TRANSCRIPTIONAL RESPONSES TO LONG-TERM SALINITY STRESS AND ACCLIMATION IN *Mytilus galloprovincialis* FROM BOSPHORUS

by

Elif İçağasıoğlu

B.S. in Information Technologies, Işık University, 2005

M.S. in Environmental Sciences, Boğaziçi University, 2011

Submitted to the Institute of Environmental Sciences in partial fulfillment of
the requirements for the degree of
Doctor of Philosophy
in
Environmental Sciences

Boğaziçi University

2021

TRANSCRIPTIONAL RESPONSES TO LONG-TERM SALINITY STRESS AND ACCLIMATION IN *Mytilus galloprovincialis* FROM BOSPHORUS

APPROVED BY:

Prof. Dr. Raşit Bilgin . . . . . .
Dissertation Advisor

Prof. Dr. Andrzej Furman . . . . . .
Dissertation Co-Advisor

Prof. Dr. Ata Akın . . . . . .

Assist. Prof. Dr. Berat Haznedaroğlu . . . . . .

Assoc. Prof. Dr. Ulaş Tezel . . . . . .

Assist. Prof. Dr. M. Baki Yokeş . . . . . .

DATE OF APPROVAL: 21/10/2021

To
my parents, Afitap and Ahmet İçağasıoğlu,
brother, Mehmet İçağasıoğlu
grandparents, Aynur and Zafer Tosun
and Alkan Şimşek

ACKNOWLEDGEMENTS

First and foremost, I would like to express my sincere gratitude to my thesis advisor, Prof. Dr. Raşit Bilgin for his support during the study, his generous time on proofreading, and all the freedom he has given me to pursue my research.

I wish to express my special thanks to Prof. Dr. Andrzej Furman for his kindness and valuable statistical advices.

It's an honor for me to thank my jury members Assist. Prof. Dr. Berat Haznedaroğlu, Assoc. Prof. Dr. Ulaş Tezel, Prof. Dr. Ata Akın, and Assist. Prof. Dr. M. Baki Yokeş for spending their valuable time to evaluate this thesis. I appreciate the effort that Assist. Prof. Dr. Berat Haznedaroğlu has spent with me during this study. I also want to thank Assoc. Prof. Dr. Ulaş Tezel for his supportive comments. I thank Prof. Dr. Ata Akın wholeheartedly for the example he provided both as a great scientist and person.

I would like to thank my dear friends and collegues, Elizabeth Hemond, Evrim Kalkan, Ayşe Mergenci, Nehir Sevim, Merve Sıvacı, Elif Şahin, Koray Sakarya, Gözde Yassal, Binnur Zaimler, Kıvanç Zaimler, Başak Savun, Hazal Pekcan, Burcu Yılmazer, and Deren Pektaş and my cousins Kübra and Zafer Tosun for supporting me in every way they can for the writing of this dissertation. I would also like to give a special thanks to Kübra Karaman, Alkan Şimşek, Melih Yazgan, Ümit Yurdakul for their efforts in collecting study samples; İlkay Civelek for her support in processing the samples; and, my cousin Elif Selin Cila for her editing.

The financial support provided by the Boğaziçi University Research Fund grant (17Y00D1) is greatly acknowledged. The numerical calculations reported in this thesis were partially performed at TUBITAK ULAKBIM, High Performance and Grid Computing Center (TRUBA resources) that is also greatly acknowledged.

Finally, words cannot express my gratitude to my parents Afitap and Ahmet İçağasıoğlu, my brother Mehmet İçağasıoğlu and my granparents Aynur and Zafer Tosun, who inspire me with their character and hard work. I could never repay them for their endless love and support. I would also like to thank Alkan Şimşek who inspires me with his stance and character as a person and for his support and encouragement to continue to persevere through to the end.

ABSTRACT

TRANSCRIPTIONAL RESPONSES TO LONG-TERM SALINITY STRESS AND ACCLIMATION IN *Mytilus galloprovincialis* FROM BOSPHORUS

Mytilus galloprovincialis is an ideal model organism for studying adaptation, as it can inhabit highly variable environments. We examined its acclimation to chronic and gradual long-term salinity stress. Gene expression, pathway and gene set enrichment analyzes were used with RNA-Seq with de novo transcriptome. In our results, low salinity was observed to be correlated with high energy expenditure. Cholinergic ciliary stimulation and calcium signalling were involved. Volume regulation was enhanced by nitrogen metabolism and alterations of membrane permeability. Arachidonic acid metabolism and Na^+/K^+ pump were inversely regulated with salinity in this context. Genes involved in the synthesis of serine, proline, glycine, ornithine and betaine were also regulated. Protein turnover and nucleotide metabolism were also inversely regulated with salinity. In addition to these regulations, some of the observed metabolic regulations are associated with cancereous cells, as well. Parallel to energy requirement, aerobic and anaerobic respiration genes were parallely regulated, as well as genes of reciprocally regulated processes of glycolysis and gluconeogenesis. Although there are many types/causes of cancer, there are common adaptations that support survival and proliferation, such as apoptosis suppression and the aforementioned metabolic regulations. In addition, in our study, parallel with these metabolic regulations, p53 and p63 originated apoptosis were triggered with participation of TP53 apoptosis effector (PERP), TLRs and TNFSF14. Understanding genes and pathways that triggers apoptosis in this context in our study, and investigating their projections in humans, may be important in our understanding of cancer and in developing therapeutic and protective products such as vaccines.

ÖZET

BOĞAZ Mytilus galloprovincialis'İNİN UZUN VADELİ TUZLULUK STRESİNE GEN ANLATIMSAL YANITLARI VE AKLİMASYONU

Ciddi çevresel koşullarının değişimlerine maruz kalmasına rağmen varlığını sürdürebilmesinden ötürü *Mytilus galloprovincialis* adaptasyon mekanizmalarını çalışmak için ideal bir türdür. Bu çalışmada bu türün kronik ve kademeli olarak uzun dönemde uygulanan tuzluluk stresi aklimasyonu, RNA-Seq ve de novo transkriptome ile gen ekspresyon, yolak ve gen seti zenginleşme analizleri kullanılarak incelenmiştir. Sonuçlarımızda; düşük tuzluluk yüksek enerji gereksinimi yaratmış, kolinerjik silyer stimülasyonu ve kalsiyum sinyalleşmesi, tranksriptomil tepkide yer almış, hacim regülasyonu ise hücre zarı geçirgenliğinin ve nitrojen metabolizmasının alterasyonu ile sağlanmıştır. Araşidonik asit metabolizması ve Na^+/K^+ pompası bu bağlamda tuzluluk ile ters yönde regüle olurken, tuzluluk stresiyle serin, prolin, glisin, ornitin ve betain sentezinde görev alan genler regüle olmuş, protein döngüsü ve nükleotid metabolizması da tuzluluk stresi ile ters regüle olmuştur. Sonuçlarımızdaki iki regülasyon özellikle dikkat çekmektedir. Enerji gereksinimiyle paralel şekilde (tuzluluk stresine ters), oksijenli ve oksijensiz solunum genleri paralel regüle olmuş, ayrıca karşılıklı düzenlenen süreçlerin, glikolizin ve glukoneogenezin genleri de paralel olarak regüle olmuştur. Bu metabolik regülasyonlara kanserde rastlanmaktadır. Kanserin pek çok çeşidi ve sebebi olmasına rağmen, apoptozun baskılanması ve sonuçlarımızda da çıkmış olan metabolik regülasyonlar gibi, ortak olarak hücrelerin hayatta kalmasını ve çoğalımını destekleyecek adaptasyonları da içerir. Önemli olarak sonuçlarımızda, bu regülasyonlara paralel şekilde p53 ve p63 odaklı, TP53 apoptoz efektör (PERP), TLR'ler ve TNFSF14'ün katılımıyla apoptoz tetiklenmiştir. Çalışmamızda çıkmış olan ve bu çerçevedeki hücre ölümünü tetikleyen mekanizmada görev alan gen ve yolakların anlaşılması ve insandaki izdüşümlerinin araştırılması, kanseri anlamamızda ve aşı gibi tedavi edici, koruyucu ürünleri geliştirmemizde önemli olabilir.

TABLE OF CONTENTS

ACKNOWLEDGEMENTS iv
ABSTRACT v
ÖZET vi
TABLE OF CONTENTS vii
LIST OF FIGURES ix
LIST OF TABLES xi
LIST OF SYMBOLS/ABBREVIATIONS xiv
1. INTRODUCTION 1
1.1. Turkey's Coastal Waters and Salinity 2
1.2. Study Organism: Mediterranean Mussel, *Mytilus galloprovincialis* 3
1.3. RNA-SEQ 5
1.4. Functional Analysis 6
1.5. The objective of the Dissertation 7
2. LITERATURE REVIEW 8
2.1. Gene Regulation as an Adaptive Response 8
2.2. Genetic Mechanisms of Adaptation to Stress 9
2.2.1. Energy Metabolism 9
2.2.2. Hypoxia 13
2.2.3. Lipid Peroxidation 17
2.2.4. Oxidative Stress 18
2.2.5. Immune Response 21
2.2.5.1. Pathogen recognition receptors (PRRs) and their related pathways 22
2.2.5.2. Complement system 27
2.2.6. DNA Damage Response (DDR) 28
2.2.7. Proteolysis 31
2.2.8. Apoptosis 31
2.2.9. Osmoregulation 35
3. MATERIALS AND METHODS 39
3.1. Sample Collection 39
3.2. Experimental Design 40
3.3. Experimental Period 41
3.4. RNA Extraction, Library Preparation and Sequencing 43

3.5. Data Analysis 44
4. RESULTS AND DISCUSSION 49
4.1. Descriptive Statistics and Data Validation 49
4.1.1. RNA Quality 49
4.1.2. Sequencing Data Quality 49
4.1.3. Data Quality Statistics 49
4.1.4. Assembly Statistics 50
4.1.5. Mapping and Alignment Statistics 51
4.1.6. Annotation Statistics 52
4.1.7. Differential Gene Expression Data Preparation Statistics 54
4.2. Differential Gene Expression 61
4.2.1. Energy Metabolism and Salinity 62
4.2.2. Oxidative Stress 101
4.2.3. Apoptosis 103
4.3. Gene Set Enrichment Analysis 114
4.3.1. Ciliary Activity 114
4.3.2. Oxidative Phosphorylation 116
4.3.3. Gene Expression Regulation 117
4.3.4. Protein Metabolism 118
4.3.5. Nucleotide Metabolism 120
4.3.6. DNA Repair 120
4.4. Pathway Enrichment Analysis 122
4.4.1. Immune System 122
4.4.2. Metabolism 125
4.4.3. Calcium Signaling 126
4.4.4. Structural Integrity of Tissues and Cells 127
4.4.5. Signaling Pathways 127
5. CONCLUSIONS AND RECOMMENDATIONS 129
5.1. Conclusions 129
5.1.1. Effect of Salinity on Distribution 135
5.2. Limitations of the Study 136
5.3. Recommendations 137
REFERENCES 140
APPENDIX A: DESCRIPTIVE STATISTICS AND DATA VALIDATION 193
APPENDIX B: GSEA ANALYSIS 220

LIST OF FIGURES

Figure 1.1. Maps of Seas of Turkey with *M. galloprovincialis* distribution and the geographic location of the sampling site from the Bosphorous 3

Figure 1.2. *M. galloprovincialis* and its worldwide distribution 5

Figure 2.1. Anaerobic metabolism in marine mollusks 16

Figure 2.2. Apoptotic pathway in mollusks 34

Figure 3.1. Schematic representation of the experiment 39

Figure 3.2. Geographic location of sampling site of *M. galloprovincialis* 40

Figure 3.3. Design of the tanks of the experiment 40

Figure 3.4. Design of the experiment with salinity adjustments 41

Figure 3.5. Flowchart of data analysis of the study 46

Figure 4.1. Second level functional annotation of assembled contigs 53

Figure 4.2. KEGG ontology distribution of enzymes 54

Figure 4.3. P-value histogram of the main contrast RTvsRC.BA with different filters 56

Figure 4.4. Multidimensional MDS graphs for dimensions 58

Figure 4.5. Distrubition of the libraries before and after filtering 60

Figure 4.6. The hypothesized model of the study 62

Figure 4.7. Electron transport chain in oxidative phosphorylation 64

Figure 4.8. Compartmentalization of the mentioned pathways 67

Figure 4.9. Malate aspartate shuttle..... 74

Figure 4.10. Pentose phosphate pathway..... 76

Figure 4.11. Regulation of lipid metabolism in the study 78

Figure 4.12. Hypothetical model of long-term salinity stress response in oyster *Crassostrea gigas* 80

Figure 4.13. Amino acid catabolism 85

Figure 4.14. Amino acid regulation in the hypothesized model 86

Figure 4.15. Glycine, serine and threonine metabolism (Map00260) for salinity increase..... 87

Figure 4.16. Arginine and proline metabolism (Map00330) for salinity increase..... 88

Figure 4.17. Arginine and proline metabolism (Map00330) for salinity decrease 90

Figure 4.18. Regulation of betA in liver mitochondria. 92

Figure 4.19. Acetylcholine release in the hypothesized model 98

Figure 4.20. Apoptotic pathway of bivalves..... 104

Figure 4.21. Apoptosis in the hypothesized model 106

Figure 4.22. Hypothetical model of the pathway which activated TAp63α dependent apoptosis by TLRs 112

Figure 4.23. Hypothesized model of the study with regulations 135

LIST OF TABLES

Table 3.1. Design of the experiment 42

Table 3.2. Design of the experiment for conditions compared in differential gene expression analysis 43

Table 3.3. Contrasts differential expression analysis tested for 47

Table 4.1. Completeness and quality statistics of the assembly 51

Table 4.2. Coverage statistics 52

Table 4.3. Annotation statistic of *de novo* assembly 53

Table 4.4. Statistics of the applied filters 55

Table 4.5. Number of contigs that were up-regulated and down-regulated at 5% FDR of the contrasts for the different filter categories 55

Table 4.6. Contrasts differential expression analysis tested for 61

Table 4.7. Regulation of contigs that were involved in oxidative phosphorylation 64

Table 4.8. Regulation of contigs related with carbohydrate metabolism 68

Table 4.9. Regulation of contigs of cathepsins, ribosomal proteins and proteoglycans 69

Table 4.10. Regulation of contigs related with nucleotide metabolism 77

Table 4.11. Regulation of contigs related to lipid metabolism 81

Table 4.12. Regulation of contigs of GPCRs 82

Table 4.13. Regulation of contigs of amino acid metabolism 85

Table 4.14. Regulation of contigs of ion channels and transporters 94

Table 4.15. Regulation of dyneins 98

Table 4.16. Regulation of contigs related to redox homeostasis..... 102

Table 4.17. Regulation of contigs related to apoptosis 105

Table 4.18. Regulation of contigs of the main innate receptors..... 110

Table 4.19. Regulation of contigs of the other innate receptors 111

Table 4.20. Regulation of contigs of DNA damage response..... 113

Table 4.21. Regulation of contigs of EGFR and MEGF 10. 114

Table 4.22. GOs of cilliary activity enriched in top 50 list by NES scores. 115

Table 4.23. GOs of oxidative phosphorylation enriched in top 50 list by NES scores. 117

Table 4.24. GOs of gene expression regulation enriched in top 50 list by NES scores. 118

Table 4.25. GOs of protein metabolism enriched in top 50 list by NES scores. 119

Table 4.26. GOs of nucleotide metabolism enriched in top 50 list by NES scores. 120

Table 4.27. GOs of DNA damage and repair enriched in top 50 list by NES scores..... 121

Table 4.28. Generic GOs enriched in top 50 list by NES scores. 121

Table 4.29. Enriched pathways related to immune system..... 124

Table 4.30. Enriched pathways related to cellular processes..... 125

Table 4.31. Enriched pathways related to metabolism of proteins, carbohydrates and lipids. 126

Table 4.32. Enriched pathways related to cell-cell and calcium signaling. 126

Table 4.33. Enriched pathways related to ECM, cytoskeleton and cell-matrix adhesions. 127

Table 4.34. Enriched pathways related to signaling. 128

Table 4.35. Generic pathways enriched. 128

LIST OF SYMBOLS/ABBREVIATIONS

Symbol	Explanation
3-PG	3-phosphoglycerate
3-PHP	3-phosphopyruvate
5,10-CH2-THF	5,10-methylenetetrahydrofolate
ACADL	Acyl-CoA dehydrogenase
ADG cells	Adipogranular cells
ADP	Adenosine diphosphate
AGTs	O6-alkylguanine-DNA alkyltransferases (MGMT)
ALOX12B	Arachidonate 12-lipoxygenase (R-type)
ALOX5	Arachidonate 5-lipoxygenase
AMP	Antimicrobial peptides
AMPK	AMP-activated protein kinase
ANXA	Annexin
APAF-1	Adaptor protein apoptotic protease activating factor 1
APE1	Apurinic/apyrimidinic endonuclease 1
ASC	Speck-like protein containing a CARD
ATG	Autophagy-related genes
ATGL	Adipose triglyceride lipase
ATP	Adenosine triphosphate
ATP1A	ATPase Na^+/K^+ transporting subunit alpha 1
ATP1B	Na^+/K^+ transporting, ATPase subunit beta 1
ATPeF0D	F-type H+-transporting ATPase subunit d
ATPeF1D	F-type H+-transporting ATPase subunit delta
ATPeV0C	V-type H+-transporting ATPase
BAD	BCL2 associated agonist of cell death
BAK	BCL2 antagonist/killer
BAX	BCL2 associated X
BCL2	B cell lymphoma 2
BCV	Biological coefficient of variation
BER	Base excision repair
betA	Choline dehydrogenase

BI-1	BAX inhibitor 1
BID	BH3 interacting domain death agonist
BIM	BCL2 interacting mediator of cell death
BIR	Baculovirus inhibitor of apoptosis
BIRCs	Baculoviral IAP repeat-containing proteins
BLM	Bloom syndrome protein
BRCA	Breast cancer gene
C1qDC	C1q domain-containing protein
CA	Carbonic anhydrase
Ca^{+2}	Calcium
CACN	Voltage-gated calcium channels (CaVs)
cAMP	Cyclic adenosine monophosphate
CARD	Caspase recruitment domain
CASP	Caspase
CAT	Catalase
CCKAR	Cholecystokinin A receptor
CCKBR	Cholecystokinin B receptor
Cd	Cadmium
CD95	Cluster of differentiation 95
cdd	Cytidine deaminase
CED-4	Cell death protein 4
CELSR3	Cadherin EGF LAG seven-pass G-type receptor 3
CLCA	Calcium-activated chloride channel regulator
CLR	C-type lectin
CNV	Copy number variation
COX	Cyclooxygenase
cPLA2	Cytosolic phospholipase A2 (PLA2G4)
CPM	Counts per million
CRD	Carbohydrate recognition domains
CRNS1	Carnosine synthase
CTLD	C-type lectin domain
Cu/ZnSOD	Copper/zinc SOD
CYP	Cytochrome p450
CYP2J	Cytochrome P450 family 2 subfamily J
D.E.	Differentially expressed

DAG	Diacylglycerol
DDB2	Damage specific DNA binding protein 2 (DDB1– XPE)
DDR	DNA damage response
DFF	DNA fragmentation factor
DGE	Differential gene expression
DHAP	Dihydroxyacetone phosphate
DNAPKcs	DNA-dependent protein kinase, catalytic subunit
dNTP	Deoxynucleoside triphosphate
DR	Direct reversal
DR4	Death Receptor 4 (TRAIL-R1, TNFRSF10A, TNF receptor superfamily member 10a)
DR5	Death Receptor 5 (TRAIL-R2, TNFRSF10B, TNF receptor superfamily member 10b)
DSBR	Double-strand break repair
dsRNA	Double-stranded RNA
ECM	Extracellular matrix
EDA-A2	Ectodysplasin A2
EET	Epoxyeicosatrienoic acid
EGFR	Epidermal growth factor receptor
EPO	Erythropoietin
EPO	Erythropoietin receptor
ER	Endoplasmic reticulum
ERCC1	ERCC excision repair 1 (RAD10)
ERCC2	ERCC excision repair 2 (XPD)
ERCC3	ERCC excision repair 3 (XPB)
ERCC4	ERCC excision repair 4 (XPF, RAD1)
ERCC5	ERCC excision repair 5 (XPG)
ERCC8	Cockayne syndrome group A (CSA)
ERK	Extracellular signal-regulated kinase
EST	Expressed sequence tag
Exo1	Exonuclease 1
FAD	Flavin adenine dinucleotide
FADD	Fas associated death domain
FAS	Fas cell surface death receptor
FBPase-1	Fructose 1,6-bisphosphatase

FBPase-2	Fructose bisphosphatase-2
FDR	False discovery rate
FEN1	Flap endonuclease 1
FeSOD	Iron superoxide dismutase
FFA	Free fatty acid
FREP	Fibrinogen-related protein
FUCA	Fucosidase
Fucolectin	F-type lectin
G6P	Glucose 6-phosphate
G6PD	Glucose-6-phosphate dehydrogenase
GAPDH	Glyceraldehyde-3-phosphate dehydrogenase
GG-NER	Global genome NER
GLUT	Glucose transporter
glyA	Glycine hydroxymethyltransferase (SHMT)
GLYT2	Glycine transporter 2
GNBPs	Gram-negative binding proteins
GO	Gene ontology
GPCRs	G-protein coupled receptors
GPx	Glutathione peroxidase
GR	Glutathione reductase
GSA	Glutamate 5-semialdehyde
GSEA	Gene set enrichment analysis
GSH	Glutathione reduced
GSSG	Glutathione oxidized
GST	Glutathione s-transferase
H2O2	Hydrogen peroxide
Hg	Mercury
HIFs	Hypoxia-inducible factors
HK	Hexokinase
HNE	4-hydroxynonenal
HPGDS	Prostaglandin-H2 D-isomerase / glutathione transferase
HRR	Homologous recombination repair
HSL	Hormone-sensitive lipase
HTRA2	HtrA serine peptidase 2
IAPs	Inhibitor of apoptosis

IKB	Inhibitor of KB
IKK	I Kappa B kinase
IMD	Immune deficiency
IP3	Inositol 1,4,5-trisphosphate
IRAK	Interleukin-1 receptor-associated kinase
IRF	Interferon regulatory factors
JNKs	c-Jun amino-terminal kinases
KAAS	KEGG Automatic Annotation Server
KCNA10	Potassium voltage-gated channel subfamily A member 10
KEGG	Kyoto Encyclopedia of Genes and Genomes
KO	KEGG Orthology
Ku70: Ku80	Ku heterodimer
LCT	Lactase-phlorizin hydrolase (LPH)
LDH	L-lactate dehydrogenase
LDHA	L-lactate dehydrogenase A
LDL	Low-density lipoproteins
LGBPs	Lipopolysaccharide and b-1, 3-glucan binding proteins
LGP2	Laboratory of genetics and physiology 2 (DHX58)
LITAF	LPS-induced TNF-α factor)
lncRNA	Long non-coding RNA
LOX	Lipoxygenase
LPS	Lipopolysaccharide
LRR	Leucine-rich repeat
LTBR	Lymphotoxin beta receptor
MAP3K7	Mitogen-activated protein kinase kinase kinase 7
MAPK	Mitogen-activated protein kinase
MASP	MBL-associated serine protease
MCL1	Myeloid cell leukemia 1
MCT	Monocarboxylate transporter
MDA	Malondialdehyde
MDA-5	Melanoma differentiation-associated gene-5 (IFIH1)
MDH	Malate dehydrogenase
MEGF10	Multiple epidermal growth factor-like domains protein 10
MIF	Macrophage migration inhibitory factor
MLH	MutL homolog

MMR	Mismatch repair
MnSOD	Manganese superoxide dismutase
MOMP	Mitochondrial outer membrane permeabilization
MRC	Mannose receptor, C type
Mre11	Meiotic recombination 11
MSH	MutS homolog
MT	Metallothionein
Mutyh	MutY DNA glycosylase
MyD88	Myeloid differentiation primary response 88
nAChRs	Nicotinic acetylcholine receptors (CHRN)
NAD	Nicotinamide adenine dinucleotide
NADPH	Nicotinamide adenine dinucleotide phosphate
NAT	Natural antisense transcription
ncRNA	Non-coding RNA
NEMO	Inhibitor of nuclear factor kappa-B kinase (IKBKG)
NER	Nucleotide excision repair
NES	Normalized enrichment scores
NF-κB	Nuclear factor kappa B
NGF	Nerve growth factor
NHEJ	Non-homologous end joining
nibrin	Nbs1
NiSOD	Nickel superoxide dismutase
NLRs	NOD-like receptors
NOD	Nucleotide-binding and oligomerization domain
NOSs	Nitric oxide synthases
NTPs	Ribonucleoside triphosphates
O2	Oxygen
OAT	Ornithine aminotransferase
Ogg1	8-oxoguanine DNA glycosylase
OsHV-1	Herpesvirus 1
P5C	Pyrroline-5-carboxylate
P5CS	Delta-1-pyrroline-5-carboxylate synthetase (ALDH18A1)
PA	Phosphatidic acid
PAMPs	Pathogen-associated molecular patterns
PARP1	Poly-ADP ribose polymerase 1

Pb	Lead
PC	Pyruvate carboxylase
PCR	Polymerase chain reaction
PDRP	P53 and DNA damage regulated protein
PEA	Pathway enrichment analysis
PEP	Phosphoenolpyruvate
PEPCK	Phosphoenolpyruvate carboxykinase
PERP	TP53 apoptosis effector
PFK-2	Phosphofructokinase-2
PFK1	Phosphofructokinase-1
PGD2	Prostaglandin D2
PGH2	Prostaglandins H2
PGHPx	Hydroperoxide glutathione peroxidase
PGK1	Phosphoglycerate kinase-1
PGN	Peptidoglycan
PGRPs	Peptidoglycan recognition receptors
PHD	Prolyl hydroxylase domain enzyme
PI3K	Phosphoinositide-3-kinase
PIDD1	P53-induced death domain protein 1
PIP2	Phosphatidylinositol 4,5-bisphosphate
PIs	Phosphoinositides
Pi	Inorganic phosphate
PK	Pyruvate kinase
PKA	Protein kinase A, cAMP-dependent protein kinase
PKC	Protein kinase C
PksJ	Polyketide synthase
PLA2	Phospholipase A2
PLC	Phospholipase C
PMS1	Postmeiotic segregation increased 1
PMS2	Postmeiotic segregation increased 2
PNKP	Polynucleotide kinase/phosphatase
PO2	Partial pressure of oxygen
Polb	DNA polymerase-beta
Pole	DNA polymerase-epsilon
Polg	DNA polymerase-gamma

PPP	Pentose-phosphate pathway
PRDX	Peroxiredoxin
proC	Pyrroline-5-carboxylate reductase
PRPP	Phosphoribosylpyrophosphate
PRPS	Ribose-phosphate pyrophosphokinase
PRRs	Pathogen recognition receptors
PSU	Practical salinity unit
PTK	Src/protein tyrosine kinase
PUFA	Polyunsaturated fatty acids
PUMA	P53 up-regulated modulator of apoptosis
PYD	Pyrin domain
R5P	Ribose-5-phosphate
RAD23B	RAD23 homolog B (HR23B)
Rad50	DNA repair protein RAD50
Rad52	DNA repair protein RAD52
Rad54	DNA repair and recombination protein RAD54
RAIDD	CASP2 and RIPK1 domain containing adaptor with death domain
RC	Rumeli Hisarı control
Relish	NF-κB related transcription factor
RIG-I	Retinoic acid-inducible gene I (DDX58)
RIN	RNA integrity number
RIP2	Receptor-interacting protein kinase 2
RLRs	RIG-I-like receptors
RNA	Ribonucleic acid
RNS	Reactive nitrogen species
ROS	Reactive oxygen species
RPA	Replication protein A
rRNA	Ribosomal ribonucleic acid
RT	Rumeli Hisarı treatment
RTKs	Receptor tyrosine kinases
RVD	Regulatory volume decrease
RVI	Regulatory volume increase
SAM	S-adenosylmethionine
SARM	Sterile alpha and armadillo-motif- containing protein
SCARF1	Scavenger receptor class F member 1

SD	Standard deviation
serA	D-3-phosphoglycerate dehydrogenase (PHGDH)
serC	Phosphoserine aminotransferase
SIRT	Sirtuin
SIRT6	NAD+-dependent protein deacetylase sirtuin 6
SLC16A12	Solute carrier family 16 member 12
SLC16A13	Solute carrier family 16 member 13
SLC16A7	Solute carrier family 16 member 7
SLC17A5	Solute carrier family 17 member 5
SLC25A38	Solute carrier family 25 member 38
SLC25A4S	Solute carrier family 25 (mitochondrial adenine nucleotide translocator), and member 4/5/6/31
SLC39A10	Solute carrier family 39 member 10 (zinc transporter)
SLC39A4	Solute carrier family 39 member 4 (zinc transporter)
SLC39A5	Solute carrier family 39 member 5 (zinc transporter)
SLC39A6	Solute carrier family 39 member 6 (zinc transporter)
SLC6A5_9	Solute carrier family 6 (neurotransmitter transporter, glycine) member 5/9
SNPs	Single-nucleotide polymorphisms
SOD	Superoxide dismutase
SR-BI	Scavenger receptor class B
SRCR-SF	Scavenger receptor cysteine-rich superfamily receptors
TAp63	Transactivating p63
TC-NER	Transcription-coupled NER
TCA cycle	Tricarboxylic acid cycle
TDP1	Tyrosyl DNA phosphodiesterase 1
TEPs	Thioester-containing proteins
TFIIH	Transcription factor II H
TGF-Beta	Transforming growth factor-beta
THF	Tetrahydrofolate
TIR	Toll interleukin 1 receptor
TIRAP	Toll interleukin 1 receptor adaptor protein
TLRs	Toll-like receptors
TLRs	Toll-like receptors
TMM	Trimmed mean of M-values

TNF	Tumor necrosis factor
TNF-α	Tumour necrosis factor alpha
TNFR1	Tumor necrosis factor receptor 1
TNFRSF27	Tumor necrosis factor receptor superfamily member 27 (EDA2R, XEDAR)
TNFSF14	Tumor necrosis factor ligand superfamily member 14 (LIGHT)
TPx	Thioredoxin peroxidase
TR	Thioredoxin reductase
TRAF	TNF receptor associated factor
TRAF3	TNF receptor associated factor 3
TRAIL	TNF-related apoptosis inducing ligand (APO2L)
TRAM	TRIF-related adaptor molecule
TRIF	TIR-domain-containing adaptor protein inducing IFNB
tRNA	Transfer RNA
TRPMs	Transient receptor potential melastatin channels
UCP4	Solute carrier family 25 (mitochondrial uncoupling protein), member 27 (SLC25A27)
UCPs	Mitochondrial uncoupling proteins
UPP	Ubiquitin-proteasome pathway
VCT cells	Vesicular connective tissue cells
VEGF	Vascular endothelial growth factor
WRN	Werner syndrome protein
XIAP	E3 ubiquitin-protein ligase XIAP
XLF	XRCC4-like factor
XPA	Xeroderma Pigmentosum Group A-Complementing Protein
XPC	Xeroderma Pigmentosum Group C-Complementing Protein (RAD4)
XRCC2	X-Ray repair cross complementing 2
XRCC3	X-Ray repair cross complementing 3
XRCC4	X-Ray repair cross complementing 4
ΔNp63	N-terminally truncated p63

1. INTRODUCTION

Biological systems are affected by changes in their environment, and understanding adaptation mechanisms of organisms to changing conditions is important in predicting the course of the species in terms of its survival *vs.* extinction. As human impact on ecosystems and climate increases, it is even more essential to understand these adaptation mechanisms. In the marine environment, these mechanisms are important in predicting distribution patterns (Hofmann, 2005), competition capacity (Lockwood and Somero, 2011; Lockwood et al., 2010), and ultimate fate of the species (Anestis et al., 2010; Fields et al., 2011).

Populations adapt to changing conditions by altering their physiology, morphology, and behavior, or through adaptation by selection (Eierman and Hare, 2014). The ability of an organism to change its phenotype due to environmental change is referred to as "phenotypic plasticity" (Yampolsky et al., 2014); or in other words, it is the ability of a genotype to create different phenotypes. It determines the acclimation capacity of the organism to change. The term encapsulates physiological mechanisms including transcription, translation, and hormonal regulation, among others (Whitman and Agrawal, 2009). Phenotypic plasticity is especially important for immobile organisms as mobile organisms can migrate to compensate for the change. Sessile organisms are exposed to extremely varied conditions in unpredictable habitats where environmental factors like temperature, oxygen, salinity, and food vary dramatically (Gracey et al., 2008). Among these, salinity is among one of the most important environmental factors that influence the distribution (Gosling, 2004; Hofmann, 2005; Fields et al., 2011) and physiology (Hofmann, 2005) of marine organisms.

Due to the warming of the seas, distribution and abundance shifts (Bethoux et al., 1998) as well local extinction "hotspots" (Bethoux et al., 1990) are expected based on the thermal tolerance of the species. Marine invasions by organisms accustomed to living in warmer waters are expected in historically cooler waters, threatening existing species therein (Lockwood et al., 2010). Like temperature, global climate change is also affecting the salinity of bodies of water globally, mainly in estuarine and coastal areas through alterations of the hydrological cycle and ocean water circulation (Durack and Wijffels, 2010). Such changes have already been documented: mainly, scientists have found increases in salinity in subtropical regions and freshening in high latitude regions (Durack and Wijffels, 2010). While changes in salinity occur regionally and decadally (Dickson et al., 1988), it is projected that global warming will hasten salinity fluctuations, negatively impacting organisms that are not able or accustomed to adapting to changes in salinity as quickly as they should (Durack and

Wijffels, 2010). Even if the change is modest and within species tolerance, in the long term it can affect species fitness and survival.

The effect of gradual or minor changes in environmental conditions on organisms can be understood by long-term acclimation stress experiments (Anestis et al., 2007). This study is focused on understanding the long-term acclimation response of *Mytilus galloprovincialis* to chronic salinity stress while accounting for the lower and upper limits of salinity encountered by this species in the Bosphorous and adjacent seas. Within this perspective gene regulatory response that ensures adaptation to long-term stress is examined using whole transcriptome profiling. Differential gene expression analysis, gene set enrichment analysis, and pathway enrichment analysis was applied to identify genes, gene ontology groups, and pathways involved in the acclimation response.

1.1. Turkey's Coastal Waters and Salinity

The effects of climate change are expected to be first be seen on the water systems, through changes in evaporation, precipitation, and runoff, which are the factors that determine the salinity of sea waters (Bakan and Büyükgüngör, 2000; Bar et al., 2015). Considering salinity, the coasts of Turkey -bordered by the Sea of Marmara, the Black Sea, the Aegean Sea, and the Mediterranean Sea- comprise a unique environment where a natural increase in sea temperature and salinity is observed as one moves south from the Black Sea (salinity ~17.5‰) through the Sea of Marmara (~24 ‰) into the Aegean (~38‰) (Figure 1.1).

The Black Sea has greater freshwater input through the inflow of rivers and precipitation than it loses with evaporation, resulting in an average salinity of 17.5‰ and an average temperature of 11.0 ºC (Zaitsev et al., 2002). The Black Sea receives about 350 km^3 of river runoff per year, making it particularly vulnerable to changes in water characteristics, as climate change alters patterns of precipitation and river runoff that feed it (Celikyilmaz-Aydemir, 2011). Furthermore, different areas of the sea may be more or less affected depending upon location and exposure to erosion (Celikyilmaz-Aydemir, 2011).

The Marmara Sea is located between the Black Sea and the Aegean sea. Low salinity water from the Black Sea flows southward through the Marmara into the Mediterranean while below, high salinity water from the Mediterranean flows in an undercurrent into the Marmara at 38.0-38.5‰ and the Black Sea at 35.5-36.5‰, forming a well-defined salt wedge (Beşiktepe et al., 1994). In this study, sampling was done from the Bosphorous, which has a salinity of 18‰ (Figure 1.1). To assess the

variation in temperature and salinity in the Bosphorous, the lower and upper layers were examined between the years 1996 and 2009 (Altiok et al., 2010). It was found that temperature variation was between 1.9°C in February 1996 and 26.7°C in July 2002, and salinity was 15.01-18.64 ‰ (Altiok et al., 2010).

In the Mediterranean Sea, precipitation and river runoff levels are lower than evaporation, causing it to be more saline, having average salinity and temperature values of 36.2‰ and 15 ºC in the western basin, and 39‰ salinity and 21 ºC in the eastern basin (Zenetos et al., 2002). An embayment of the Mediterranean Sea, the Aegean Sea shows the characteristics of the Mediterranean Sea. The South Aegean Sea has an average salinity of 38.7‰ and average temperatures of 16-24 ºC (Zenetos et al., 2002). It is reported that Mediterranean sea temperature and salinity have been increasing for the last three decades (Anestis et al., 2010; Bethoux et al., 1990; Bethoux et al., 1998). For example, the deep layer of the Mediterranean was measured to be 0.12 ºC warmer and ≈0.03 PSU more saline in 1988-1989 than it was in 1959 (Bethoux et al., 1990).

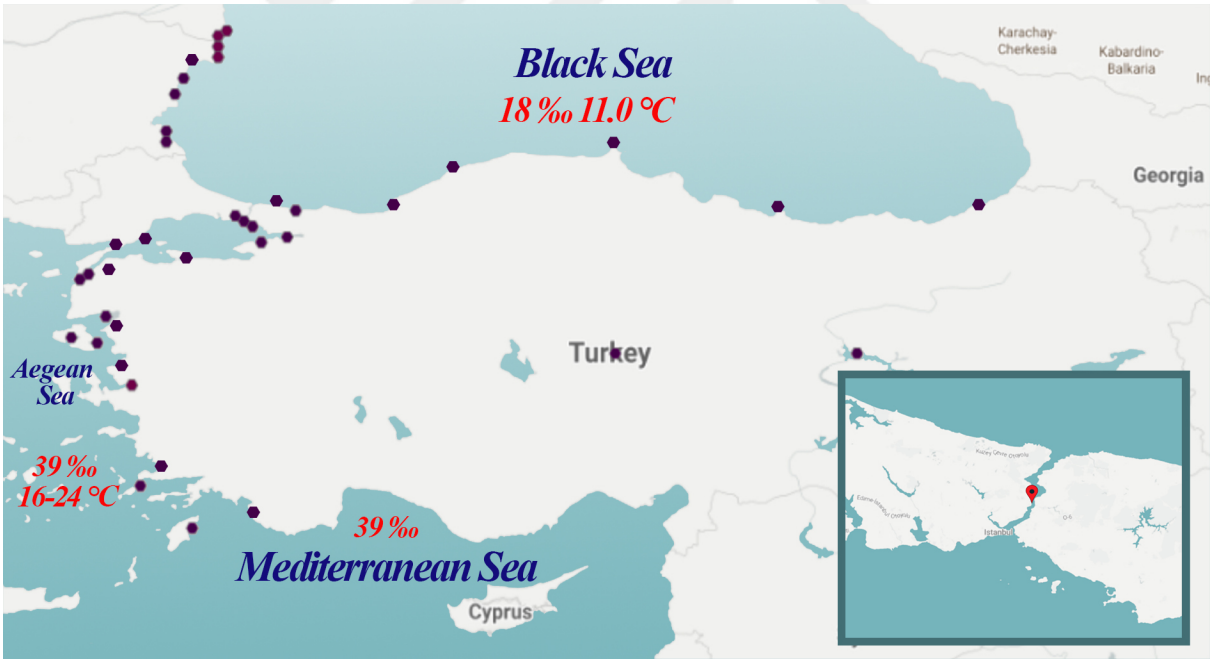


Figure 1.1. Maps of Seas of Turkey with M. galloprovincialis distribution (modified from GBIF (2021) and Kalkan (2013)) and the geographic location of the sampling site from the Bosphorous.

1.2. Study Organism: Mediterranean Mussel, *Mytilus galloprovincialis*

The Mediterranean mussel, *M. galloprovincialis* (Lamarck, 1819) is a bivalve marine mollusk with a blue-black shell belonging to the phylum Mollusca, class Bivalvia, genus *Mytilus* (Figure 1.2). It is one of the three sibling species of *Mytilus edulis* complex of blue mussels (McDonald et al.,

1991); the others being *Mytilus edulis* (Linnaeus, 1758) and *Mytilus trossulus* (Gould, 1850), which can hybridize when in contact (McDonald et al., 1991). It is one of the most ecologically important marine organisms globally, as well as in Turkey. As being edible, it is also commercially important (Gosling, 2004). Between 2006 and 2010, Turkish fishermen collected 18311 tons of black mussels from wild populations and 3270 tons from aquacultured populations, exporting 812 tons in 2010 alone (Turan et al., 2012).

M. galloprovincialis is widely distributed in the Northern and Southern hemispheres (McDonald et al., 1991). It is native to the Mediterranean, Black, and Adriatic Seas, and is found along the coasts of Algeria, Bosnia And Herzegovina, Bulgaria, Croatia, Egypt, Slovenia, France, Greece, Italy, Libya, Morocco, Portugal, Romania, Russian Federation, Spain, Tunisia, Turkey, and Ukraine (ISSG, 2015) (Figure 1.2). However, the species is alien to the non-Mediterranean African countries, including Australia, Canada, North Korea, Hong Kong, Ireland, Japan, Mexico, Namibia, the Netherlands, South Korea, the United Kingdom, and the United States (including Hawaii) (ISSG, 2015) (Figure 1.2).

Considering its habitat, it attaches to the surface of rocky shores of intertidal and subtidal zones, as well as sandy bottoms (Tagliarolo et al., 2012; ISSG, 2015). *M. galloprovincialis* found on intertidal rocky shores and estuaries experience drastic fluctuations in environmental conditions as temperature, salinity, and oxygen availability, and are therefore constantly exposed to high levels of abiotic stress (Hofmann, 2005). Due to exposure to different conditions, it is a euryoxic, facultative anaerobe (De Zwaan and Mathieu,1992). It is an ectothermic organism found between water temperatures of 7°- 28°C (Fields et al., 2011). It is also a euryhaline species occurring in the 12-38‰ salinity range (Bayne, 1976) and an osmoconformer (Hamer et al., 2008; Lockwood and Somero, 2011). The sessile *M. galloprovincialis* can adapt to these ever-changing local conditions and respond to extreme environmental changes that make them an ideal model organism for studying animal adaptation (Hofmann, 2005).

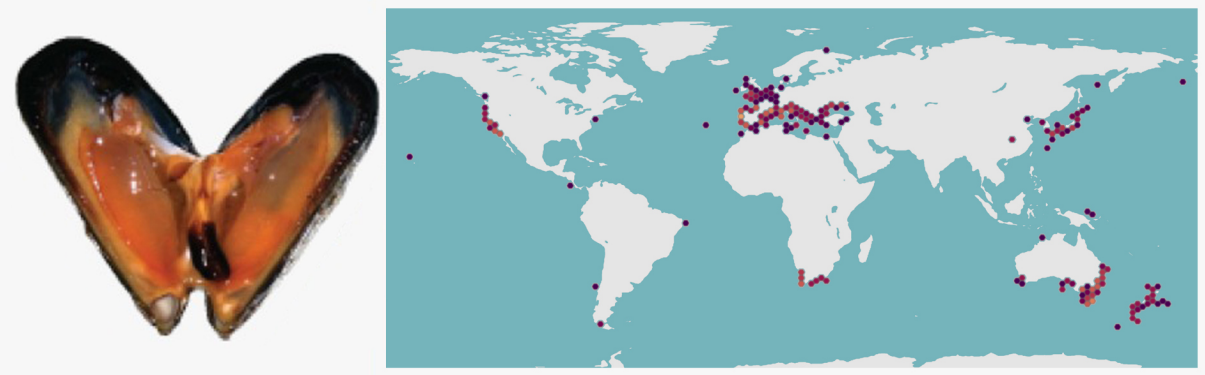


Figure 1.2. *M. galloprovincialis* on the left and its worldwide distribution (GBIF, 2021) on the right.

1.3. RNA-SEQ

For two and a half decades, Edward Sanger's 1975 genomic sequencing method (Sanger Sequencing) was widely used for sequencing the genome. It is based on the incorporation of chain-terminating dideoxynucleotides during in vitro DNA replication (Grada and Weinbrecht, 2013). The DNA fragments are separated by size using gel electrophoresis and visualized. Relatively long (500–1000 bp) and high-quality reads are generated using capillary sequencers (Besser et al., 2018). The first completed genome of a human was also sequenced by this method. Sanger Sequencing is considered "first-generation" sequencing technology (Metzker, 2010).

"Second-generation"(next-generation) sequencing technologies have caused a rapid decline in the cost of generating DNA sequence, surpassing Moore's law (NHGRI, 2020). The huge amount of complex data produced in a short time increased the usage of bioinformatic tools and statistical methods. Next-generation sequencing is used in

- *de novo* sequencing of genomes,
- whole or targeted resequencing of genomes,
- identifying SNPs, indels, CNVs by comparing with a reference genome,
- gene expression profiling,
- quantification of transcripts,
- examining epigenetic modifications like DNA methylation, and post-translational modifications of histones, among others (Mutz et al., 2013).

Next-generation sequencing technology based on sequencing by synthesis technology is called pyrosequencing (Mutz et al., 2013). Fluorescently labeled dNTPs are added and nucleotide incorporation is monitored by luminescence (Mutz et al., 2013). As a result, thousands of DNA

fragments are sequenced parallelly at the same time (Grada and Weinbrecht, 2013). Next-generation sequencers produce short (50 – 400 bp) and long reads (1 – 100 kb) depending on the platform that is being used (Besser et al., 2018). The read length is related to the signal-to-noise ratio of the platform which is associated with sequencing errors. Shorter read lengths can make assembling the genome harder if the genome is highly polymorphic and abundant in repetitive sequences (Mardis, 2013; Zhang et al., 2012), and special algorithms have been developed to assemble short reads.

Rna-Seq is the transcriptomic variant of next-generation sequencing (Mutz et al., 2013), and does not need prior information of the genes that are examined (Metzker, 2010). With Rna-Seq whole transcriptome sequencing of both coding and non-coding RNA genes, or targeted transcripts of interest can be made (Mercer et al., 2012; Nagalakshmi et al., 2008). For coding sequences, transcript identification and quantification can be both done. For organisms that have a reference genome, reads can be mapped and identified. If a reference genome is not available or is not comprehensive, mapping reads to the *de novo* constructed transcriptome can be used for quantification (Conesa et al., 2016). Statistical analysis of quantification of genes between conditions ensures detection of differentially expressed genes between altered conditions. In bivalves, transcriptome analyses have been widely used to understand the molecular basis of adaptation to stress (Prego-Faraldo et al., 2018; Eierman and Hare, 2014; Prentis and Pavasovic, 2014).

1.4. Functional Analysis

Genome-scale datasets like proteome, transcriptome, genome or epigenome data are high throughput that is hard to interpret due to their complexity and volume. Strong analytical methods are necessary to obtain meaningful biological information like geneset/pathway enrichment analysis or pathway-topology methods (Wang et al., 2015). In this study, geneset enrichment analysis (GSEA) and pathway enrichment analysis were used for finding enriched gene ontologies and pathways in the study.

GSEA is a widely used enrichment method that determines statistically significant set of genes between conditions (Subramanian et al., 2005). In other words, it identifies overrepresented functional groups in a dataset. Genes are annotated and a ranked list composed of all of the genes without applying a threshold value is used. Different rank metric calculations can be applied (Zyla et al., 2017) or only differential expression value can be used. For each set of elements, the enrichment score value showing overrepresentation is calculated by scanning the rank list (Wang et al., 2015). Normalized enrichment scores for gene set size differences and false discovery rate (FDR) for

multiple hypothesis testing is calculated (Subramanian et al., 2005). With GSEA, enrichment of gene ontology (GO) terms can be assessed. GO provides standardized terminology and annotation of genes and gene products. It is hierarchical and composed of sets of classes and relations between them, and is composed of three domains: cellular component, molecular function, and biological process (Ashburner et al., 2000; Gene Ontology Consortium, 2021).

Pathway enrichment analysis is a powerful analytical method for biological information inference like GSEA. It identifies enriched pathways that are expected more than by chance by using genetic associations in a gene list (Reimand et al., 2019). It uses a filtered gene list with a threshold value queried against pathway databases that are holding data of pathways and their interactions, such as WikiPathways, Reactome, KEGG, NetPath, and MSigDB.

1.5. The objective of the Dissertation

Understanding molecular mechanisms and interactions involved in stress response is important and promoted by scientists, as it improves our knowledge about the physiology of the cell and contributes to a broad range of biological applications such as developing stress-tolerant crops or understanding the resistance of cancer cells to drugs (Grover, 2002). It is also important for predicting the fate of the species. *M. galloprovincialis* is an invasive species in many parts of the world outside of its native Mediterranean range. Genomic responses to environmental stress have been previously studied for M. galloprovincialis from other geographic locations (Lockwood et al., 2010; Lockwood and Somero, 2011; Fields et al., 2011; Hamer et al., 2004; Dutton and Hofmann, 2009; Hamer et al., 2008) yet no study exists on the genomic responses of populations from the Marmara Sea. The project focused on gene regulation as an adaptive response to osmostress in *M. galloprovincialis* from Bosphorus. Specifically, using the Rna-Seq approach and by exposing the Bosphorus mussels to salinity levels observed in the Aegean Sea in an experimental set-up, I tried to try to better understand the plasticity of the expression and repeatability of the plastic response for osmoregulation. By examining the genes and pathways, I tried to understand and interpret the mechanisms and interactions involved in the stress adaptation of this mussel species.

2. LITERATURE REVIEW

2.1. Gene Regulation as an Adaptive Response

Organisms show adaptive responses to changes in their environments to preserve cellular and organismal homeostasis. When the environment changes, rapid responses are given in seconds by signal transduction mechanisms, physical regulation of ion channels and transporters, post-translational mechanisms, and post-transcriptional mechanisms afterward (De Nadal et al., 2011; Lopez-Maury et al., 2008). *De novo* synthesis of proteins takes few minutes, but gene expression regulation is the major adaptive mechanism in stress response ensuring proper adaptation to stronger stress (De Nadal et al., 2011; Lopez-Maury et al., 2008). Therefore, the ability of an organism to initiate changes in gene expression corresponds to its ability to respond to environmental stress (Lockwood and Somero, 2011).

The response depends on the organism, its current physiological state, its evolutionary history as well as type and intensity of the stress (De Nadal et al., 2011; Lopez-Maury et al., 2008). For example, moderate heat stress induced genes for protein chaperones, whereas extreme heat stress induced genes for degradation of denatured proteins in the ribbed mussel, *Mytilus californianus* (Gracey et al., 2008). Even the responsiveness of a gene can change among conditions for the same individual, or under the same condition among individuals. The variability of gene expression under different environmental conditions is termed ‘expression plasticity’, whereas the variability of gene expression levels under the same conditions among individuals is termed ‘expression noise’ (Hirao et al., 2015). Expression plasticity can be affected by the evolutionary history of the organism. Interaction between expression plasticity and evolutionary history were examined in the osmoregulatory genes of *Crassostrea virginica* by Eierman and Hare (2016) and ethanol exposure of *Drosophila melanogaster* populations by Yampolsky et al. (2012), where they compared populations coming from different evolutionary histories and exposure to stress. Both studies found a significant effect of evolutionary history on the plasticity of gene expression. Variability and stochasticity of gene expression may ensure adaptation to unpredictable environmental stresses, even those not encountered before in the evolutionary history of the organism, facilitating evolvability of gene expression (Lopez-Maury et al., 2008).

Prolongation of adaptive response can impair cellular functions. When encountered with change, cells direct energy from routine cellular processes to stress response. Therefore, adaptive stress

responses need to be temporally constrained, tightly regulated, and reversible (De Nadal et al., 2011; Lopez-Maury et al., 2008). Even when the stress continues, new steady-state levels that are close to unstressed levels are reached (Lopez-Maury et al., 2008). For example, tuning of cellular processes with environmental change was seen in the ribbed mussel, *Mytilus californianus*, an inhabitant of the rocky intertidal zone. Distinct phases of physiological states were linked to phases of the tidal cycle, and cellular functions like growth, division, and repair were found to be correlated with changing conditions (Gracey et al., 2008). In addition to the fact that stress responses decrease the production of growth-related proteins, growth-related genes and stress-related genes have different regulatory characteristics. Stress-related genes have different transcriptional mechanisms, have high plasticity, and are generally characterized by TATA boxes in their promoters associated with high gene expression noise facilitating long-term evolvability of the response (Lopez-Maury et al., 2008; Zou et al., 2011). In contrast, cell proliferation or development processes can be negatively influenced by too much noise (Lopez-Maury et al., 2008).

2.2. Genetic Mechanisms of Adaptation to Stress

Salinity is one of the most important factors besides temperature that affects physiology, cellular homeostasis, development, abundance, distribution, feeding, reproduction, growth, respiration, and interspecific interactions of *M. galloprovincialis* (Gosling, 2004; Freitas et al., 2017; Pourmozaffar et al., 2019; Zhang *et al.* 2012b). *M. galloprovincialis* adapt to changing salinities with behavioral and molecular responses. All of the processes occur by the expression of genes that are triggered through signaling pathways to ensure organismal homeostasis (De Nadal et al., 2011). While some of these changes in gene expression occur in response to salinity stress only, others respond with changes to any kind of stress an organism might encounter. In addition to osmotic alterations, salinity change can alter organisms' metabolism, energy reserves, oxidative status (Hu et al., 2015; Freitas et al., 2017), anabolic and catabolic processes, DNA damage and repair response (cellular damage), among others that related with degree and time of exposure to the stress. If irreparable damage occurs apoptosis can also be triggered (Sun and Zhou, 2017).

2.2.1. Energy Metabolism

Energy metabolism is important for organismal homeostasis in determining the ability to cope with changing conditions. Balance is established between ATP generation, ATP utilization, and potential ATP sources, such as nutrient intake and energy reserves. In any circumstance, with changing conditions, this balance is regulated accordingly. For example, researchers found that the

amount of energy allocated to immune defense is adjusted based on energy reserves and food availability (Houston et al, 2007). Another example is metabolic rate depression in marine invertebrates to preserve energy reserves under unfavorable conditions. By suppressing basal metabolic rate, energy expenditure decreases, expanding the use of fuel reserves for the long term. Another example is modified fuel catabolism pathways to increase ATP production efficiency in organisms that frequently experience changing oxygen levels, such as in bivalves (Storey, 2004).

Under stress, various energy-demanding mechanisms are activated to tolerate damage and ensure homeostasis. These mechanisms for response and restoration of the normal state are energy-consuming, such as immune response against pathogens, regulation of ATP-driven ion pumps for osmoregulation, synthesizing molecular chaperones for denaturing proteins, and repair of DNA damage and antioxidant mechanisms for maintaining redox balance. In turn, alterations in energy metabolism cause alteration in the oxidative status of the cells as mitochondria is a source of reactive oxygen (ROS) and reactive nitrogen species (RNS) (Rivera-Ingraham and Lignot, 2017).

Many authors investigated energy metabolism alterations in response to stress. To assess the glycolytic rate, pyruvate kinase (PK, EC:2.7.1.40) that is involved in the last step of glycolysis was examined as pyruvate is at the heart of energy metabolism (Anestis et al., 2007). Anestis et al. (2007) also found a decrease in PK in *M. galloprovincialis*, when exposed to long-term temperature stress, where chronic stress resulted in metabolic depression and a shift to anaerobic metabolism. Normally switching to anaerobic metabolism causes increases in the glycolytic rate to compensate for the free ATP deficit (Halliwell and Gutteridge, 2015; Seagroves et al., 2001); O_2 consumption and glycolytic rate have an inverse relation called the Pasteur effect (Hochachka, 1986). As metabolic rate is suppressed (metabolic rate depression), a reversed-Pasteur effect is seen with unchanged (or reduced) glycolytic flux (Hochachka, 1986). Facultative anaerobes such as *M. galloprovincialis* do not exhibit the Pasteur effect (Storey and Storey, 1990).

Acidification was also found to alter energy metabolism in the Pacific oyster, *Crassostrea gigas* (Cao et al. 2018) and the Yesso scallop, *Patinopecten yessoensis* (Liao et al., 2019) by stimulating anaerobic metabolism. Metabolic rate depression was found to be activated by acidification, decreasing energy expenditure (higher lipid, glycogen, and protein content was observed) (Freitas et al., 2017; Fernández-Reiriz et al., 2011).

Osmoregulation and energy metabolism are also tightly connected. Osmoregulation is a costly process (Rivera-Ingraham and Lignot, 2017) and the cost of osmoregulation in terms of energy

consumed is reflected in metabolism and respiration (Rivera-Ingraham and Lignot, 2017). Moreover, the cost of osmoregulation affects growth rates and other cellular processes in terms of the energy budget. It was found that energy expenditure of *Mytilus edulis* mussels at low and high salinities was different, low salinity being less energy-favorable (Freitas et al., 2017), and also culminating in lower growth rates (Riisgård et al., 2013; Tedengren and Kautsky, 1987). For example, Baltic Sea mussels at 6.5 PSU are dwarfed compared to the North Sea mussels at 28.8 PSU (Tedengren and Kautsky, 1987; Sanders et al., 2018; Riisgård et al., 2013). With decreasing salinities, the growth rate also tends to decrease (Riisgård et al., 2012 in Riisgård et al., 2013). When additional stress was applied such as diesel oil, stress was often exacerbated by salinity reductions and balanced by increased salinity (Tedengren and Kautsky, 1987). Also, filtration rate was higher in Baltic Sea mussels than in North Sea mussels (Gilek et al., 2001 in Riisgård et al., 2013). However, when mussels from the Baltic and North Seas are transplanted, transplanted mussels have growth rates that were comparable to native mussels, but with North Sea mussels having high mortality rates (Kautsky et al., 1990 in Riisgård et al., 2013). Mortality was related to specific enzyme loci, where North Sea mussels that had the Baltic Sea genotype survived (Johannesson et al., 1990 in Riisgård et al., 2013).

Freitas et al. (2017) examined the effect of chronic salinity increase and decrease on the energy metabolism of *M. galloprovincialis*. A salinity increase (from 28‰ to 35‰) caused lower metabolic activity due to lower energetic expenditure. The inverse was seen with a salinity decrease (to 14‰ from 28‰). Probably due to high metabolic activity at low salinities, ROS increase caused lipid peroxidation, although antioxidant enzymes also increased. These findings indicate that low salinity has a less favorable energy metabolism due to amino acid metabolism and nitrogen excretion, causing *M. edulis* mussels of lower salinities to have a lower growth rate, agreed with Riisgård et al. (2013) and Tedengren and Kautsky (1987). Sanders et al. (2018) attributed reduced growth rates at low salinities to high calcification costs rather than metabolic maintenance costs (due to unfavorable protein metabolism and physiological costs) as oxygen consumption rates were not impacted by salinity. On the other hand, Hamer et al. (2008) found increased oxygen consumption rates with lowered salinities.

Carbohydrates, lipids, and proteins are used as metabolic fuels in energy metabolism (Storey and Storey, 1990), whose regulation is crucial for energy homeostasis. Excess energy that is not converted to ATP is stored as energy reserves. In some animals, excess carbohydrates are converted to fatty acids for long-term energy storage, as carbohydrates have a high affinity to water. In *M. edulis* two types of energy reserves were identified (Kellner et al., 2002). The first type is adipogranular cells (ADG cells) that exist in mantle tissue and mainly contain lipid droplets (and minute quantities of

proteinic granules and glycogen particles). The second type is the glycogen-specific vesicular connective tissue cells (VCT cells) that exist in the mantle and labial palps. Of the two, glycogen is the main energy reserve in Mytilidae (Kellner et al., 2002).

The mobilization of these reserves is determined by the circulating glucose and by energy sensors like Axin, AMPK, and sirtuin (SIRT). These sensors detect low energy status and activate catabolic pathways of lipid and glucose (Cao et al., 2018). When glucose levels are high inside the cell, glycogenesis enhances, keeping the osmotic pressure stable. Glucose is stored as energy reserves through glycogenesis or it can be used to supply ATP through glycolysis. On the contrary, when glucose levels are low -like in fasting conditions- glycogenesis is inhibited, and lipolysis, gluconeogenesis, and glycogenolysis are promoted, to supply glucose for use in ATP generation. Glucagon and insulin are two hormones that act oppositely to regulate these processes.

Glucagon is released to promote gluconeogenesis and glycogenolysis when the available circulating glucose levels are low. Triglycerides in lipid droplets and glycogen energy reserves are mobilized to supply energy. Glucagon signals the G protein-coupled receptor (GPCR) cascade, which activates PKA (Protein kinase A, cAMP-dependent protein kinase, EC:2.7.11.11). Activated PKA phosphorylates proteins and directs them to supply glucose.

One enzyme PKA phosphorylates is the regulatory enzyme, fructose bisphosphatase-2 (FBPase-2) of fructose bisphosphatase-2 (FBPase-2)/Phosphofructokinase-2 (PFK-2, EC: 2.7.1.105) bifunctional enzyme. FBPase-2 dephosphorylates fructose 2,6-bisphosphate to produce fructose 6-phosphate, also activating fructose 1,6-bisphosphatase (FBPase-1, EC:3.1.3.11) to further produce glucose by gluconeogenesis. FBPase-1 is involved only in gluconeogenesis and not in glycolysis. Other enzymes that are part of gluconeogenesis, but not of glycolysis, are pyruvate carboxylase (PC, EC:6.4.1.1) and phosphoenolpyruvate carboxykinase (PEPCK, EC: 4.1.1.49).

Another enzyme that is phosphorylated by PKA is phosphorylase kinase (EC: 2.7.11.19) activating glycogenolysis. Glycogen branches are cleaved and converted to glucose 1-phosphate by glycogen phosphorylase (EC: 2.4.1.1) and then converted to glucose-6-phosphate by phosphoglucomutase. Glucose-6-phosphate is then converted to glucose (Venugopal and Jialal, 2020).

PKA also phosphorylates hormone-sensitive lipase (HSL) and adipose triglyceride lipase (ATGL) that breaks down triglyceride to glycerol and fatty acids (Marvyn et al., 2015; Pagnon et al.,

2012; Han et al ., 2019). The degradation of triglycerides to glycerol and fatty acids is called lipolysis. At the same time, fatty acid synthesis is prevented by inhibiting acetyl-CoA carboxylase (EC:6.4.1.2). Generated fatty acids can be oxidized by beta-oxidation in mitochondria or peroxisomes to produce acetyl-CoA to be used in the TCA cycle, and NADH and $FADH_2$ to be used in oxidative phosphorylation. Acyl-CoA dehydrogenase (ACADL), enoyl-CoA hydratase, 3-hydroxyacyl CoA dehydrogenase, acetyl-CoA C-acyltransferase (EC: 2.3.1.9), and mitochondrial trifunctional protein are involved in the beta-oxidation process (Houten and Wanders, 2010; Rismani-Yazdi et al., 2011). Generated glycerol is phosphorylated into glycerol 3-phosphate (glycerophosphate) by glycerol kinase (EC:2.7.1.30), and then further oxidized into dihydroxyacetone phosphate (DHAP, dihydroxyacetone) by glycerol 3-phosphate dehydrogenase (glycerophosphate dehydrogenase) to advance glycolysis or glucogenesis.

When the available circulating glucose level is high, insulin is released. The increase in insulin promotes glycolysis. Insulin activates protein phosphatases that dephosphorylate regulatory enzyme FBPase-2 of FBPase-2/PFK-2 bifunctional enzyme activating PFK-2. PFK-2 converts fructose 6-phosphate to fructose 2,6-biphosphate that binds to phosphofructokinase-1 (PFK1, EC:2.7.1.11). Fructose 6-phosphate is converted to fructose 1,6-biphosphate leading to glycolysis. When the available glucose level is high, glycogenesis is also activated converting glucose into glycogen. The key enzyme of glycogenesis is glycogen synthase (UDP-glucose-glycogen glucosyltransferase, EC: 2.4.1.11). The mobilization of fats is also decreased and fatty acid synthesis is increased with high glucose levels (Behari, 2011). Acetyl-CoA carboxylase (EC:6.4.1.2), fatty acid synthase (Behari, 2011), and adipose lipoprotein lipase are also upregulated with high glucose levels (Spooner et al., 1979).

In the genus *Mytilus*, the insulin-like hormone was found to increase glycogen storage, and metabolic neurohormone was found to increase storage of lipids, glycogen, and protein (Willmer et al., 2005). Glucagon-like peptides were identified in *M. edulis*, however, the involvement of glucagon-like peptides in hyperglycemia is not clear (Kellner et al., 2002). In mollusks, the central nervous system originated factor was found to be involved in glycogen mobilization, however, a clear relationship has not been identified (Kellner et al., 2002).

2.2.2. Hypoxia

Oxygen concentration is tightly controlled as oxygen can be reduced by leaked electrons from oxidative phosphorylation (Goda and Kanai, 2012). Under normal conditions, oxygen delivery is

controlled by the oxygen demand of the cells that is determined by metabolic rate (Bakker, 1997). Hypoxia occurs when environmental oxygen concentrations drop abnormally so that cells cannot compensate O_2 demand for mitochondrial ATP production. Hypoxia also occurs when enough oxygen cannot be carried to tissues due to the failure of oxygen-carrying systems. For sufficient oxygen delivery to tissues, regulatory mechanisms have evolved, such as cardiovasculatory, respiratory, and neuroendocrine systems in humans (Halliwell and Gutteridge, 2015).

Normally under aerobic conditions, pyruvate generated from glycolysis is oxidized to acetyl-CoA and enters into the tricarboxylic acid cycle (TCA cycle) for further production of molecules (NADH and $FADH_2$) used in oxidative phosphorylation. In oxidative phosphorylation, electrons from NADH and $FADH_2$ are transferred to O_2 by the electron transfer chain to produce ATP. 36-38 ATP molecules are generated from the oxidization of a glucose molecule.

Under hypoxia, ATP is directed to essential processes, like maintaining homeostasis rather than RNA and protein synthesis (Halliwell and Gutteridge, 2015). The most prominent adaptation to hypoxia is the metabolic adjustment, which decreases oxidative phosphorylation and increases anaerobic glycolysis (Halliwell and Gutteridge, 2015; Seagroves et al., 2001). In anaerobic glycolysis, pyruvate is converted to lactate by lactate dehydrogenase (LDH) and 2 mol ATP/mol is generated. Due to differences in the amount of ATP generated between aerobic and anaerobic pathways, decrease in oxidative phosphorylation and increase in anaerobic glycolysis cause more glucose intake and increased activity of glycolytic pathway to compensate for the free ATP deficit (Halliwell and Gutteridge, 2015; Seagroves et al., 2001). Therefore, enzymes in the glycolytic pathway (e.g., hexokinase (HK1, HK2), glyceraldehyde-3-p dehydrogenase, aldolase A and C, lactate dehydrogenase A, phosphoglycerate kinase-1(PGK1), pyruvate kinase M), and glucose transporter genes 1 and 3 (GLUT1, GLUT3) increase (Madhavan, 2006) under the control of hypoxia-inducible factor (HIF). Cells lacking hypoxia-inducible factor 1 (HIF-1) decrease in glycolytic capacity, and exhibit low levels of ATP and lactate production, and decreased acidosis (Seagroves et al., 2001).

HIF sense molecular oxygen, and plays a regulatory role in adaptation to low oxygen levels. It also acts as a metabolic switch, coordinating the switching from oxidative phosphorylation to anaerobic glycolysis (Goda and Kanai, 2012; Seagroves et al., 2001), regulates carbohydrate energy metabolism (Halliwell and Gutteridge, 2015) and lipid metabolism, and is involved in the conversion of pyruvate to acetyl-CoA (Goda and Kanai, 2012). Evolutionarily conserved suppression of lipid utilization by HIF pathway is found in *Caenorhabditis elegans* and mammalian adipocytes during hypoxia. Under normal conditions during fasting, lipolysis is increased for ATP production from

lipids. Under hypoxia, the HIF pathway downregulates fasting-induced lipolysis by suppressing PKA and ATGL proteins. The benefit of suppression of lipid utilization is the conservation of energy reserves (Han et al., 2019).

HIF also regulates inducible nitric oxide synthase and heme-oxygenase (Madhavan, 2006), promotes key mediator vascular endothelial growth factor (VEGF) for angiogenesis (Carmeliet, 2005), erythropoietin (EPO) for erythropoiesis (Haase, 2013), and proteins involved in iron delivery (Halliwell and Gutteridge, 2015). When low oxygen levels are persistent, these mechanisms ensure high oxygen delivery to cells by increasing the oxygen-carrying capacity of the blood by uptake and binding capacity of iron (Haase, 2013). However, bivalves have open circulatory systems where hemolymph directly flows through tissues (Gosling, 2008, pp. 35). Also there is no respiratory pigment, and the oxygen concentration of the hemolymph is close to the oxygen concentration of the seawater (Bayne et al., 1976 in Gosling, 2008, pp. 36). Hypoxia-inducible factor (HIF-1, HIF-1-Alpha) and its regulatory hydroxylase, the prolyl hydroxylase domain enzyme (HIF-P4H, PHD) were identified in *M. galloprovincialis* (Giannetto et al., 2015). They were especially abundant in gills and share features with orthologues pointing to conserved oxygen sensing pathways (Giannetto et al., 2015). An ortholog of the EPO receptor (EPOR) has been reported in *M. edulis* (Gerber et al., 2007 in Litwack, 2017) and VEGF has been reported in *C. gigas* (Ivanina et al., 2018).

M. galloprovincialis belongs to the family Mytilidae that includes euryoxic and facultative anaerobes (De Zwaan and Mathieu,1992), but tends to use oxygen when available (Gosling, 2003). Bivalves that inhabit intertidal and shallow waters are exposed to air with tides, making them very tolerant to anoxic conditions. Besides tides, dissolved oxygen levels can change due to other factors like eutrophication, and changes in salinity and/or temperature. Because of fluctuations in environmental O_2 concentrations, bivalves evolved adaptations to tolerate anoxic conditions. They have self-sufficient tissues with large glycogen reserves, fermentable amino acids (aspartate, asparagine, glutamate, glutamine) and lipids (Meng et al., 2018), minimized toxicity of end products (succinate, opines, ethanol, acetate, propionate, and malate), the capability of metabolic rate depression and modified fuel catabolism pathways addition to glycolysis (Storey, 2004). In marine invertebrates, mainly bivalves, integration of anaerobic catabolism of glycogen and aspartate is the initial response (Figure 2.1A). Aspartate is catabolized to succinate as a part of the reverse TCA cycle. As input, glycogen and aspartate decrease, and end-products, alanine and succinate increase. For example, it was found that during four days of anoxia of the clam *Mercenaria mercenaria*, glycogen and aspartate were used as substrate, and succinate and alanine were produced as end-products in the gill tissue (Korycan and Storey, 1983 cited in Storey, 2004).

Also, bivalves regulate anaerobic energy metabolism to increase anaerobic glycolysis ATP yield by coupling it with additional phosphorylation reactions catalyzed with phosphoenolpyruvate carboxykinase (PEPCK) (Meng et al., 2018; Storey and Storey, 1990). If anoxia prolonges and aspartate decreases, direct fermentation of glucose to succinate (Figure 2.1B) is performed yielding 4 mol ATP/mol glucose. In one study (Meng et al., 2018), an increase in ATP yield was assessed by coupling anaerobic energy metabolism with additional phosphorylation reactions catalyzed with PEPCK. Rather than continuing to form pyruvate with pyruvate kinase (PK), as in a normal glycolytic pathway, phosphoenolpyruvate (PEP) was directed to form oxaloacetate with PEPCK (Figure 2.1B) and later to produce succinate. If it is further catabolized to propionate, 6 mol ATP/mol glucose is produced in total. Normally in humans and other animals, PEPCK is the control point of gluconeogenesis, reconverting pyruvate to PEP together with pyruvate carboxylase, which is the opposite reaction of invertebrates under anoxia (PEPCK oppositely converts PEP to oxaloacetate, Fig 3.1B)

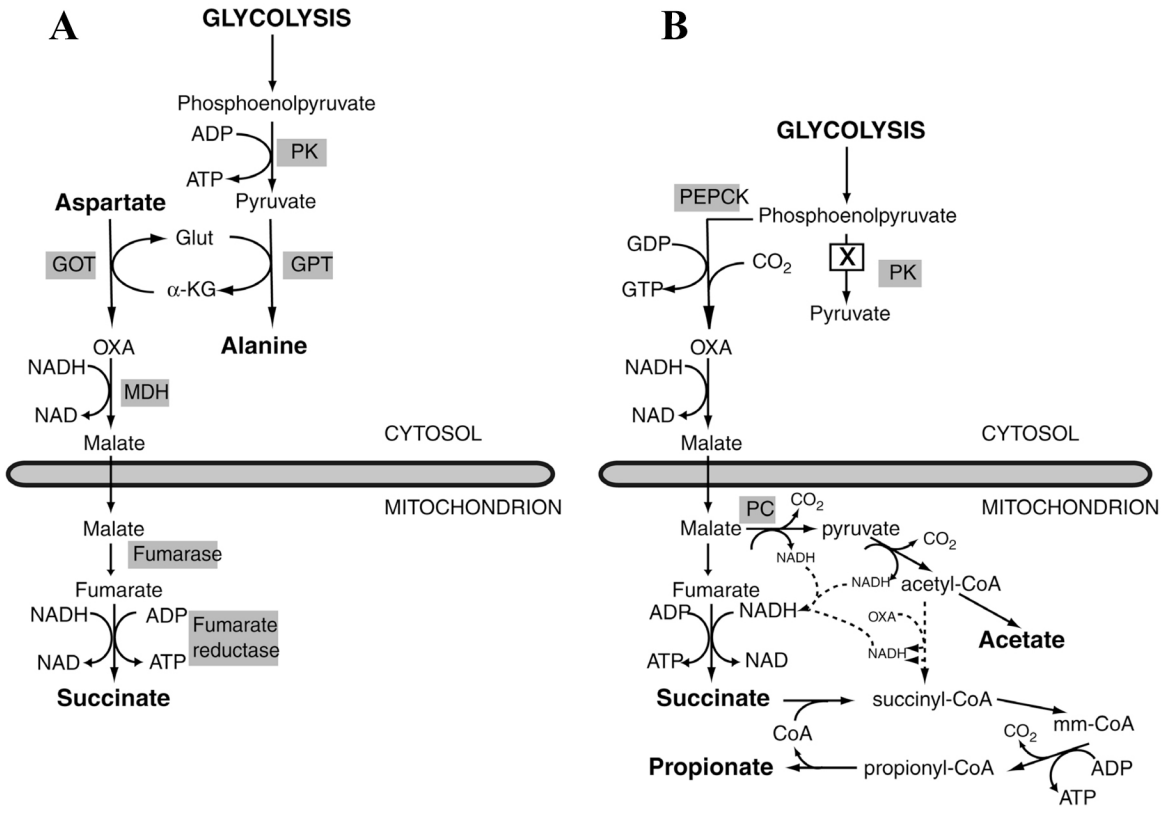


Figure 2.1. Anaerobic metabolism in marine mollusks. A) Anaerobic catabolism of glycogen and aspartate. B) Direct fermentation of glucose to succinate (Storey, 2004).

2.2.3. Lipid Peroxidation

Lipids are used as energy storage and fuels in energy metabolism. They are also the main component of the cell membrane which separates intracellular and extracellular space, keeping molecules at the right concentrations inside and outside. The membrane lipid composition determines membrane integrity and is very important for cell survival. Changes in lipid composition and membrane fluidity cause destabilization of the membrane and can result in ion leakage. Moreover, alteration of it can result in many diseases (Choi et al., 2016).

Lipid peroxidation involves oxidative degradation of lipids, especially polyunsaturated fatty acids (PUFA) (Ayala et al., 2014) which are mainly localized in membranes (Aslan and Aslan, 2017). Oxidants attack PUFA by targeting carbon to carbon double bonds, resulting in lipid radicals. Lipid radicals further generate lipid peroxyl radicals with O_2. These can further react with fatty acids and form fatty acid radicals and lipid peroxides (Rivera-Ingraham and Lignot, 2017). Malondialdehyde (MDA) and 4-hydroxynonenal (HNE) are lipid peroxidation products used in studies as markers (Tsikas, 2017). Antioxidants, glutathione peroxidase (GPx), and Glutathione s-transferases (GST) are involved in the reduction of lipid hydroperoxides with reduced glutathione (GSH), and protect lipids from peroxidation (Halliwell and Gutteridge, 2015; Kisic et al., 2012). GST is also involved in the conversion of leukotriene A4 to leukotriene C4 (Agarwal et al., 1992).

Injury caused by free radicals alters ion concentrations, especially in the form of an increase in intracellular calcium levels (Borza et al., 2013). Under normal conditions, intracellular and extracellular levels of calcium are tightly regulated, as it acts like a second messenger (Tsunoda and Owyang, 1993) and takes part in many cellular processes (Modica et al., 2019). High concentrations of calcium cause loss of membrane integrity, can form phosphate precipitates, protein and nucleic acid aggregates (Roch and Sherwood, 2011). Lipid peroxidation can also occur enzymatically which results in calcium increase and signaling lipid generation. Enzymes like phospholipases, lipid kinases, or phosphatases generate signaling lipids. Examples of some signaling lipids are phosphatidic acid (PA) (Hou et al., 2016), its metabolite key signaling molecule lysophosphatidic acid, phosphoinositides (PIs), sphingolipids, lysophospholipids, oxylipins, N-acylethanolamines, free fatty acids (FFAs), among others (Wang & Chapman 2013 cited in Hou et al., 2016).

Phospholipases are the key enzymes that catalyze the hydrolysis of phospholipids at specific ester bonds into fatty acids including arachidonic acid. They are involved in membrane remodeling and maintenance, altering cell membrane permeability and ion channels activity (Ortiz et al., 2017;

Nelson et al., 2011). They cause the generation of lipid mediators and are involved signal transduction of many cellular processes (Richmond and Smith, 2011) such as apoptosis, proliferation (Bamji-Mirza and Yao, n.d.), and stress response (Hou et al., 2016). Based on the ester bond that is cleaved, they are divided into four major groups: A, B, C, and D and further divided into subgroups (Bamji-Mirza and Yao, n.d.)

The main enzymes that generate signaling lipids are lipoxygenase and cyclooxygenase of arachidonic acid metabolism (Ayala et al., 2014). Arachidonic acid is mobilized by phospholipase A_2 (PLA_2) or phospholipase C (PLC) from membrane phospholipids which both can cause calcium increase (Ting and Khasawneh, 2010). PLC is involved in membrane phospholipid, phosphatidylinositol 4,5-bisphosphate (PIP2) metabolism in a calcium-dependent manner that mediates the production of diacylglycerol (DAG) and inositol 1,4,5-trisphosphate (IP_3) (Haas and Stanley, 2007). DAG and IP_3 are second messenger signaling molecules that activate protein kinase C (PKC) and cause calcium increase due to release from the endoplasmic reticulum. PLA_2 hydrolyzes phospholipids into fatty acids including arachidonic acid, which is the rate-limiting step in eicosanoid generation, is very important for cell membrane homeostasis, and is involved in lipid peroxidation. Its expression is triggered by the influx of calcium to the cell (Ortiz et al., 2017). Arachidonic acid generated by hydrolysis of phospholipids can be metabolized by cyclooxygenase (COX, prostaglandin G/H synthase), lipoxygenase (LOX), cytochrome p450 (CYP4A11, CYP4A22 (Pikuleva and Waterman, 2013), CYP4F2, CYP4F3 (Costea et al., 2010)), and anandamide pathways (Hanna and Hafez, 2018) and further form bioactive eicosanoids, including prostaglandins, thromboxanes, prostacyclins, and leukotrienes (Yui et al., 2015). While arachidonic acid is oxidized, ROS can be generated (Kim et al., 2008a).

2.2.4. Oxidative Stress

Oxidative stress arises when antioxidant enzyme capacity is not sufficient to transform free radicals and their byproducts into nontoxic molecules. It has adverse effects on cell functions, causing lipid peroxidation, protein degradation, and DNA damage. In marine bivalves, oxidative stress can be caused by many stressors like salinity stress (Hu et al., 2015; Freitas et al., 2017), heat and cold stress (Wang et al., 2018a), hypoxia (Almeida et al., 2005), metal contamination (Pytharopoulou et al., 2011; Vlahogianni and Valavanidis, 2007), and genotoxicity (Gravato et al., 2005), among others.

Antioxidant enzymes protect cells from oxidative damage of free radicals; ROS and RNS. ROS are produced by peroxisomes, ER, and mitochondria. Most importantly they are produced under

normal aerobic metabolism as byproducts due to electron leakage in the electron transfer chain and are increased under stress conditions. ROS can also be beneficial, for instance an increase of ROS after pathogen recognition (Torres et al., 2006) improves defense against pathogens (Song et al., 2010). But when excessive, it causes impairment in cell functions that can lead to apoptosis. Examples of ROS include superoxide, singlet oxygen, peroxides, hydroxyl radical, and alpha-oxygen (Di Meo et al., 2016). RNS is also a by-product of mitochondrial activity (Rivera-Ingraham and Lignot, 2017). Examples of RNS are nitric oxide and peroxynitrite (Di Meo et al., 2016). Nitric oxide synthases (NOSs) or oxidases like NADPH oxidase and xanthine oxidase can also result in ROS and RNS production (Kim et al., 2008a). In the Korean mussel *Mytilus coruscus*, it was found that gills have the highest oxidative load, and antioxidants are expressed highest, mostly at gills (Wu et al., 2017). The most known antioxidant enzymes found in bivalves are superoxide dismutase (SOD), catalases (CAT), glutathione reductase (GR), Glutathione s-transferases (GST), glutathione peroxidase (GPx), peroxiredoxin (PRDX), and metallothioneins (MT). Thioredoxin peroxidase (TPx) (Rocher et al., 2015), thioredoxin reductase (TR, a major antioxidant), and malondialdehyde (MDA, lipid marker of oxidative stress) are also used as oxidative damage markers in bivalves (Box et al., 2009).

The main source of superoxide is oxidative phosphorylation in the mitochondrial electron transport chain (Halliwell and Gutteridge, 2015). Superoxide and hydrogen peroxide (H_2O_2) can form more reactive hydroxyl radicals. Superoxide dismutase (SOD) efficiently dismutases superoxide to H_2O_2 and oxygen. It is classified according to the metal content it contains, such as manganese SOD (MnSOD), copper/zinc SOD (Cu/ZnSOD), iron SOD (FeSOD), and nickel SOD (NiSOD). Bivalves have only manganese SOD (MnSOD) and copper/zinc SOD (Cu/ZnSOD) (Song et al., 2010). SODs have been involved in response to many stressors, such as pH decrease in Yesso Scallop *Patinopecten yessoensis* (Liao et al., 2019), copper contamination in bivalve mollusk *Scapharca inaequivalvis* (CuZnSOD increase, MnSOD not changed) (Isani et al., 2002), invasive alga *Lophocladia lallemandii* colonization of *Pinna nobilis* (Box et al., 2009), organic pollutants in *M. galloprovincialis* (Fernández et al., 2010), heavy metal pollution in *M. galloprovincialis* (Vlahogianni et al., 2007), temperature stress in *C. gigas*, *M. galloprovincialis*, and *Katelysia rhytiphora* (Rahman et al., 2018), and also in defense response against pathogens in *M. galloprovincialis* (Wang et al., 2013) and *Chlamys farreri* (Xing et al. 2008). It was also found that SOD expression changed with tolerance to stress (Rahman et al., 2018) upon tissues (Song et al., 2010; Box et al., 2009)) and isoforms (Isani et al., 2002).

H_2O_2 is disintegrated by peroxidases and catalases (CATs) to oxygen and water. CATs have a high turnover number and thermal stability (Tehrani et al., 2018). Proteins with catalase activities have also been reported in bivalves (Song et al., 2010). CATs activity is found to increase with metal

exposure (cadmium, lead, and copper) in the brown mussel *Perna perna*, moreover, induction was concentration/mixture dependent (Boudjema et al., 2014). Like SOD, CATs increased in Yesso Scallop *Patinopecten yessoensis* with pH decrease (Liao et al., 2019), with organic pollutants and physiological activity in *M. galloprovincialis* (Fernández et al., 2010). On the other hand, Isani et al. (2002) found a decrease in CATs where CuZnSOD activity was increased with copper contamination. In the colonization of *Pinna nobilis* with the invasive algae *Lophocladia lallemandii*, CATs were increased in the digestive gland, but not in the gills (Box et al., 2009) indicating involvement with higher oxidation states.

Another antioxidant is glutathione. It is found in reduced (GSH) and oxidized (GSSG) forms. GSH neutralizes ROS species. Glutathione peroxidase (GPx) removes H_2O_2 by oxidizing GSH. It may also be involved in immune defense against pathogens (Song et al., 2010). Glutathione reductase (GR) produces GSH with NADPH from GSSG. Glutathione s-transferases (GST) catalyzes the conjugation of reduced glutathione (GSH) with electrophilic substrates (Croom, 2012). GST is upregulated in response to oxidative stress, and protects the cell from xenobiotics and lipid peroxidation (Halliwell and Gutteridge, 2015). GST may also function as transport proteins for low solubility compounds in water by binding to them (Orhan and Şahin, 1995). GST is also used in environmental assessment as a biomarker (Song et al., 2010; Vidal-Liñán et al., 2014). In the study of Fernández et al. (2010), GR, GPs, and GST were found to be activated with high levels of metal contamination (Hg, Pb, and Cd), unlike SOD and CAT activation with organic pollutants. GPx and GST activities were increased in the study of Box et al. (2009) of algae colonization of *Pinna nobilis*, mentioned above.

Other antioxidants, such as peroxiredoxin (PRDX) and metallothioneins (MT) scavenge ROS. Metallothioneins protect the cell from oxidative stress and are important for copper and zinc homeostasis. They are also involved in cell differentiation and proliferation, along with the p63 gene (Brandão et al., 2018). MT, glutathione, GPx, SOD, and CAT levels increase with exposure to H_2O_2 (Cavaletto et al., 2002).

An important point is related to antioxidant enzyme efficiencies in scavenging ROS relying on a supply of NADPH (Singh et al., 2007). Glucose has two pathways; first, glycolysis mainly for the production of pyruvate and ATP, and second, pentose-phosphate pathway (PPP) for the production of precursors for nucleotides and NADPH. It is found that in humans and mice, P53 gene can regulate oxidative homeostasis by directing glucose 6-phosphate (G6P) to PPP for NADPH generation (Napoli and Flores, 2017). In aerobic respiration, an adequate supply of NADPH is necessary for enhancing

a reducing environment for the inactivation of ROS species (Singh et al., 2007). NADPH is also involved in generating reduced glutathione (GSH) used in detoxifying peroxides. For example, during an oxidative challenge in *Pseudomonas fluorescens*, the concentration of NADPH and activity and expression of its generators malic enzyme (malate dehydrogenase, MDH), glucose-6-phosphate dehydrogenase (G6PD), and $NADP^+$-isocitrate dehydrogenase are increased. G6PD is the rate-limiting enzyme of PPP and is therefore important in antioxidant homeostasis (Almeida et al., 2005). TCA cycle enzymes that generate NADH for oxidative phosphorylation are downregulated on the other hand (Singh et al., 2007).

Besides these, uncoupling proteins (UCPs) also protect from oxidative stress by decreasing ROS generation in the electron transport chain. Electron flow generates proton flow from matrix to intermembrane, generating mitochondrial membrane potential. This membrane potential is used to convert ADP to ATP. In neurons that have high mitochondrial ATP synthesis, consumption, and turnover, leakage of protons back to the matrix by UCPs (UCP4 and UCP5) decreases ROS formation with little impact on membrane potential and ATP generation, in a process referred to as 'mild uncoupling' (Ramsden et al., 2012).

2.2.5. Immune Response

Mussels are used as pollution sentinels as they have widespread distributions globally and are filter-feeders (Figueras et al., 2019). They continuously filter high volumes of water, the average being 7.5 lt/hr per mussel (Figueras et al., 2019). Waters they filter contain microorganisms and pathogens, and moreover it was found that the number of bacteria (Vibrio spp.) found inside the mussels was higher than the surrounding water (Stabili et al., 2005) probably due to filtering. Although they are exposed to high levels of pathogens, they are much less susceptible to infectious outbreaks and mass mortality compared to other bivalves like oysters and clams (Gerdol and Venier, 2015; Venier et al., 2011; Figueras et al., 2019).

Susceptibility to pathological invasions increases with stress, e.g. environmental change. *M. galloprovincialis* has evolved a highly complex immune system as they are constantly exposed to microorganisms and changing environments (Gerdol and Venier, 2015). Bivalves, including mussels, do not have adaptive immunity but have innate immunity that is not pathogen-specific, and this immunity also lacks memory and rather depends on recognizing and inactivating non-self molecules from their common and chemical properties. Without adaptive immunity, vaccination is not possible for controlling infectious outbreaks in mussels, and the approach is also not feasible in the open sea

they reside in. However, even though they do not have immune memory, they might have a kind of short-term memory. For instance, it was found that oyster larvae have better protection against herpesvirus 1 (OsHV-1) if their parents are treated with immunostimulants (Green et al., 2016). Also, although they do not have adaptive immunity, variability and abundance of involved genes enhance pathogen specificity (Figueras et al., 2019). Mussel genome has high heterozygosity, is highly polymorphic, has high repetitive sequences, and has high interspecific diversity (Figueras et al., 2019). Mussel transcriptome is also highly variable between individuals (Figueras et al., 2019, Rey-Campos et al., 2019). The abundance and variability of immune receptors elicit pathogen specificity and immune priming (Allam and Raftos, 2015), and together with effector variability and abundance may result in the advancement of successful immunity (Figueras et al., 2019).

First-line defense in the mussel defense system is enhanced by mucus release in the external epithelium (Figueras et al., 2019). Next, immunocompetent cells, primarily hemocytes found in the hemolymph and tissues of invertebrates, are involved in recognizing and inactivating invading pathogens. Recognition is undertaken by common properties of molecules of pathogens. Examples include recognition of double-stranded RNA molecules of viruses or pathogen-associated molecular patterns (PAMPs) such as molecular motifs (e.g. LPS or peptidoglycan (PGN)) by pathogen recognition receptors (PRR). Afterward, signal transduction pathways activate immune processes like complement system, phagocytosis, prophenoloxidase system, apoptosis, inflammation, lysozyme activation by inflammatory and effector molecules such as hydrolytic enzymes, proteolytic cascades, adhesion molecules, chemokines, cytokines, and antimicrobial peptides (AMP). The signaling pathways most involved in the immune response are MAPK (Mitogen-activated protein kinase, MAPKs EC:2.7.11.24) and NF-κB (Nuclear Factor kappa B). NF-κB is a transcription factor that is involved in pro-inflammatory gene expressions like cytokines, chemokines, and adhesion molecules (Lawrence, 2009; Song et al., 2010) produced in response to stimuli like stress and free radicals. At resting state NF-κB and IKB (Inhibitor of KB, I Kappa B) are bound in an inactive state (Song et al., 2010). When activated, IKK (I Kappa B kinase) catalyzes the degradation of IKB, and NF-κB is released for transcription (Song et al., 2010). Similarly, the MAPK pathway can be stimulated by stress, cytokines, hormones and bacteria, and participate in many processes including cell differentiation, proliferation, death, and immune function (Song et al., 2010). The signal is regulated by kinases (ERKs), c-Jun amino-terminal kinases (JNKs), and p38 MAPKs that activate each other by phosphorylation (Song et al., 2010).

2.2.5.1. Pathogen recognition receptors (PRRs) and their related pathways. There are four main receptor families; CLRs (C-type lectins), TLRs (Toll-like receptors), NLRs (NOD-like (nucleotide-

binding and oligomerization domain) receptors), and RLRs (RIG-like (retinoic acid-inducible gene 1) receptors). Lectins and TLRs are membrane-bound PRRs, and NLRs and RLRs families are intracellular cytosolic PRRs.

Specifically, NLRs recognize the peptidoglycan and flagellin of bacteria. Although they are important receptors in the innate immune system, NLRs are not as conserved as RLRs and TLRs throughout the animal kingdom (Philipp et al., 2012). NLRs are composed of C-terminal leucine-rich repeat (LRR) recognition domain, central NATCH domain and N-terminal effector binding domain (DEATH, Pyrin domain (PYD), baculovirus inhibitor of apoptosis protein repeat (BIR) or caspase recruitment domain (CARD)) (Song et al., 2010; Gerdol and Venier, 2015). NLRs are involved in the activation of proinflammatory NF-κB pathway or proinflammatory caspases (Song et al., 2010). In mammals, they are involved in inflammasome complex formation, but inflammasomes are not encountered in invertebrates (Latz et al., 2013 cited in Gerdol and Venier, 2015). Also, NLRs have not been identified in bivalves although metazoans have a high diversity of NACHT domain-containing proteins (Gerdol and Venier, 2015). In the comprehensive study of the immune gene repertoire of *M. edulis* by Philipp et al. (2012), no NLRs and NATCH domains were found. Moreover, key adaptor molecules such as RIP2 (receptor-interacting protein kinase 2) and ASC (speck-like protein containing a CARD) were also absent. However, Gerdol and Venier (2015) identified one NLR-like sequence in *M. galloprovincialis* which had three domains of NLRs; central NATCH domain, N-terminal CARD effector domain, and C-terminal LRRs. They suggested NLRs in bivalves need deeper transcriptome analysis.

On the other hand, RLRs recognize viral RNA and DNA (Gerdol and Venier, 2015). Examples of RLRs include laboratory of genetics and physiology 2 (LGP2, DHX58), retinoic acid-inducible gene I (RIG-I, DDX58), and the melanoma differentiation-associated gene-5 (MDA-5, IFIH1) (Philipp et al., 2012). RLR pathways also have common genes with TLR pathways, and both can trigger inflammation by interferon regulatory factors (IRF) and NF-κB. Similar Rel/NF-κB proteins are induced by different intermediary molecules through the immune deficiency (IMD) pathway (Toubiana et al., 2014). Vertebrate RLRs have two N-terminal CARD, central helicase and C-terminal RIG repressor domains (Gerdol and Venier, 2015), except LGP2 lacks the CARD domain. In bivalves, RIG-like receptor was previously identified in the pacific oyster *C. gigas* (Zhang et al., 2014) and *M. galloprovincialis* (Gerdol and Venier, 2015). Both RIG-I-like (lacks N-terminal CARD domain) and MDA-5-like (includes N- terminal CARD domain, helicase domain, and a C-terminal helicase-c domain) gene fragments were found in *M. edulis* (Philipp et al., 2012). Also, genes of the RLR pathway (also genes of autophagy), autophagy-related-12 (ATG12), and autophagy-related-5

(ATG5) were found in *M. edulis*. However, the signaling adaptor, MAVS (IPS-1, Cardif, Visa (IMCV)) was not detected (Philipp et al., 2012).

TLRs are very important in pathogen recognition and most researched PRRs of metazoans. In 2011, the Nobel prize in medicine went to the discovery of the role of TLRs in pathology and physiology (Nobel Prize, 2021). TLR pathway is a key pathway of the innate immune response, and in mammals, it influences the types of response of the adaptive immune system through immunomodulatory cytokines (Brightbill and Modlin, 2000). For example, due to having an immunostimulatory effect, TLR agonists (CpG oligodeoxynucleotides) are used to activate TLR signaling in cancer immunotherapy studies (Adamus and Kortylewski, 2018). TLRs recognize conserved PAMPs of bacteria, viruses, protozoa, and fungi (Pålsson-McDermott and O'Neill, 2007). These receptors are composed of intracellular C-terminal TIR (Toll-interleukin-1-receptor) domain for signal transduction, a transmembrane region, and extracellular LRRs for recognition (Zhang et al., 2013).

Activation TLR signaling is tightly regulated (O'Neill and Bowie, 2007) as it has immunostimulatory effects. Activation is triggered with ligand binding and TLR dimerization, TIR domain-containing adaptors attach to intracellular TIR domain of TLR initiating signaling that leads to activation of transcription factors (O'Neill and Bowie, 2007). There are five TIR domain-containing adaptors: MyD88 (Myeloid differentiation primary response 88), TIRAP (Toll interleukin 1 receptor adaptor protein, MyD88-adaptor- like, MAL), TRIF (TICAM1, TIR-domain-containing adaptor protein inducing IFNB), TRAM (TICAM2, TRIF-related adaptor molecule), and SARM (sterile alpha and armadillo-motif- containing protein) (O'Neill and Bowie, 2007). These molecules activate transducer TRAF6 and kinases such as IRAK, IKK, IKB, MAP3K7(TAK1) and transcription factors such as NF-κB, IRF (Interferon regulatory factors) that induce proinflammatory cytokines as interleukins, macrophage migration inhibitory factor (MIF), tumor necrosis factor (TNF), transforming growth factor-beta (TGF-Beta) and interferons for immune response (Gerdol and Venier, 2015; Coscia et al., 2011). With LPS induction of TLR, LITAF (LPS-induced TNF-α factor) transcription factor is involved in TNF-α and other cytokine productions via MyD88 and p38 MAPK (Tang et al., 2006).

In humans, 10 TLRs were identified each with specific ligands (Brown et al., 2011). On the other hand, as an echinoderm representative, sea urchins have a much higher diversity of TLRs with 222 TLRs and 26 adaptors (Leulier and Lemaitre, 2008). This high diversity reflects “diversification of recognition specificity” in the absence of an adaptive immune system (Leulier and Lemaitre, 2008).

Leulier and Lemaitre (2008) attributed the high diversity in sea urchins TLR to "complex life history, intricate water vascular system, large body size (compared to other invertebrates), long lifespan (more than 30 years)" and also endosymbiotic microorganisms they interact with. Likewise, relatively high abundance and diversity of TLRs have also been observed in bivalves, thought to be due to similar reasons (Philipp et al., 2012). In bivalves, TLRs are seen in many species such as *C. farreri* (Wang et al., 2018c), *C. gigas* (Zhang et al., 2013), *M. galloprovincialis* (Toubiana et al., 2014), *M. edulis* (Philipp et al., 2012) and *Bathymodiolus* mussels (Zheng et al., 2017).

The last category of receptor families to be discussed in this section, C-type lectins (CLRs), are involved in immune processes like pathogen recognition (Gerdol and Venier, 2015), complement activation (Gerdol and Venier, 2015), inflammation (Cummings and McEver, 2009), phagocytosis (Song et al., 2010) and also in other biological processes such as particle capture in feeding (Gerdol and Venier, 2015). They are Ca^{+2} dependent glycan-binding proteins with carbohydrate recognition domains (CRD) (Cummings and McEver, 2009). Collectins and proteoglycans are examples of C-type lectins. CLRs bind to glycoproteins and glycolipids with different carbohydrate-binding specificities (Song et al., 2010). They harbor the C-type lectin domain (CTLD) which is also present in many proteins that do not bind to carbohydrates (Cummings and McEver, 2009). A high number of CLRs were identified in bivalves with diverse domain structures and organizations, such as *C. farreri* that contains CLRs with more than one CRD-like domain (Cflec-3, Cflec-4) like insects (Song et al., 2010). Both *M. galloprovincialis* and *C. gigas* also have a very high abundance of CLRs (Gerdol, M., & Venier, P. 2015; Wang et al., 2018b; Venier et al., 2011; Zhang et al., 2012b).

Other than these main receptor families, other lectins, peptidoglycan recognition proteins (PGRPs), gram-negative binding proteins (GNBPs), galectins, thioester-containing proteins (TEPs) (Song et al., 2010), scavenger receptor cysteine-rich superfamily receptors (SRCR-SF) (Gerdol and Venier, 2015), fibrinogen-related proteins (FREPs) (Gerdol and Venier, 2015), f-type lectins (fucolectins) (Gerdol and Venier, 2015; Venier et al., 2011), C1qDC (C1q domain-containing proteins) (Venier et al., 2011), ficolins (lectin) and chitotriosidase-1 (chitinase-1, lectin) (Venier et al., 2011) are involved in pattern-recognition in bivalves.

Many types of lectins that are involved in pathogen recognition are identified in bivalves. Fibrinogen-related proteins (FREPs) are lectins with fibrinogen-like domains. A high number of FREPs have been identified in *M. galloprovincialis* (Romero et al., 2011; Gerdol and Venier, 2015), *Argopecten irradians* (Zhang et al., 2009), and *C. gigas* (Zhang et al., 2012b; Zhang et al., 2012c). Another type of lectin is galectins. Galectins are Ca^{+2} independent beta-galactosyl-binding lectins.

Although they are the most conserved lectins, they show functional diversity involving other biological processes besides immune processes; mainly recognition of glycans on the surface of pathogens. They show different domain organizations with having one CRD per subunit (Cooper, 2018). Invertebrate galectins do not agree with vertebrate types (Cooper, 2018). They have two or four CRDs. Galectins were identified in many bivalve species such as *C. gigas* (Yamaura et al., 2008), *R. philippinarum* (Kim et al., 2008b), and *M. galloprovincialis* (Venier et al., 2009). F-type lectins are also pathogen recognition receptors of bivalves identified in *Pinctada spp* (Anju et al., 2013; Chen et al., 2011; Chen et al., 2011 cited in Wang et al., 2018b) and *C. gigas* (Chen et al., 2011 cited in Wang et al., 2018b). F5/8 type C domain (IPR000421) of F-type lectins are seen in mussels (Gerdol and Venier, 2015). Other identified lectins include chitinase-like lectin in *C. gigas* (Badariotti et al., 2006 cited in Wang et al., 2018b) and ficolin-like lectins in *C. hongkongensis* (Xiang et al., 2014 cited in Wang et al., 2018b).

Peptidoglycan recognition receptors (PGRPs) recognize peptidoglycan (PGN) of the bacterial cell wall. They are highly conserved PRRs that are found in all metazoans. They were identified in many bivalve species as well (Gerdol and Venier, 2015). They can be membrane-bound or secreted. They activate toll and IMD pathways in insects and are involved in immune functions such as phagocytosis. Peptidoglycan recognition proteins 1, 2, 3 (PGRP1, PGRP2, PGRP3) were identified after bacterial challenge in *M. galloprovincialis* (Gerdol and Venier, 2015). In bivalves, the IMD pathway is thought to be involved with PGRPs in the recognition of gram-bacteria (Gerdol and Venier, 2015). IMD pathway genes (TAK1 (Mitogen-activated protein kinase kinase kinase 7, MAP3K7), NEMO (Inhibitor of Nuclear Factor Kappa B Kinase, IKBKG), IKK-b and Relish (NF-κB related transcription factor)) were also detected in *M. galloprovincialis* (Gerdol and Venier, 2015).

Scavenger receptors are another diverse superfamily of receptors coded from class A to class J. They bind to low-density lipoproteins (LDL) and are involved in phagocytosis. Sea urchins have a high diversity of scavenger receptor genes; 218 genes comprising a total of 1095 SRCR domains (Hibino et al., 2006). Scavenger receptor class B (SR-BI) was identified in the oyster subspecies *Pinctada fuctada martensii* (Lei et al., 2017). Scavenger receptor cysteine-rich domain superfamily (SRCR-SF) was also identified in *C. farreri* (Liu et al., 2011). SRCR-SF was annotated in the oyster *C. gigas* and the mussel *M. galloprovincialis* (Gerdol and Venier, 2015).

Thioester-containing proteins have unique intrachain beta-cysteinyl-gamma-glutamyl thioester involved in innate immune response (Zhang et al., 2007). TEP genes are “complement component C3, C4, C5 and protease inhibitor alpha2-macroglobulin, CD109 and a set of insect TEPs” (Song et

al., 2010). Considering marine invertebrates, CfTEP was identified in *C. farreri* (Zhang et al., 2007) and C3-like protein (Rd-C3 and Rd-Bf-like) in *Ruditapes decussatus* (Prado-Alvarez et al., 2009).

Gram-negative binding protein (GNBP) recognizes LPS and beta-1,3-glucan to bind to gram-negative bacteria (Song et. al 2010). In bivalves both of these binding abilities encountered in lipopolysaccharide and b-1, 3-glucan binding proteins (LGBPs) are involved in many processes like melanization and opsonic reaction. LGBPs were identified in *P. fucata* (Zhang et al., 2010 cited in Gerdol and Venier, 2015) and in *C. farreri* (Wang et al. 2009). In *Drosophila*, GNBP and PGRP together activate toll signaling and melanization, however, in mussels this remains hypothetical (Gerdol and Venier, 2015).

C1q is a protein complex of complement cascade with the C1q conserved domain. C1q domain is also involved in non-complement proteins integral to many biological processes like apoptosis and inflammation. (Gerdol et al., 2011). C1q domain-containing (C1qDC) proteins comprise important, divergent, and abundant pathogen recognition receptors of bivalves (Gerdol et al., 2015 cited in Gerdol and Venier, 2015). They are usually composed of N-terminal signal peptide, central region, and C-terminal C1q domain. It was found that C1qDC is overexpressed in *M. galloprovincialis* (Gestal et al. 2010 cited in Gerdol and Venier, 2015) and *M. coruscus* (Liu et al., 2014b cited in Gerdol and Venier, 2015) after bacterial challenge. The abundance of C1qDC proteins (168 in Gerdol et al., 2011 and 1274 putative loci in Gerdol and Venier, 2015) in *M. galloprovincialis* indicates gene duplication (Gerdol et al., 2011), selection of specific variants (Gerdol et al., 2011), and recognition of a wide variety of pathogens (Gerdol and Venier, 2015).

2.2.5.2. Complement system. The complement system is part of innate and adaptive immunity that helps to fight against pathogens by inflammation, opsonization, and killing of pathogens (Janeway et al., 2001). Most of the complement cascade enzymes are inactive when not triggered. When triggered, each enzyme activates the next enzyme in line through proteolytic cleavage (Alberts et al., 2008). The complement system can be triggered by classical, alternative, and lectin pathways (Alberts et al., 2008). Blood coagulation can also trigger the complement cascade (Janeway et al., 2001). In the classical pathway, C1q protein is attached to the pathogen's surface, marking it for phagocytosis. In the lectin pathway, Ca^{+2} dependent mannan-binding lectin is attached to the mannose-rich surface of bacteria. The alternative pathway is triggered by the surface of the bacteria itself. All three pathways lead to the activation of C3. After C3 is immobilized on the surface of a pathogen, membrane attack complexes are formed for lysis of the pathogen. Other genes of the pathway include C1–C9, MBL-associated serine protease (MASP), and factors B and D (Alberts et al., 2008). There is not a lot of

information about the functioning of the complement system in bivalves; complement C1 was identified in *M. edulis*, and C3 was identified in *M. coruscus* (Chen et al., 2018) and *M. edulis* (Wu et al., 2020). Also, C3-like protein (Rd-C3 and Rd-Bf-like) was identified in *Ruditapes decussatus* (Prado-Alvarez et al., 2009).

2.2.6. DNA Damage Response (DDR)

Cells face various kinds of stress throughout their life that can cause DNA damage. Maintaining genome stability and integrity is vital for living organisms, as deterioration of genomic integrity can lead to immune deficiency, aging, neurological degeneration, and/or diseases (Hakem, 2008; Giglia-Mari et al., 2011). Chakarov et al. (2014) define DNA damage as "any modification in the physical and/or chemical structure of DNA resulting in an altered DNA molecule which is different from the original DNA molecule with regard to its physical, chemical and/or structural properties". The damage can be caused by endogenous sources such as ROS, metabolic processes, replication errors, or exogenous sources such as chemical toxins, ionizing radiation, and UV light. To deal with DNA damage, adaptations, checkpoints, and repair mechanisms evolved (Hakem, 2008). If damage is beyond repair and extensive, apoptosis is triggered (Morandell and Yaffe, 2012). Cells sense and repair DNA damage via the DNA damage response (DDR) system composed of DNA repair mechanisms, damage tolerance processes, and cell-cycle checkpoint pathways (Giglia-Mari et al., 2011).

DNA repair mechanisms broadly have four steps: recognition, removal, resynthesis, and restoration (Kelley and Fishel, 2013). At the recognition step, glycosylases and helicases are involved in the recognition of damaged parts. At the removal step, endonucleases and lyases are involved in the removal of damaged parts, and the region to be repaired is prepared for further steps. At the resynthesis step, polymerases and progressivity factors are involved in new oligo synthesis. Finally, the involvement of ligases and exonucleases comprises the restoration step (Kelley and Fishel, 2013). Each DNA repair mechanism has its specificity but influences each other with crosstalk. These mechanisms are direct reversal (DR), mismatch repair (MMR), base excision repair (BER), nucleotide excision repair (NER), and double-strand break repair (DSBR) (Yi and He, 2013; Giglia-Mari et al., 2011).

DR is the direct reversal of the damage by a single repair protein non-enzymatically, in an error-free and simple manner. Three major sub-mechanisms use a protein of i) photolyase, ii) alkyltransferase (O6-alkylguanine-DNA alkyltransferases (AGTs), MGMT) or iii) dioxygenase to

reverse UV light, O-alkylated, N-alkylated DNA damage, respectively (Yi and He, 2013). Without MGMT, thymine mispairings would happen during replication due to alkyls (Kelley and Fishel, 2013).

MMR repairs insertions and deletions during replication and helps to impede permanent mutations (Kelley and Fishel, 2013). Defects in MMR result in increases in the rate of mutations due to the skipping of cell cycle checkpoints and continuing replication (Kelley and Fishel, 2013). MutS, MutL, MutL homolog (MLH), MutS homolog (MSH), postmeiotic segregation increased 1 (PMS1), postmeiotic segregation increased 2 (PMS2) and exonuclease 1 (Exo1) are the most known DNA mismatch repair genes (Hakem, 2008). MSH2:MSH6 or MSH2:MSH3 heterodimers are involved in damage recognition of insertions-deletions and single-base mismatches. MSHs enlist MLH1, PMS1, and PMS2 for ordaining strand error. Mismatched sections are removed by MutL. New DNA nucleotides are synthesized by DNA polymerase, where Exo1 removes nucleotides, and DNA ligase completes repair (Kelley and Fishel, 2013).

NER repairs a variety of kinds of DNA damage. Global genome NER (GG-NER) identifies damage throughout the genome, and transcription-coupled NER (TC-NER) identifies actively transcribed genes. NER recognizes and removes damaged sections, and newly synthesized oligos are attached. Genes involved in recognition include XPC (RAD4), RAD23 Homolog B (RAD23B, HR23B), and Damage Specific DNA Binding Protein 2 (DDB2, DDB1– XPE) in GG-NER and cockayne syndrome group A (CSA) (ERCC8), and CSB (RAD26, ERCC6) in TC-NER (Hakem, 2008). Subsequent steps are the same for both pathways. Transcription Factor II H (TFIIH) is a damage sensing protein complex, which contains ERCC Excision Repair 3 (ERCC3, XPB) and XPD (ERCC2), unwind DNA, and open double helix. The damaged section is removed by ERCC1 (RAD10), Xeroderma Pigmentosum Group A-Complementing Protein (XPA), and endonucleases XPG (ERCC5) and XPF (RAD1, ERCC4). With DNA polymerase-epsilon (Pole) and DNA polymerase-gamma (Polg) new nucleotides are synthesized. XPG removes overhanging flap, and ligase I completes repair (Kelley and Fishel, 2013).

BER is important for genomic integrity, and it repairs base damage that would cause incorrect base pairing. Damage can be due to oxidation, deamination, and alkylation. There are two pathways; short patch BER that replaces one nucleotide and long patch BER that replaces 2-13 nucleotides. DNA glycosylases, Ogg1 (8-oxoguanine DNA glycosylase) and Mutyh (MutY DNA glycosylase) recognize the site and endonuclease APE1 (apurinic/apyrimidinic endonuclease 1) removes it (Hakem, 2008). DNA polymerase-beta (Polb) in short patch BER, and DNA polymerase-epsilon

(Pole) and DNA polymerase-gamma (Polg) in long-patch BER synthesize new bases (Kelley and Fishel, 2013). Ligase III in short patch BER and ligase I in long patch BER completes the repair (Kelley and Fishel, 2013). Scaffolding proteins, XRCC1 (x-ray repair cross-complementing 1) and PARP1 (poly-ADP ribose polymerase 1) are involved in BER. PARP1 also determines the repair pathway. FEN1 removes overhanging flaps in the long patch BER (Kelley and Fishel, 2013).

DSBR is the most dangerous DNA damage that can lead to "mutations, deletions, translocations, and genome amplification" (Willers et al., 2012 cited in Kelley and Fishel, 2013). Two pathways exist: non-homologous end joining (NHEJ) and homologous recombination repair (HRR). The pathway is selected according to the properties and state of the damage. In the NHEJ pathway, two broken ends of the DNA are simply rejoined. Accuracy is not guaranteed, deletions can arise, which can subsequently lead to mutation. Broadly speaking, genes involved are Ku heterodimer (Ku70: Ku80), DNA-dependent protein kinase (DNAPKcs), tyrosyl DNA phosphodiesterase 1 (TDP1), polynucleotide kinase/phosphatase (PNKP), Artemis, and Werner syndrome protein (WRN). Ku heterodimer recognizes break and recruits other proteins for progression. DNAPKcs works with Ku heterodimer for preparation to ligation. Other proteins including artemis, PNKP, WRN, and TDP1 may also be involved depending on the damage. MRN complex has endonuclease and exonuclease properties and is involved in the process with various functions, such as binding of double-strand breaks and tethering of ends before repair. MRN complex is composed of Mre11 (Meiotic Recombination 11), Rad50, and Nbs1 (nibrin) proteins. Ligase IV joins the ends in the next step. X-Ray repair cross complementing 4 (XRCC4) and XRCC4-Like Factor (XLF) scaffolding proteins are also involved in the process (Kelley and Fishel, 2013). It was previously thought that invertebrates did not have XRCC4, XLF, ligase 4 (Hecox-Lea and Welch, 2018), DNAPKcs, and artemis, and also artemis function was thought to be undertaken by the RAD50:MRE11:NBS1 complex (Lieber et al., 2010). Subsequently, however, DNAPKcs and artemis homologs were identified in multiple invertebrate genomes (Hecox-Lea and Welch, 2018).

HRR is a very important and the most guaranteed DNA repair pathway. It is a conserved pathway from bacteria to humans (Hiom, 2001). Alternative to the NHEJ pathway, breaks are repaired with high fidelity by recombination with homologous DNA duplex molecule (Featherstone and Jackson, 1999). It is a complex process, and the main steps are strand exchange, branch migration, and resolution (Hiom, 2001). Genes involved in the process are MRN complex, gamma-H2AX, breast cancer gene 1 (BRCA1), Rad50, replication protein A (RPA), Rad52, breast cancer gene 2 (BRCA2), X-Ray repair cross complementing 2 (XRCC2), X-Ray repair cross complementing 3 (XRCC3),

Rad54, Bloom syndrome protein (BLM), Werner syndrome protein (WRN), TOPOIII-alpha, and resolvase (Kelley and Fishel, 2013).

2.2.7. Proteolysis

Proteins are involved in every process in the cell, determining the healthy functioning of the organism and its capability to adapt to changing environments (Clausen et al., 2019). Therefore, it is very important to control their concentration, conformation, stability, location, and turnover for cellular homeostasis (Clausen et al., 2019). Proteins are continuously synthesized, modified, and degraded if they are functionally expired, misfolded, or damaged beyond repair. Stressors like temperature, salinity, and other factors can cause the dysfunction of proteins (Wang et al., 2004). For a protein to be functional, it must be folded in its native conformation. Chaperons are conserved proteins involved in protein folding, assembly, translocation, and degradation of other proteins (Wang et al, 2004; Lodish et al., 2000). Under stress, they stabilize proteins and inhibit aggregation of misfolded proteins. Stress-inducible molecular chaperones are upregulated in response to any type of stress, as they play a role in protein homeostasis and protein folding (Hofmann, 2005), and stabilize denaturing proteins (Buckley *et al.*, 2001). They are therefore indirect indicators of protein damage (Hofmann, 2005). Denaturing proteins that are not stabilized by molecular chaperones are degraded by the ubiquitin-proteasome pathway (UPP). UPP pathway is involved in almost all cellular processes. In the UPP, the target protein to be degraded is tagged with ubiquitin, in the process of ubiquitination and degraded by 26S proteasome. Three enzymes are involved in the process: E1 ubiquitin-activating enzyme, E2 ubiquitin-conjugating enzyme, and E3 ubiquitin ligase. The other pathway of protein degradation is the lysosomal pathway (Cooper, 2000). In the lysosomal pathway, proteins to be degraded are encapsulated in membrane vesicles and transported to the lysosome which has catalytic enzymes including cathepsins, other proteases, and other hydrolytic enzymes used for digestion.

2.2.8. Apoptosis

Apoptosis is programmed cell death without inflammation. It is an energy-dependent and a vital mechanism for normal cell turnover, involved in various natural physiological processes to eliminate unwanted cells, such as those produced through embryogenesis, hormone-dependent atrophy, and immune response (Elmore, 2007). It is also activated in pathological conditions to eliminate cells with damaged DNA (Roos and Kaina, 2006), unfolded protein accumulations (Fribley et al., 2009), oxidative stress (Kannan and Jain, 2000), salt stress (Yazdani and Mahdieh, 2012) and viral infections

(Kvansakul, 2017). Apoptosis can be initiated by two alternative pathways, by surface receptors (the extrinsic pathway) or through mitochondria (the intrinsic pathway). In all metazoans, the main executors of apoptosis are caspases for both of the pathways (Julien and Wells, 2017).

Caspases are cysteine proteases (Julien and Wells, 2017), which are divided into two, as initiator and effector/executioner caspases (Matsuura et al., 2016). As their name implies, initiator caspases initiate apoptosis, whereas executioners execute apoptosis. Caspases 2 and 9 are initiators of intrinsic apoptosis; caspases 8 and 10 are initiators of extrinsic apoptosis; caspases 1,4,5, and 12 are inflammatory initiator caspases, and lastly, caspases 3, 6, and 7 are executioner caspases (Matsuura et al., 2016). Initiator caspases are activated by the intrinsic or the extrinsic pathway, and subsequently, they activate executioner caspases through cleavage. Nucleus, cytoskeleton, and protein substrates are cleaved by executioner caspases, generating apoptotic bodies to be engulfed by phagocytic cells. In bivalves, homologs of these caspases show difference and expansion compared to vertebrate ones, and require detailed examination to understand their full function (Vogeler et al., 2021).

The intrinsic pathway is mediated by the integrity of mitochondrial structure when severe stress and cellular damage are detected. With severe stress, sensors of cellular damage, BCL2 associated agonist of cell death (BAD), BCL2 interacting mediator of cell death (BIM), BH3 interacting domain death agonist (BID), and p53 up-regulated modulator of apoptosis (PUMA) are activated. These are also proapoptotic regulators that activate proapoptotic genes and inactivate antiapoptotic genes (Sinicrope et al., 2008). Activated proapoptotic genes, namely BCL2 Associated X (BAX), BCL2 Antagonist/Killer (BAK) and BCL-xS trigger mitochondrial outer membrane permeabilization (MOMP) (Suhaili et al., 2017), and proteins in the intermembrane space are released to the cytosol. These proteins are cytochrome c, endonuclease G, Smac/DIABLO, and HtrA serine peptidase 2 (HTRA2) (Galluzzi et al., 2014). Cytochrome c, adaptor protein apoptotic protease activating factor 1 (APAF-1), ATP and procaspase 9 form the apoptosome complex (Pelzel and Nickells, 2010), and with apoptosome formation, procaspase 9 is activated. In addition, caspase 9 cleaves caspase 3, which activates DNA fragmentation factor (DFF) for the fragmentation of DNA (Estévez-Calvar et al., 2013). Smac/DIABLO, and HTRA2 activate caspases by neutralizing inhibitor of apoptosis (IAPs). Endonuclease G mediates DNA degradation that is independent of caspases (Galluzzi et al., 2014). On the other hand, the stimulation of cells by growth factors can activate antiapoptotic genes. Antiapoptotic genes are B cell lymphoma 2 (BCL2), BCL-xL, myeloid cell leukemia 1 (MCL1) that inhibit MOMP, and prevent leakage of intermembrane proteins to the cytosol by maintaining BAK and BAX in an inactive conformation (Galluzzi et al., 2014).

Extrinsic pathway (death receptor initiated) of apoptosis is triggered by extracellular ligands that bind to death receptors, FAS (ligand: CD95), TNFR1(Tumor necrosis factor receptor 1, ligand: TNF-α), and DR4 (Death Receptor 4, TRAIL-R1, TNFRSF10A, TNF Receptor Superfamily Member 10a, ligand: APO2L) and DR5 (Death Receptor 5, TRAIL-R2, TNFRSF10B, TNF Receptor Superfamily Member 10b, ligand: APO2L) (Elmore, 2007). Fas Associated Death Domain (FADD) adaptor is attached to the death domains of the clustered receptors and activates caspase 8. Like in the intrinsic pathway, executioner caspases 3, 6, and 7 are activated afterwards (Kumar et al., 2015).

In invertebrates, apoptosis is frequently associated with stress. DNA fragmentation, a hallmark of apoptosis, is used in pollution monitoring (Estévez-Calvar et al., 2013). P53 mitochondrial apoptotic gene is used as a marker of cellular stress in mussels. P53 acts as a transcription factor, binds to proapoptotic and antiapoptotic BCL2 family proteins, and regulates their activity. Other members of the p53 gene family, p63 and p73 also mediate apoptosis. Moreover, p53 gene family is suggested to have evolved for mediating apoptosis of damaged germ cells (Walker et al., 2011). Other than apoptosis, these genes are involved in other processes such as development, energy metabolism, and differentiation (Bourdon, 2007). Many apoptosis genes in vertebrates have also been identified in invertebrates. Estévez-Calvar et al. (2013) identified p53, p53 and DNA damage regulated protein (PDRP), BCL2, BAX, BAX inhibitor 1 (BI-1) and Dff-A in *M. galloprovincialis*. Caspase 2, caspase 8 and caspase 3/7 (caspase 3/7-1, caspase 3/7-2, caspase 3/7-3 and caspase 3/7-4) were also identified by Romero et al. (2011) in *M. galloprovincialis*. Summary of apoptosis genes identified in mollusks (Estévez-Calvar et al., 2013) is given in Figure 2.2.

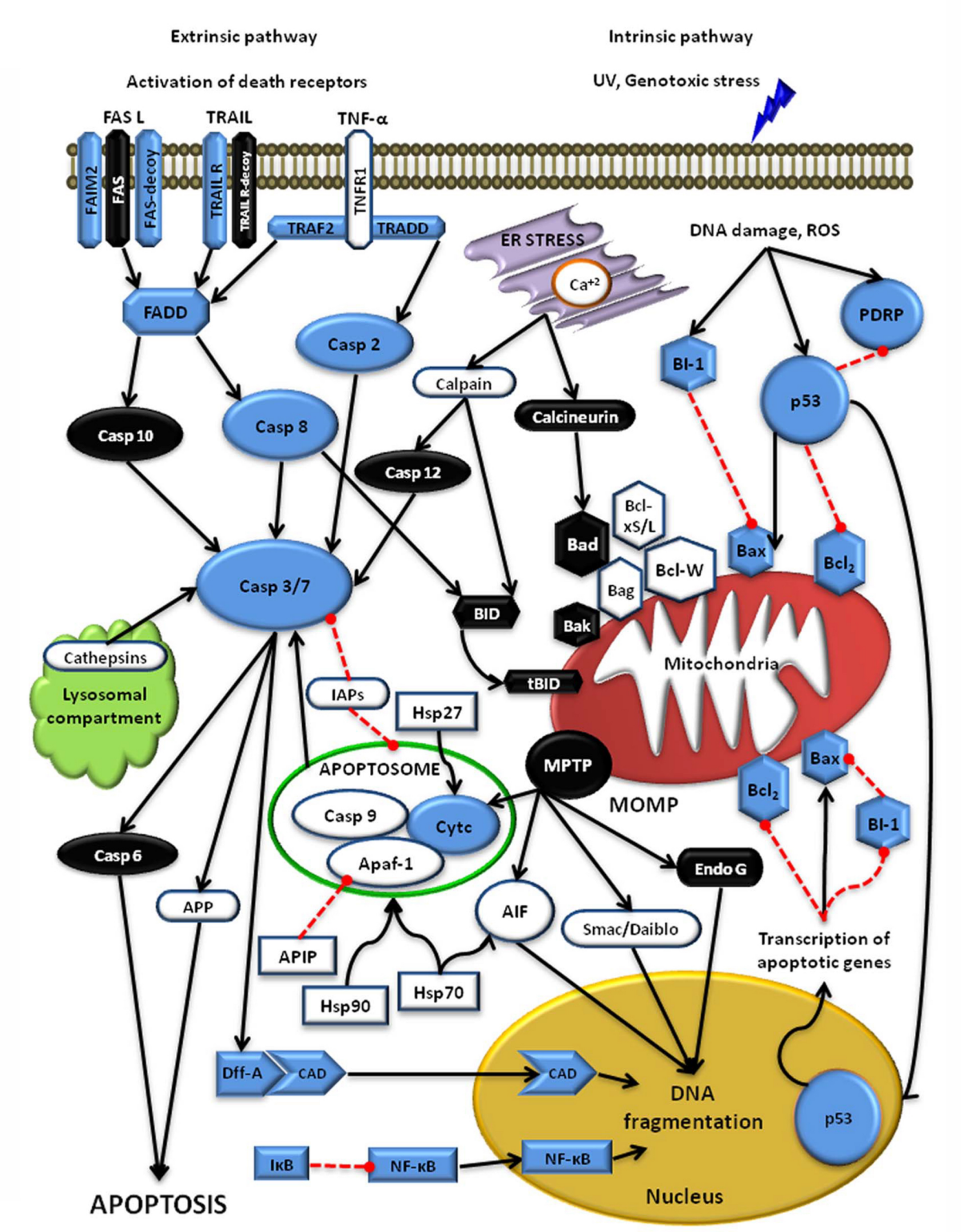


Figure 2.2. Apoptotic pathway in mollusks (Estévez-Calvar et al., 2013). The blue-colored genes are identified in bivalves, white-colored are available ESTs, and black-colored are genes that have not been described in mollusks (Estévez-Calvar et al., 2013).

2.2.9. Osmoregulation

Like *M. galloprovincialis*, most bivalves are osmoconformers that have extracellular fluid and intracellular cytoplasm isosmotic to the surrounding water, unlike osmoregulators that regulate osmotic gradient with the surrounding medium (Bradley, 2009, Zhao et al., 2012). To adapt to the changing osmolarity of the surrounding water, osmoconformers undergo energetically costly processes to balance internal salinity (Eierman and Hare, 2014). The initial short-term behavioral response to salinity change in bivalves is visible in the closing of the shells. However, food and oxygen demand in the long term requires the opening of their shells and an adjustment in cell volume (Gosling, 2004). Also, behavioral responses adjusting the siphons and adjusting the rate of beating of the cilia on the gills ensures a slower rate of exposure to changing environmental conditions (Deaton, 2008). Changing the permeability of water and ions across the cell membrane enables the cell to gain time to respond to the shock (Deaton, 2008). As the extracellular fluid becomes isosmotic with the ambient water, cells swell or shrink due to osmosis (Deaton, 2008; Toyohara, 2005a). To regain volume, organic and inorganic osmolytes are exported in the former in a process referred to as regulatory volume decrease (RVD) and imported or synthesized in the latter under regulatory volume increase (RVI) (Toyohara, 2005a, Deaton, 2008). This cell volume regulation is very important and its dysfunction leads to protein denaturation and apoptosis (Gómez-Angelats and Cidlowski, 2002 cited in Rivera-Ingraham and Lignot, 2017). Rather than inorganic osmolytes, organic osmolytes, which "stabilize proteins and protect cells from oxidative stress", are used first (Eierman and Hare, 2014). This is because, unlike inorganic osmolytes, most of the organic osmolytes can be accumulated at high concentrations in the cell without perturbing protein function (Burg and Ferraris, 2008). Therefore, cells that reside at high osmotic pressure, such as the cells of marine water organisms, preferentially comprise organic osmolytes (Sidney et al., 2001). Cells that reside at low osmotic pressure, such as the cells of freshwater organisms, can also rely on inorganic osmolytes (Sidney et al., 2001). Examples of organic osmolytes that act as antioxidants include taurine and hypotaurine (Yancey, 2005). Glycerol also maintains redox balance (Yancey, 2005). However, some of the organic osmolytes should not be accumulated at high concentrations in order to stay beneficial and needs to be adjusted like methylamines as they stabilize macromolecules (Yancey, 2005).

Response to osmotic stress can vary due to multipe factors. For example, it can change among tissue types within the same specimen. Such variation was seen between ventricle, gill and mantle cells of *Geukensia demissa*. The ventricles initiate volume regulation in response to moderate change, but show no response in the gills and the mantle (Deaton, 2008). Another example is change with the composition of the ambient medium (Cornet, 2006). In vitro tissue culture of *M. galloprovincialis*,

toleration of hypoosmotic shock was better when the medium provided had higher concentrations of amino acids (Cornet, 2006). The concentration and composition of organic osmolytes changes among species and populations within species, as well (Deaton, 2008).

For volume regulation, firstly, organic osmolytes are used. Free amino acids and quaternary amines, which compose organic osmolytes, play an important role in osmoregulation. In marine bivalves, free amino acids are primarily involved (Toyohara, 2005a). In *C. gigas*, the amino acid transporter gene which is responsible for membrane transport of the amino acids was upregulated both in hypoosmotic and hyperosmotic stresses where the response was more intense and acute in the former (Toyohara et al., 2005a). With increases in salinity, free amino acids are increased, whereas, with a decrease in salinity, free amino acids and amino-nitrogens are decreased due to ammonia excretion (Gosling, 2004; Meng et al., 2013). The most prominent hyperosmotic volume regulation responses of amino acids in bivalves are seen as increases in alanine, glycine and betaine (Deaton, 2001). In acute hyperosmotic volume regulation, a rapid increase in betaine and alanine level, and slower increase in glycine and proline levels were observed in the gills of the ribbed mussel, *G. demissa* (Deaton, 2001), which suggested that rapid increase in betaine levels was indicative of gene expression not being involved in volume regulation (Deaton, 2001).

Taurine is another essential osmolyte, constituting one-fifth of total intracellular osmolality and 80% of the total amino acid pool (Hosoi et al., 2005). In the mantle of *M. galloprovincialis* and several tissues of *C. gigas*, the taurine transporter gene was upregulated during hyperosmotic stress. It was also upregulated in hypoosmotic stress due to the decrease in the concentration of taurine. In hypoosmolality, regulation of the taurine transporter is not only related to ambient osmolality but also decreases in tissue taurine concentration and availability of NaCl (Hosoi et al, 2005, Hosoi et al., 2007). The Toyohara et al. (2005b) study on the mantle of *M. galloprovincialis* agreed with these hypoosmotic stress findings, whereas it diverged in the inferences with regards to hyperosmotic stress being associated with the downregulation of the taurine transporter. Another important osmolyte, which functions similarly to taurine, is glycine betaine (betaine) (de Vooys and Geenevasen, 2002). In the short term, its regulation is controlled by inorganic ions and free amino acids, especially glycine and alanine (de Vooys and Geenevasen, 2002). In *M. galloprovincialis*, a change in glycine betaine and several amino acids were observed in the posterior adductor muscle with changing salinities (de Vooys and Geenevasen, 2002).

Secondarily, inorganic osmolytes (ions such as Na^+, K^+, Ca^{2+} and Cl^-) are used to adjust cell volume. With decreases in salinity, ion channel genes such as the potassium voltage-gated channel

subfamily A member 10 (KCNA10) are upregulated, preventing cell swelling by allowing ions to move freely across the membrane. Simultaneously, ion and amino acid transporter genes solute carrier family 17 member 5 (vesicular H^+/aspartate-glutamate cotransporter, SLC17A5), glycine transporter 2 (GLYT2), ATPase Na^+/K^+ transporting subunit alpha 1 (ATP1A) and monocarboxylate transporter (MCT) are downregulated, preventing active transport of these to the cytosol where the concentration of solutes is too high (Lockwood and Somero, 2011).

Mostly, the balance of Na^+ and K^+ ions across the membrane ensures that the cell sustains its volume and integrity (Deaton, 2008). The membrane-bound protein Na^+/K^+-ATPase actively pumps Na^+ ions out of cells and K^+ ions into the cell (Deaton, 2008). This process requires a large portion of the cell's energy since it must move against the concentration gradient, as Na^+ ions are lower inside the cell than outside, and for K^+ ions the situation is vice versa (Deaton, 2008). Na^+/K^+-ATPase is found in the ion-transporting epithelia of all euryhaline species - specifically in the gills- although other transport proteins can differ between tissues and species (Henry et al., 2003, Henry, 2001). In bivalves, Na^+/K^+-ATPase alpha subunit, and Na^+/K^+-ATPase beta subunit are found to be involved in salinity stress (Lockwood and Somero, 2011; Prentis and Pavasovic, 2014).

Like Na^+/K^+-ATPase, carbonic anhydrase (CA), is an enzyme that is involved in the transportation of all ions (Henry et al., 2003). This enzyme is also found in the gills of the ion-transporting epithelia of all euryhaline species. CA increases at both high and low salinity stress in *M. galloprovincialis* for osmotic homeostasis (Freitas et al., 2017). It is especially upregulated as a response to low salinity after cell swelling and is important for long-term adaptation to low salinity (Henry, 2001). It is also upregulated in acidification to ensure acid-base balance (Freitas et al., 2017). In the green crab, *Carcinus maenas*, which is an osmoconformer when the salinity is 26‰ or more, and an osmoregulator below this limit, following low salinity stress the mRNA CA increased in 24 hours, and protein-specific CA increased in 48 hours, indicating de novo synthesis of the CA (Henry et al., 2003). Jillette et al. (2011) also examined CA activity for low and high salinity acclimation in the gills of *C. maenas*. They found induction of CA activity and mRNA of CA isoforms (CAc 100-fold, and CAg 7-fold) and the α-subunit of the Na^+/K^+-ATPase (8-fold) when crabs were acclimated to low salinity for one week. When crabs moved to 32‰ from 15‰, hemolymph osmolality recovered in 6h back to 32‰ levels, mRNA levels returned to low baseline levels within one week, and CA activity was stable for one week and subsequently returned to baseline levels in four weeks. These results suggest rapid regulation of expression of mRNA for high and low salinity stress, and slower changes in CA activity due to "long biological life span" of CA (Jillette et al., 2011). Carbonic

anhydrase alpha and carbonic anhydrase 2 were also found to be involved in the salinity stress of bivalves (Prentis and Pavasovic, 2014).

3. MATERIALS AND METHODS

In this project, chronic salinity stress was applied to *M. galloprovincialis* mussels collected from Rumeli Hisarı (Bosphorus) and mRNAs of gill tissues were extracted to generate transcript catalogs of genes using RNA-Seq. Afterwards, processes, genes and pathways were examined. A schematic representation of the process is given in Figure 3.1.

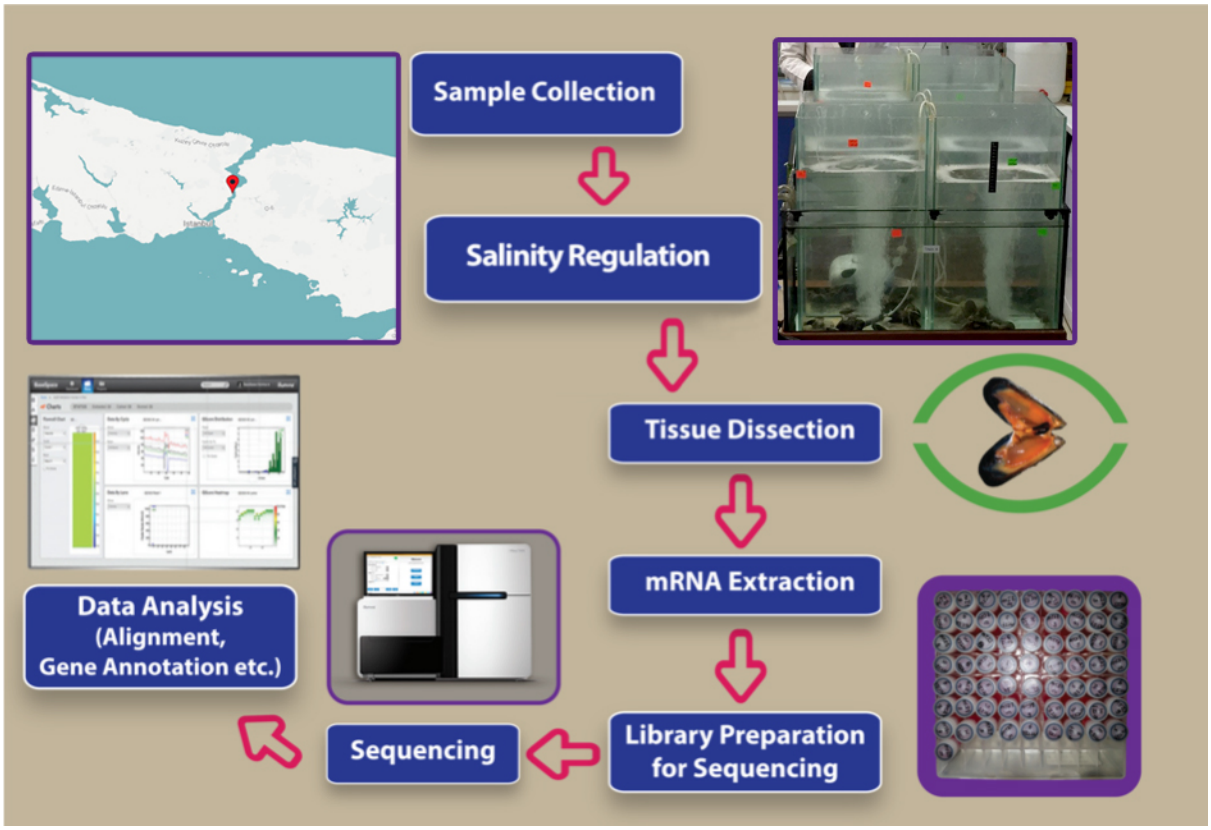


Figure 3.1. Schematic representation of the experiment.

3.1. Sample Collection

We collected 96 adult mussels from Rumeli Hisarüstü (41° 5'16.60"N 29° 3'24.95"E) (Figure 3.2) having salinity of 18.7‰ and temperature of 18.1 ºC. Only adult mussels were collected as "Mytilus transcriptome has only been characterized in adults" (Lockwood and Somero, 2011). The temperature and salinity of the site were measured using the WTW Multi 340i instrument. Samples were transported to the laboratory in seawater taken from the sea at the time of the sampling.

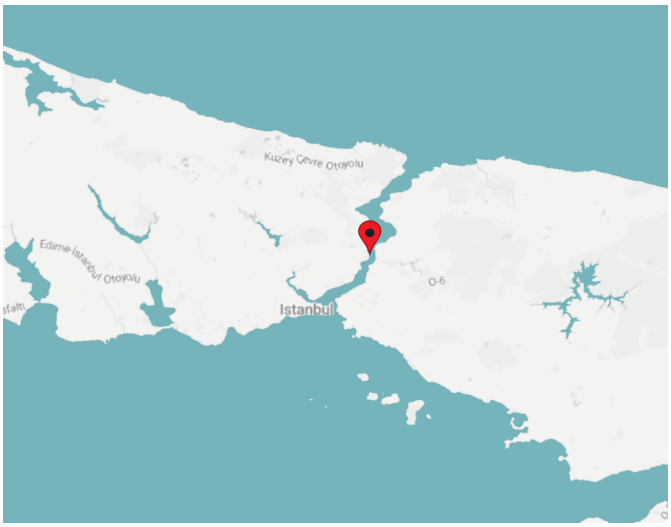


Figure 3.2. Geographic location of sampling site of *M. galloprovincialis*.

3.2. Experimental Design

In the laboratory, four tanks having size of 31x14x55h cm were prepared with artificial seawater (Instant Ocean). Two of the tanks were placed inside a bigger tank, Tank A, to share the same aeration pump and the cooling unit. The remaining two tanks were placed inside another big tank, Tank B, again to share the same aeration pump and the cooling unit. Bigger tanks, Tank A and Tank B, were arranged as technical replicates of each other having different aeration pumps and different cooling units. Experimental units in Tank A and Tank B were arranged as Rumeli Hisarı Treatment (RT), Rumeli Hisarı Control (RC) (Figure 3.3).

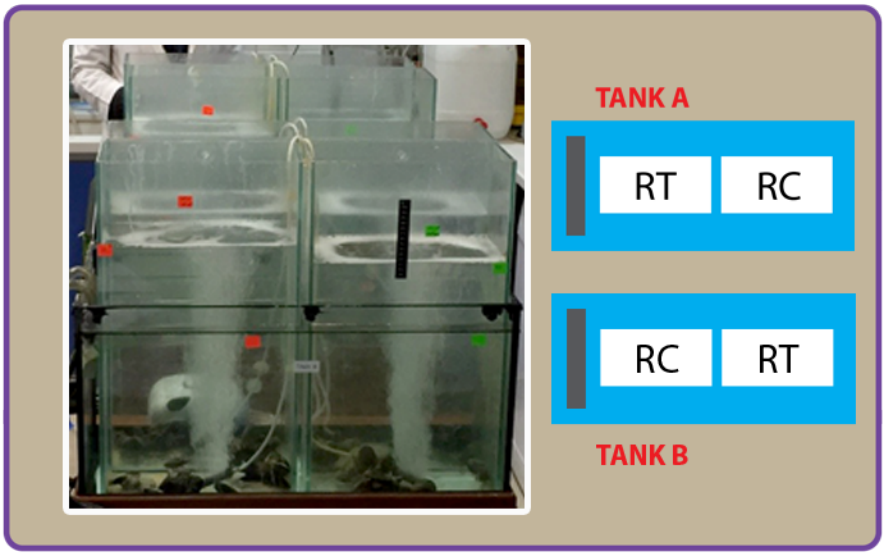


Figure 3.3. Design of the tanks of the experiment. Tank A and Tank B were replicates of each other with different cooling units and different aeration pumps. RT and RC were different experimental units sharing the same aeration pump and cooling unit (within Tank A or Tank B).

Tanks were prepared to have 18.0 ºC temperature and baseline salinities of 18‰. Each tank had 30 mussels with approximately 800 ml of water per mussel. Each tank was constantly aerated. Mussels were fed daily (20 µl/mussel) with phytoplankton of PhytoGreen-M (Brightwell Aquatics). Every week, approximately 1/3 of the water was changed with artificial seawater having the same salinity and temperature conditions.

3.3. Experimental Period

The experiment was planned to last 84 days in total. Four timepoints, A, B, C and D, with time intervals of 21 days were determined for sampling to observe treatment effects (Figure 3.4, Table 3.1). Control groups were kept at constant salinity of 18‰ (salinity of Bosphorus) to be used as time controls throughout the study.

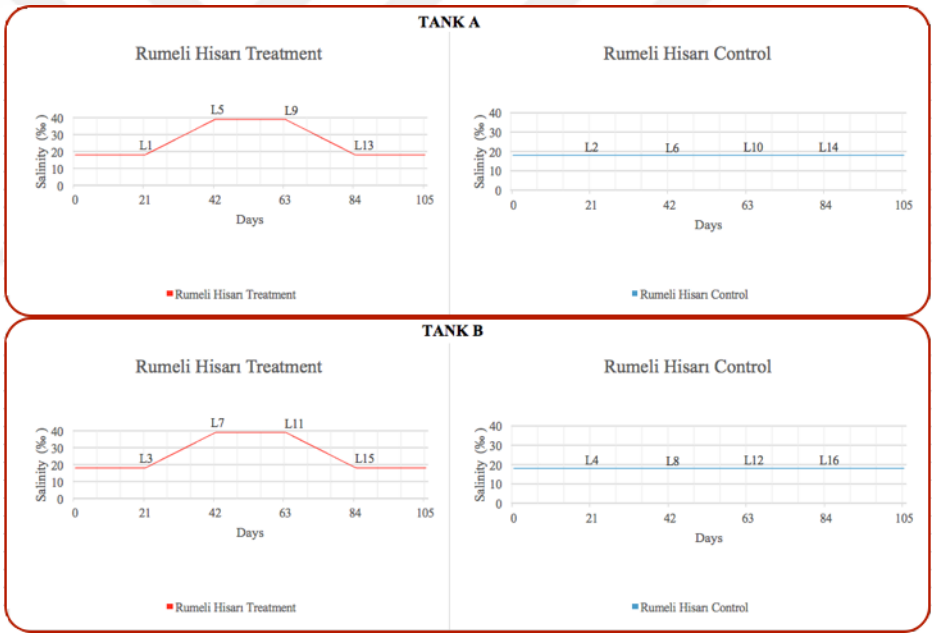


Figure 3.4. Design of the experiment with salinity adjustments. Salinity adjustments were applied to the tanks at timepoints A, B, C and D. The temperature was kept constant at 18.0 ºC throughout the experiment. A total of 16 libraries were constructed for eight conditions. Three samples were pooled for each library.

The first sampling was at timepoint A, in which mussels were acclimated to baseline salinity of 18‰ for 21 days to eliminate the effect of other stressors. Next, salinity was increased by 1‰ per day until reaching 39‰ (salinity of Aegean Sea) within 21 days for the treatment groups. At timepoint B, the second sampling was conducted at 39‰ for the treatments and 18‰ for the control groups. The treatment groups were kept 21 days at 39‰ salinity for acclimation while the control groups

were still at constant salinity of 18‰. After this acclimation period sampling was conducted at timepoint C for both groups. Lastly, the salinity of the treatment groups was decreased by 1‰ per day until reaching 18‰ (within 21 days) while control groups were at constant salinity of 18‰. The last sampling at timepoint D was conducted at the end of this period (Figure 3.4, Table 3.1).

Table 3.1. Design of the experiment. Samples are RNA-Seq libraries that were constructed. Tank A and Tank B, replicates of each other, were incorporated into the model to control for batch effects. RT (Rumeli Hisarı treatment) are units where time series of salinity stress were applied, and RC (Rumeli Hisarı control) are time control units with constant salinity. Timepoint A, B, C and D were 21st, 42nd, 63rd and 84th days of the experiment, respectively.

Sample	Tank	Treatment	Timepoint	Acronym
L1	A	RT	A	ARTA
L2	A	RC	A	ARCA
L3	B	RT	A	BRTA
L4	B	RC	A	BRCA
L5	A	RT	B	ARTB
L6	A	RC	B	ARCB
L7	B	RT	B	BRTB
L8	B	RC	B	BRCB
L9	A	RT	C	ARTC
L10	A	RC	C	ARCC
L11	B	RT	C	BRTC
L12	B	RC	C	BRCC
L13	A	RT	D	ARTD
L14	A	RC	D	ARCD
L15	B	RT	D	BRTD
L16	B	RC	D	BRCD

Out of 96 specimens, we analyzed only half with RNA-Seq by pooling three samples per experimental unit for each timepoint. The other half was collected considering the chances of mortality and/or experimental problems, as backup. The amount of food and water available *per* mussel was kept constant by adjusting their volumes according to the number of live samples that remained in the tank, after the death of individual mussels during the experiments.

3.4. RNA Extraction, Library Preparation and Sequencing

The experiment was conducted between November 2016 and February 2017. For the sampling, gill tissue was dissected, finely cut into pieces and frozen at -80 °C in DNA/RNA/Protein isolation reagent (Tri Reagent). The gill tissue was used as it is shown to be responsive to environmental stress in *Mytilus* (Lockwood and Somero, 2011). Total RNA was extracted with spin column purification using Direct-Zol RNA MiniPrep Plus Kit following the manufacturer's protocol in March 2019. Extracted total RNAs were sent to Macrogen Inc. on dry ice for library preparation and sequencing. Quantification and quality control of total RNA was measured with 2200 TapeStation by Macrogen Inc. RNAs of three individuals for each library were pooled in equal quantities generating 16 RNA-seq libraries (Table 3.1) to increase library complexity and decrease inter-individual variability. Pooling averages biological variability within-group and improves detection of differentially expressed genes (Kendziorski et al., 2005; Mors et al., 2015). In differential gene expression analysis, libraries should be constructed with biological replicates for robust statistical inference (Schurch et al., 2016). Therefore, eight treatment points (condition, Table 3.2), each with a replicate (from replicated tanks, Figure 3.4, Table 3.1) was chosen for RNA-Seq. As replicates were coming from different tanks, the tank effect was incorporated into the model matrix when building the model.

Table 3.2. Design of the experiment. Conditions compared in DGE.

Conditions	Treatment	Timepoint
RT.A	RT	A
RC.A	RC	A
RT.B	RT	B
RC.B	RC	B
RT.C	RT	C
RC.C	RC	C
RT.D	RT	D
RC.D	RC	D

Library preparation was done non-stranded using TruSeq RNA Sample Prep Kit v2, following TruSeq RNA Sample Preparation v2 Guide Part # 15026495 Rev. F by Macrogen Inc. Libraries were sequenced with Illumina HiSeq2500 yielding 100 bp paired-end reads, ~1Gb/sample.

3.5. Data Analysis

During size selection in library preparation, fragment lengths are obtained as a distribution rather than a specific size, leading necessity to check for adaptor contamination in raw reads. As adaptors do not occur in genomic sequences, their existence leads to alignment errors and an increased number of unaligned reads. For the preparation of the raw reads, sequencing primers (SP1, SP2) and MID sequences (i5, i7) were removed with Cutadapt v1.16 (Martin, 2011) and low quality reads (Phred score < 15) and short reads (reads < 25 bp) were removed with Trimmomatic 0-2.38 (Bolger et al., 2014) (Figure 3.5). Quality was analyzed with FastQC v0.11.7 (Andrews, 2010) before and after removal of adaptors, and low quality and short reads.

After filtering, for comprehensive reference assembly, reads of all samples were merged. Trinity v2.8.3 (Grabherr et al., 2013) was used for constructing de novo assembly with a default k-mer size of 25. Completeness of the transcriptome was assessed by BUSCO v3 (Seppey et al., 2019), which queries the assembly against a set of single-copy orthologs present in at least 90% of the species (Waterhouse et al., 2011; Waterhouse et al., 2018). To remove redundancy, assembled transcripts were clustered with CD-HIT-EST v4.6 (Li and Godzik, 2006).

Clustered assembly was queried to the following databases with an e-value of $1x10^{-7}$ as cut-off: blastx against NCBI NR, blastx against NCBI RefSeq protein invertebrate, blastx against Swiss-Prot, blastn against NCBI NT, blastn against NCBI RefSeq RNA, blastx against TrEMBL, blastx against NCBI RefSeq protein and blastn against RefSeq genomic (Figure 3.5). At each step results without hit were selected and queried against the next database. Blastx searches were used to identify protein products in NR, RefSeq or Swiss-Prot databases. If no protein products were found, blastn searches were conducted. Open reading frames and coding sequences were checked. The contigs that did not map to protein products can be pre-mRNAs, ncRNAs or can be encountered due to contamination of genomic DNA. Contigs that had no blast hits could also be due to long non-coding RNAs (lncRNA) (Prego-Faraldo et al. 2018). Milan et al. (2011) also showed that natural antisense transcription (NAT), a category of ncRNA, constituted 10% of the transcriptome of the clam *Ruditapes philippinarum*, and this process is also observed in other bivalves. NATs were suggested to regulate the expression of sense transcripts and are involved in gene silencing (Wight and Werner, 2013).

After the blast step, OmicsBox was used for mapping and annotation (Götz et al., 2008). Transcripts were assigned enzyme commission numbers by running KEGG (Ogata et al., 1999) services from OmicsBox (2019). InterProScan was run through OmicsBox for annotation. Orthology

assignment by eggNOG mapper was also conducted (Huerta-Cepas et al., 2019). After annotation, gene set enrichment analysis (GSEA) was done through OmicsBox (2019). FDR was used as a rank metric in GSEA analysis. REVIGO (Supek et al., 2011) was used for gene ontology visualization.

For differential gene expression analysis, count files were generated following the recommended workflow of StringTie (Pertea et al., 2015) with a modification. Sample reads were mapped to de novo assembled transcriptome by HISAT2 alignment software (Kim et al., 2015). Reference annotation information was not used in the mapping process. Mapped reads were assembled using StringTie for each sample. StringTie was run with --merge option for merging assembled transcripts of samples and removing redundant transcripts. Count files were generated by HTSeq (Anders et al., 2015) with sorted mapped files of each sample and merged transcripts generated in the previous step.

A negative binomial generalized linear model was used for differential gene expression analysis using Bioconductor package edgeR (Robinson et al., 2010; McCarthy et al., 2012). For the 16 libraries that were constructed for RNA-Seq, counts per million (CPM) and log CPM transformations were used to quantify library size differences. For normalizing distributions across samples, trimmed mean of M-values (TMM) was used.

Transcripts lowly expressed or with zero counts were removed from the transcript lists for all samples. Filtering lowly expressed transcripts improves the reliability of the estimation of the mean-variance relationship of RNA-Seq count data, as variance depends on the mean of this statistic (Law et al., 2014). In edgeR, the degree of filtering can be selected by the user and should be adjusted according to the aim of the study (Chen et al., 2020). To select the degree of filtering, different filtering criteria were examined based on the general rules of filtering described below.

For a gene (contig) to be considered expressed, it should be responding to at least one condition that differential expression analyses were tested for, that is, it should be expressed in RNA-Seq libraries of that condition. For our experiment, the differential expression condition tested for was salinity stress between timepoints. In the main contrast calculations between timepoints (Table 3.3), treatment libraries were used, and control libraries were incorporated into calculations and subtracted from treatment libraries, for time control and adjustment. Hence, each group of libraries based on timepoint grouping factor (Table 3.1), consisting of four RNA-Seq libraries, represents one of the conditions of the main differential expression tests (main contrasts, Table 3.3) of this experiment. Therefore, for filtering criteria, for a contig to be kept and considered expressed, it should have a

worthwhile expression in at least four libraries for our experimental design. In order not to introduce bias, group membership of libraries is not accounted for in filtering (Chen et al, 2020).

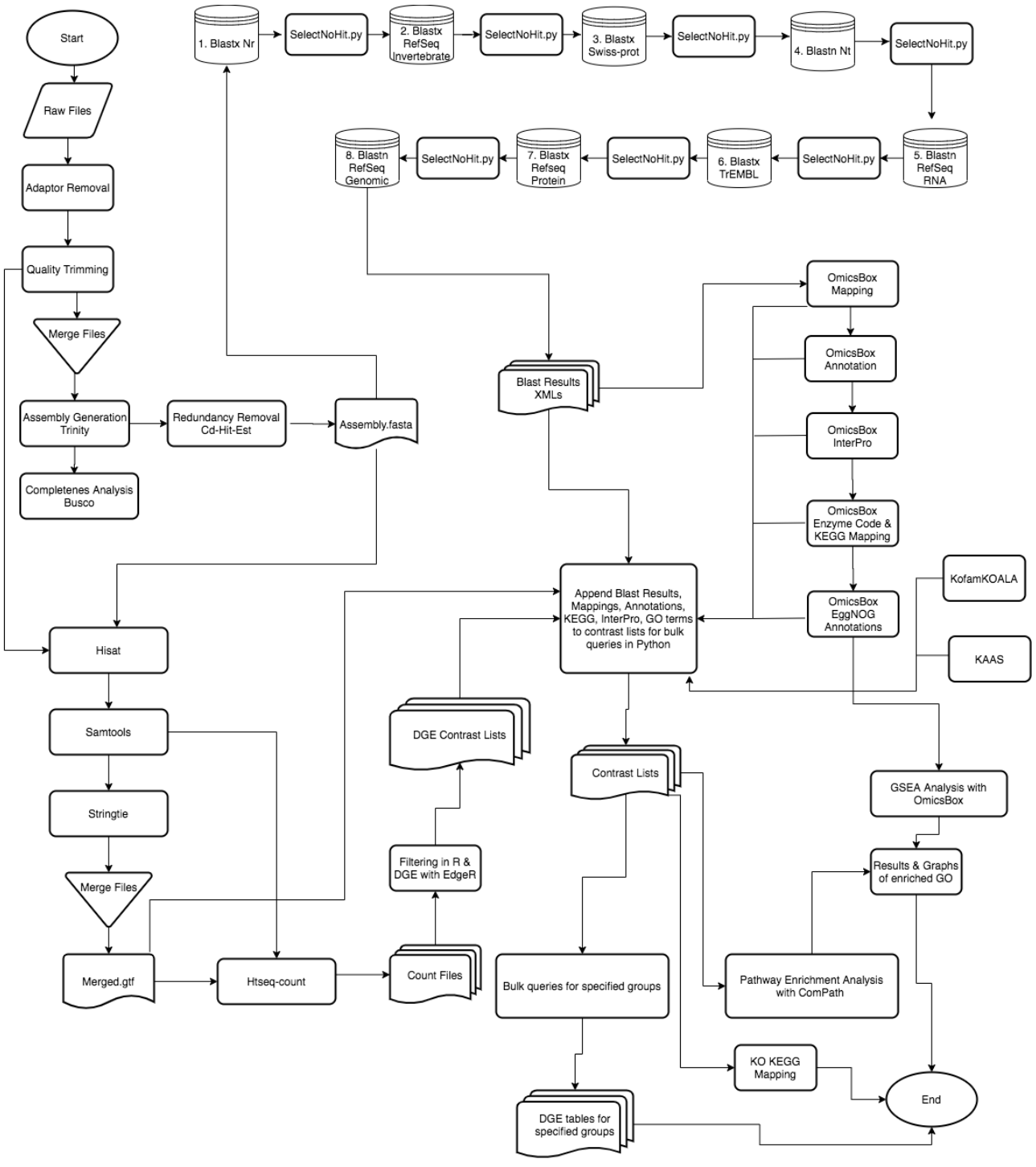


Figure 3.5. Flowchart of data analysis of the study.

The approach mentioned above was implemented by the edgeR function ‘FilterByExpr’. ‘FilterByExpr’, as its name suggests, filters genes by expression levels, keeping rows in a minimum number of samples that have “worthwhile” counts. For this study, worthwhile expression is a count value of 10 in CPM (Eq. 3.1). CPM format is used as it accounts for library size differences.

$$CPM(10) = \frac{10^6 * 10}{Average\ size\ of\ 16\ libraries} \quad (3.1)$$

Roughly speaking, 'FilterByExpr' keeps contigs having worthwhile expression in a number of samples defined by the user based on design matrix or grouping factors (Chen et al., 2016). According to Chen et al. (2020) 'scientific interest', that is differential expression analysis tested for, should determine grouping factors. As stated, the main focus of this experiment, salinity stress, was applied between different timepoints of treatment libraries and control libraries were incorporated for time control. Based on Chen et al. (2020) definition, grouping factor becomes timepoint for the purpose of this experiment. 'FilterByExpr' function, with its grouping factor defined as timepoint, keeps contigs having worthwhile expression in at least four libraries, as in any timepoint group, the smallest group size is four.

As other contrasts were also examined and the amount of filtering that can be done is not strictly defined (but is based on the aim of the study), alternative filtering options were also evaluated. Contigs having worthwhile expression in at least two libraries (as the smallest group size is two, also equivalent to 'FilterByExpr' function with design matrix), eight libraries and 15 libraries (equivalent to 'FilterByExpr' function without any arguments) were also examined**.**

After filtering, dispersion and biological coefficient of variation (BCV) were calculated. The experiment comprised a multi-factor experimental design as seen in Table 3.1. Likelihood ratio test with tagwise dispersion (as it is recommended for multi-factor experimental designs) was applied (Chen et al., 2008). False discovery rate (FDR) was adjusted by Benjamini- Hochberg method (Benjamini and Hochberg, 1995). Differential gene expression lists constructed with cut-off values of FDR < 0.05 and |LogFoldChange| > 2 for contrasts are given in Table 3.3.

Table 3.3. Contrasts differential expression analysis tested for.

Contrasts	Formula
RTvsRC	RTvsIntercept
RTvsRC.DA	(RT.D-RT.A)-(RC.D-RC.A)
RTvsRC.DB	(RT.D-RT.B)-(RC.D-RC.B)
RTvsRC.CA	(RT.C-RT.A)-(RC.C-RC.A)
Main Contrasts	
RTvsRC.BA	(RT.B-RT.A)-(RC.B-RC.A)
RTvsRC.CB	(RT.C-RT.B)-(RC.C-RC.B)
RTvsRC.DC	(RT.D-RT.C)-(RC.D-RC.C)

In this perspective two design matrixes were constructed:

1. model.matrix(~ tank + treatment + timepoint + treatment:timepoint)
2. model.matrix(~ 0 + group + tank)

model.matrix 1 was mainly used for the comparison of the treatment group to the control group (contrast RTvsRC in Table 3.3). Tank B, control groups and timepoint A were used as reference levels and adjustments were made accordingly. model.matrix 2 was constructed for pairwise comparisons given in Table 3.3. Treatment and timepoint pairs are represented as 'group' in the design matrix. Reference levels were the same as in model matrix 1 and adjustments were manually calculated as given in Table 3.3.

For pathway enrichment analysis ComPath (Domingo-Fernández et al., 2019), which works with WikiPathways (Slenter et al., 2017; Kutmon et al., 2016; Kelder et al.2012), Reactome (Fabregat et al., 2018; Croft et al., 2014) and KEGG (Kanehisa et al., 2017; Kanehisa et al., 2016, Kanehisa and Goto, 2000) databases, was used. The program identifies enriched pathways from a geneset without using a ranked list. Therefore, as genesets, differentially expressed genes having FDR < 0.05 were selected for the contrasts given in Table 3.3. Enriched pathways that have adjusted p-values lower than 0.05 were sorted in descending order according to the number of genes mapped to each pathway. As *M. galloprovincialis* is a non-model species, orthologs genes and pathways of other species were not removed from the results except for human-specific diseases, as one of the main objectives of the study is to determine target genes and pathways and check if results support previous findings.

4. RESULTS AND DISCUSSION

4.1. Descriptive Statistics and Data Validation

4.1.1. RNA Quality

For the 48 samples that were analyzed, the average RIN value was 9.3 (SD = 0.6). All RIN values were higher than 7.0, except one sample (from tank A, belonging to the treatment group at timepoint B) with a RIN of 5.7 (Figure A.1 and Table A.1, Appendix A). As mentioned in Materials and Methods 3.4. RNA Extraction, Library Preperation and Sequencing section, each of the three samples belonging to the same experimental condition was pooled that resulted in 16 RNA-Seq libraries. For each of these libraries, the average RIN values were calculated based on the constituent samples. For these final libraries, the smallest RIN value was 8 and the average RIN value was 9.3 (SD = 0.4) (Figure A.2 and Table A.1, Appendix A). rRNA ratios were not considered as *Mytilus* has molluscan type RNA profile that only has an 18S band due to a break in 28S rRNA (Muttray *et al.*, 2008).

4.1.2. Sequencing Data Quality

The next-generation sequencing of the 16 RNA-seq libraries generated a total of ~687M 100bp paired-end reads, for a total of ~69B read bases. The average number of reads per library was ~43M (SD = ~6M). The average GC content was 38.81% (SD = 0.36), which is comparable to the species GC content (Moreira et al., 2015). The average Q20 was 98.87% (SD = 0.05) and Q30 was 96.14% (SD = 0.11) suggesting very high quality of the data. Detailed statistics are provided in Table A.2 (Appendix A).

4.1.3. Data Quality Statistics

Quality checks of raw, adaptor trimmed and quality filtered data were done with FastQC. All of the FastQC criteria were passed except for per base sequence content, sequence duplication levels and overrepresented sequences, which are typical for RNA-Seq (Michigan State University, n. d.). I discuss the possible reasons behind these three parameters not passing the FastQC threshold criteria below. All of the other plots, including per base sequence quality, per tile sequence quality, per sequence quality scores, per sequence GC content, per base N content, sequence length distribution and adapter content, indicated high quality of the data.

Per base sequence content shows the proportion of nucleotides (A, T, C, G) at each position. In a random library little or no difference should be observed. However, in RNA-Seq studies, the plot is typically biased by the first 10-15 of the reads, due to random hexamer priming (Babraham Bioinformatics, n. d.). This does not have an adverse effect in downstream analyses, and cannot be corrected by trimming (Babraham Bioinformatics, n. d.).

The second threshold that was not passed, sequence duplication, measures if a library is unenriched and diverse. Ideally, in a diverse library, sequences occur only once, and duplicates indicate sequences with high coverage. Mostly, sequence duplication occurs due to PCR enrichment bias. On the other hand, expression levels of transcripts differ in RNA-Seq studies, which can result in high and low abundance of transcripts, and failure of this test (Babraham Bioinformatics, n. d.).

Overrepresented sequences also had a "warning" flag in the reports. A read is categorized as overrepresented if it comprises more than 0.1% of total sequences. An overrepresented sequence can be biologically meaningful or can indicate library contamination, such as adaptor contamination (Babraham Bioinformatics, n. d.). To check for the presence of possible adaptors, overrepresented sequences were queried against the NR database. The resultant hits were matching to *Mytilus* species ribosomal RNAs, suggesting that adaptor contamination was not likely. As these overrepresented sequences were also observed to be non-coding RNAs, they were not trimmed. In addition, even though polyA selection was used in the library preparation step, it is normal for a small amount of ribosomal RNA to remain (Sims et al., 2014). To check for possible rRNA contamination, the amount of ribosomal RNA was examined using SortMeRNA (Kopylova et al., 2012) software. rRNA sequences for SILVA (Quast et al., 2013), SSURef_NR99, and LSURef_NR99 databases were used for this purpose. An average of 2.7 % (SD = 0.7) of reads was mapped to rRNA considering all of the libraries, indicating an acceptable level of ribosomal RNA contamination (Table A.3 and Table A.4, Appendix A).

4.1.4. Assembly Statistics

The quality and completeness of the assembly statistics are given in Table 4.1. De novo assembly of all libraries generated 834,295 trinity contigs, with an average contig length of 747.53 bp. A total of ~624M bases assembled with an N50 statistic value of 1,213. BUSCO analysis that shows the completeness of the assembled transcriptome was undertaken with the metazoa_odb9 reference database and resulted in a score of 99.8% (976 complete orthologs), and there were 0.2% (2) fragmented orthologs and no missing orthologs.

Table 4.1. Completeness and quality statistics of the assembly.

Trinity Statistics	BUSCO Result
Total trinity 'genes': 438,285 Total trinity transcripts: 834,295 Percent GC: 34.15 Stats based on ALL transcript contigs: Contig N10: 4712 Contig N20: 3147 Contig N30: 2277 Contig N40: 1679 Contig N50: 1213 Median contig length: 400 Average contig: 747.53 Total assembled bases: 623656913 Stats based on ONLY LONGEST ISOFORM per 'GENE': Contig N10: 3703 Contig N20: 2271 Contig N30: 1496 Contig N40: 1006 Contig N50: 703 Median contig length: 338 Average contig: 562.46 Total assembled bases: 246519298	C:99.8%[S:25.1%,D:74.7%],F:0.2%,M:0.0%,n:978 976 Complete BUSCOs (C) 245 Complete and single-copy BUSCOs (S) 731 Complete and duplicated BUSCOs (D) 2 Fragmented BUSCOs (F) 0 Missing BUSCOs (M) 978 Total BUSCO groups searched

Clustering of assembled contigs with CD-HIT-EST resulted in 493,815 contigs, with an average contig length of 629.40 bp, and the total number of assembled bases was 310,805,708. The number of contigs over 5 Kb in length was 2,883, and the longest contig length was 36,320 bp.

4.1.5. Mapping and Alignment Statistics

Libraries were aligned to the de novo assembly (of our 16 libraries) using HISAT2 (Kim et al., 2015). All libraries had an overall alignment rate of > 85%. The average alignment was 87.12% (SD = 0.91) (Table A.4.1, detailed alignment statistics are given in Table A.4.2 in Appendix A).

Bam file statistics were calculated using Samtools (Li et al., 2009) -depth and -flagstat (Table A.4.3, Appendix A) commands. Coverage statistics are given in Table 4.2. Average breadth of coverage was 41% (SD = 3), calculated as the total number of covered bases divided by the reference assembly length (310,805,708). The average depth was ~9X (SD = 0.9) and was calculated as the total number of bases of all mapped reads divided by reference assembly length (310,805,708). Average mean read depth was 21.22 (SD = 1.7) and was calculated as the total number of bases of all mapped reads divided by the total number of covered bases.

Table 4.2. Coverage statistics.

Libraries	Mean Read Depth	Total number of bases mapped	Depth of Coverage	Total number of covered bases	Coverage breadth (%)
Library1	17.69	2,243,870,263	7.22	126,861,950	40.82
Library2	20.00	2,533,477,425	8.15	126,698,918	40.76
Library3	20.63	2,896,794,769	9.32	140,424,176	45.18
Library4	22.89	2,975,010,965	9.57	129,983,211	41.82
Library5	21.25	2,805,784,670	9.03	132,044,257	42.48
Library6	20.47	2,216,844,694	7.13	108,293,392	34.84
Library7	20.12	2,646,586,303	8.52	131,539,684	42.32
Library8	20.80	2,530,133,003	8.14	121,646,153	39.14
Library9	24.57	2,863,398,353	9.21	116,563,228	37.50
Library10	22.52	2,946,733,038	9.48	130,844,846	42.10
Library11	19.83	2,799,871,434	9.01	141,179,880	45.42
Library12	21.22	2,606,269,257	8.39	122,800,661	39.51
Library13	20.75	2,331,678,758	7.50	112,365,376	36.15
Library14	21.25	2,741,405,563	8.82	129,021,444	41.51
Library15	24.24	3,244,688,673	10.44	133,832,240	43.06
Library16	21.34	2,518,205,118	8.10	118,017,982	37.97
Total		42,900,752,286	138.03		
Average	21.22	2,681,297,017.88	8.63		40.66
SD	1.70	282,173,683.51	0.91		2.99

4.1.6. Annotation Statistics

Among 493,815 contigs of the assembly, 144,459 had blast hits. After results were imported to Omicsbox, 143,999 contigs with blast hits remained, and 80,507 of these were mapped. The most blast hits were found in *C. virginica*, followed by *Mizuhopecten yessoensis, C. gigas*, and *M. galloprovincialis*. On the other hand, *M. galloprovincialis* was the most prominent species in the top hit species distribution, followed by *M. yessoensis, C. virginica and C. gigas*. Orthology assignment, undertaken by eggNOG mapper, resulted in 87,900 contigs. When eggNOG mapper results were merged, the number of GOs assigned increased from 85,837 to 480,376, and the number of ECs assigned increased from 8,789 to 57,565. Annotation statistics of de novo assembly are given in Table 4.3.

Considering the second level functional annotation for biological process category, “cellular process” (39,970), “metabolic process” (31,258), “biological regulation” (25,352), “regulation of biological process” (23,901), and “response to stimulus” (20,723) were enriched (Figure 4.1). Top GOs for the molecular function category were “binding” (44,586) and “catalytic activity” (24,834)

(Figure 4.1). For the cellular component category, “cellular anatomical entity” (35928) and “intracellular” (23,149) were enriched (Figure 4.1).

Table 4.3. Annotation statistic of de novo assembly.

Annotation Statistics	Number of contigs
Contigs with blastx hit to NR	116,225
Contigs with blastx hit to RefSeq Invertebrate	3,485
Contigs with blastx hit to Swiss-Prot	103
Contigs with blastn hit to NT	20,792
Contigs with blastn hit to RefSeq RNA	39
Contigs with blastx hit to TrEMBL	584
Contigs with blastx hit to RefSeq Protein	22
Contigs with blastn hit to RefSeq Genomic	3,209
Total of blast hits	144,459
Contigs with InterProScan	108,887
Contigs with EggNOG	87,900
Contigs with Blast Hits	143,999
Contigs with Mapping	80,507
Contigs with GO Annotation	69,399

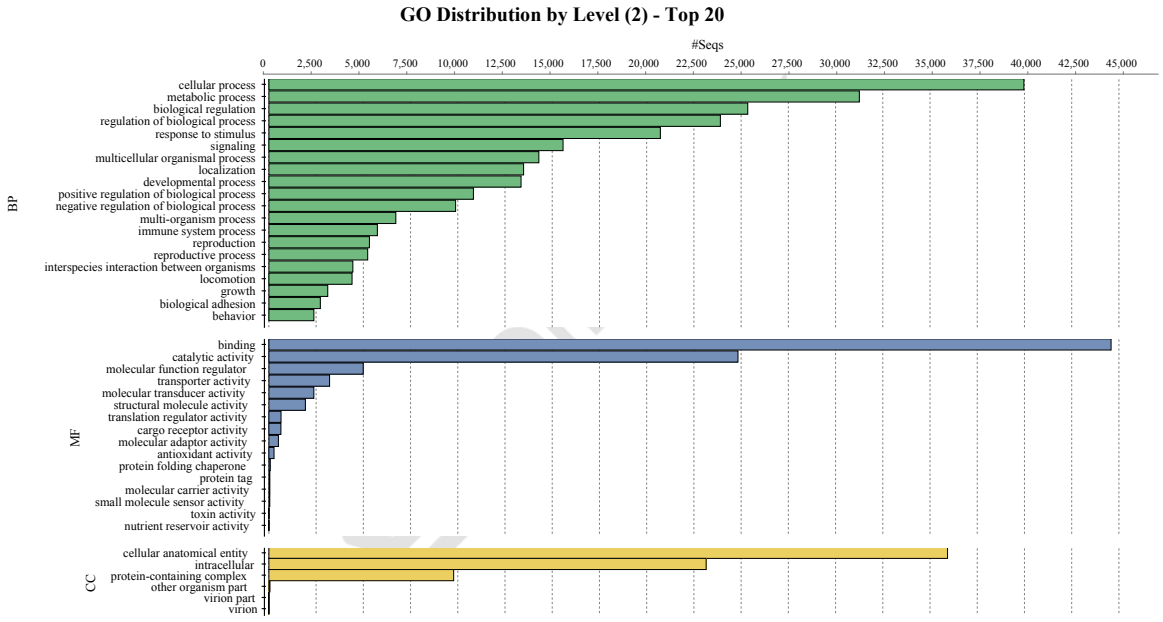


Figure 4.1. Second level functional annotation of assembled contigs based on gene ontology for biological process, molecular function and cellular component categories.

Enzymes are categorized into oxidoreductases, transferases, hydrolyses, lyases, isomerases and ligases. Most abundant forms of enzymes, hydrolases, transferases and oxidoreductases (Creative Enzymes, n. d.) were also the most abundant categories found in the assembly (Figure 4.2). 13,396

contigs were assigned to hydrolase enzymes that catalyze bond cleavages of compounds and oxidoreductase enzymes, by using water (Alberty, 2005). 4,060 contigs were assigned as transferases, which transfer groups from donor to acceptor such as methyl, carboxyl or amine groups (Alberty, 2005). And lastly, oxidoreductases that catalyze redox reactions (Alberty, 2005) were assigned to 1,612 contigs. Less common groups of enzymes, translocases which assist movement of molecules by ATP hydrolysis (Uniprot, n.d. (a)), isomerases which catalyze the interconversion of isomers of a molecule (Cuesta et al. 2016), lyases which cleave bonds other than hydrolysis and oxidation (Mahdi and Kelly, 2008), and ligases which catalyze joining of two molecules (Manubolu et al., 2018) were assigned to 419, 406, 398 and 304 contigs, respectively.

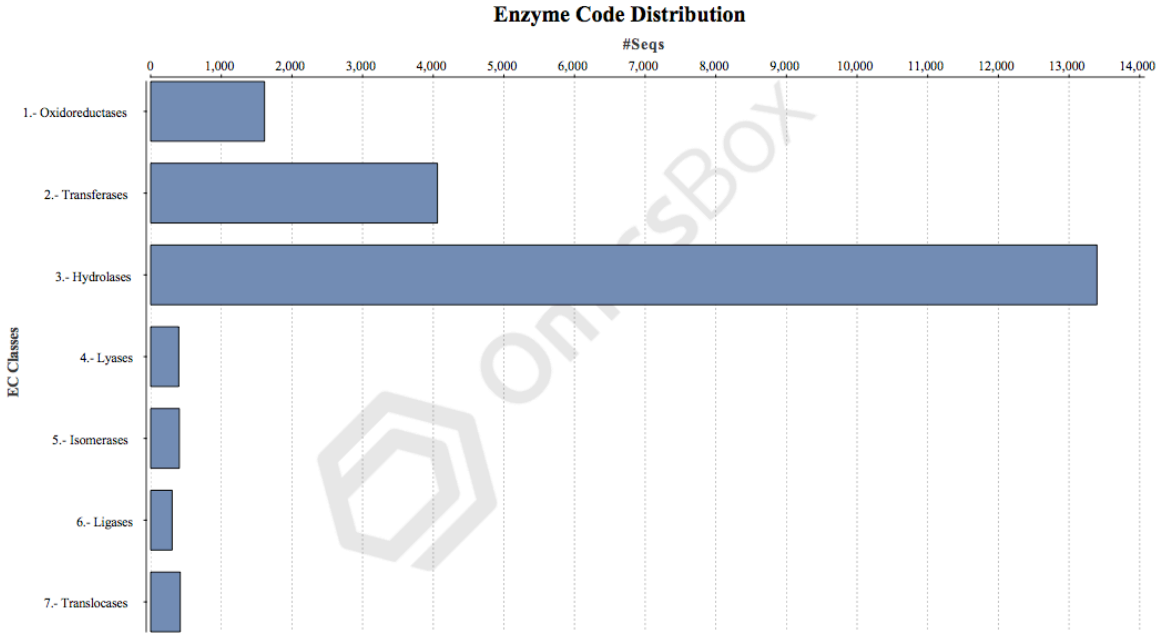


Figure 4.2. KEGG ontology distribution of enzymes.

4.1.7. Differential Gene Expression Data Preparation Statistics

Filters were compared in terms of the number of genes in significant lists at 5% FDR and p-value histograms of the main contrasts. Filters that keep contigs having worthwhile expression in at least 2, 4, 8 and 15 libraries were named as F2, F4, F8 and F15, respectively. There was a total of 237,591 contigs for all libraries combined. 3,797 contigs with zero counts were removed for all filters. Lowly expressed contigs were removed, as mentioned above, and filtering results are given in Table 4.4.

Table 4.4. Statistics of the applied filters.

	F2	F4	F8	F15
Number of contigs filtered	103,785	151,174	182,779	207,230
Number of contigs left	130,009	82,620	51,015	26,564
Common dispersion	1.36	1.02	0.6	0.2
BCV	1.17	1.01	0.77	0.45

The F4 filter had the highest number of contigs in significant lists for the main contrasts (Table 4.5). For example, for the contrast RTvsRC.BA, the total number of contigs up-regulated and down-regulated at 5% FDR for filters F2, F4, F8, and F15 were 500, 660, 368, and 73, respectively (Table 4.5). With the filter F15, very few contigs were left at 5% FDR: for instance the main contrast RTvsRC.BA had only 58 contigs with blast hits. When the number of significant contigs was considered, the most preferable filtering scheme was F4.

Table 4.5. Number of contigs that were up-regulated and down-regulated at 5% FDR of the contrasts (Table 3.3) for the different filter categories. EdgeR 'decideTests' (Ritchie et al., 2015) function was used for the calculations.

at 5% FDR		RTvsRC.BA	RTvsRC.CA	RTvsRC.CB	RTvsRC.DA	RTvsRC.DB	RTvsRC.DC	Total
F2	Down	286	206	249	138	239	207	
	Up	214	166	234	114	240	284	
	Total	500	372	483	252	479	491	2,577
F4	Down	392	221	256	173	293	201	
	Up	268	123	234	128	294	315	
	Total	660	344	490	301	587	516	2,898
F8	Down	202	116	174	80	184	128	
	Up	166	62	133	64	197	213	
	Total	368	178	307	144	381	341	1,719
F15	Down	42	17	22	7	51	41	
	Up	31	13	28	8	89	60	
	Total	73	30	50	15	140	101	409

P-values of gene-wise likelihood ratio test for contrasts were plotted to evaluate the overall distribution of contigs. The most preferable p-value histogram is where values get denser near zero, representing differentially expressed genes (Gonzalez, 2014). Genes that are not differentially expressed exhibit a uniform spread from 0 to 1. Bimodal (U-shaped) p-value histograms can also be acceptable for RNA-Seq, as genes having low counts take discrete values and increase in frequency near 1 (Gonzalez, 2014). When examining p-value histograms of the main contrasts, the left peak of the histogram compared to other bars was the highest in the timepoint grouping (F4), indicating

significant genes (Figure 4.3 and Figure A.3, A.4, A.5 and A.6 in Appendix A). In F8 and F15, in some of the main contrasts, the histograms showed a trend of increase when approaching 1 (RTvsRC.CA and RTvsRC.DA in A.4.3 and A.4.4, Appendix A). With the design matrix filtering (F2), high enrichment near the value of one was observed in p-value histograms of the main contrast (Figure 4.3 and Figure A.3, Appendix A). Therefore, again, the filter based on timepoint grouping (F4) was preferable when p-value histograms were considered.

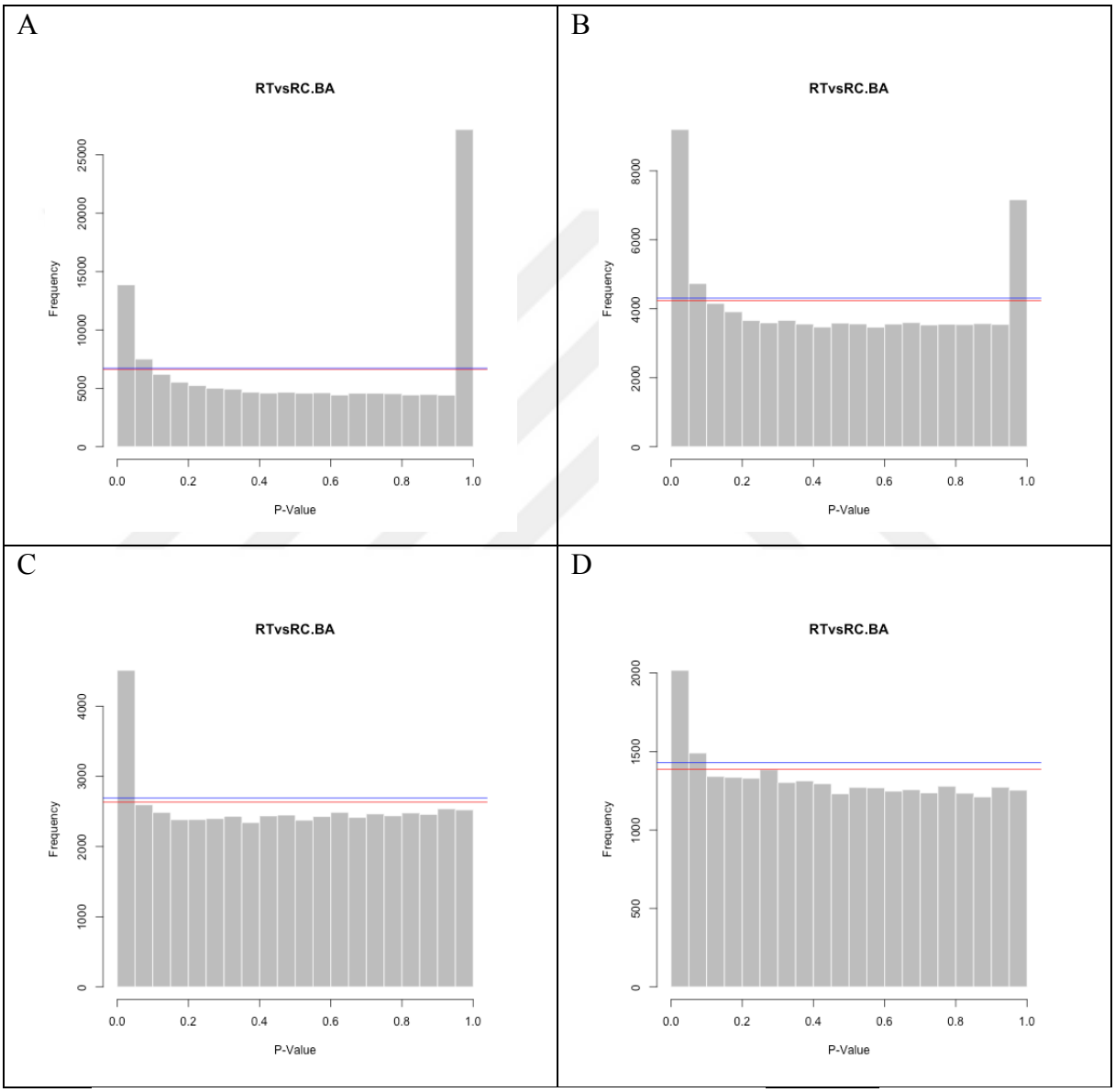


Figure 4.3. P-value histogram of the main contrast RTvsRC.BA (Table 3.3) with different filters. Filters, F2, F4, F8 and F15 are labeled as A, B, C and D, respectively. Higher criticism threshold line, calculated as qbinom(0.95, length(pValues), 0.05) (R Core Team, 2019), is in red. Quality control threshold line, calculated as qbinom(1 – 0.05*0.05, length(pValues), 0.05), is in blue (Breheny et al., 2018).

As a result of the evaluations above, the filter based on timepoint grouping factor (F4) was chosen. In an initial MDS analysis, L9 (ARTC, Table 3.1) was not clustered with the other samples as expected (Figure 4.4B), however it was not removed from the subseqent analyses for two reasons. Firstly, the amount of variance explained in the first two dimensions and other dimensions of MDS plot was examined. In experimental designs with multiple factors like the one in this project, examination of dimensions other than the first two is suggested (Law et al., 2016). Clustering in any of these dimensions indicates that they could be contributing to expression differences and it might be desirable to keep them in the linear model (Law et al., 2016).

According to Figure 4.4, the first dimension was only explaining 0.08 of the variance. Other dimensions (2-8) were also explaining similar levels of variance (around 0.07) in each, and also being parallel to the first one rather than being orthogonal (Figure 4.4A). When other dimensions' pairwise MDS plots were examined, L9 was not separated like in the first dimension, although explaining similar levels of variance (Figure 4.4B-G). Therefore, it was concluded that L9 contributes to expression difference, comprising the main argument for not removing it from the study.

And secondly, incorporation of L9 did not change BCV and dispersion values (actually its removal slightly increased the already high dispersion: when the analysis was run without it, common dispersion and BCV increased to 1.11 and 1.05, respectively). Dispersion is the BCV squared which shows the true abundance of gene variability between replicates. Common dispersion was high, indicating high variability of the samples. Common dispersion was 1.02 and BCV was 1.01 (Figure A.7, Appendix A). Since dispersion is not the same for all genes, gene-wise dispersion was used in the final model-fitting.

Before filtering, average, minimum and maximum library sizes were 14,982,107 (SD = 1,798,216), 11,644,588, and 18,415,555, respectively. After filtering, 14,174,023 (SD = 1,684,538), 10,996,814, and 17,457,548 were obtained for these values. Distribution graphs are given in Figure 4.5. Counts followed expected patterns in the distribution graphs. Filtering and normalization ensured more uniform (Figure 4.5B) and similar (Figure 4.5C) log CPM distributions throughout libraries. After filtering, differential gene expression lists were constructed for contrasts in Table 3.3, with cut-off values of FDR < 0.05 and |LogFoldChange| > 2. Subsequently, a total of 2944 genes, 2034 of them being unique, were left in the significant gene lists of the main contrasts after the cut-off. KofamKOALA (Aramaki et al., 2020), EggNOG (Huerta-Cepas et al., 2019) and KAAS (Moriya et al., 2007) mappings were added for KEGG Orthology (KO). Regulation tables for differentially

expressed genes of contrasts were prepared based on contigs and KO terms. Finally, KEGG maps were created and colored based on net log-fold change of unique KO terms.

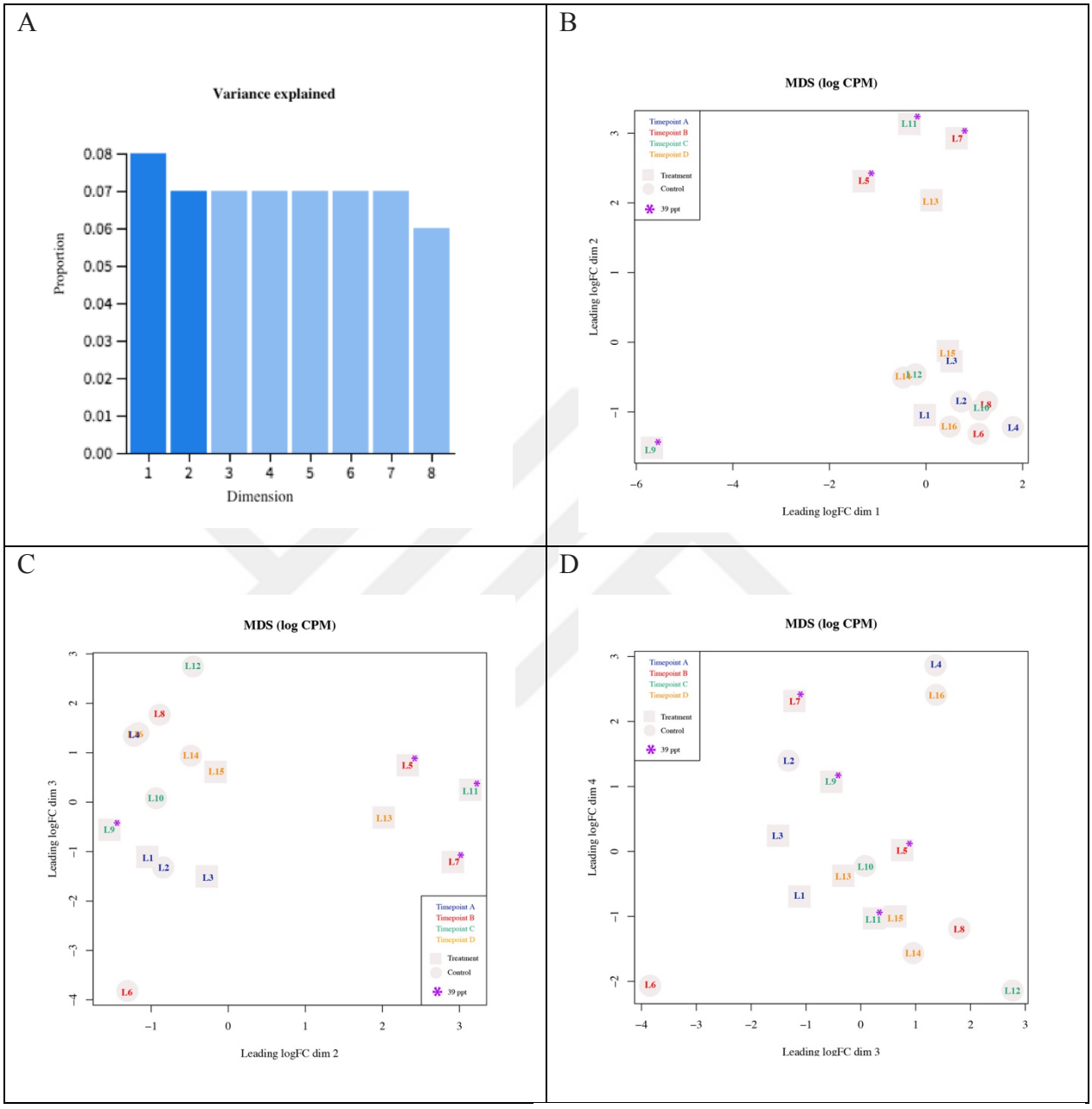


Figure 4.4. Multidimensional MDS graphs for dimensions. Variance explained for dimensions is also given.

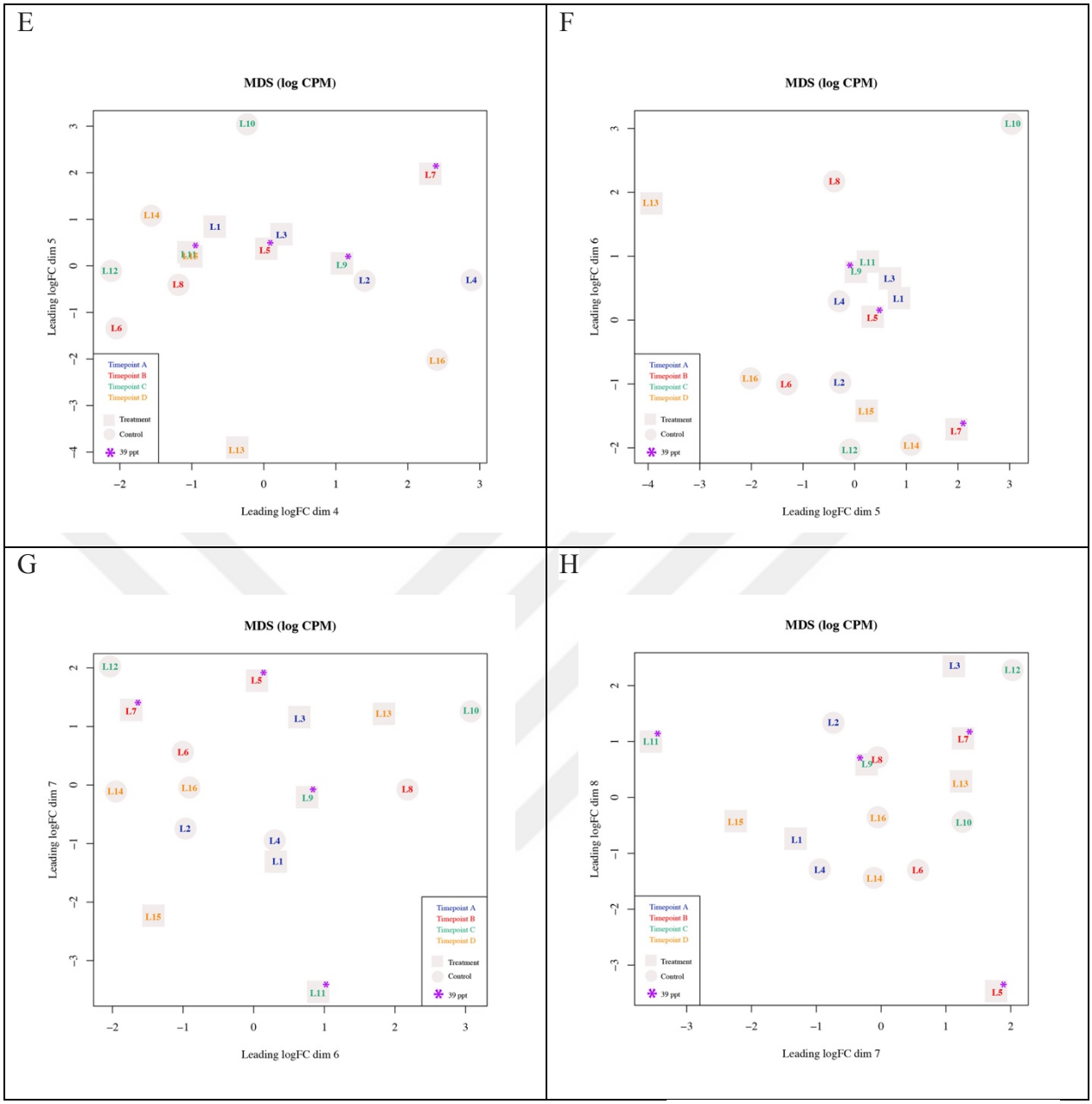


Figure 4.4 continued. Multidimensional MDS graphs for dimensions. Variance explained for dimensions is also given.

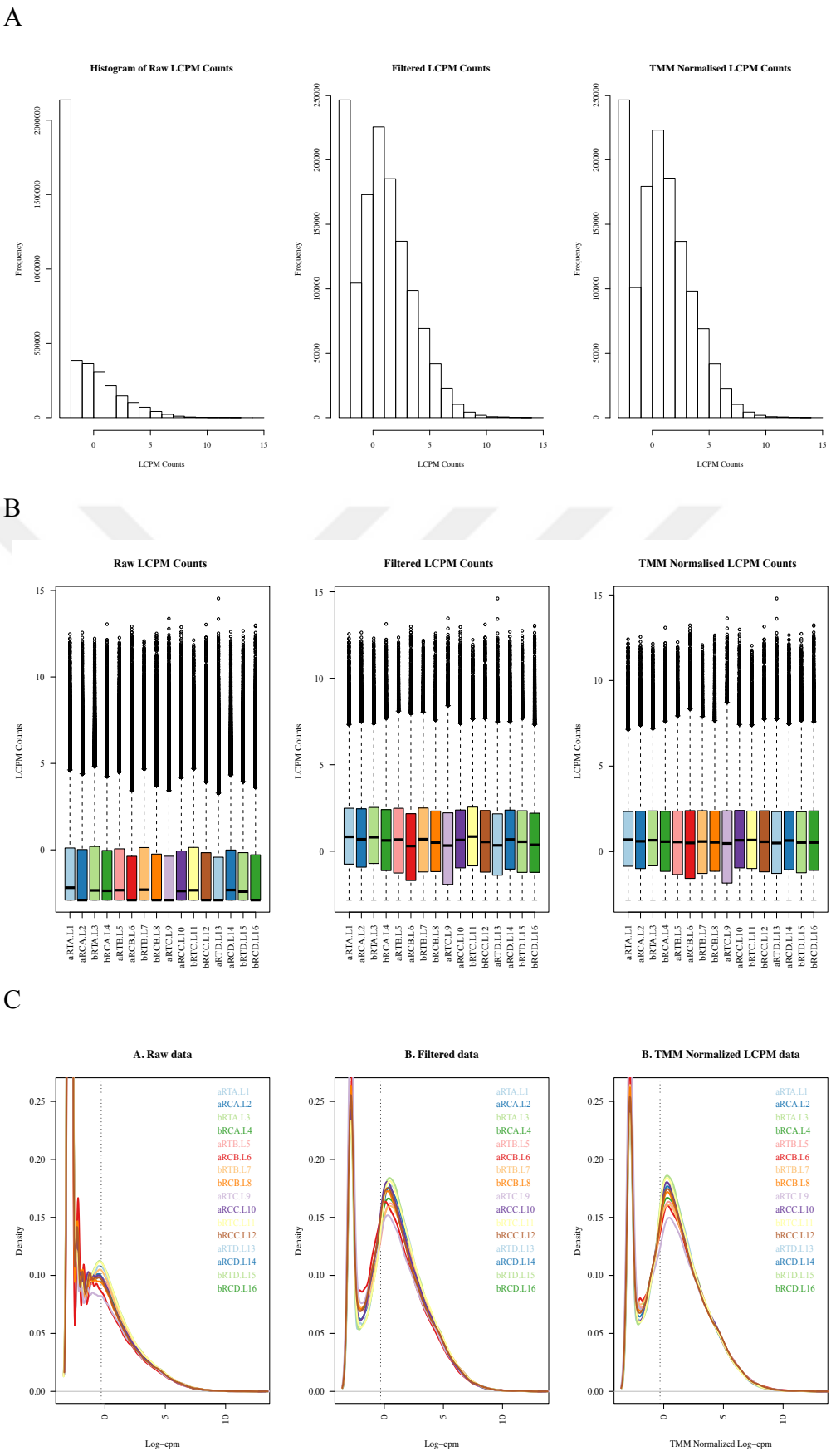


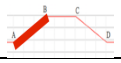
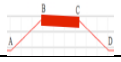
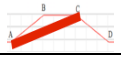
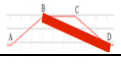
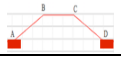
Figure 4.5. Distrubition of the libraries before and after filtering. On the bottom graph, the dotted line is the log-CPM cut-off used in the filtering step.

The MD plots (Figure A.8, A.9 and A.10, Appendix A), p-value histograms (Figure A.3, A.4, A.5 and A.6 in Appendix A), volcano plots (Figure A.11, A.12 and A.13, Appendix A) and heatmaps (Figure A.14, A.15 and A.16, Appendix A) were calculated for all contrasts in Table 3.3. Symbols of contigs of heatmaps were labeled based on blast and KO mappings. If a symbol was not assigned to a contig, blast GI identifiers were used for labeling. Significant contigs were selected for each contrast and log CPM values of these contrasts for related libraries were used for drawing heatmaps, as suggested by EdgeR (Chen et al., 2020).

4.2. Differential Gene Expression

To understand *M. galloprovincialis* genomic adaption and the plasticity of its response to long-term salinity stress, differentially expressed (D.E.) genes in response to gradual salinity increase, acclimation and decrease were examined (Table 4.6). RTvsRC was examined for examining D.E. genes between treatment and control groups. RTvsRC.BA, RTvsRC.CB and RTvsRC.DC were examined for D.E. genes involved in adaptation to salinity increase from home condition, acclimation to high salinity stress, and returning to home condition, respectively. Genes that were D.E. in these contrasts were also checked in significant lists of contrasts, namely RTvsRC.DA, RTvsRC.DB, RTvsRC.CA and RTvsRC (Table 4.6). The hypothesized model for regulations are given in Figure 4.6.

Table 4.6. Contrasts differential expression analysis tested for.

Contrasts	
RTvsRC.BA	
RTvsRC.CB	
RTvsRC.DC	
RTvsRC.CA	
RTvsRC.DB	
RTvsRC.DA	
RTvsRC	

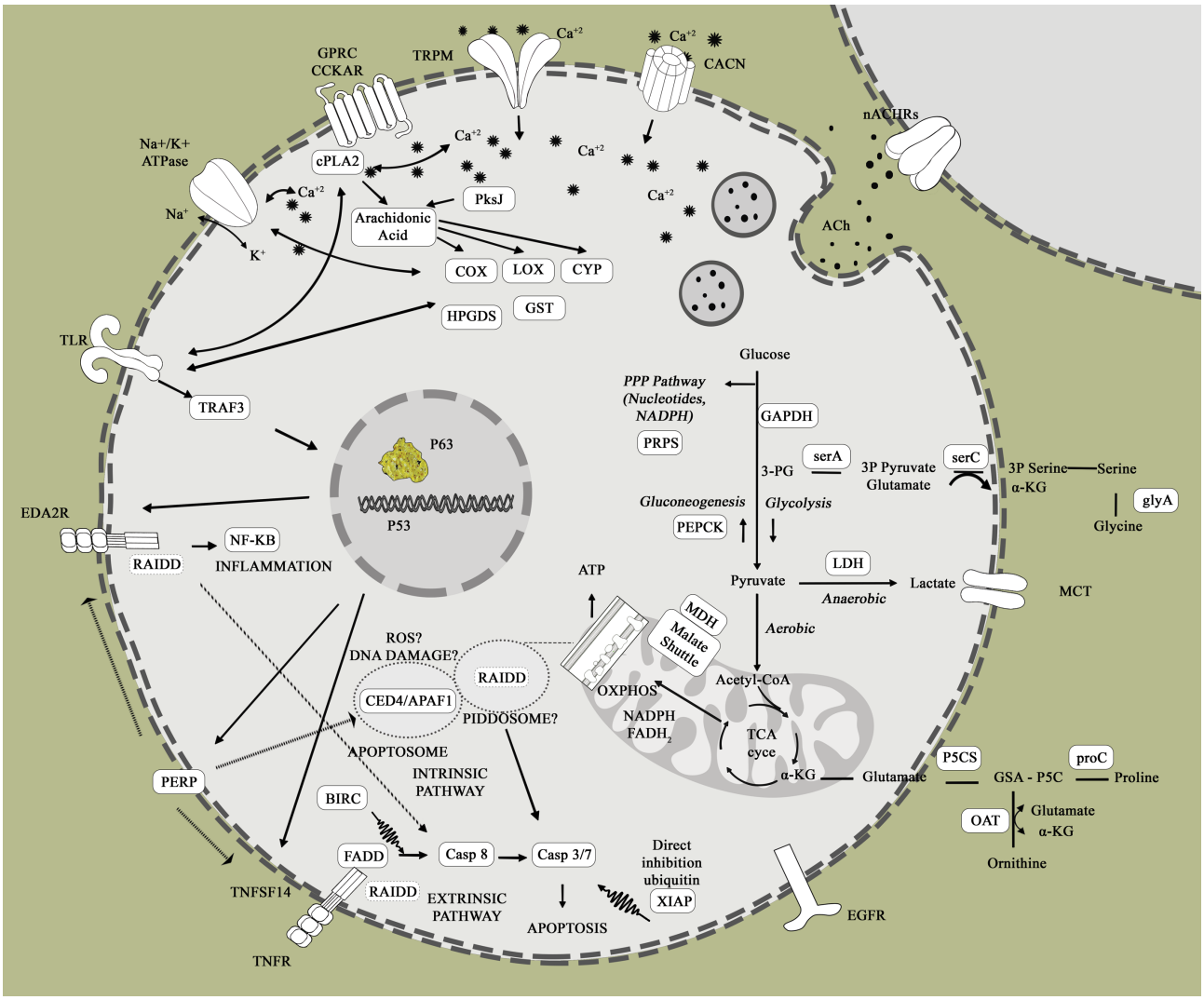


Figure 4.6. The hypothesized model of the study.

4.2.1. Energy Metabolism and Salinity

Osmoconformers have an osmotic concentration of internal fluids that is equal to the surrounding environments. However, for various reasons, osmolyte composition within and outside of the cells can be different and this requires regulation through energy allocation to preserve cell volume and integrity. Regulation of cell volume is mainly enhanced by nitrogen metabolism in bivalves which increases demands of oxidative metabolism, and mobilization of reserves and oxygen consumption rates (Peteiro et al., 2018). In aerobic organisms, energy is harnessed through the process of oxidative phosphorylation (Berg et al., 2002b), and therefore, it is critical to examine oxidative phosphorylation genes to understand the ongoing processes in energy metabolism. In addition, genes involved in carbohydrate, lipid, nucleotide, amino acid, and glycan metabolisms are critical components of energy metabolism and therefore are examined in this section (Table 4.7).

High salinity is associated with low energy expenditure and vice versa in *Mytilus* species (Freitas et al., 2017; Riisgard et al., 2013; Tedengren and Kautsky, 1986; Tedengren and Kautsky, 1987; Sanders et al., 2018). In this study, in agreement with the literature, metabolism genes in D.E. lists indicate high glycolytic and metabolic rate at steady state, when compared to high salinity. Increase in salinity generally caused downregulation of genes of metabolism and translation, as explained in greater detail below. Chronic salinity decrease also supported high energy expenditure of low salinity with carbohydrate catabolism for energy production. Detailed examination of genes regulated for these categories is explained below.

4.2.1.1. Oxidative phosphorylation. Oxidative phosphorylation is the last stage of cellular respiration and is the main process for ATP generation in aerobic organisms that synthesize massive amounts of ATP (Berg et al., 2002b). In the electron transport chain of mitochondria, NADH and $FADH_2$ (Figure 4.7(1)) are oxidized and their electrons are transferred through electron carriers, in the end reducing O_2 to water (Figure 4.7(2)). The generated energy is used to pump protons from matrix to intermembrane space (Figure 4.7(3)) leading to an electrochemical gradient generating chemiosmotic potential, referred to as protonmotive force (Jastroch et al., 2010). Protonmotive force drives a flow of protons back to the matrix through ATP synthase and is used in ADP phosphorylation (Figure 4.7(4)).

All of the contigs involved in oxidative phosphorylation were downregulated in BA(↑) (↑ indicates that salinity was increased from 18‰ to 39‰ between the two time points B and A). Downregulation with increasing salinity indicates a decrease in metabolic rate and energy production compared to the steady-state. The contigs related to oxidative phosphorylation that were D.E. in the study mainly included ATPases and transporters. Specifically, the D.E. ATPases were F-type H^+-transporting ATPase subunit delta (ATPeF1D, K02134), F-type H^+-transporting ATPase subunit d (ATPeF0D, K02138) and V-type H^+-transporting ATPase (ATPeV0C, K02155), and transporters were solute carrier family 25 (mitochondrial uncoupling protein), member 27 (SLC25A27, UCP4, K15112) and solute carrier family 25 (mitochondrial adenine nucleotide translocator), and member 4/5/6/31 (SLC25A4S, K05863). Regulation of these contigs are given in Table 4.7 and are explained in greater detail below.

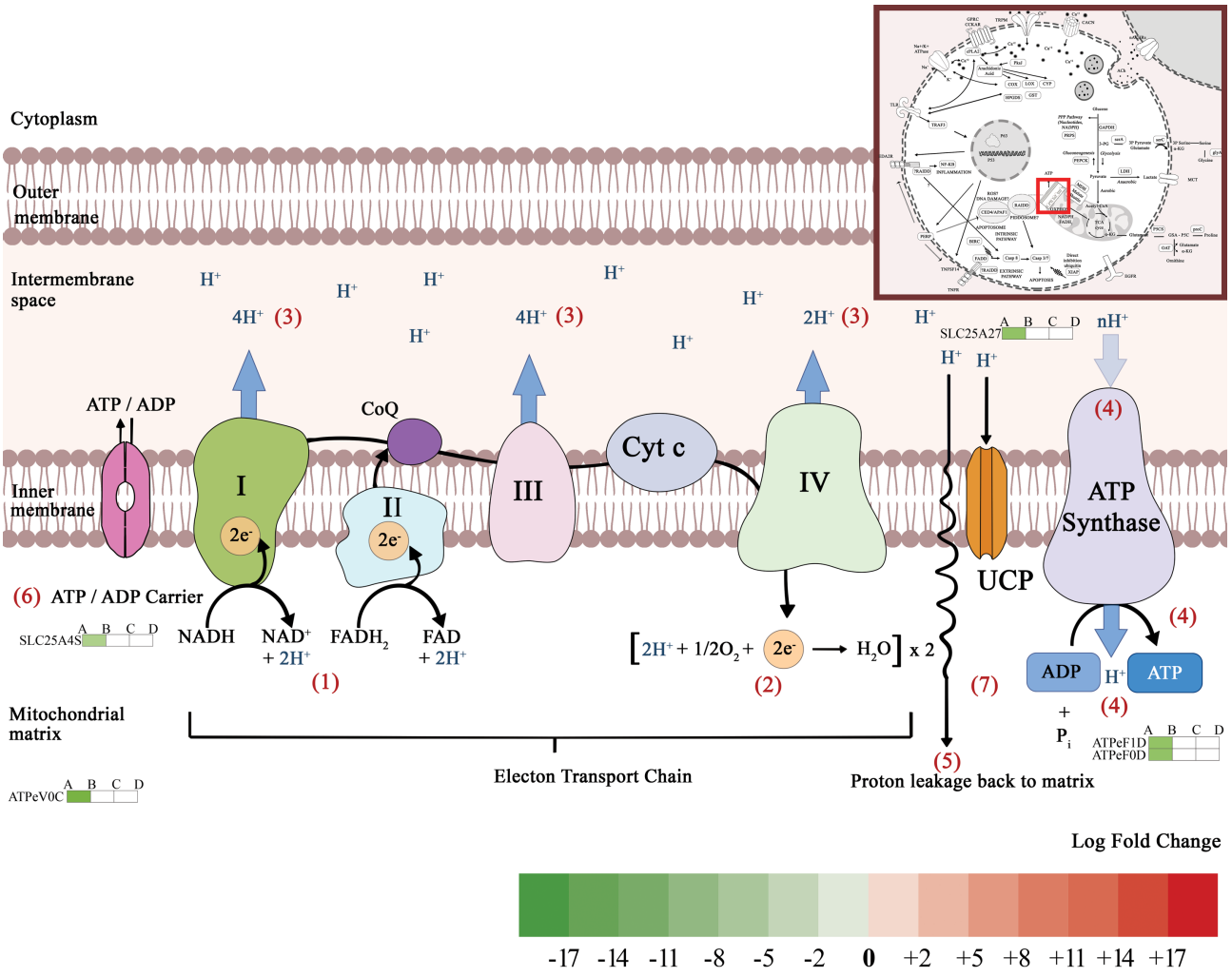


Figure 4.7. Electron transport chain in oxidative phosphorylation (modified from BioRender, 2021). In the legend, green and red colors represent downregulation and upregulation with higher color intensity denoting greater log-fold change.

Table 4.7. Regulation of contigs that were involved in oxidative phosphorylation. In the legend, green and red colors represent downregulation and upregulation with higher color intensity denoting greater log-fold change.

	Symbol	Name	RTvsRC.BA logFC	RTvsRC.BA FDR	RTvsRC.CB logFC	RTvsRC.CB FDR	RTvsRC.DC logFC	RTvsRC.DC FDR	RTvsRC.CA logFC	RTvsRC.CA FDR	RTvsRC.DB logFC	RTvsRC.DB FDR	RTvsRC.DA logFC	RTvsRC.DA FDR	RTvsRC logFC	RTvsRC FDR
Oxidative phosphorylation	ATPeV0C	V-type H+-transporting ATPase 16kDa proteolipid subunit	-12.410177	6.41E-03												
	ATPeF1D	F-type H+-transporting ATPase subunit delta	-8.889290	4.66E-02												
	ATPeF0D	F-type H+-transporting ATPase subunit d	-8.525942	4.05E-02												
Transporters	SLC25A27	solute carrier family 25 (mitochondrial uncoupling protein), member 27	-9.809311	3.07E-03							9.329050	6.24E-03				
	SLC25A4S	solute carrier family 25 (mitochondrial adenine nucleotide translocator), member 4/5/6/31	-6.311012	4.66E-02												

-17 -14 -11 -8 -5 -2 0 +2 +5 +8 +11 +14 +17

ATPases

ATPases involved in oxidative phosphorylation were downregulated in BA(↑) (Table 4.7). Among these, ATPeF0D and ATPeF1D are F-ATPases (ATP synthases) that are found in mitochondria, chloroplasts, and bacterial plasma membranes. In oxidative phosphorylation (mitochondria) or photosynthesis (chloroplasts), ATP is synthesized from ADP and Pi by ATP synthases, driven by an electrochemical proton gradient, as stated above. As ATP synthases are involved in synthesizing ATP in oxidative phosphorylation, downregulation in BA(↑) shows higher energy production at timepoint A when compared to timepoint B.

Another ATPase, also downregulated in BA(↑) was a V-ATPase, ATPeV0C (Table 4.7). ATPeV0C not only participates in oxidative phosphorylation but also is involved in diverse processes such as endocytosis and protein degradation (Toei et al., 2010). It is an ATP-driven proton pump that produces a proton gradient and mediates acidification of intracellular compartments in eukaryotic cells containing acidification of cytosol and extracellular space (Jäättelä and Kallunki, 2016). It is also needed for low pH and calcium homeostasis in lysosomes. H^+ concentration is very important in affecting transmembrane electrochemical gradients, ATP synthesis, and transport processes (Wessner et al., 2018). For example, lactate generated by anaerobic metabolism is transported between cells by monocarboxylate transporters (MCTs) through cotransport of H^+ that serves as a signal for metabolic processes (Deitmer et al., 2019). Besides ATP synthesis, downregulation in BA(↑) was also probably important for lactate transportation, altered metabolism and pH homeostasis, as discussed in greater detail below.

Transporters

Oxidative phosphorylation can also reflect reactive oxygen species (ROS) production, as ROS can be generated as byproducts of aerobic metabolism. In the electron transport chain, electrons can leak before reducing oxygen to water. These electrons can react with oxygen and form superoxide radicals, which in turn can generate the highly reactive hydroxyl radicals (Halliwell and Gutteridge, 2015). Like electrons, protons can also leak back to the matrix (Figure 4.7(5)) rather than passing through ATP synthase, which results in a decrease in the protonmotive force. Research shows that superoxide formation is negligible below a threshold of protonmotive force and exponentially increases once above that threshold (Papa and Skulachev, 1997). Therefore, a small decrease in protonmotive force can switch off superoxide accumulation, referred to as ‘mild uncoupling’, without significant effects on ATP production (Papa and Skulachev, 1997). Mitochondrial uncoupling

proteins (UCPs) facilitate proton leaks (Figure 4.7(7)) and attenuate protonmotive force, thus decreasing ROS generation (Azzu and Brand, 2010). For example, in neurons that have high mitochondrial ATP synthesis, high ATP consumption and turnover, leakage of protons back to the matrix by UCPs (UCP4 and UCP5) decreases ROS formation with little impact on membrane potential and ATP generation (Ramsden et al., 2012). By decreasing ROS, UCPs protect cells from oxidative stress (Ramsden et al., 2012). In this study, contig mapping to UCP4 (SLC25A27) was also assigned the gene ontology term 'response to oxidative stress' (GO:0006979). SLC25A27 was downregulated in BA(↑) and upregulated in DB(↓), in the same direction with oxidative phosphorylation genes, probably decreasing ROS generation in the electron transport chain and helping protect the cell from oxidative stress (Table 4.7).

Another transporter downregulated in BA(↑) (Table 4.7) that is related to oxidative phosphorylation was the ADP and ATP carrier protein, SLC25A4S (Figure 4.7(6)). ADP, ATP carrier proteins import ADPs and export ATPs across the inner membrane of the mitochondria (Mehnert et al., 2014). To synthesize ATP, ADP is needed, and ADP/ATP exchange is vital for the operation of oxidative phosphorylation (Traba et al., 2009 cited in Mehnert et al., 2014). Downregulation of this contig also supports downregulation of ATP synthases and indicates that aerobic energy production was more intense at timepoint A compared to timepoint B (Table 4.7), in parallel with the theoretical expectation of higher energy expenditure at low salinity and vice versa.

4.2.1.2. Carbohydrate metabolism. Carbohydrates comprise one of the fundamental sources of energy for all organisms, and bivalves also prefer carbohydrates as a respiratory substrate when carbon resources are not limiting (Hawkins et al., 1985). Carbohydrates are named according to the number of monomeric units they carry, such as monosaccharides and polysaccharides (glycans). Polysaccharides such as glycogen, starch, chitin, and cellulose can be used for energy storage that can be utilized in need. In energy demand, polysaccharides are catabolized to monosaccharides and the chemical energy of monosaccharides is harnessed to synthesize ATP. Glycolysis is the metabolic pathway that breaks down monosaccharide glucose to pyruvate, to produce energy and NADH (Figure 4.8(1)). In aerobic conditions, the generated pyruvate can be further oxidized to acetyl CoA (Figure 4.8(2) to enter the TCA cycle (Figure 4.8(7)) which mainly produce energy precursors for oxidative phosphorylation (Figure 4.8(3), Figure 4.7). In anaerobic conditions, the generated pyruvate is reduced to lactate (Figure 4.8(4)). Parallel to glycolysis, glucose can also be directed to the pentose phosphate pathway for the generation of NADPH and nucleotide precursors (Figure 4.8(5)). In case of its shortage, glucose can be generated from nonsugar precursors through the process of gluconeogenesis (Figure 4.8(1) in the reverse direction).

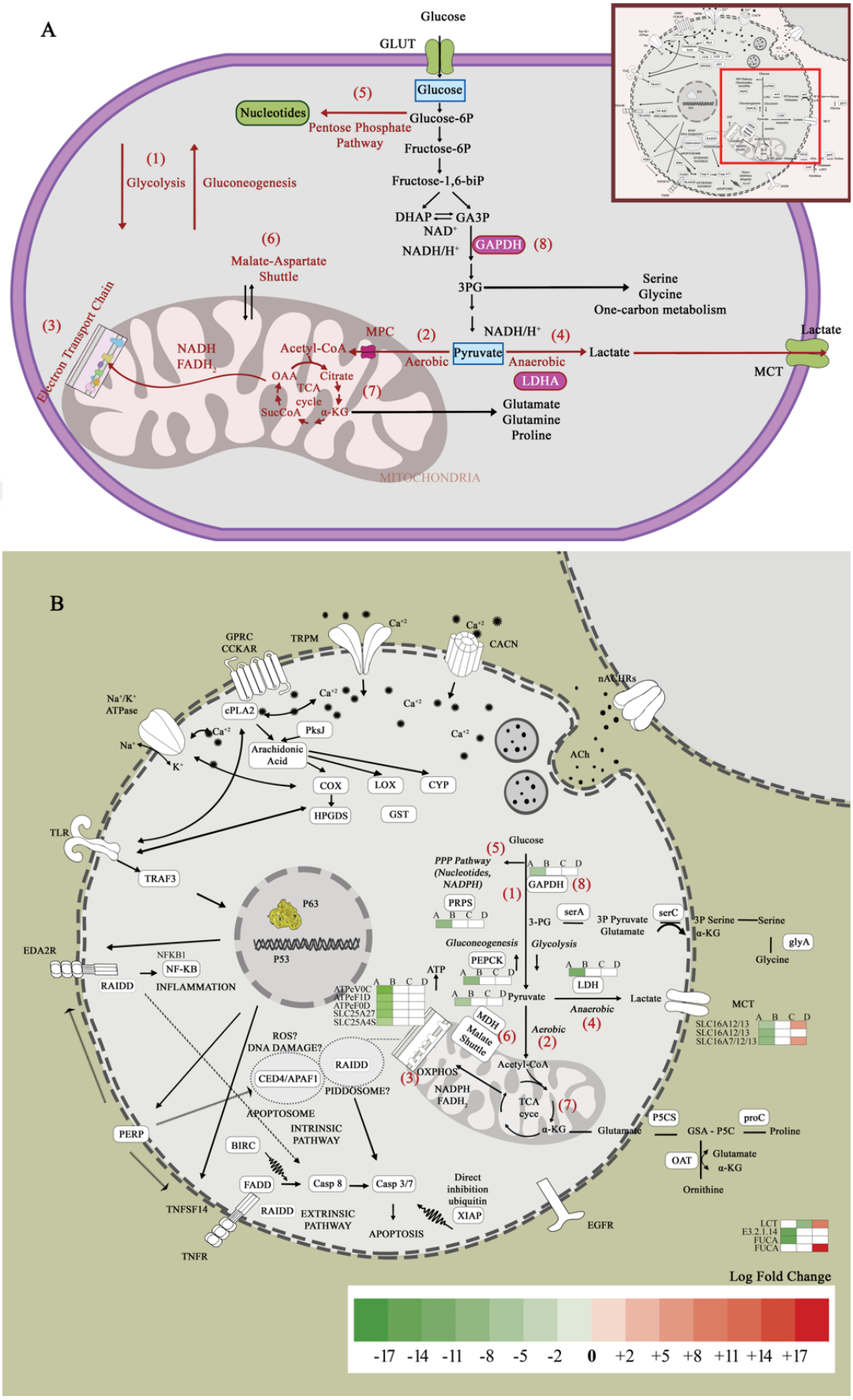


Figure 4.8. Compartmentalization of the mentioned pathways (modified from Lehninger et al. (2005)). In the legend, green and red colors represent downregulation and upregulation with higher color intensity denoting greater log-fold change.

In our study, the genes of carbohydrate metabolism that are involved in the catabolism of carbohydrates, namely fucosidase (FUCA, K01206), lactase-phlorizin hydrolase (EC: 3.2.1.108, EC: 3.2.1.62, K01229) (LPH, LCT), and chitinase (K01183) were D.E. in the contrasts. Other D.E. genes related to carbohydrate metabolism were glycolysis and gluconeogenesis enzyme glyceraldehyde-3-phosphate dehydrogenase (GAPDH, EC:1.2.1.59, EC:1.2.1.12, K00134), gluconeogenesis enzyme phosphoenolpyruvate carboxykinase (PEPCK, EC:4.1.1.32, K01596), TCA cycle enzyme that is also involved in the malate-aspartate shuttle (Figure 4.8(6)), malate dehydrogenase (MDH, EC 1.1. 1.37, K00025), anaerobic metabolism enzyme L-lactate dehydrogenase (LDHA, EC:1.1.1.27, K00016), and pentose-phosphate shunt enzyme ribose-phosphate pyrophosphokinase (PRPS, K00948). PRPS is examined in 4.2.1.3., nucleotide metabolism section, as it is involved in the generation of nucleotide precursor phosphoribosylpyrophosphate (PRPP) that is the key molecule in nucleotide synthesis. Related to carbohydrate metabolism, NAD^+-dependent protein deacetylase sirtuin 6 (SIRT6, K11416, EC:2.3.1.286) involved in PEPCK regulation was also DE. Regulation of these contigs is given in Table 4.8 and discussed in greater detail below.

Table 4.8. Regulation of contigs related with carbohydrate metabolism. In the legend, green and red colors represent downregulation and upregulation with higher color intensity denoting greater log-fold change.

			RTvsRC.BA		RTvsRC.CB		RTvsRC.DC		RTvsRC.CA		RTvsRC.DB		RTvsRC.DA		RTvsRC	
	Symbol	Name	logFC	FDR	logFC	FDR	logFC	FDR	logFC	FDR	logFC	FDR	logFC	FDR	logFC	FDR
Carbohydrate Metabolism	GAPDH	glyceraldehyde 3-phosphate dehydrogenase	-7.548939	1.18E-02												
	LDH	L-lactate dehydrogenase	-12.557895	1.74E-03												
	E4.1.1.32	phosphoenolpyruvate carboxykinase (GTP)	-10.847751	3.75E-02												
	PRPS	ribose-phosphate pyrophosphokinase	-9.081637	7.56E-03												
	MDH1	malate dehydrogenase	-6.927828	2.67E-02												
	LCT	lactase-phlorizin hydrolase			-9.819807	3.22E-02	10.109770	3.51E-02	-11.018403	2.47E-02						
	E3.2.1.14	chitinase	-16.196906	3.73E-02												
Glycan Degradation	FUCA	alpha-L-fucosidase	-15.293666	4.07E-05					-8.160787	2.89E-02	10.540486	5.79E-03				
	FUCA	alpha-L-fucosidase					21.632906	8.74E-03			20.142547	1.41E-02				
Other	SIRT6	NAD+-dependent protein deacetylase sirtuin 6	3.917646	4.15E-02					4.047373	4.65E-02						

-17 -14 -11 -8 -5 -2 0 +2 +5 +8 +11 +14 +17

Carbohydrate catabolism

Fucosidase

Fucosidase (FUCA) contigs ‘alpha-L-fucosidase- like isoform X1’ and ‘alpha-L-fucosidase-like isoform X2’ were regulated inversely with salinity (Table 4.8). FUCA is involved in glycan metabolism, in the degradation of L-fucose located on the oligosaccharide chains of glycoproteins, glycolipids, and glycosaminoglycans (Reglero and Cabezas, 1976). In lysosomes, FUCA is involved in the first step of glycoprotein degradation reflecting protein turnover (Artigaud et al., 2015).

Downregulation of FUCA reduces protein turnover in scallop *Pecten maximus* at hypoxia suggesting an energy-saving strategy (Artigaud et al., 2015 cited in Prego-Faraldo et al., 2018). Likewise, downregulation (between A and B) of FUCA with salinity increase and upregulation (between B and D, and C and D) with salinity decrease is probably directly proportional to the protein turnover which contributes to the high energy expenditure of low salinity (seen both in the study and in the literature) (Freitas et al., 2017; Riisgard et al., 2013; Tedengren and Kautsky, 1986; Tedengren and Kautsky, 1987; Sanders et al., 2018). To investigate protein turnover in more detail, i) cysteine proteases that participate in protein turnover, cathepsin B, L (Mohamed and Sloane, 2006), and K, ii) proteoglycans that are subclasses of glycoproteins, and iii) ribosomal proteins that are mainly involved in protein synthesis and ribosomal biogenesis, (Pollutri & Penzo, 2020; Yang et al., 2016) were also analyzed. Proteoglycans, cysteine proteases and ribosomal proteins were also inversely regulated with salinity like FUCA (Table 4.9) supporting protein turnover. Protein synthesis is one of the most energy-consuming process in the cell (Guimaraes & Zavolan, 2016), and regulation of ribosomal proteins was consistent with energy expenditure in the study and was probably increasing energy demand agreeing with the literature of high energy demand of altered nitrogen metabolism (Peteiro et al., 2018).

Table 4.9. Regulation of contigs of cathepsins, ribosomal proteins and proteoglycans. In the legend, green and red colors represent downregulation and upregulation with higher color intensity denoting greater log-fold change.

			RTvsRC.BA		RTvsRC.CB		RTvsRC.DC		RTvsRC.CA		RTvsRC.DB		RTvsRC.DA		RTvsRC	
	Symbol	Name	logFC	FDR	logFC	FDR	logFC	FDR	logFC	FDR	logFC	FDR	logFC	FDR	logFC	FDR
Cathepsins	CTSB	cathepsin B	-11.351435	2.30E-02												
	CTSB	cathepsin B	-7.039516	3.75E-02												
	CTSK / CTSL	cathepsin K / cathepsin L	-7.373894	8.86E-03												
	CTSL	cathepsin L			13.559638	1.86E-02					13.351451	2.85E-02				
	CTSL	cathepsin L	-8.148590	4.66E-02												
	CTSL	cathepsin L	-5.026500	1.79E-02												
Ribosomal Proteins	RP-L10Ae	large subunit ribosomal protein L10Ae	-8.469609	1.32E-02												
	RP-L11e	large subunit ribosomal protein L11e	-8.333504	4.66E-02												
	RP-L34e	large subunit ribosomal protein L34e	-12.618357	7.50E-03												
	RP-LP0	large subunit ribosomal protein LP0	-8.044966	1.78E-02												
	RP-LP1	large subunit ribosomal protein LP1	-9.939559	2.29E-02					-9.774686	3.26E-02			-10.584333	2.21E-02	9.864265	2.57E-02
	RP-S10e	small subunit ribosomal protein S10e	-10.792946	4.27E-02												
	RP-S14e	small subunit ribosomal protein S14e	-9.354905	3.75E-02												
	RP-S17e	small subunit ribosomal protein S17e	-10.725850	4.84E-03	8.681865	3.04E-02										
	RP-S25e	small subunit ribosomal protein S25e	-10.854419	3.18E-02												
	RP-S2e	small subunit ribosomal protein S2e	-12.671792	2.78E-03												
	RP-S30e	small subunit ribosomal protein S30e	-9.761040	1.85E-02												
Proteoglycans	AGC1	aggrecan 1			6.540026	1.52E-02										
	AGC1	aggrecan 1									14.259789	1.66E-03				
	AGC1	aggrecan 1							-19.044135	1.53E-02						
	AGC1 / BCAN	aggrecan 1 / brevican			10.998009	1.47E-02										
	AGC1 / BCAN	aggrecan 1 / brevican									9.979629	1.82E-02				
	AGC1 / NCAN / VCAN	aggrecan 1 / neurocan core protein / versican core protein			-7.856964	3.21E-02	8.614681	1.32E-02	-8.833866	1.18E-02						
	BCAN / NCAN	brevican / neurocan core protein			11.159161	1.26E-02					9.899319	2.11E-02				
	BCAN / NCAN	brevican / neurocan core protein	-17.030086	3.17E-02												
	COL12A	collagen type XII alpha			-9.728983	1.18E-02	11.891107	7.93E-04	-8.809164	3.25E-02						
	NCAN	neurocan core protein	-7.123122	4.50E-02												
	NCAN	neurocan core protein					21.532091	1.60E-02								
	NCAN	neurocan core protein			-11.833061	1.68E-02					-11.734162	3.44E-02				
	TSK	tsukushi (leucine-rich repeat-containing protein 54)			15.785456	4.69E-02										

-17 -14 -11 -8 -5 -2 0 +2 +5 +8 +11 +14 +17

Lactase-phlorizin hydrolase

Another contig involved in the catabolism of carbohydrates, LCT, has both phlorizin hydrolase and lactase activities (GenomeNet, n. d. (b)). Lactose is converted to glucose and galactose, which can be used in energy production and other cellular processes, and it was upregulated with salinity decrease between timepoints C and D (Table 4.8), probably due to high energy expenditure of low salinity, in a parallel manner with FUCA. LCT was also downregulated between timepoints B and C (Table 4.8), as the mussels became more acclimated to the low energy expenditure of high salinity.

Chitinase

The last contig involved in the catabolism of carbohydrates in the study, chitinase, was downregulated in BA(↑) (Table 4.8), *i.e.* in the same direction as FUCA and LCT. Chitinase is involved in nitrogen and carbon generation by degradation of chitin, an abundant polymer in the marine world (Hamid et al., 2013; Birkbeck and McHenery, 1984), and bivalves regularly consume chitin containing diatoms and debris (Smucker and Wright, 1984). For instance, in the Fujian Oyster *Crassostrea angulata*, chitinase is found to be involved in digestion in the visceral mass and is regulated through feeding (Yang et al., 2015). Chitin is also a structural component of bivalve shell and nacre formation. In this study, chitin degradation probably contributed nitrogen molecules to the altered nitrogen metabolism, due to osmoregulation and energy metabolism. It also likely contributed carbon molecules for metabolic processes and energy production. It is concluded that metabolic activity was higher in 18‰ compared to 39‰, and chitinase, FUCA and LCT were all downregulated accordingly, consistent with the lower energy demand expected from higher salinity.

Glycolysis/gluconeogenesis

GAPDH (Figure 4.8(8)) is a glycolytic pathway enzyme involved in glucose metabolism, specifically glycolysis and gluconeogenesis. It is also involved in many cellular functions such as protein binding, cell signaling (Purves et al., 2010), and apoptosis initiation. It is highly conserved and used as a housekeeping gene for glycolysis (Treaster et al., 2015), but is elevated in some cancer types (Zhang et al., 2015) and stress conditions. For instance, GAPDH was upregulated in the scallop *Pecten maximus spermatozoa* under oxidative stress or apoptosis (Boonmee et al., 2016). The contig mapped to GAPDH was downregulated in BA(↑) (Table 4.8), indicating a high glycolytic rate at timepoint A compared to timepoint B, again concordant with expectations of energy metabolism.

Anaerobic metabolism

Probably, the most notable enzyme related to energy metabolism that was D.E. in the contrasts was LDHA (Figure 4.8(4)), which was also downregulated in BA(↑) (Table 4.8). LDHA is involved in the synthesis of lactate from pyruvate in anaerobic glycolysis within the cytoplasm. Normally, the production of lactate from pyruvate happens when there is not sufficient oxygen (Melkonian and Schury, 2020), and LDHA is expected to be upregulated under these circumstances as anaerobic metabolism kicks in. Oxygen solubility in water decreases with increase in salinity, and LDHA regulation in this study was in the opposite direction: LDHA activity was higher in lower salinity, indicating that the LDHA regulation in the study was not related to oxygen solubility of water due to salinity change. Also, genes involved in hypoxia such as hypoxia-inducible factors (HIFs) were examined, and no significant changes indicative of lack of oxygen were detected between contrasts. Beyond oxygen levels, in bivalves, switching to anaerobic metabolism coupled with depressed metabolism is an energy-saving strategy in response to environmental stressors like temperature, salinity changes, or nutrient availability (De Zwaan and Mathieu, 1992). As hypoxia genes were not found to be D.E., the involvement of anaerobic metabolism (LDHA) could be due to environmental stress (De Zwaan and Mathieu 1992), specifically the salinity increase in our experiment. However, rather than shifting to anaerobic metabolism, genes of aerobic metabolism were also downregulated in BA(↑) (Table 4.7), pointing to high metabolic rates at steady-state compared to chronic salinity increased state. Increased metabolic activity and oxidative phosphorylation genes at 18‰ indicate increased oxygen consumption, therefore metabolic depression was not thought to be involved: metabolic depression is normally associated with decreased energy demand through decreasing of activities such as cardiac activity, filtration rate, muscular activity, and food uptake (De Zwaan, 1977).

Parallel regulation of aerobic and anaerobic metabolism genes can occur to provide additional energy to the cells. For example, in Tilapia (*Oreochromis mossambicus*), alteration of ion channels and enzymes related to osmoregulation causes high energy demand in mitochondrial rich cells of the gills. Tseng et al. (2008) proposed the involvement of LDH to supply additional energy to aerobic metabolism to support high energy demand due to osmoregulation. Likewise, in bivalves, De Zwaan and Mathieu (1992) also stated that the involvement of functional anaerobism can provide additional ATP when energy production of aerobiosis is not sufficient when compared to the energy demand. Besides, during conversion of pyruvate to lactate, NAD^+ necessary for glycolysis is also regenerated (Figure 4.8(4)). In contrasts, genes involved in oxidative phosphorylation and LDHA were D.E. in

the same direction, and this can be due to the activation of functional anaerobism to provide additional ATP to aerobic metabolism.

High expression of GAPDH and LDHA at timepoint A, when compared to B (Table 4.8) could also potentially indicate the Pasteur effect, which refers to the inverse relation between O_2 consumption and glycolytic rate (Hochachka, 1986) (see the Literature Review 2.2.1. Energy Metabolism section above for an explanation of the Pasteur effect). However, due to two reasons, this probably was not the case: First, bivalves can depress metabolism to decrease energy demand by decreasing energy expenditure rather than increasing glycolytic rate to compensate ATP deficiency of anaerobic metabolism, and therefore, can reverse the Pasteur effect (Hochachka, 1986; Storey and Storey, 1990) And second, aerobic metabolism genes were also highly expressed, indicating the involvement of anaerobic metabolism as an additional energy supply to aerobic metabolism, as stated above.

Gluconeogenesis

Another notable regulation was the parallel regulation of glycolysis (Figure 4.8(1)) and gluconeogenesis (Figure 4.8(1) in reverse order) genes. In vertebrates, mainly the liver and to a lesser extent kidney, are specialized organs for gluconeogenesis (Phillips and Hird, 1977; Miyamoto and Amrein, 2017). On the other hand, in bivalves, gluconeogenesis is probably carried out in all organs, similar to the storage of glycogen that takes place in all tissues and organs, as well (De Zwaan, 1983). Glycolysis is the breakdown of glucose to produce energy, and gluconeogenesis refers to glucose production from non-carbohydrate sources like lactate. Normally glycolysis and gluconeogenesis are reciprocally regulated processes that are regulated by allosteric enzymes. When the energy charge of the cell is low, glycolysis is promoted for energy production. And when it is high, glycolysis is switched off, and gluconeogenesis is promoted. In BA(↑), phosphoenolpyruvate carboxykinase (PEPCK, EC:4.1.1.32, K01596), the key enzyme of the gluconeogenesis, and the glycolysis enzyme glyceraldehyde-3-phosphate dehydrogenase (GAPDH, EC:1.2.1.59, EC:1.2.1.12, K00134) were regulated in the same direction (downregulated, see Table 4.8). Although the processes are reciprocally regulated (*i.e.* one is active while the other is inhibited or *vice versa*), this pattern of regulation is seen in some cancer cells. In cancer cells that rely on oxidative phosphorylation in limited glucose supply, PEPCK is regulated to replenish glycolysis intermediates (Leithner, 2015), as it is involved in adaptation to glucose deprivation by utilizing TCA metabolites and carbon metabolites, as alternative carbon sources (Leithner, 2015, Leithner et al., 2014). In lung cancer cells, for instance, when glucose levels are low, lactate is used and converted to phosphoenolpyruvate with

PEPCK (Leithner et al., 2014). In this study, the regulation of oxidative phosphorylation, glycolysis, and gluconeogenesis genes were parallel to the regulation in cancer (Leithner, 2015, Leithner et al., 2014), as PEPCK was activated when energy demand was high at low salinity.

Regarding the regulation described, SIRT6 (a sirtuin) that is related to glycolysis and gluconeogenesis, was upregulated in BA(↑) and CA(↑) (Table 4.8). Sirtuins are energy sensors (Houtkooper et al., 2012) and SIRT6 is "central regulator of glucose metabolism" (Kugel & Mostoslavsky, 2014), affecting both glycolysis and gluconeogenesis. Its deficiency causes higher expression of gluconeogenic genes and increase in glucose uptake (Kugel & Mostoslavsky, 2014). Regulation of PEPCK parallel with oxidative phosphorylation genes can utilize TCA metabolites, as an alternative carbon source to meet the high energy demand of steady-state (18‰) compared to high salinity (39‰). In the study, SIRT6 probably enhanced glucose uptake and gluconeogenesis at the steady-state (timepoint A) compared to high salinity, and upregulation in BA(↑) with salinity increase probably downregulated gluconeogenesis (as there was no more need to utilize TCA metabolites as an alternative carbon source) and glucose uptake, as high salinity requires low energy expenditure. This pattern with SIRT6 also resembles regulation in cancer literature, probably due to energy demand and alternative metabolite requirement conditions. In cancer metabolism, Zhang et al. (2014a) found that SIRT6 downregulates PEPCK through the tumor suppressor p53 (Leithner et al., 2014), which was linked to the tumor-suppressive function of p53. In our study, p53 was not D.E., however, its apoptosis effector gene, TP53 apoptosis effector PERP (examined in Results 4.2.3. Apoptosis section) was D.E., showing possible involvement of p53 in these regulations.

TCA cycle / malate-aspartate shuttle

MDH is another important gene that catalyzes malate-oxaloacetate conversion in a NAD/NADH dependent manner (Minárik et al., 2002), and is involved in many metabolic pathways; the TCA cycle (Figure 4.8(7)), malate-aspartate shuttle (Figure 4.8(6), Figure 3), as well as modified anaerobic metabolism pathways of bivalves (as explained in detail in Literature Review 2.2.2. Hypoxia section). Malate-aspartate shuttle ensures oxidative phosphorylation to proceed by translocating electrons from the cytosol across the mitochondrial membrane in the form of malate (Figure 4.9(1)), as the inner membrane of mitochondria is impermeable to NADH (Berg et al., 2002a). Cytosolic malate dehydrogenase catalyzes the conversion of oxaloacetate to malate and NADH is oxidized to NAD^+, and subsequently, NAD^+ needed for glycolysis to operate is produced (Figure 4.9(2)). Malate transported across the mitochondrial inner membrane and mitochondrial isoform that is also involved in the TCA cycle converts malate to oxaloacetate (Figure 4.9(3)). NAD^+ is reduced to NADH and

can be used further in oxidative phosphorylation (Figure 4.9(4)). As oxaloacetate can not pass the mitochondrial inner membrane, aspartate is formed (Figure 4.9(5)) and transported to the cytosol (Figure 4.9(6)). In the cytosol, oxaloacetate is formed again (Figure 4.9(7)) and the cycle restarts (Berg et al., 2002a).

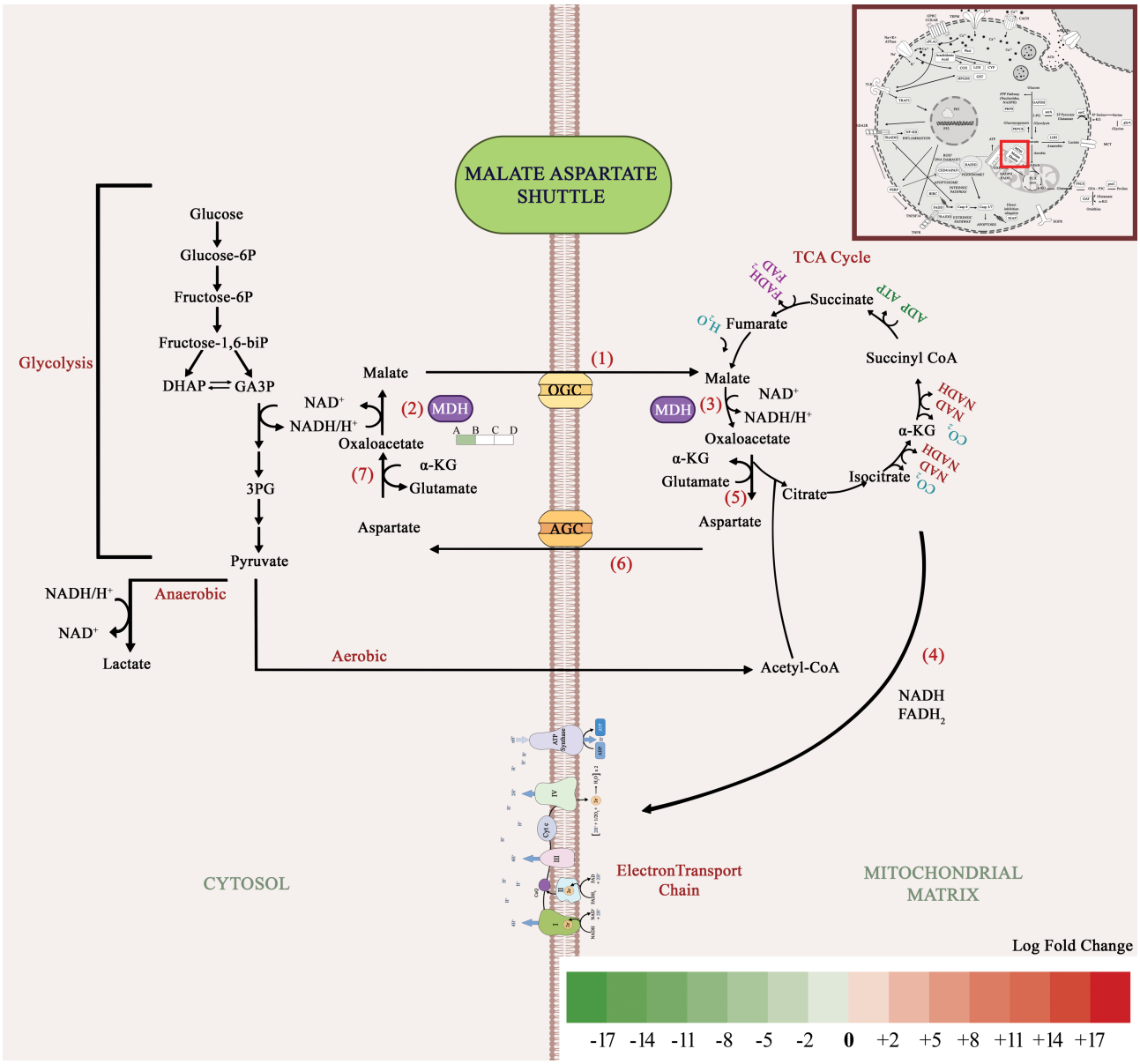


Figure 4.9. Malate aspartate shuttle. Zoomed version of Figure 4.8(6) (Pathways are modified from Lehninger et al. (2005)). In the legend, green and red colors represent downregulation and upregulation with higher color intensity denoting greater log-fold change.

In our experiment, the MDH contig mapped to 'cytosolic malate dehydrogenase' (Figure 4.9(2)), which is involved in malate aspartate shuttle, was downregulated between timepoints A and B (Table 4.8). This downregulation probably supported increased glycolytic rate by regenerating NAD^+ for glycolysis in addition to LDHA, and also by its role in aerobic metabolism; ensuring oxidative

phosphorylation to proceed by translocating electrons from the cytosol across the mitochondrial membrane. Cytosolic MDH can also be involved in modified anaerobic metabolism pathways with PEPCK (Literature Review, Figure 2.1). However, this probably was not the case, as modified anaerobic pathways involve part of the reverse TCA cycle and NAD^+ production in the mitochondrial matrix that can be more efficient and are more likely to occur under oxygen-deficient conditions. There was no evidence for oxygen deficiency for timepoints A and B, as indicated by parallel regulation of oxidative phosphorylation genes and lack of expression of genes involved in oxygen deprivation, such as HIF as stated above.

4.2.1.3. Nucleotide metabolism. Nucleotides are subunits of genetic acids, DNA and RNA, composed of nitrogenous bases, a five-carbon sugar, and a phosphate group. Nucleotide synthesis is a high-energy, carbon and nitrogen consuming process that is regulated tightly at multiple levels. Nucleotide metabolism can be altered in conditions such as replication, DNA damage and gene expression regulation for protein synthesis (Lane and Fan, 2015; Janero et al., 1993). In the study contigs related to nucleotide metabolism, namely ribose-phosphate pyrophosphokinase (PRPS, K00948, EC:2.7.6.1) (Figure 4.10(1) and cytidine deaminase (cdd, K01489, EC:3.5.4.5)), were inversely regulated with salinity (Table 4.10).

PRPS (Figure 4.10(1)) catalyzes the conversion of ribose-5-phosphate (R5P) to PRPP. PRPP is a key molecule in nucleotide synthesis (Figure 4.10(2)) and is very important since the generation of many key molecules such as the energy currency ATP, nucleic acids DNA and RNA, cofactors (e.g. NAD), second messengers (e.g. c-AMP), and pathway intermediates (e.g. UDP-glucose) depend on it (Hove-Jensen et al., 2016). During the nucleotide synthesis process, R5P is generated by nucleotide breakdown (Figure 4.10(3)) or by pentose phosphate shunt from glucose-6-phosphate (Figure 4.8(5), Figure 4.10(4)). R5P can be i) redirected to nonoxidative pentose phosphate shunt and generate glycolytic intermediates for the generation of ATP/glucose (Figure 4.10(5)) or ii) can be converted to PRPP for nucleotide synthesis (Figure 4.10(1), Figure 4.10(2)). The contig annotated as PRPS was downregulated in BA(↑) indicating decreased nucleotide synthesis with salinity increase (Table 4.10).

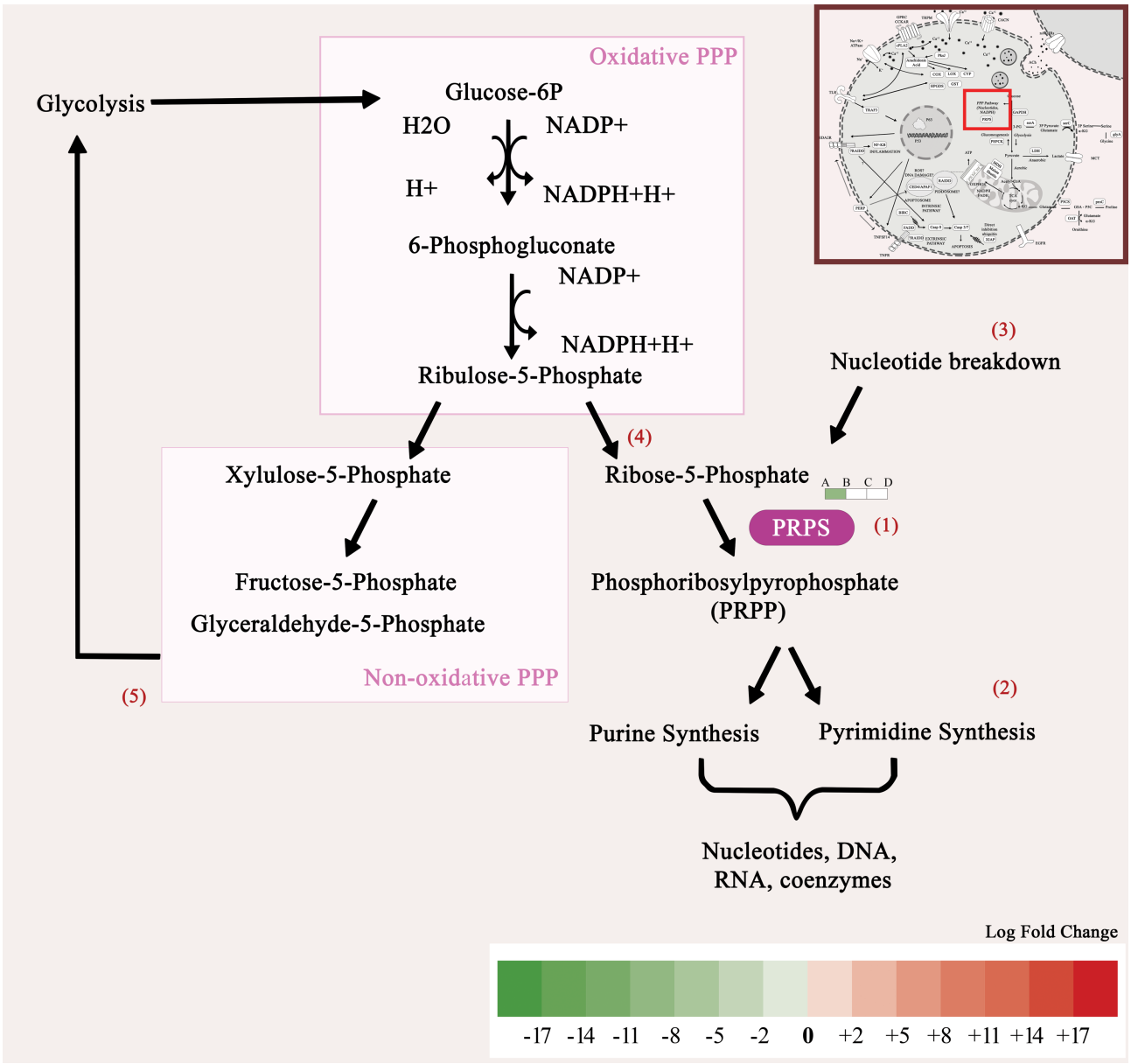
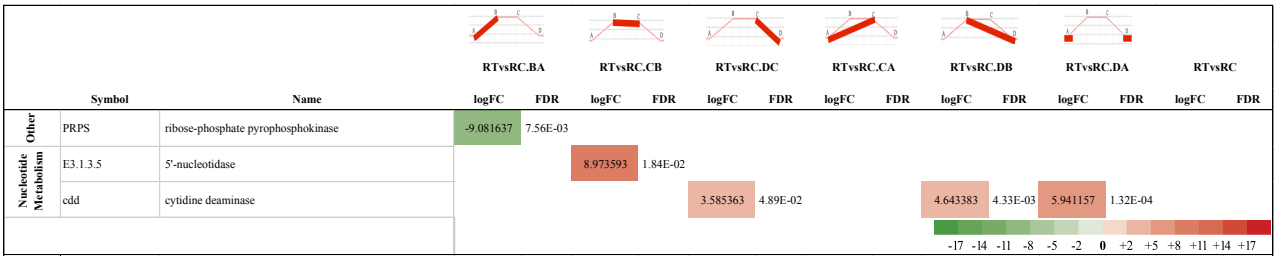


Figure 4.10. Pentose phosphate pathway. Multiple enzymatic steps are indicated with an arrow (modified from Lehninger et al. (2005)). Zoomed in version of Figure 4.8(5). In the legend, green and red colors represent downregulation and upregulation with higher color intensity denoting greater log-fold change.

The other contig related to nucleotide metabolism, cdd, is a key enzyme in the pyrimidine salvage pathway, essential for nucleic acid synthesis and recycling of pyrimidines (Frances & Cordelier, 2020). In nucleotide salvage pathways, bases and nucleosides from degraded nucleic acids are recovered. In our experiment, it was upregulated in DC(↓), under salinity decrease, indicating higher pyrimidine recycling at lower salinities (Table 4.10).

Table 4.10. Regulation of contigs related with nucleotide metabolism. In the legend, green and red colors represent downregulation and upregulation with higher color intensity denoting greater log-fold change.



	Symbol	Name	RTvsRC.BA logFC	RTvsRC.BA FDR	RTvsRC.CB logFC	RTvsRC.CB FDR	RTvsRC.DC logFC	RTvsRC.DC FDR	RTvsRC.CA logFC	RTvsRC.CA FDR	RTvsRC.DB logFC	RTvsRC.DB FDR	RTvsRC.DA logFC	RTvsRC.DA FDR	RTvsRC logFC	RTvsRC FDR
Other	PRPS	ribose-phosphate pyrophosphokinase	-9.081637	7.56E-03												
Nucleotide Metabolism	E3.1.3.5	5'-nucleotidase			8.973593	1.84E-02										
	cdd	cytidine deaminase					3.585363	4.89E-02			4.643383	4.33E-03	5.941157	1.32E-04		

4.2.1.4. Lipid metabolism. Genes of lipid metabolism that were D.E. were mainly related to arachidonic acid metabolism (Figure 4.11) (Table 4.11). In addition, a contig involved in fatty acid synthesis was D.E (Table 4.11). Genes of arachidonic acid metabolism were involved in the degradation of membrane phospholipids by cytosolic phospholipase A_2 ($cPLA_2$) and generation of signaling eicosanoids (Figure 4.11). $cPLA_2$ has a major role in membrane lipid remodeling (Uniprot, n.d. (b)); it causes hydrolysis of membrane phospholipids and generation of lysophospholipids and polyunsaturated fatty acids (PUFA) such as arachidonic acid (Figure 4.11(3)). The fatty acids generated through hydrolysis of membrane phospholipids can be degraded to acetyl-CoA and used in the TCA cycle for energy production. Free arachidonic acid can be metabolized by cyclooxygenase (Figure 4.11(4)), lipoxygenase (Figure 4.11(5)), cytochrome p450 (Figure 4.11(9)), and anandamide pathways (Hanna and Hafez, 2018) and further form bioactive signaling eicosanoids, including prostaglandins (Figure 4.11(6)), thromboxanes (Figure 4.11(7)), prostacyclins, and leukotrienes (Figure 4.11(8)) (Yui et al., 2015). Eicosanoids initiate signaling cascades and are involved in pathological and physiological processes such as inflammation, immune response, growth regulation and stress adaptation (Panigrahy et al., 2010).

Genes involved in these processes that were D.E. in our experiment for phospholipase activity were cytosolic phospholipase A_2 (PLA2G4, $cPLA_2$, K16342) (Figure 4.11(2)), and for eicosanoids production were i) arachidonate 5-lipoxygenase (ALOX5, K00461) (Figure 4.11(5)), ii) arachidonate 12-lipoxygenase (R-type) (ALOX12B, K08021) (Figure 4.11(5)), iii) cytochrome P450 family 2 subfamily J (CYP2J, K07418) (Figure 4.11(9)), and iv) prostaglandin-H2 D-isomerase / glutathione transferase (HPGDS, K04097) (Figure 4.11(10)). In addition, antioxidant Glutathione s-transferase (GST, K00799) was D.E. in this process. GST is an antioxidant, and along with another antioxidant glutathione peroxidase (GPx) reduce lipid hydroperoxides with GSH, to help protect the cell from lipid peroxidation caused by metabolization of arachidonic acid by LOX (Figure 4.11(5)) and COX (Figure 4.11(4)) (Speed and Blair, 2011). Finally, other than arachidonic acid metabolism, but related

to lipid metabolism, a lipid biosynthesis protein polyketide synthase PksJ (pksJ, K13611) was also D.E.

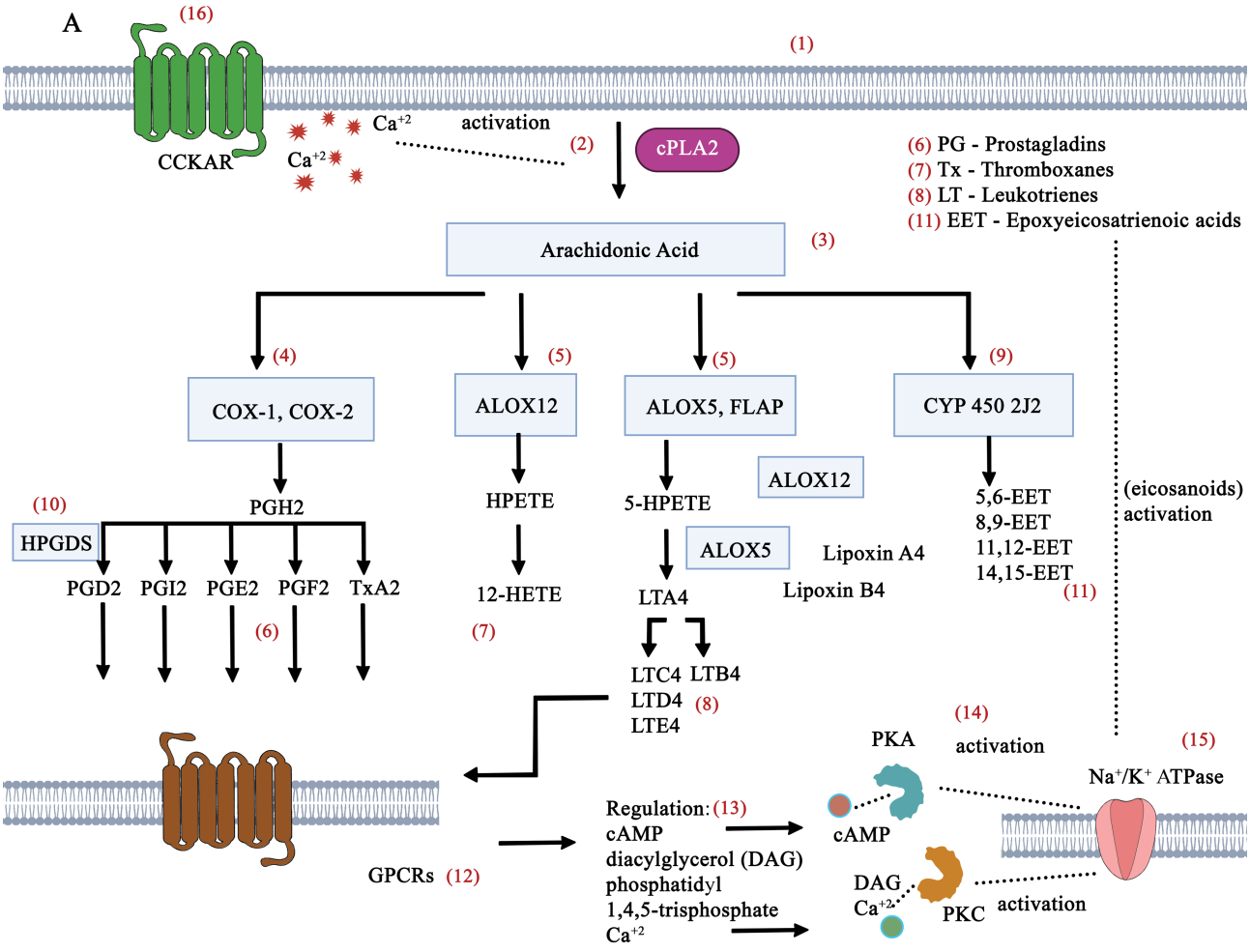


Figure 4.11. Regulation of lipid metabolism in the study. A) Phospholipase activity, metabolization of arachidonic acid by cytochrome P450 2J2, cyclooxygenase, and lipoxygenase, and regulation of Na+/K ATPase by generated eicosanoids (modified from van Kranen and Siezen, 2016; Wang et al., 2020; Korotkova and Lundberg, 2014; Therien and Blostein, 2000; Farooqui and Farooqui, 2016; Pirahanchi et al., 2021).

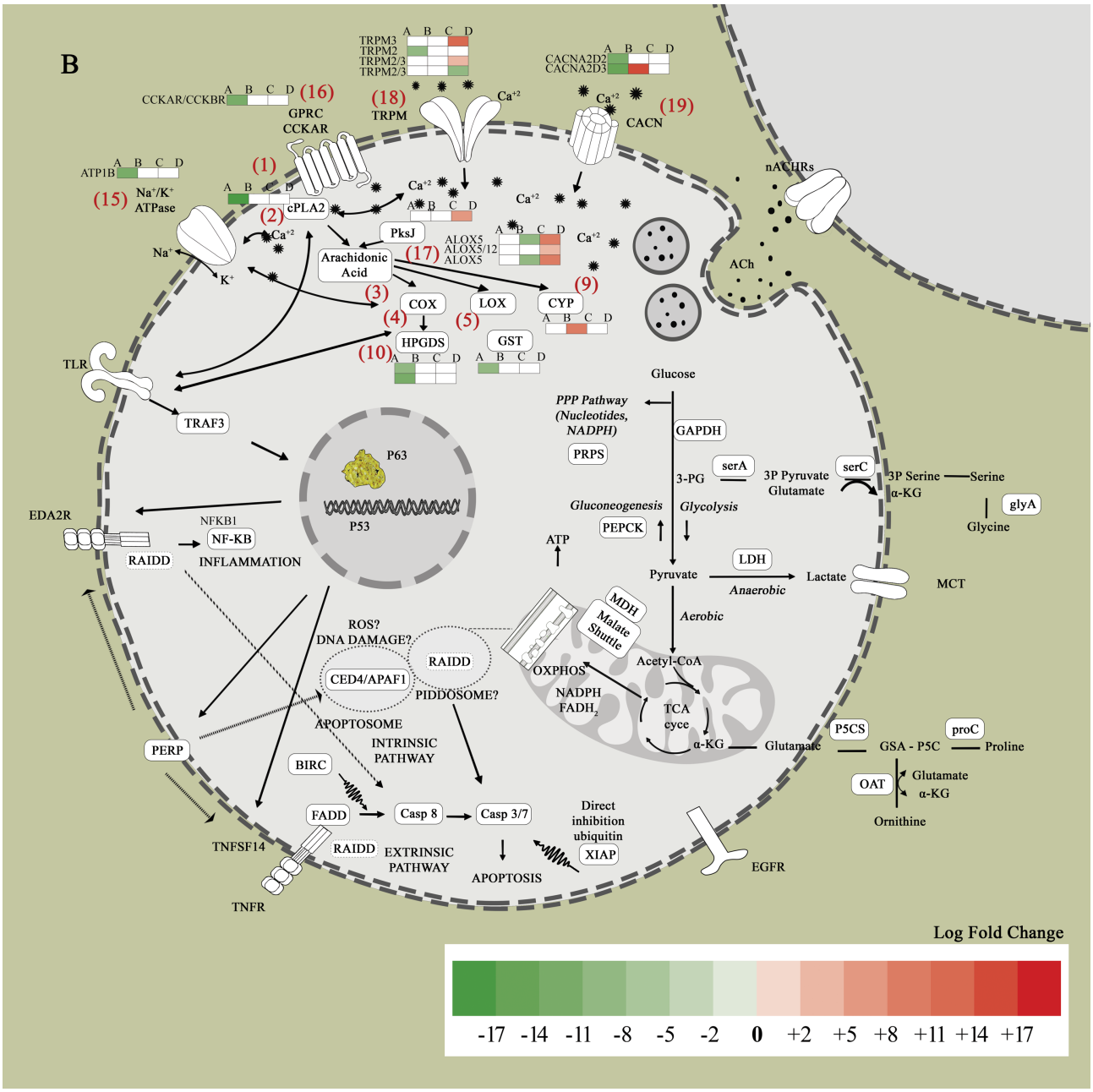


Figure 4.11 continued. Regulation of lipid metabolism in the study. B) Lipid metabolism in the hypothesized model of the study. In the legend, green and red colors represent downregulation and upregulation with higher color intensity denoting greater log-fold change.

Arachidonic acid metabolism enzymes and fatty acid synthesis enzyme were D.E. in this study. These enzymes alter membrane lipid composition and fluidity, which enhance adaptation to changing conditions such as salinity and temperature (Bhoite and Roy, 2013) by altering the activity of ion channels (Ortiz et al., 2017; Nelson et al., 2011). For example, in the mud crab, *Scylla serrata*, change in lipid composition and membrane fluidity enhances salinity adaptation by modulating the activity of Na^+/K^+-ATPase pump (Bhoite and Roy, 2013) (Figure 4.11(15)), as osmolyte regulation is connected to alteration of the lipid composition of the cell membrane. Arachidonic acid metabolism

is involved in a signaling cascade that leads to the release of osmolytes triggered by cell swelling (Lambert, 2004). For example, taurine (an osmolyte) release in humans is modulated by leukotrienes formed by $cPLA_2$ activity induced by cell swelling (Lambert, 2004). Also, in the oyster species, *C. gigas*, cell swelling activates arachidonic acid metabolism that releases osmolytes (Figure 4.12(1), Figure 4.12(2), Figure 4.12(5)). G-proteins (Erickson and Guilak, 1999) and G-protein coupled receptors (GPCRs) (Figure 4.12(3)) (Meng et al., 2013) were also found to be involved in this process. The hypothetical model of the processes is given in Figure 4.12 (Meng et al. (2013)).

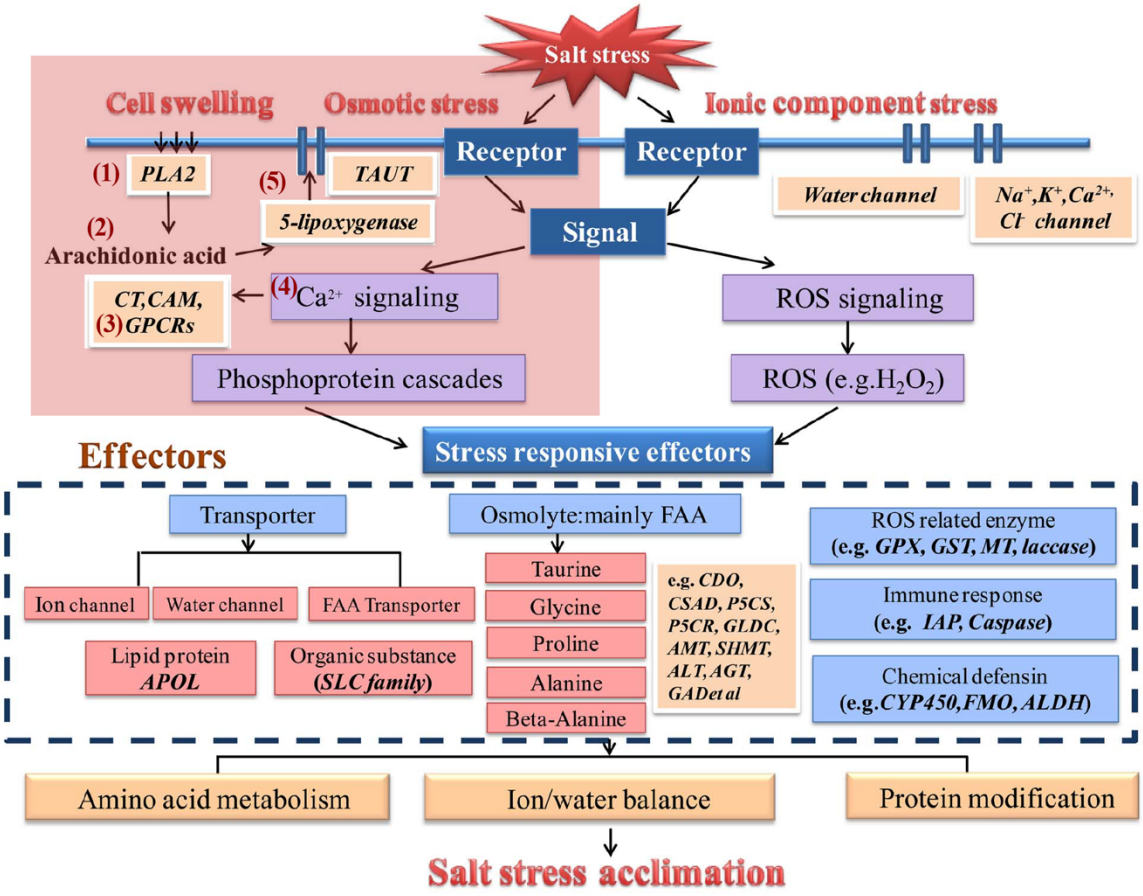


Figure 4.12. Hypothetical model of long-term salinity stress response in oyster *C. gigas* by Meng et al. (2013).

Regulation of Na^+/K^+-ATPase activity by arachidonic acid metabolism ($cPLA_2$ and generated eicosanoids) is well studied in many tissues and species (Figure 4.11(15)) (Therien and Blostein, 2000). Generated eicosanoids in arachidonic acid metabolism can regulate cAMP, diacylglycerol, phosphatidyl 1,4,5-trisphosphate and calcium levels (Figure 4.11(13)) by binding to eicosanoid receptors which are mostly GPCRs (Figure 4.11(12)) (Farooqui and Farooqui, 2016). Change in cAMP levels also activates protein kinase A (PKA) which can directly phosphorylate and regulate Na^+/K^+-ATPase (Figure 4.11(14)) (Therien and Blostein, 2000).

In this study, $cPLA_2$ and arachidonic acid metabolizing enzymes were higher in low salinity compared to high salinity, in agreement with the literature (Meng et al., 2013; Lambert, 2004; Bhoite and Roy, 2013) (Table 4.11). The contig involved in fatty acid synthesis (pksJ, K13611) was also matching with this regulation pattern. Metabolism of arachidonic acid in the study was probably altered with Ca^{+2} influx, as explained in greater detail in Results 4.2.1.6., Ion Channels and Transporters section, see below. It has been observed that Ca^{+2} is involved in osmostress response and regulates both hypoosmotic and hyperosmotic stress (Erickson and Guilak, 1999; Hasegawa et al., 2000). In mollusks, cytosolic Ca^{+2} regulation and calcium signaling is suggested to alter membrane fluidity under hypoosmotic stress conditions (Figure 4.12(4)) (Meng et al., 2013). Similar results were also encountered in some studies (Meng et al., 2013) that involved hyperosmotic stress.

Table 4.11. Regulation of contigs related to lipid metabolism. In the legend, green and red colors represent downregulation and upregulation with higher color intensity denoting greater log-fold change.

			RTvsRC.BA		RTvsRC.CB		RTvsRC.DC		RTvsRC.CA		RTvsRC.DB		RTvsRC.DA		RTvsRC	
	Symbol	Name	logFC	FDR	logFC	FDR	logFC	FDR	logFC	FDR	logFC	FDR	logFC	FDR	logFC	FDR
Lipid Metabolism	PLA2G4 (cPLA2)	cytosolic phospholipase A2	-19.796411	4.09E-02							22.295117	5.40E-03				
	PLA2G4 (cPLA2)	cytosolic phospholipase A2									15.399480	3.96E-02				
	PLA2G4 (cPLA2)	cytosolic phospholipase A2							-15.716666	1.27E-02						
	ALOX5	arachidonate 5-lipoxygenase									-12.652147	3.34E-02				
	ALOX5	arachidonate 5-lipoxygenase			-9.211039	3.91E-03	9.684387	1.48E-03	-8.112629	2.62E-02						
	ALOX12B / ALOX5	arachidonate 12-lipoxygenase (R-type) / arachidonate 5-lipoxygenase					4.762356	4.20E-05			4.789789	2.03E-05	2.934678	4.53E-02		
	ALOX5	arachidonate 5-lipoxygenase											-15.653868	4.84E-02		
	ALOX5	arachidonate 5-lipoxygenase			-8.544695	2.57E-03	8.728440	1.48E-03	-8.145011	5.00E-03						
	HPGDS	prostaglandin-H2 D-isomerase / glutathione transferase	-8.570366	7.44E-03												
	HPGDS	prostaglandin-H2 D-isomerase / glutathione transferase	-11.140583	1.52E-02												
	CYP2J	cytochrome P450 family 2 subfamily J			10.918017	1.12E-02										
	CYP2J	cytochrome P450 family 2 subfamily J											-12.072218	2.31E-02		
	pksJ	polyketide synthase PksJ					6.100513	1.04E-02								
Other	ANXA7_11	annexin A7/11	-8.459426	4.63E-02												
		stanniocalcin-like protein	-14.667656	3.75E-02					-16.892835	2.14E-02						
		stanniocalcin-like protein					18.492386	1.10E-03	-17.079104	2.65E-03	12.296981	2.70E-02				

-17 -14 -11 -8 -5 -2 0 +2 +5 +8 +11 +14 +17

Arachidonic acid Metabolism

Phospholipase activity

Cytosolic phospholipase A_2 (PLA2G4, $cPLA_2$, K16342) (Figure 4.11(2)) was downregulated in BA(↑) and CA(↑) (salinity increase), and upregulated in DB(↓) (salinity decrease) (Table 4.11), which is involved in cell signaling, and is important for cell membrane homeostasis and cellular processes such as inflammation, osmoregulation, and immune response (Ricciotti and FitzGerald, 2011). It can be activated by GPCRs (González et al, 1999; Kano et al., 2002; Lankisch et al, 1999; Tsunoda and Owyang, 1995) and calcium influx (Ortiz et al., 2017). In this study, phospholipase activity that was accompanied by GPCR activity and calcium influx (Figure 4.11(2), Figure 4.11(16), Figure 4.11(18),

Figure 4.11(19)) was in concordance with the literature (Figure 4.12(3), Figure 4.12(4))(Meng et al., 2013).

GPCRs are conserved receptors of eukaryotes and are the largest and most diverse group of receptors that are involved in sensing the extracellular environment in the form of different molecules such as mating factors, glucose, lipids, light energy, etc. (O'Connor & Adams, 2010). Upon binding with the signaling molecule, they interact with G proteins and further initiate related signaling cascades with second messengers (O'Connor & Adams, 2010). In our study, the GPCR cholecystokinin receptor (CCKAR, K04194, CCKBR, K04195) was inversely regulated with salinity (Table 4.12, Figure 4.11(16)). CCKAR activates $cPLA_2$, phospholipase C (PLC) and src/protein tyrosine kinase (PTK) pathways and regulates Ca^{+2} levels (Lankisch et al, 1999; González et al, 1999; Kano et al., 2002; Tsunoda and Owyang, 1995). In this study CCKAR (GPCR) (Table 4.12) (Figure 4.11(16)) could cause calcium oscillations (Table 4.14) and phospholipase activation (Table 4.11). The direction of the observed phospholipase activity in this study was parallel to the CCKAR (GPCR) activity (Table 4.12) (Figure 4.11(16)), which can cause calcium oscillations (Figure 4.12(4)) and phospholipase activation (Table 4.12) (Figure 4.11(2)). Additionally, $cPLA_2$ can also be activated by TNF receptors (MacEwan, 2002). In the study, TNFSF14 was downregulated in BA(↑), like $cPLA_2$, which is examined in greater detail in Results 4.2.3., Apoptosis section, below.

Table 4.12. Regulation of contigs of GPCRs. In the legend, green and red colors represent downregulation and upregulation with higher color intensity denoting greater log-fold change.

		RTvsRC.BA		RTvsRC.CB		RTvsRC.DC		RTvsRC.CA		RTvsRC.DB		RTvsRC.DA		RTvsRC	
Symbol	Name	logFC	FDR	logFC	FDR	logFC	FDR	logFC	FDR	logFC	FDR	logFC	FDR	logFC	FDR
ADGRA3	adhesion G protein-coupled receptor A3	-16.729648	4.05E-02												
ADGRB3	adhesion G protein-coupled receptor B3					14.247495	3.54E-02								
ADGRE1	adhesion G protein-coupled receptor E1			-10.642739	4.68E-02	10.513224	4.66E-02								
ADGRL1	adhesion G protein-coupled receptor L1					9.561978	3.90E-02								
ADGRL1	adhesion G protein-coupled receptor L1					-10.045453	4.49E-02								
CCKAR	cholecystokinin A receptor									4.102762	3.84E-02				
CCKAR / CCKBR	cholecystokinin A receptor / cholecystokinin B receptor	-13.436199	1.75E-02									-12.937285	3.80E-02		
CELSR3	cadherin EGF LAG seven-pass G-type receptor 3					6.299563	1.19E-02								

-17 -14 -11 -8 -5 -2 **0** +2 +5 +8 +11 +14 +17

$cPLA_2$ becomes catalytically active by the influx of calcium to the cell (Ortiz et al., 2017), as stated above. Calcium binds to the C2 domain (calcium-dependent lipid-binding domain) of $cPLA_2$ that enhances translocation of $cPLA_2$ to the membrane from the cytosol and subsequent metabolization of phospholipid to arachidonic acid (Evans et al., 2004; Clapham, 2007). In our study, it was seen that calcium-related channels that import calcium were D.E., as examined in Results 4.2.1.6., Ion Channels and Transporters section (Table 4.14).

$cPLA_2$ can also cause membrane destabilization and lipid peroxidation, and therefore is used as a stress indicator in biomonitoring programs (Prego-Faraldo et al. 2018). Consistent with possible effects of $cPLA_2$ on membrane stability, a contig annotated as annexin (ANXA7_11, K17095) was downregulated in BA(↑) (with blast hit of annexin A6 [*M. galloprovincialis*]) (Table 4.11). Annexins are calcium-regulated, calcium/phospholipid-binding proteins, with the capacity to suppress phospholipase A_2 (Oktay et al., 2013). They are involved in membrane-related processes such as ion channel formation, membrane repair, membrane trafficking, and calcium signaling (Tao et al., 2020). Annexin A6 plays a central role in membrane repair and is also identified as a therapeutic target for it (Demonbreun et al., 2019). Downregulation of annexin in BA(↑) probably was related to the possible effects of $cPLA_2$ on the cell membrane.

Contigs involved in calcium homeostasis were also D.E., including stanniocalcin-like proteins that were downregulated in BA(↑) and CA(↑) (salinity increase), and upregulated in DC(↓) and DB(↓) (salinity decrease) (Table 4.11). Stanniocalcin is involved in calcium/phosphate homeostasis in the gills, intestine, and kidneys of fishes (Yeung et al., 2012; Wagner and Dimattia, 2006). In teleost fish, it inhibits calcium uptake from the environment (Wagner et al., 1986 cited in Roch and Sherwood, 2011). In this study, stanniocalcin-like protein regulation was observed at different stages of the experiment and is likely to be associated with calcium homeostasis.

Eicosanoids production

Finally, considering the lipid metabolism, cyclooxygenase (Figure 4.11(4)), lipoxygenase (Figure 4.11(5)), and cytochrome p450 (Figure 4.11(9)) enzymes were D.E. (Table 4.11) in the contrasts that were involved in the metabolization of arachidonic acid produced by phospholipases. These enzymes are involved in eicosanoids production; prostaglandins (Figure 4.11(6)), leukotrienes (Figure 4.11(8)), and epoxyeicosatrienoic acids (EETs) (Figure 4.11(11)), respectively. Considering the pathway, prostaglandins H2 (PGH2) that are generated from arachidonic acid by the cyclooxygenase (COX) enzyme system (Nørregaard et al., 2015) are further catalyzed into prostaglandin D_2 (PGD_2) by the bifunctional enzyme HPGDS in the presence of GSH (Williams, 2012). Specifically, eicosanoid production was downregulated in BA(↑) and upregulated in DC(↓) (Table 4.11). Lipoxygenases (ALOX5 and ALOX12B) (Figure 4.11(5)) were downregulated in CB(→) (constant salinity) and upregulated in DC(↓). Among the cytochrome p450 superfamily of enzymes that can metabolize arachidonic acid, CYP2J (Figure 4.11(9)) was found to be upregulated in CB(→). None of the lipoxygenase and cytochrome p450 contigs were D.E. in BA(↑). HPGDS (Figure 4.11(10)) contigs were downregulated in BA(↑) indicating generation of PGD_2 (Table 4.11).

Fatty acid synthesis

Adjusting the fatty acid composition of the membrane with enzymes such as $cPLA_2$ and fatty acid synthetase alters membrane permeability and facilitates adaptation to environmental changes such as salinity (Bhoite and Roy, 2013). Fatty acid synthesis is essential for membrane phospholipids. As stated above, $cPLA_2$ mobilizes PUFA of membrane phospholipids (such as arachidonic acid) with the result of the destabilization of the membrane. Lipid biosynthesis protein PksJ (Figure 4.11(17)) is involved in PUFA synthesis in cold marine ecosystems (Metz et al., 2001). Normally, PUFA is synthesized in primary producers such as microalgae, but some mollusks including bivalves are also able to synthesize PUFA (Zhukova, 2019; Metz et al., 2001; Monroig et al., 2013). In the study, upregulation of PksJ in DC(↓) (Table 4.11) parallelly with lipoxygenases can be related to membrane lipid remodeling for the osmoregulatory response.

4.2.1.5. Amino acid metabolism. The energy requirement of a cell is mainly supplied through carbohydrates and lipids, and carbohydrates are priority respiratory substrates in bivalves (Hawkins et al., 1985), as mentioned earlier. Amino acids are mainly used as building blocks of proteins, although they can also be used to supply energy. However, excess amino acids can be deaminated and enter the TCA cycle at multiple locations to be utilized in the glucose catabolism (Figure 4.13) (Nelson and Cox, 2008). For euryhaline marine invertebrates, free amino acids, their derivatives, and methylamines are also used to buffer osmotic changes (Pourmozaffar et al., 2019), and for bivalves, amino acids are very important in osmoregulatory response (Fuhrmann et al., 2018). Regulating different compensatory organic osmolytes such as amino acids enables maintaining cell volume and osmolarity (Gilles, 1988).

In our study, D.E. contigs that were related to amino acid metabolism are D-3-phosphoglycerate dehydrogenase (PHGDH, serA, K00058, EC:1.1.1.95 1.1.1.399), phosphoserine aminotransferase (serC, K00831, EC:2.6.1.52), glycine hydroxymethyltransferase (glyA, SHMT, K00600, EC:2.1.2.1), pyrroline-5-carboxylate reductase (proC, K00286, EC:1.5.1.2), delta-1-pyrroline-5-carboxylate synthetase (ALDH18A1, P5CS, K12657, EC:2.7.2.11 1.2.1.41), ornithine aminotransferase (OAT, K00819, EC:2.6.1.13), choline dehydrogenase (betA, K00108, EC: EC:1.1.99.1), and carnosine synthase (CRNS1, K14755, EC: 6.3.2.11) (Table 4.13). Glycine (an amino acid) transporter genes, solute carrier family 6 (neurotransmitter transporter, glycine) member 5/9 (SLC6A5_9), and solute carrier family 25 member 38 (SLC25A38) are also examined in this section.

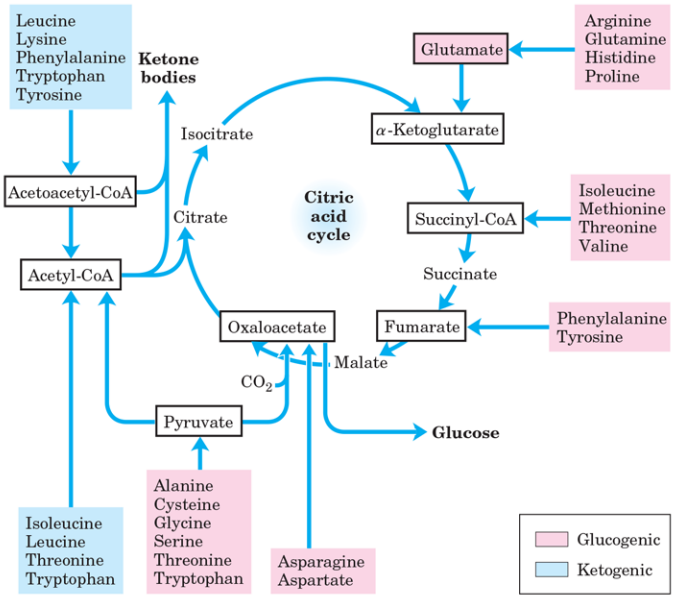


Figure 4.13. Amino acid catabolism. Amino acids can enter the TCA cycle from various locations (Nelson and Cox, 2008).

Table 4.13. Regulation of contigs of amino acid metabolism. In the legend, green and red colors represent downregulation and upregulation with higher color intensity denoting greater log-fold change.

			RTvsRC.BA		RTvsRC.CB		RTvsRC.DC		RTvsRC.CA		RTvsRC.DB		RTvsRC.DA		RTvsRC	
	Symbol	Name	logFC	FDR	logFC	FDR	logFC	FDR	logFC	FDR	logFC	FDR	logFC	FDR	logFC	FDR
Aminoacid Metabolism	serA	D-3-phosphoglycerate dehydrogenase / 2-oxoglutarate reductase	4.234619	7.80E-03	-3.664317	3.04E-02					-4.278530	6.39E-03				
	betA	choline dehydrogenase			-7.376840	1.34E-02	7.358080	1.24E-02	-6.365559	4.16E-02						
	serC	phosphoserine aminotransferase	4.601218	3.23E-04												
	glyA	glycine hydroxymethyltransferase	3.600619	2.70E-03							-3.240458	8.57E-03				
	SETD2	[histone H3-lysine36 N-trimethyltransferase			-13.750364	8.56E-03	9.884237	3.98E-02								
	rocD (OAT)	ornithine--oxo-acid transaminase					2.735351	1.91E-02			2.748342	1.55E-02				
	proC	pyrroline-5-carboxylate reductase	7.669431	3.15E-02												
	proA / ALDH18A1 (P5CS)	glutamate-5-semialdehyde dehydrogenase / delta-1-pyrroline-5-carboxylate synthetase					3.361447	4.84E-02			3.727850	2.23E-02				
	CRNS1	carnosine synthase	-4.550986	5.03E-05			5.631142	8.81E-08	-4.257606	2.43E-04	5.924521	2.69E-09				
	TYR	tyrosinase	-6.877305	7.68E-03					-9.436488	9.31E-05			-5.923750	3.18E-02	5.534514	1.81E-02
	GST	glutathione S-transferase	-9.230499	1.57E-02												
Transporters	SLC6A5_9	solute carrier family 6 (neurotransmitter transporter, glycine) member 5/9	3.937095	1.13E-02							-3.375954	4.30E-02				
	SLC25A38	solute carrier family 25, member 38	-2.458080	4.34E-02												
	SLC25A38	solute carrier family 25, member 38	-4.258738	1.55E-02							4.671407	5.82E-03				

-17 -14 -11 -8 -5 -2 0 +2 +5 +8 +11 +14 +17

Under hyperosmotic stress, intracellular organic osmolytes such as alanine, betaine (glycine betaine), proline, and glycine are accumulated to maintain cell volume (Deaton, 2001). In bivalves, serine, proline, and glycine are among the most common amino acids involved in osmoregulation (Deaton, 2001; Hanson and Dietz, 1976). In this study, genes involved in the synthesis of these amino acids were upregulated when salinity was gradually increased from timepoint A to B over a span of 21 days. Contigs annotated as serA, serC, glyA, proC were upregulated between A and B (Figure 4.14(1), Figure 4.14(2), Figure 4.14(4) and Figure 4.14(8)). serA and serC are involved in serine

synthesis, where serA initially converts 3-phosphoglycerate (3-PG) to 3-phosphopyruvate (3-PHP) (Figure 4.15(1)), followed by convertion of 3-PHP to phosphoserine by serC (Figure 4.15(2)). Lastly, phosphoserine is converted to serine, completing the process (Figure 4.15(3)). Serine-glycine (reversible) conversion is carried out by glyA (Figure 4.15(4)) that is also involved in one-carbon metabolism with the conversion of tetrahydrofolate (THF) to 5,10-methylenetetrahydrofolate (5,10-CH2-THF) (Figure 4.15(5)). proC, another D.E. gene in amino acid metabolism, as mentioned above, catalyzes the last step of proline biosynthesis (Figure 4.16(1)).

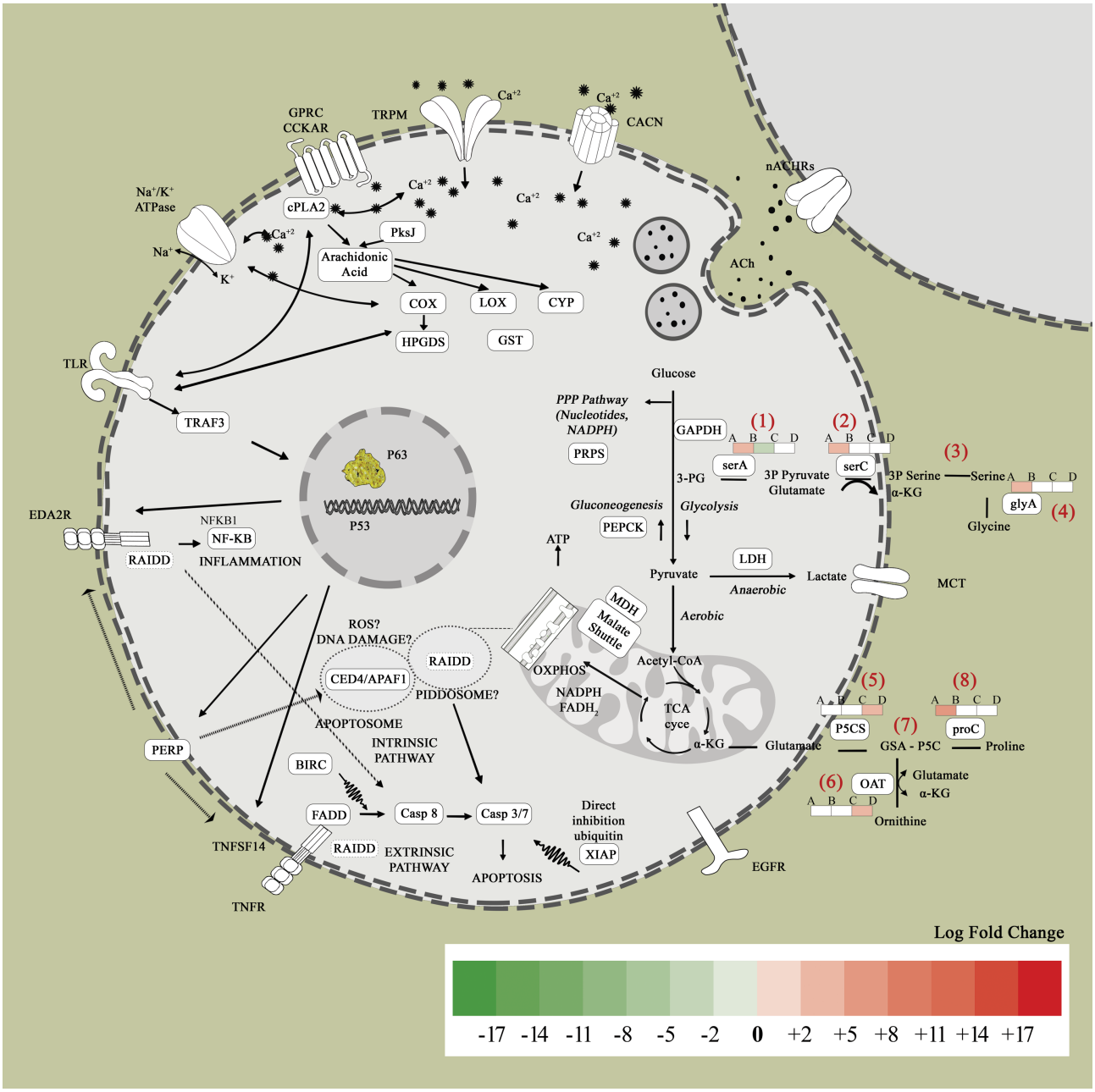


Figure 4.14. Amino acid regulation in the hypothesized model. In the legend, green and red colors represent downregulation and upregulation with higher color intensity denoting greater log-fold change.

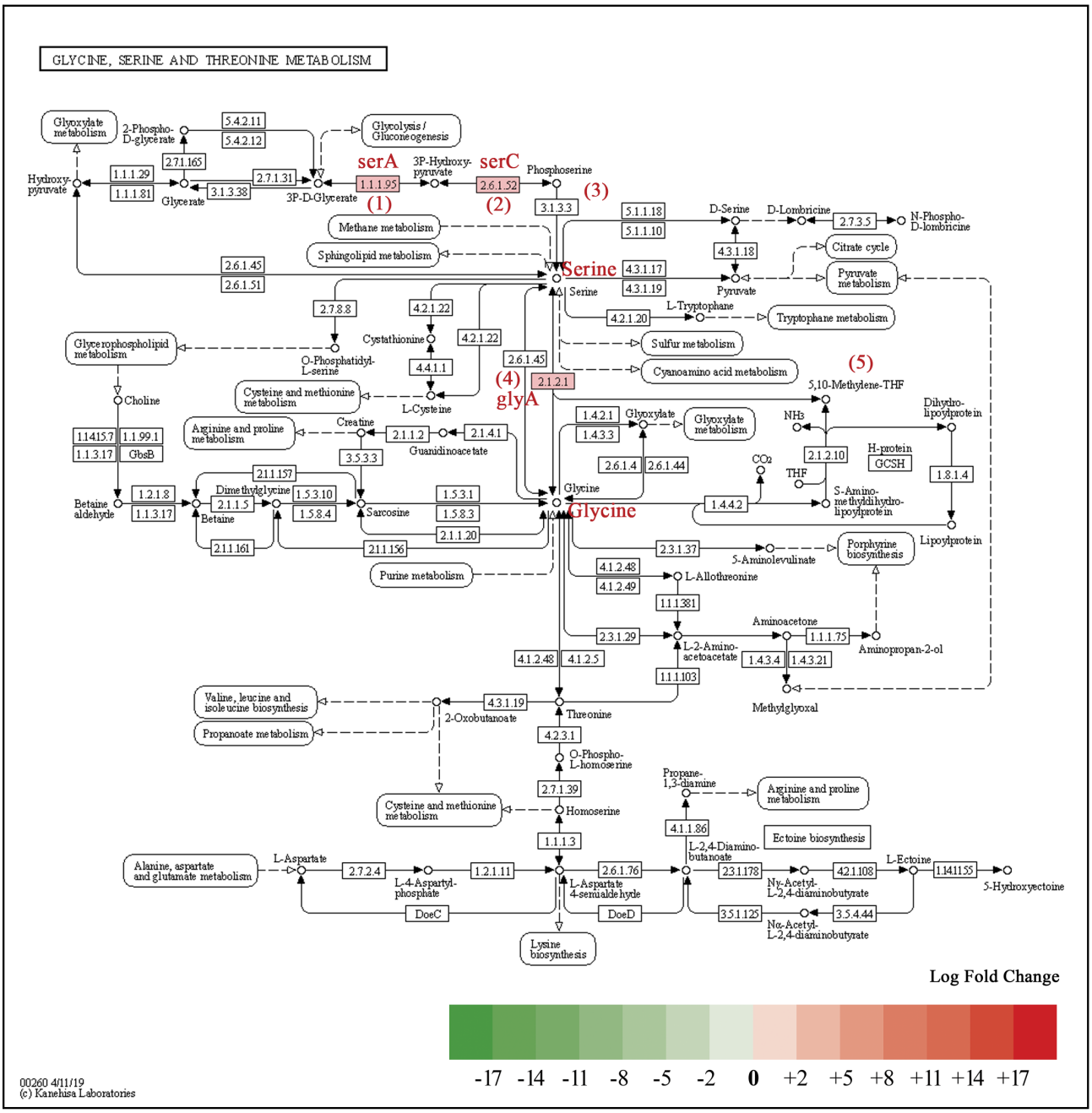


Figure 4.15. Glycine, serine and threonine metabolism (Map00260) for the contrast BA(↑). In the legend, green and red colors represent downregulation and upregulation with higher color intensity denoting greater log-fold change.

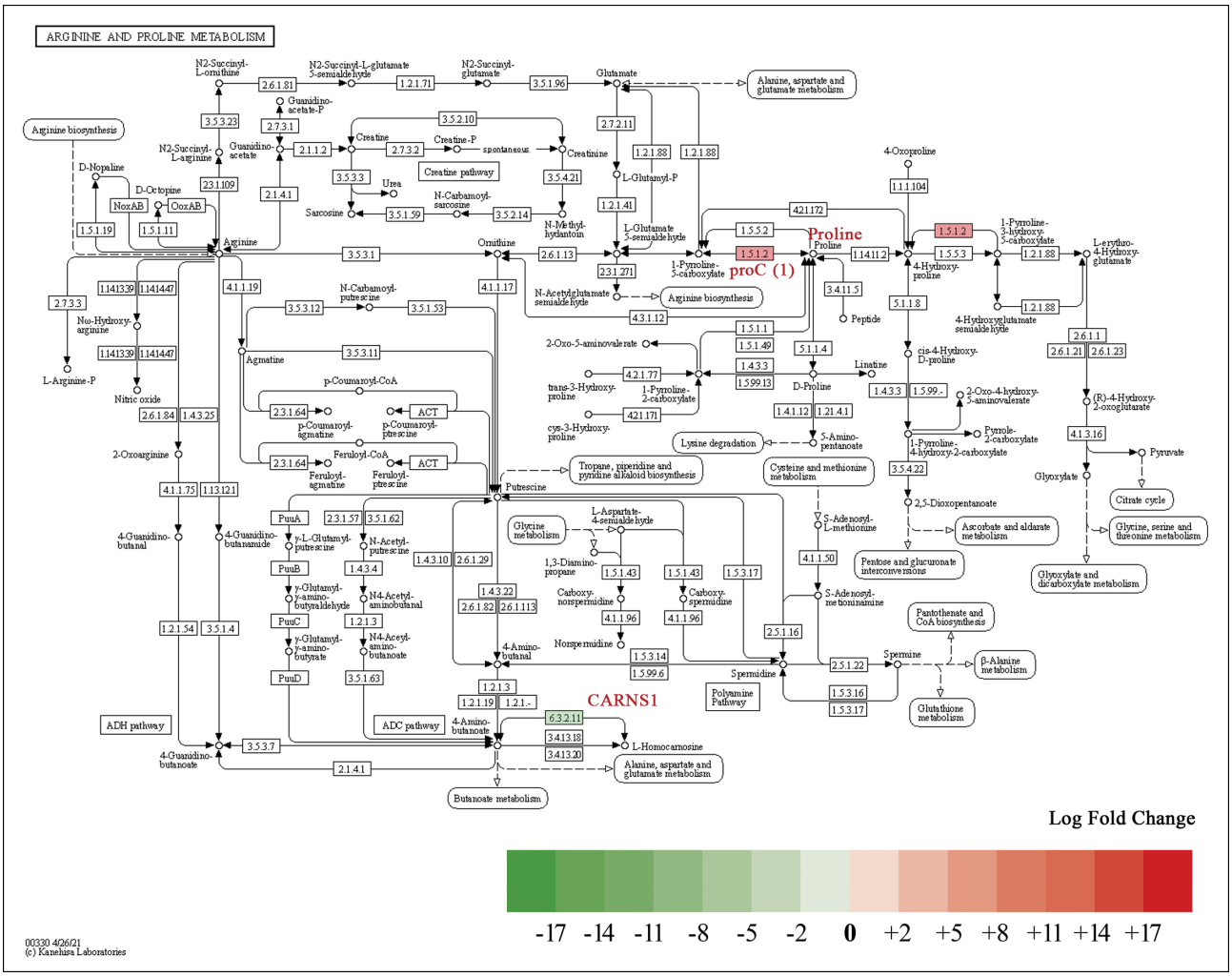


Figure 4.16. Arginine and proline metabolism (Map00330) for contrast BA(↑). In the legend, green and red colors represent downregulation and upregulation with higher color intensity denoting greater log-fold change.

Glycine transporter genes, solute carrier family 6 (neurotransmitter transporter, glycine) member 5/9 (SLC6A5_9), and solute carrier family 25 member 38 (SLC25A38) were D.E. in the contrasts as well. SLC6 are plasma membrane-located transporters that actively import substrates into the cell (Rudnick et al., 2014). SLC6A5_9 is a sodium and chloride dependent glycine transporter, and cotransports glycine, chloride and sodium into the cytosol (Reactome, 2009), which is involved in neuronal excitability and hypoosmotic stress response (e.g. under low salinities of 10‰ and 15‰, where normal salinity was 30‰) in the oyster *C. gigas* (Meng et al., 2013)). In our study, SLC6A5_9 was expressed in the opposite direction to that observed in Meng et al. (2013): upregulated with salinity increase between BA(↑) and downregulated with salinity decrease between DB(↓). In addition, in our study, serine synthesis and serine-glycine conversion (glyA) was in line with the regulation of SLC6A5_9, also upregulated in BA(↑), showing involvement of glycine as an osmolyte in hyperosmotic stress, which agrees with Deaton (2001). Finally, in this category, SLC25 are

mitochondrial transporters used in energy conversion and cell maintenance (Ruprecht and Kunji, 2020). SLC25A38 was inversely regulated with salinity and in the same direction with energy demand, downregulated in BA(↑), and upregulated in DB(↓). This suggests that as salinity increases, energy demand and expression of SLC25A38 decreases.

Symmetrically with salinity decrease between B and D, contigs of serine and glycine synthesis, serA and glyA were downregulated. Serine and glycine synthesis was in the same direction as salinity stress. On the other hand, contigs that are intermediates of proline synthesis, P5CS and OAT were upregulated with salinity decrease in DC(↓) (Figure 4.14(5), Figure 4.14(6), and Figure 4.17) and DB(↓), showing the possibility of involvement of proline in responding to chronic salinity decrease as well (Figure 4.17A, the scenario is shown with red arrows). In Figure 4.17, P5CS catalyzes the conversion of glutamate to glutamate 5-semialdehyde (GSA) with EC:2.7.2.11 and EC:1.2.1.41 (GenomeNet, n. d.) (Figure 4.17(1)). OAT catalyzes the conversion of GSA and glutamate to ornithine and 2-oxoglutarate (α-ketoglutarate) (Eq. 4.1) (Figure 4.17(2)). Spontaneously, interconversion occurs between P5C and GSA (Figure 4.17(3)). A more probable scenario is that (Figure 4.17B, the scenario is shown with red arrows) ornithine and α-ketoglutarate (2-oxoglutarate) form with OAT (Eq. 4.1), rather than synthesis of proline with proC. Thereby, α-ketoglutarate can feed the TCA cycle for energy production, a regulation pattern that is in concordance with the energy demand of low salinity.

L-Ornithine + 2-Oxoglutarate <=> L-Glutamate 5-semialdehyde + L-Glutamate (4.1)

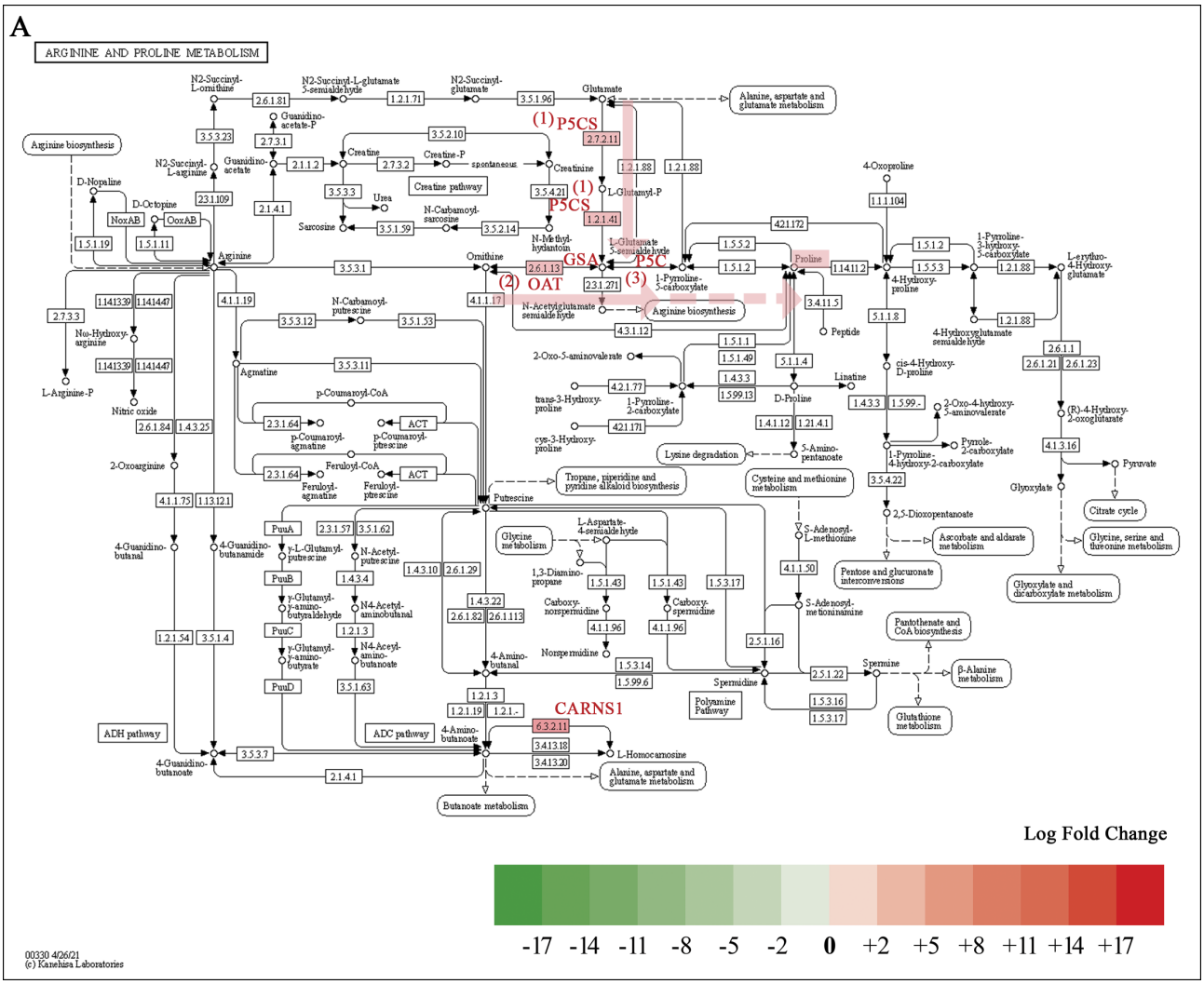


Figure 4.17. Arginine and proline metabolism (Map00330) for contrast DC(↓). P5CS and OAT were upregulated. Reaction of OAT (EC:2.6.1.13) is given in (Eq. 4.1). Red arrows indicate regulation scenarios for A) proline synthesis B) ornithine synthesis. In the legend, green and red colors represent downregulation and upregulation with higher color intensity denoting greater log-fold change.

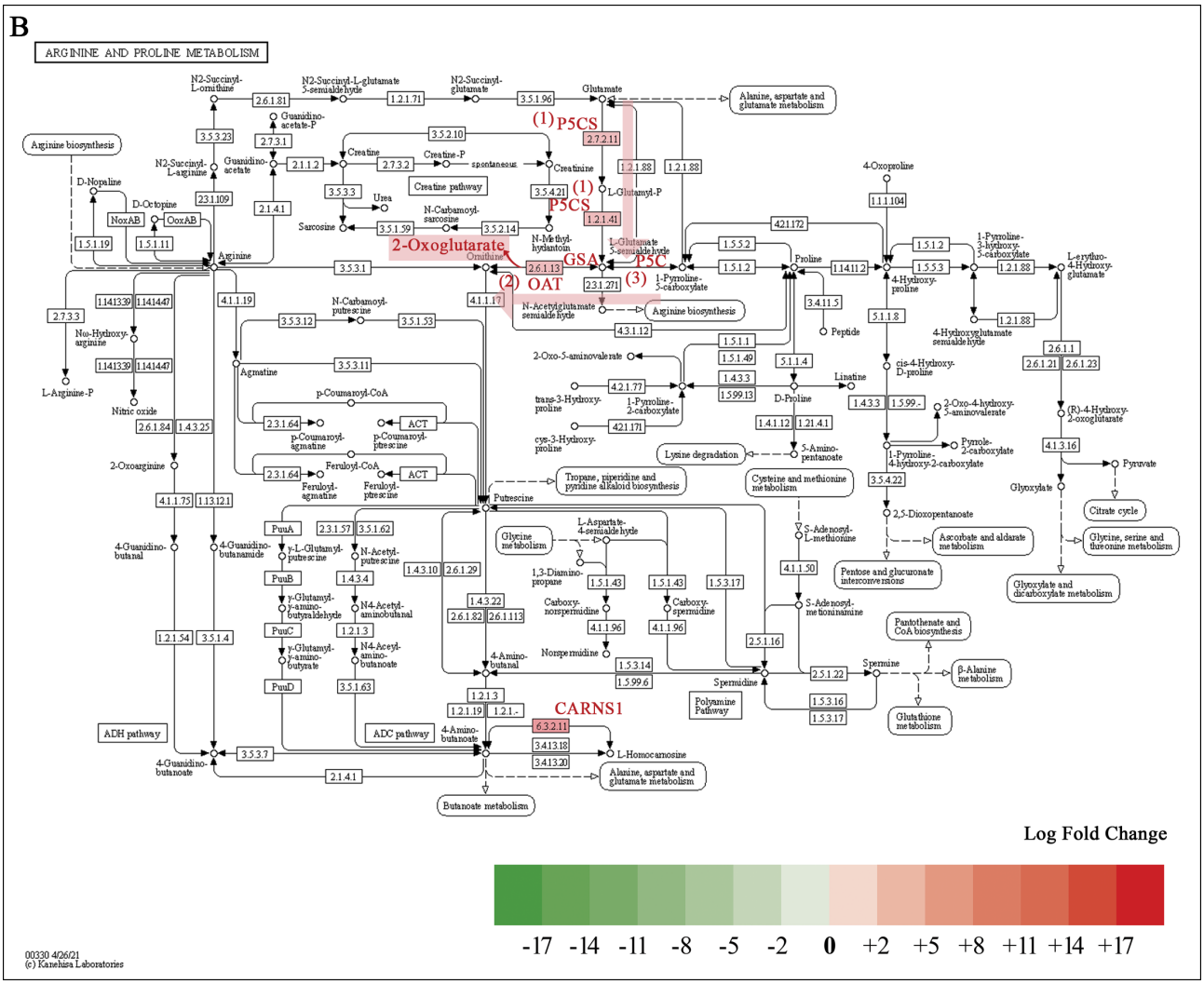


Figure 4.17 continued. Arginine and proline metabolism (Map00330) for contrast DC(↓). P5CS and OAT were upregulated. Reaction of OAT (EC:2.6.1.13) is given in (Eq. 4.1). Red arrows indicate regulation scenarios for A) proline synthesis B) ornithine synthesis. In the legend, green and red colors represent downregulation and upregulation with higher color intensity denoting greater log-fold change.

betA was also inversely regulated with salinity in DC(↓) and CA(↑), *i.e.* downregulated with salinity increase, and vice versa, although it was not D.E. in BA(↑). It was also downregulated in the acclimation period to high salinity between CB(→). betA catalyzes the oxidation of choline to betaine aldehyde (Figure 4.18(1)) and is involved in the synthesis of glycine betaine (betaine) (Figure 4.18(2)). Choline is involved in the synthesis of acetylcholine and membrane phospholipids (Salvi and Gadda, 2013), phosphatidylcholine and sphingomyelin, which are both major components of bilayer membranes (Steinbauer et al., 2003). Betaine is an osmoprotectant and regulates transcription factors of protein synthesis (Figueroa-Soto and Valenzuela-Soto, 2018), and carbohydrate and lipid metabolism. Betaine is also the key modulator of one-carbon metabolism (Ueland et al., 2005) whose metabolization provides tetrahydrofolate-linked one-carbon units (Figure 4.18(4)) for the synthesis

of amino acids, as well as nucleotide, DNA, creatine, and phospholipids. It is also a methyl donor in methionine synthesis from homocysteine by betaine-homocysteine methyltransferase (Ueland et al., 2005) (Figure 4.18(3)) and further methionine is used to generate SAM which is essential for methylation reactions of DNA, RNA and proteins (Mailloux et al., 2016) (Figure 4.18(4)). In bivalves and also in other species, betaine is accumulated with hyperosmotic stress as an osmoprotectant (de Vooys and Geenevasen, 2002; Deaton, 2001). In our study, betA was inversely regulated with salinity in DC(↓) and CA(↑), which is in contradiction with the expectation of its regulation as an osmoprotectant under hyperosmotic stress. Therefore, other functions likely determined its regulation more so than the osmoprotective function, such as the role of betaine in one-carbon metabolism, or nucleotide, DNA, creatine, and phospholipid synthesis, as outlined above. Moreover, its upregulation with salinity decrease supports enrichment of 'methylation' term in GSEA analysis of salinity decrease (see below), as choline metabolization provides SAM for methylation reactions. Although betaine is an osmoprotectant and is expected to increase with hyperosmotic stress, betA was not D.E. in BA(↑), supporting its function with high energy metabolism, as further metabolization of choline may supply electron carriers (NADH (Figure 4.18(5)) and ubiquinol (Figure 4.18(6))) for oxidative phosphorylation (Mailloux et al., 2016). As an example, the incorporation of choline oxidation to energy metabolism in liver mitochondria can be given (Figure 4.18, based on Mailloux et al. (2016)).

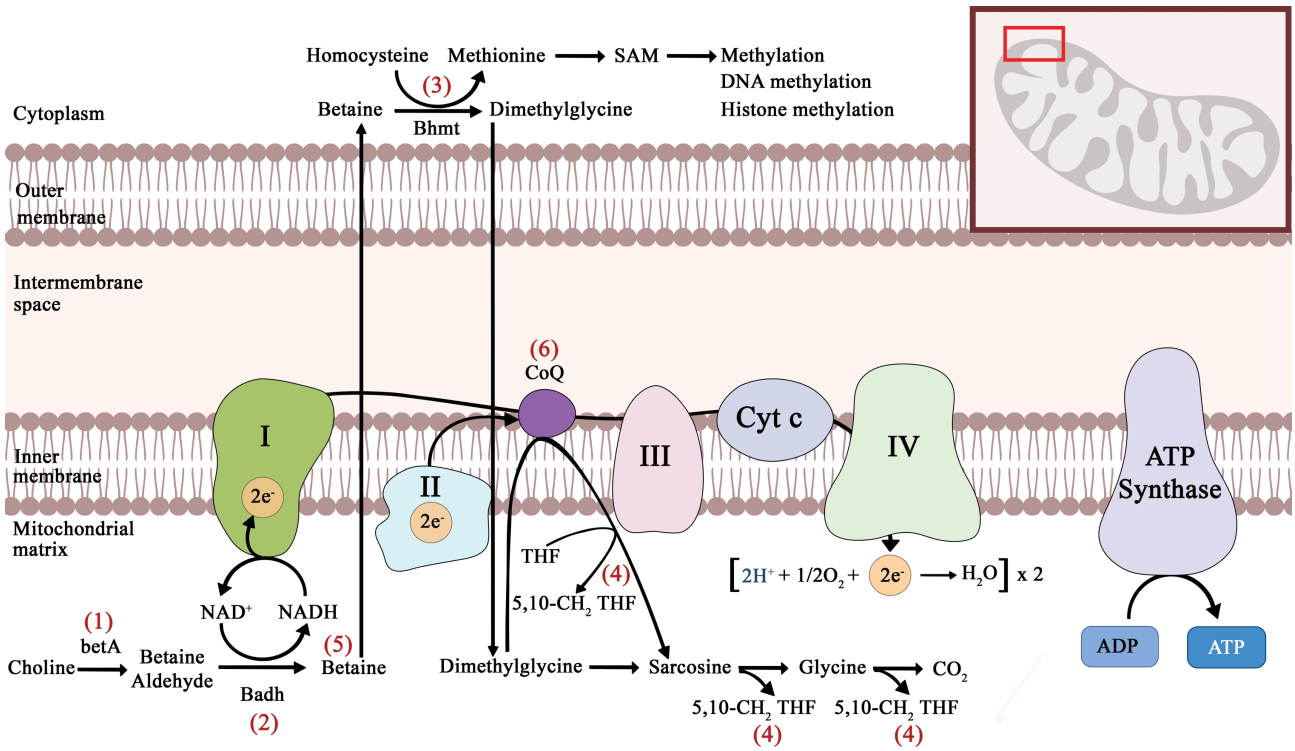


Figure 4.18. Regulation of betA in liver mitochondria (modified from Mailloux et al., 2016).

Finally, in terms of amino acid metabolism, carnosine synthase (CRNS1) catalyzes the synthesis of carnosine from beta-alanine and histidine. Expression of CRNS1 is increased with hypoosmotic stress in the oyster *C. gigas* showing involvement of beta-alanine metabolism in hypoosmotic stress (Meng et al., 2013). In our study, CRNS1 was downregulated between BA(↑), and upregulated between DB(↓) and between DC(↓) (Table 4.13), in agreement with Meng et al. (2013). This might be related to the function of carnosine as a buffer against acidification. For increasing buffering capacity, CRNS1 can also activate carbonic anhydrase. White muscles that have high glycolysis and produce high lactic acid also have been observed to exhibit high carnosine levels (Doğru-Abbasoğlu et al., 2018). Besides buffering against acidification, carnosine is a natural antioxidant inhibiting lipid peroxidation and can scavenge ROS (Szabadfi et al., 2014). It also has antiapoptotic and anti-inflammatory properties (Doğru-Abbasoğlu et al., 2018). In the contrasts, its expression is seen to be inversely regulated to salinity, probably buffering against acidification that can be caused by LDHA and ATPV0C, and lipid peroxidation that can be caused by arachidonic acid metabolism of the further steps of $cPLA_2$, as discussed in the Results 4.2.1.4. Lipid Metabolism section above.

4.2.1.6. Ion channels and transporters. In osmostress, cell volume is regulated with organic and inorganic osmolytes to prevent the dysfunction of the cell due to osmosis. Also, molecules involved in cellular processes that are altered with osmostress are transported across the membranes, inter- and intra-cellularly. Selective passage of molecules/osmolytes across the cell membrane is ensured by ion channels and transporters that are transmembrane proteins. Inorganic ions, such as Na^+, K^+, Cl^-, protect bivalves from rapid salinity changes, and ion channels such as K^+/Cl^- contransporter, Na^+/H^+ and $Cl^-/HCO3^-$ exchangers ensure ion exchange in response to osmostress (Pourmozaffar et al., 2019). Our experiment examined chronic long-term salinity stress and acclimation, and genes that were regulated in the study were mainly related to calcium flux and calcium signaling pathways that can be altered due to cell swelling activated membrane lipid remodeling for osmolyte release (Meng et al., 2013), and cell-to-cell signaling (Clapham, 2007) or ciliary activity (Zagoory et al., 2002; Jokura et al., 2020). Also, ion channels and transporters that are involved in other cellular processes altered with osmoregulation, such as energy metabolism and nitrogen metabolism, were D.E.

Contigs in our study that mapped to ion channels and transporters are given in Table 4.14. D.E. contigs that are related to this category were ion pump subunit sodium/potassium-transporting ATPase subunit beta (ATP1B, K01540), ion channels voltage-dependent calcium channels (CACNA2D2, K04859, CACNA2D3, K04860), nicotinic acetylcholine receptors (CHRNA2, CHRNA6, CHRND, CHRNN), calcium-activated chloride channel regulator (CLCA3_4, K05030, CLCA1), transporters MFS transporter, MCT family, solute carrier family 16 (monocarboxylic acid

transporters) (SLC16A12, SLC16A13, SLC16A7), solute carrier family 25 (mitochondrial uncoupling protein), member 27 (SLC25A27), solute carrier family 25, member 38 (SLC25A38), solute carrier family 6 (neurotransmitter transporter, glycine) member 5/9 (SLC6A5_9), solute carrier family 25 (mitochondrial adenine nucleotide translocator), member 4/5/6/31 (SLC25A4S), solute carrier family 39 (zinc transporter) (SLC39A4 / SLC39A5 / SLC39A6 / SLC39A10), and transient receptor potential cation channel subfamily M (TRPM2 / TRPM3).

Table 4.14. Regulation of contigs of ion channels and transporters. In the legend, green and red colors represent downregulation and upregulation with higher color intensity denoting greater log-fold change.

		RTvsRC.BA		RTvsRC.CB		RTvsRC.DC		RTvsRC.CA		RTvsRC.DB		RTvsRC.DA		RTvsRC	
Symbol	Name	logFC	FDR	logFC	FDR	logFC	FDR	logFC	FDR	logFC	FDR	logFC	FDR	logFC	FDR
ATP1B	sodium/potassium-transporting ATPase subunit beta	-11.358764	4.97E-02												
CACNA2D2	voltage-dependent calcium channel alpha-2/delta-2	-13.614783	3.68E-02												
CACNA2D3	voltage-dependent calcium channel alpha-2/delta-3	-16.484786	1.73E-02	15.171934	3.09E-02							-15.845905	3.28E-02		
CLCA1 / CLCA3_4	calcium-activated chloride channel regulator 1 / calcium-activated chloride channel regulator 3/4					-7.063468	2.24E-02								
TRPM2 / TRPM3	transient receptor potential cation channel subfamily M member 2 / transient receptor potential cation channel subfamily M member 3					-8.807222	2.95E-02			-9.073344	2.24E-02				
TRPM2 / TRPM3	transient receptor potential cation channel subfamily M member 2 / transient receptor potential cation channel subfamily M member 3					3.912835	2.95E-02			3.838714	3.15E-02				
TRPM2	transient receptor potential cation channel subfamily M member 2	-10.603246	1.36E-02					-10.907916	1.25E-02			-10.937361	1.77E-02	9.106610	4.22E-02
TRPM3	transient receptor potential cation channel subfamily M member 3					12.561163	4.31E-02								
CHRNA2 / CHRNN	nicotinic acetylcholine receptor alpha-2 / nicotinic acetylcholine receptor, invertebrate	14.461246	4.30E-02							-15.475262	3.35E-02				
CHRNA2 / CHRNA6 / CHRND	nicotinic acetylcholine receptor alpha-2 / nicotinic acetylcholine receptor alpha-6 / nicotinic acetylcholine receptor delta	-17.562370	4.47E-02												
CHRNA6	nicotinic acetylcholine receptor alpha-6									-16.788099	8.71E-03				
SLC6A5_9	solute carrier family 6 (neurotransmitter transporter, glycine) member 5/9	3.937095	1.13E-02							-3.375954	4.30E-02				
SLC25A38	solute carrier family 25, member 38	-4.258738	1.55E-02							4.671407	5.82E-03				
SLC25A38	solute carrier family 25, member 38	-2.458080	4.34E-02												
SLC16A12 / SLC16A13	MFS transporter, MCT family, solute carrier family 16 (monocarboxylic acid transporters), member 12 / MFS transporter, MCT family, solute carrier family 16 (monocarboxylic acid transporters), member 13	-8.180274	1.91E-02												
SLC16A12 / SLC16A13	MFS transporter, MCT family, solute carrier family 16 (monocarboxylic acid transporters), member 12 / MFS transporter, MCT family, solute carrier family 16 (monocarboxylic acid transporters), member 13	-6.064342	1.40E-02			6.256915	8.06E-03			7.367088	1.82E-03				
SLC16A12 / SLC16A13 / SLC16A7	MFS transporter, MCT family, solute carrier family 16 (monocarboxylic acid transporters), member 12 / MFS transporter, MCT family, solute carrier family 16 (monocarboxylic acid transporters), member 13 / MFS transporter, MCT family, solute carrier family 16 (monocarboxylic acid transporters), member 7	-9.133253	8.94E-03			7.845020	1.37E-02	-7.335023	2.47E-02	9.643251	5.18E-03				
SLC1A2 / SLC1A6	solute carrier family 1 (glial high affinity glutamate transporter), member 2 / solute carrier family 1 (high affinity glutamate/aspartate transporter), member 6			8.359408	9.62E-03										
SLC22A4_5	MFS transporter, OCT family, solute carrier family 22 (organic cation transporter), member 4/5			-9.498179	4.45E-02										
SLC25A27	solute carrier family 25 (mitochondrial uncoupling protein), member 27	-9.809311	3.07E-03							9.329050	6.24E-03				
SLC35B1	solute carrier family 35 (UDP-galactose transporter), member B1					3.965460	4.48E-02					4.099301	4.50E-02		
SLC39A10 / SLC39A4 / SLC39A5 / SLC39A6	solute carrier family 39 (zinc transporter), member 10 / solute carrier family 39 (zinc transporter), member 4 / solute carrier family 39 (zinc transporter), member 5 / solute carrier family 39 (zinc transporter), member 6					4.076970	2.58E-02								
SLC39A10 / SLC39A4 / SLC39A6	solute carrier family 39 (zinc transporter), member 10 / solute carrier family 39 (zinc transporter), member 4 / solute carrier family 39 (zinc transporter), member 6					3.613607	4.31E-02								
SLC6A2	solute carrier family 6 (neurotransmitter transporter, noradrenalin) member 2	-25.678497	4.98E-02												
STRA6	vitamin A receptor/transporter (stra6) family protein	-13.415371	2.97E-02												

-17 -14 -11 -8 -5 -2 0 +2 +5 +8 +11 +14 +17

Ion channels

One contig that mapped to Na^+/K^+ transporting, ATPase subunit beta 1 (ATP1B), was downregulated with salinity increase from steady-state in BA(↑) (Table 4.14). As animal cells do not have cell walls, alterations of cell volume can be detrimental to the cell membrane and cellular functions. Even in the absence of osmostress, cell volume regulation is essential, as high molecular weight polymers are continuously converted to osmotically active low molecular compounds for cellular processes (Mongin and Orlov, 2001). Under isosmotic condition (steady-state), cells have high concentrations of K^+ and low concentrations of Na^+ inside, whereas the opposite is true for the extracellular fluid. Low permeability of the membrane to Na^+ causes the Donnan effect and swelling tendency in the cell due to osmotic pressure (Mongin and Orlov, 2001). Under these conditions, cell volume regulation by active pump Na^+/K^+ ATPase is activated. Na^+/K^+ ATPase pumps ions Na^+ and K^+ against their concentration gradient, however, this requires a large portion of the cell's energy (Deaton, L. 2008; Mongin and Orlov, 2009; Sardini et al., 2003). For a typical animal cell, one third of its energy is consumed by this pump, and the value is much higher for the nerve cells (Alberts et al., 2008, p. 661). Moreover, activation of this pump is found to be coupled with glycolysis in many studies (Sanderson et al., 2020; Dutka & Lamb, 2007; Sepp et al., 2014). Exporting Na^+ out of the cell by this pump enhances sodium gradient to be used in the uptake of nutrients, such as glucose and amino acids by membrane transport proteins. This pump also contributes to the regulation of pH and Ca^{+2} levels (Sanderson et al., 2020). The pump was downregulated with salinity increase from steady-state in BA(↑), in concordance with the literature, as it is activated in steady-state condition for volume regulation due to Donnan effect and swelling tendency caused by osmotic pressure (Mongin and Orlov, 2001). The pump was downregulated as salinity was increased, probably with a decrease in swelling tendency. The regulation of this pump in the study was in line with alteration of membrane lipid composition (explained in Results 4.2.1.4. Lipid Metabolism section) with phospholipase activity, as eicosanoids are modulators of this pump (Therien and Blostein, 2000). The pump can also be regulated by cAMP levels, and therefore can be regulated by GPCR and protein kinase A (PKA) which directly phosphorylate the pump (Therien and Blostein, 2000) (Figure 4.11(14), Figure 4.11(15)). However, the effect of cAMP on the pump varies between species and tissues (Therien and Blostein, 2000), and was also found to be related with Ca^{+2} concentration (Therien and Blostein, 2000). The pump also interacts with signaling proteins PKC (Figure 4.11(14)) and PI3K (Pirahanchi et al., 2021).

In the study, calcium-related ion channels and calcium-activated proteins (phospholipases, annexin) were also found to be D.E. In bivalves, calcium is involved in calcification; calcium from

the gills, mantle, and gut is transported to extrapallial space to be used in the process (Sillanpää et al., 2020). Moreover, calcium was found to be the primary limiting factor for reduced calcification rates of Baltic mytilid mussels that inhabit low salinities (Sanders et al., 2020). Besides calcification, calcium is also involved in signal transduction, as it is a universal second messenger in eukaryotes that triggers complex signaling cascades and regulates various cellular processes with the change in its concentration (Modica et al., 2019). Activation of calcium signaling was seen with stress in bivalves (Prego-Faraldo et al., 2018; Zhao et al., 2012) and was linked to immune-related parameters (Zhao et al., 2012). In response to salinity stress, Zhao et al. (2012) found change in TRPM, Ca^{+2} binding proteins and Ca^{+2} binding EGF domain protein that controls signaling process and defense response.

Upon binding with calcium, calcium-binding proteins undergo conformational changes that trigger cellular processes (Clapham, 2007). Therefore, intracellular calcium concentration is tightly regulated and kept very low (Tsunoda and Owyang, 1993). Even very small changes in calcium concentrations are detected (Clapham, 2007), as uncontrolled levels of calcium increase can cause loss of membrane integrity, and form phosphate precipitates and protein and nucleic acid aggregates (Roch and Sherwood, 2011). Cells perform calcium regulation by various mechanisms, such as with calcium-binding proteins that lower its concentration with different binding affinities and calcium pumps (Clapham, 2007).

In the resting state, calcium is actively exported to extracellular space or intracellular stores by pumps such as Ca^{+2} ATPase, Na^{+}/ Ca^{+2} exchanger and Na^{+}/Ca^{+2}-K^{+} exchanger (Guerini, 1998). Upon signaling initiation by ligand binding or membrane depolarization, calcium is imported from extracellular space through ion channels or is released from intracellular stores. The fastest calcium signaling is provided by voltage-gated calcium channels (CaVs, CACN) (Figure 4.19(1)) that are capable of achieving folded intracellular calcium concentrations within very short periods of time (Clapham, 2007), due to the high electrochemical gradient across the cell membrane (Blaustein, 1985). Opening of CaVs increases periplasmic calcium that causes the release of acetylcholine from synaptic vesicles (Figure 4.19(2)) to bind to nicotinic acetylcholine receptors (nAChRs) (Figure 4.19(3)) of the adjacent cell membranes (Clapham, 2007). Upon binding to its ligand, nAChR allows cation influx (Na^{+}, K^{+}, and Ca^{+2}) that depolarizes the membrane (Figure 4.19(4)). Local membrane depolarization can open nearby voltage-gated calcium and sodium channels that cause an influx of $Na^{+}$and Ca^{+2}.

In addition, nAChRs (Figure 4.19(3)) are ligand-gated ion channels that respond to both the neurotransmitter acetylcholine and nicotine (Changeux, 2020). They are conserved channels found in the nervous system, muscle tissue, and in many other organs of vertebrates and invertebrates. The response triggered with acetylcholine differs with cell type and receptor. Even if the same ligand binds to the same receptor, a different response can be achieved in different cell types by the activation of different genes (Alberts et al., 2008, p. 885-886). Unlike vertebrates that have specialized nAChRs with the advanced nervous system, bivalves have highly diversified and expanded nAChRs that are suggested to have diversified functions and are involved in adaptation to sedentary life with a reduced nervous system. In bivalves, nAChRs are involved in various processes such as immune and stress responses (Jiao et al., 2019). In *M. edulis* gills, acetylcholine, generated in the nerve-free tissue of the gill plates regulates ciliary activity (Bülbring et al., 1953; Aiello, 1960) which is also linked to cytosolic calcium increase and signaling (Zagoory et al., 2002; Jokura et al., 2020; Catapane et al., 2016).

In the study, contigs of voltage-dependent calcium channel (CACNA2D2, CACNA2D3) were downregulated in BA(↑), indicating possible downregulation of calcium influx with salinity increase, as expected (Table 4.14). CACNA2D3 was also downregulated in DA and upregulated in CB(→). Contigs mapped to acetylcholine receptors (CHRNA2, CHRNA6, CHRND, CHRNN) were regulated in both directions in BA(↑). Acetylcholine receptors are involved in the ciliary activity of the gills, which is essential for feeding and respiration activities. Cilia assemble and disassemble with osmostress, acting as osmosensors and transmitting that signal to cells for response (Pedersen et al., 2012). Related to ciliary activity, a contig mapping to light chain of outer dynein arm which is involved in driving ciliary beating activity (Oda et al., 2016) was also downregulated in BA(↑) (Table 4.15). Another dynein contig with a blastx hit 'dynein heavy chain, axonemal [*Mytilus galloprovincialis*]' was upregulated with salinity decrease in DC(↓). Axonemal dyneins are motor proteins forming inner and outer arms of cilia that ensure motive force for the beating of the cilia (King, 2018). Another contig of GPRC, cadherin EGF LAG seven-pass G-type receptor 3 (CELSR3) was upregulated in DC(↓) (Table 4.12) which is involved in cell to cell signaling and cilium assembly (Uniprot, n.d. (i)). Regulation of these contigs indicates involvement of ciliary activity in osmosensing and regulation associated with salinity changes induced in our study.

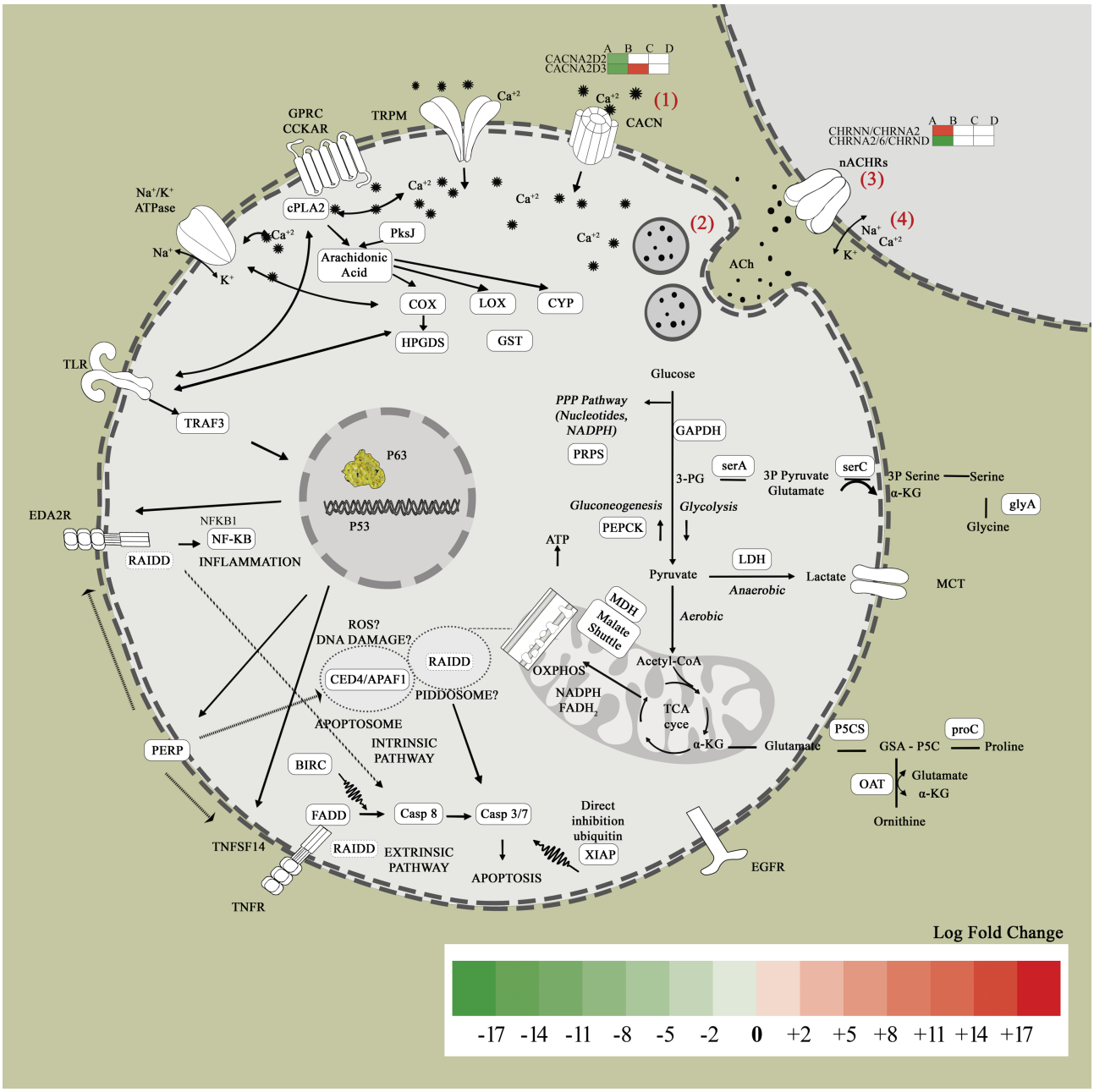


Figure 4.19. Acetylcholine release in the hypothesized model.In the legend, green and red colors represent downregulation and upregulation with higher color intensity denoting greater log-fold change.

Table 4.15. Regulation of dyneins. In the legend, green and red colors represent downregulation and upregulation with higher color intensity denoting greater log-fold change.

		RTvsRC.BA		RTvsRC.CB		RTvsRC.DC		RTvsRC.CA		RTvsRC.DB		RTvsRC.DA		RTvsRC	
Symbol	Name	logFC	FDR	logFC	FDR	logFC	FDR	logFC	FDR	logFC	FDR	logFC	FDR	logFC	FDR
DYNLL	dynein light chain LC8-type	-10.144597	2.20E-02												
	dynein heavy chain, axonemal [Mytilus galloprovincialis]					5.370446	2.74E-02								

-17 -14 -11 -8 -5 -2 0 +2 +5 +8 +11 +14 +17

Another set of calcium-related channels in the study that were D.E. (Table 4.14) included transient receptor potential melastatin channels (TRPMs). TRPMs belong to melastatin subfamily of TRP channels. TRP channels are involved in sensory signaling and alter membrane potential to generate calcium influx (Fernández et al., 2011). TRPMs are categorized into four groups according to sequence homology: TRPM1/ TRPM3, TRPM2/ TRPM8, TRPM4/ TRPM5 and TRPM6/ TRPM7 (Samanta et al., 2018). In the study, contigs mapped to TRPMs were TRPM2 and TRPM3 in KO mappings and TRPM1, TRPM2, TRPM3, and TRPM8 in blastx mappings.

TRPM2 is activated by calcium increase, ROS, cell signaling, and adenosine dinucleotides (Ahern, 2013). It increases cytoplasmic Ca^{+2} levels (Uniprot, n.d. (c)), and regulates insulin secretion, glucose metabolism (Uchida et al., 2011), and energy expenditure in mice (Zhang et al., 2012a). In controlled studies of Uchida et al. (2011) and Zhang et al. (2012a), TRPM2 knockout mice had impaired insulin secretion and had low weight gain in a high-fat feeding experiment, due to having higher energy expenditure. For contigs that mapped to TRPM2, TRPM8 was also examined as it shares the highest blast hit score with TRPM2. TRPM8 is a cold-activated channel, however high levels of expression are seen in constant temperatures as well (Vanden Abeele et al., 2006) by membrane depolarization, lipids, and compounds that imitate a cooling effect (Fernández et al., 2011). It was found to activate uncoupling protein 1 (UCP1) and inhibit weight gain and glucose intolerance in high-fat diets (Ma et al., 2012 cited in Ahern, 2013). TRPM1, on the other hand, was involved in melanocyte pigmentation and calcium homeostasis (Oancea et al., 2009), and TRPM3 was associated with calcium homeostasis and was expressed in hypotonic stress and osmotic cell swelling in HEK293 cells (Grimm et al., 2003). In DGE lists, TRPM2 (TRPM8 in bivalve blast hit) was downregulated in BA(↑) indicating downregulation of calcium influx, similar to the voltage-gated channels. Between timepoints C and D, TRPM contigs were regulated in both directions indicating active calcium regulation mechanisms.

In addition, downregulation of a contig mapped to calcium-activated chloride channel regulator (CLCA) in DC(↓) was observed (Table 4.14). CLCAs are involved in signal transduction and modulate chloride channels with calcium concentration for various cellular functions such as osmotic regulation, cell adhesion, cell proliferation, cell migration and mucus production (Reactome, 2014; Leblanc et al., 2005; Hu et al., 2019; Liu & Shi, 2019).

To sum up, the response of the calcium signaling can be hard to predict as complex signaling cascades and various processes are involved, and the response is determined not only by the concentration of the calcium but also by other factors such as the frequency of the calcium oscillations

(Alberts et al., 2008, p. 912). For example, an increase in intracellular calcium can activate opposing processes such as synaptic strengthening and synaptic weakening by binding to different proteins (Evans & Blackwell, 2015). Factors determining the preference of these binding proteins were suggested to be the amplitude of calcium concentration, duration of calcium increase, and location of the calcium influx (Evans & Blackwell, 2015). In our study, in the contrasts, overall, contigs of calcium regulation and signaling were D.E. Between timepoints A and B, calcium influx was decreased with salinity increase according to ion channels (Figure 4.19(1), Figure 4.11(18), Figure 4.11(19)). This could cause parallel regulation of contigs of phospholipase and arachidonic acid metabolism genes (Figure 4.11(1-10)). For timepoints B and C, upregulation of voltage-gated calcium channel also indicates calcium influx with acclimation to high salinity (Figure 4.19(1)). In DC(↓), with salinity decrease, TRPMs were regulated in both directions and CLCAs were downregulated, indicating calcium influx regulation in both directions.

Transporters

Contigs mapping to monocarboxylate transporters, SLC16A12, SLC16A13, SLC16A7 comprised another set of D.E. transporter genes. Contig expressions were inversely regulated with salinity, downregulated in BA(↑), upregulated in DC(↓), downregulated in CA(↑), and upregulated in DB(↓) (Table 4.14). Monocarboxylate transporters carry monocarboxylates such as lactate and pyruvate with the exchange of proton across the plasma membrane. Lactate from anaerobic metabolism can be transported through cotransport of H^+, and can then be oxidized further to regenerate pyruvate and NADH or be excreted (Ellington, 1983). In our study, monocarboxylate transporters were regulated in the same direction with LDHA (parallel to lactate generation) matching with the literature (Tseng et al., 2008), probably transporting lactate to be used in downstream processes such as excretion or to be used in gluconeogenesis.

Zinc transporter, solute carrier family 39 (zinc transporter), member 12 (mapped to KOs, 14710, K14711, K14712, K14716), was upregulated with salinity decrease in DC(↓) (Table 4.14). SLC39 (ZIP) family of zinc transporters are involved in cellular zinc homeostasis, increasing cytoplasmic zinc concentrations (Bafaro et al., 2017). Zinc is imported from extracellular space and intracellular compartments to cytosol (Baltaci and Yüce, 2018), and it enhances chemical catalysis and protein stability of more than 300 enzymes from all of the six enzyme classes and is important for various processes such as DNA replication, cell cycle, apoptosis, immune response, oxidative stress, and cytoprotection (Hambidge et al., 2000). It is especially important for energy metabolism due to being conducive in the electron transport chain, and mitochondrial pyruvate transport, and being involved

in lipid, nucleotide, protein, and carbohydrate metabolisms (Yang et al, 2017). Zinc supplementation was found to improve normal and impaired energy metabolism (Yang et al, 2017), whereas its excess inhibits energy production (Dineley et al., 2003). In this study, we have seen that chronic salinity alteration stimulated energy metabolism, and zinc influx might enhance adaptation to the more energy-demanding low salinity condition in DC(↓).

Genes regulated in our study, nicotinic acetylcholine receptor, glycine transporter (GLYT2, SLC6A5), a subunit of Na^+/K^+ ATPase (ATP1A), and monocarboxylate transporter (MCT) were also regulated in the study of Lockwood and Somero (2011). In both studies, regulation of nicotinic acetylcholine receptors can be related to the involvement of ciliary activity in osmosensing. GLYT2 was regulated in parallel with salinity. On the other hand, ATP1A and MCT were downregulated with salinity increase in our study while it was downregulated with salinity decrease in Lockwood and Somero (2011).

The regulation differences can be related to changing cellular requirements due to different treatments applied in each study. Our study examined exposure to long-term, chronic salinity increase and decrease whereas Lockwood and Somero (2011) simulate freshwater input by a 4-h exposure to decreased salinity from 35‰ to 29.75‰. Therefore Lockwood and Somero (2011) measured acute response and we measured long-term acclimation response. In our study, we have associated MCTs with anaerobic metabolism which supported aerobic metabolism. In Lockwood and Somero (2011), MCT downregulation with salinity decrease was associated with decreasing transportation of solutes into the cytosol. Similarly, downregulation of ATP1B with salinity increase was associated with a decrease in swelling tendency in our study. Na^+/K^+ pump maintains Na^+ and K^+ gradients across the cell membrane and is regulated by multiple mechanisms such as physiological stimuli or changes in Na^+ and K^+ concentrations (Therienand Blostein, 2000). In the study of Lockwood and Somero (2011), downregulation of Na^+/K^+ pump can related to other mechanisms rather than swelling, such as K^+ concentration, as KCNA10 was upregulated with salinity decrease in their study.

4.2.2. Oxidative Stress

Antioxidant expression was in opposite direction with salinity, downregulated with salinity increase and upregulated with salinity decrease (Table 4.16). Glutathione s-transferases (GSTs) were downregulated in BA(↑) and metallothionein (MT) was upregulated in DB(↓) (Table 4.16). Both of these antioxidants, GST and metallothionein, can increase with exposure to H_2O_2, protecting cells from oxidative stress and lipid peroxidation (Halliwell and Gutteridge, 2015). GSTs are also involved

in the conversion of unstable leukotriene A4 to leukotriene C4 (NCBI, n. d.). Some GSTs also have phospholipid hydroperoxide glutathione peroxidase (PGHPx) activity on membrane lipid peroxides (Halliwell and Gutteridge, 2015).

Table 4.16. Regulation of contigs related to redox homeostasis. In the legend, green and red colors represent downregulation and upregulation with higher color intensity denoting greater log-fold change.

		RTvsRC.BA		RTvsRC.CB		RTvsRC.DC		RTvsRC.CA		RTvsRC.DB		RTvsRC.DA		RTvsRC	
Symbol	Name	logFC	FDR	logFC	FDR	logFC	FDR	logFC	FDR	logFC	FDR	logFC	FDR	logFC	FDR
HPGDS	prostaglandin-H2 D-isomerase / glutathione transferase	-8.570366	7.44E-03												
HPGDS	prostaglandin-H2 D-isomerase / glutathione transferase	-11.140583	1.52E-02												
GST / HPGDS	glutathione S-transferase / prostaglandin-H2 D-isomerase / glutathione transferase	-9.230499	1.57E-02												
	RecName: Full=Metallothionein 10-III: Short=MT-10-III									4.546483	3.96E-02				
	RecName: Full=Metallothionein 10-III: Short=MT-10-III									3.972217	4.91E-02				

-17 -14 -11 -8 -5 -2 0 +2 +5 +8 +11 +14 +17

In this vein, timepoint A had higher metabolic rate and phospholipase activity compared to timepoint B, as discussed in Results 4.2.1.1. Oxidative Phosphorylation, 4.2.1.2. Carbohydrate Metabolism, and 4.2.1.4. Lipid Metabolism sections. With metabolic rate, reactive oxygen species (ROS) increase as well, due to electron leakage in the electron transport chain. To attenuate, the contig UCP4 was also downregulated in BA(↑), decreasing ROS formation (Azzu and Brand, 2010; Ramsden et al., 2012). Additionally, phospholipase activity was higher at timepoint A compared to timepoint B. Phospholipase activity causes hydrolysis of phospholipids that can further result in the generation of eicosanoids, and lipid peroxidation by the enzymes LOX and COX (Speed and Blair, 2011). GST downregulation between timepoints A and B could therefore be a response to both protect from ROS due to energy metabolism and lipid peroxidation due to COX and LOX.

Metallothionein also protects the cell from oxidative stress and DNA damage, and in our study, metallothionein contigs were upregulated between timepoints B and D. If metabolic rate increases at lower salinities, metallothionein upregulation can protect from H_2O_2 and lipid peroxidation. MT is also important for copper and zinc homeostasis. Zinc protects from oxidative stress by participating in the synthesis of metallothioneins and contributing to the catalysis of antioxidant enzymes and stabilization of the membrane (Marreiro et al., 2017). In another contrast, DC(↓), contig belonging to SLC39 (ZIP) family of zinc transporter was upregulated with salinity decrease (Table 4.14), which causes zinc influx as explained in the Results 4.2.1.6., Ion Channels and Transporters section. Zinc can interfere with calcium, and other metal-dependent processes and proteins if it overly increases.

Metallothionein controls its concentration (Maret, 2000), and it is likely that MT upregulation probably protected the cells from oxidative stress and help enhance zinc homeostasis in the study.

4.2.3. Apoptosis

In cells, death and proliferation are always in balance and apoptosis ensures organismal homeostasis by maintaining normal cell turnover, necessary to eliminate unwanted or damaged cells. Apoptosis can be initiated under stress and responses are regulated by a network of apoptotic and antiapoptotic pathways; with stress duration and intensity determining whether a cell will adapt and survive (signaled via antiapoptotic pathways) or die from necrosis, autophagy or apoptosis (signaled via apoptotic pathways) (Milisav et al., 2017). In the cell undergoing apoptosis, nucleus, cytoskeleton and protein substrates are cleaved, generating apoptotic bodies that are marked to be engulfed by phagocytic cells (Romero et al., 2015). Apoptosis has two alternative pathways, namely intrinsic and extrinsic pathways, both of which are executed by caspases (Julien and Wells, 2017). The intrinsic pathway is mediated by the integrity of the mitochondrial structure when cellular stress and damage are detected. By the activation of proapoptotic genes (Figure 4.20(1)) that trigger mitochondrial outer membrane permeabilization (MOMP) (Figure 4.20(2)), mitochondrial proteins are released to the cytosol (Figure 4.20(3)),a which neutralize inhibitor of apoptosis (IAP) (Figure 4.20(4)), form apoptosome complex (Figure 4.20(5)), activate caspases (Figure 4.20(6)) and lastly cause DNA fragmentation (Figure 4.20(7)). The extrinsic pathway is mediated by the binding of extracellular ligands (Figure 4.20(8)) to death receptors (Figure 4.20(9)) (Romero et al., 2015). Here, Fas Associated Death Domain (FADD) (Figure 4.20(10)) adaptor attaches to clustered receptors and activates caspase 8 (Figure 4.20(11)), which further activates executioner caspases (Figure 4.20(12)) (Kumar et al., 2015).

Apoptosis is important for the control of immune response for destroying cells that are infected and also are no longer needed. It is especially important for bivalves which are constantly exposed to changing environments and microorganisms. In bivalves, apoptosis is a highly complex process, similar to that in vertebrates. Key genes such as p53, BCL2, BI-1, and PDRP are more closely related to those vertebrates, while initiator caspases and Dff-A are more closely related to those in invertebrates (Romero et al., 2015). There is a high abundance and diversity of caspases, and some of them are functionally different from vertebrate homologues and detailed examination is necessary to identify their precise functions (Vogeler et al., 2021). Genes of apoptosis in bivalves are given in Figure 4.20 (Vogeler et al., 2021).

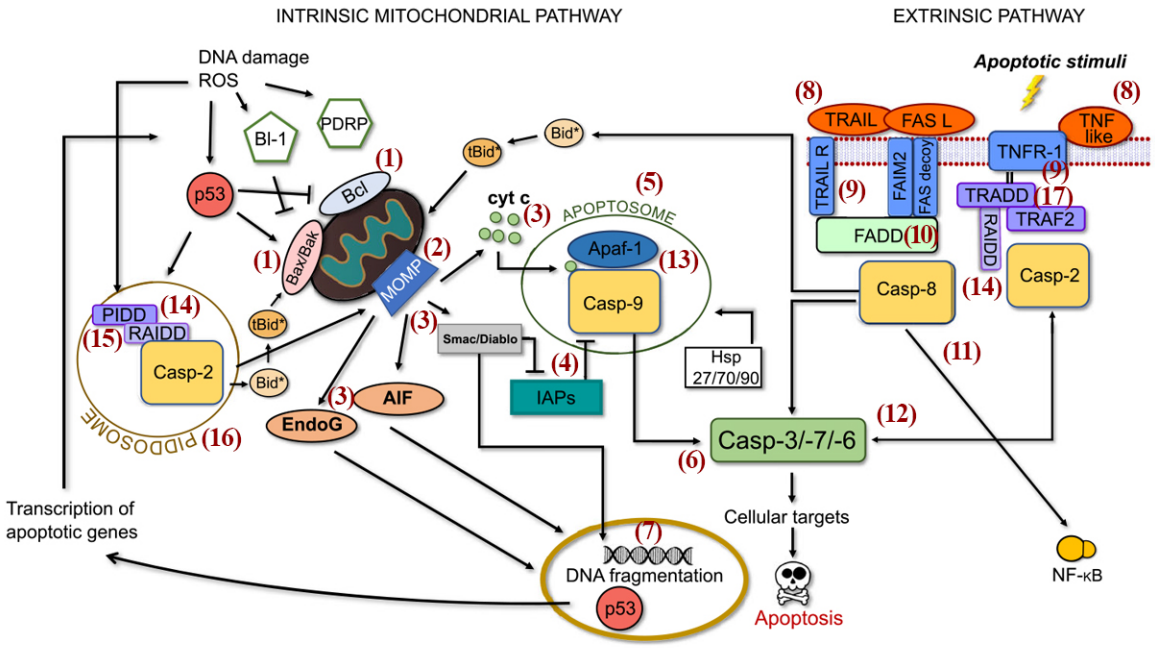
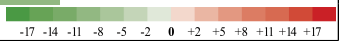


Figure 4.20. Apoptotic pathway of bivalves (Vogeler et al., 2021).

In this study, D.E. contigs (Table 4.17, Table 4.18) related to apoptosis were caspases (caspase 8 (K04398, CASP8) and caspase 7 (K04397, CASP7)), apoptotic inhibitors, baculoviral IAP repeat-containing proteins (BIRCs, K16060, K16061) and E3 ubiquitin-protein ligase XIAP (K04725), tumor necrosis factor (TNF) family genes, tumor necrosis factor ligand superfamily member 14 (TNFSF14, LIGHT, K05477) and tumor necrosis factor receptor superfamily member 27 (TNFRSF27, EDA2R, XEDAR; K05163), adaptor molecules, FAS-associated death domain protein (FADD, K02373) and CASP2 and RIPK1 domain containing adaptor with death domain (RAIDD, K02832), caspase activator, apoptotic protease-activating factor/ cell death protein 4 (APAF1/ CED-4, K02084/ K20105), and lastly effector, TP53 apoptosis effector (K10136, PERP) (Table 4.17). D.E. main innate receptors that can trigger apoptosis in the study were C-type lectins (CLRs), Toll-like receptors (TLRs), RIG- like receptors (RLRs) and NOD-like receptors (NLRs) (Table 4.18). A proapoptotic signal transducer, TNF receptor-associated factor 3 (TRAF3, K03174) was also D.E (Table 4.17). Epidermal growth factor receptor (EGFR, K04361, EC:2.7.10.1) and multiple epidermal growth factor-like domains protein 10 (MEGF10, K24068) were also examined in relation to apoptosis.

Table 4.17. Regulation of contigs related to apoptosis. In the legend, green and red colors represent downregulation and upregulation with higher color intensity denoting greater log-fold change.

		Symbol	Name	RTvsRC.BA logFC	RTvsRC.BA FDR	RTvsRC.CB logFC	RTvsRC.CB FDR	RTvsRC.DC logFC	RTvsRC.DC FDR	RTvsRC.CA logFC	RTvsRC.CA FDR	RTvsRC.DB logFC	RTvsRC.DB FDR	RTvsRC.DA logFC	RTvsRC.DA FDR	RTvsRC logFC	RTvsRC FDR
Apoptosis	IAP	BIRC2_3	baculoviral IAP repeat-containing protein 2/3	23.541959	8.94E-03												
		BIRC2_3 / BIRC7_8 / XIAP	baculoviral IAP repeat-containing protein 2/3 / baculoviral IAP repeat-containing protein 7/8 / E3 ubiquitin-protein ligase XIAP	-12.593723	2.25E-02												
		BIRC2_3 / BIRC7_8	baculoviral IAP repeat-containing protein 2/3 / baculoviral IAP repeat-containing protein 7/8									7.322288	3.44E-02				
		BIRC2_3 / BIRC7_8	baculoviral IAP repeat-containing protein 2/3 / baculoviral IAP repeat-containing protein 7/8					-12.962622	3.45E-02								
		BIRC2_3 / BIRC7_8 / XIAP	baculoviral IAP repeat-containing protein 2/3 / baculoviral IAP repeat-containing protein 7/8 / E3 ubiquitin-protein ligase XIAP			-12.484040	7.76E-03	8.541313	3.69E-02								
		BIRC2_3 / BIRC7_8	baculoviral IAP repeat-containing protein 2/3 / baculoviral IAP repeat-containing protein 7/8	6.201727	3.29E-02												
		BIRC2_3	baculoviral IAP repeat-containing protein 2/3									8.344666	2.30E-02				
		BIRC2_3	baculoviral IAP repeat-containing protein 2/3	-18.098976	1.87E-02												
		BIRC2_3 / BIRC7_8 / XIAP	baculoviral IAP repeat-containing protein 2/3 / baculoviral IAP repeat-containing protein 7/8 / E3 ubiquitin-protein ligase XIAP					-10.849273	2.58E-02	13.868603	6.04E-03						
		BIRC2_3 / BIRC7_8 / XIAP	baculoviral IAP repeat-containing protein 2/3 / baculoviral IAP repeat-containing protein 7/8 / E3 ubiquitin-protein ligase XIAP	3.221638	4.24E-02												
		BIRC2_3 / BIRC7_8 / XIAP	baculoviral IAP repeat-containing protein 2/3 / baculoviral IAP repeat-containing protein 7/8 / E3 ubiquitin-protein ligase XIAP	-9.873921	1.63E-02												
		BIRC2_3	baculoviral IAP repeat-containing protein 2/3			15.821827	3.95E-02										
		BIRC2_3 / BIRC7_8 / XIAP	baculoviral IAP repeat-containing protein 2/3 / baculoviral IAP repeat-containing protein 7/8 / E3 ubiquitin-protein ligase XIAP					18.948429	3.11E-02								
		BIRC2_3	baculoviral IAP repeat-containing protein 2/3	13.361301	5.03E-05					13.346427	8.09E-05			12.071797	9.14E-04	-12.060287	6.00E-05
		BIRC2_3	baculoviral IAP repeat-containing protein 2/3	8.564452	1.75E-02					9.797249	3.15E-03			10.069213	4.22E-03	-10.164760	3.46E-04
		BIRC2_3 / XIAP	baculoviral IAP repeat-containing protein 2/3 / E3 ubiquitin-protein ligase XIAP			-22.130648	5.62E-03					-21.874482	5.01E-03				
		BIRC2_3 / XIAP	baculoviral IAP repeat-containing protein 2/3 / E3 ubiquitin-protein ligase XIAP			-9.967991	2.66E-02	9.464662	3.68E-02	-10.030079	3.01E-02						
		BIRC7_8	baculoviral IAP repeat-containing protein 7/8			-20.312062	1.03E-02										
		BIRC7_8 / XIAP	baculoviral IAP repeat-containing protein 7/8 / E3 ubiquitin-protein ligase XIAP	15.760147	4.08E-02												
	CASP	CASP7	caspase 7							-13.697356	4.17E-02						
		CASP7	caspase 7	15.848817	1.36E-02			-16.598153	3.74E-03	17.973722	2.41E-03	-14.473248	1.14E-02				
		CASP8	caspase 8	-7.996524	3.17E-02									-10.809435	3.54E-02		
	Intrinsic	APAF1 / CED-4	apoptotic protease-activating factor / cell death protein 4					12.644579	3.32E-02								
	Intrinsic /Extrinsic	RAIDD	CASP2 and RIPK1 domain containing adaptor with death domain	10.928137	8.94E-03	-11.540273	1.34E-02										
		RAIDD	CASP2 and RIPK1 domain containing adaptor with death domain					9.641791	2.99E-02								
	TNF (Extrinsic)	PERP	TP53 apoptosis effector	-6.743645	4.34E-02												
		TRAF3	TNF receptor-associated factor 3	-12.668058	4.59E-02												
		EDA2R	tumor necrosis factor receptor superfamily member 27	2.944643	2.25E-02												
		TNFSF14 / TNFSF11	tumor necrosis factor ligand superfamily member 14 / tumor necrosis factor ligand superfamily member 11	-19.353102	1.40E-02									-18.919754	2.77E-02		
		FADD	FAS-associated death domain protein					10.312144	4.14E-02								
		EGFR	epidermal growth factor receptor			-6.322112	1.52E-02										
		EGFR	epidermal growth factor receptor									-7.907320	3.95E-02				
NF-κB	NF-κB	NFKB1	nuclear factor NF-kappa-B p105 subunit									-5.801149	1.97E-02				
		NFKB1	nuclear factor NF-kappa-B p105 subunit			-11.901170	2.06E-02					-12.230672	1.45E-02				
		NFKB1	nuclear factor NF-kappa-B p105 subunit							-20.345815	5.88E-03						
		NFKB1	nuclear factor NF-kappa-B p105 subunit									-9.616200	3.44E-02				



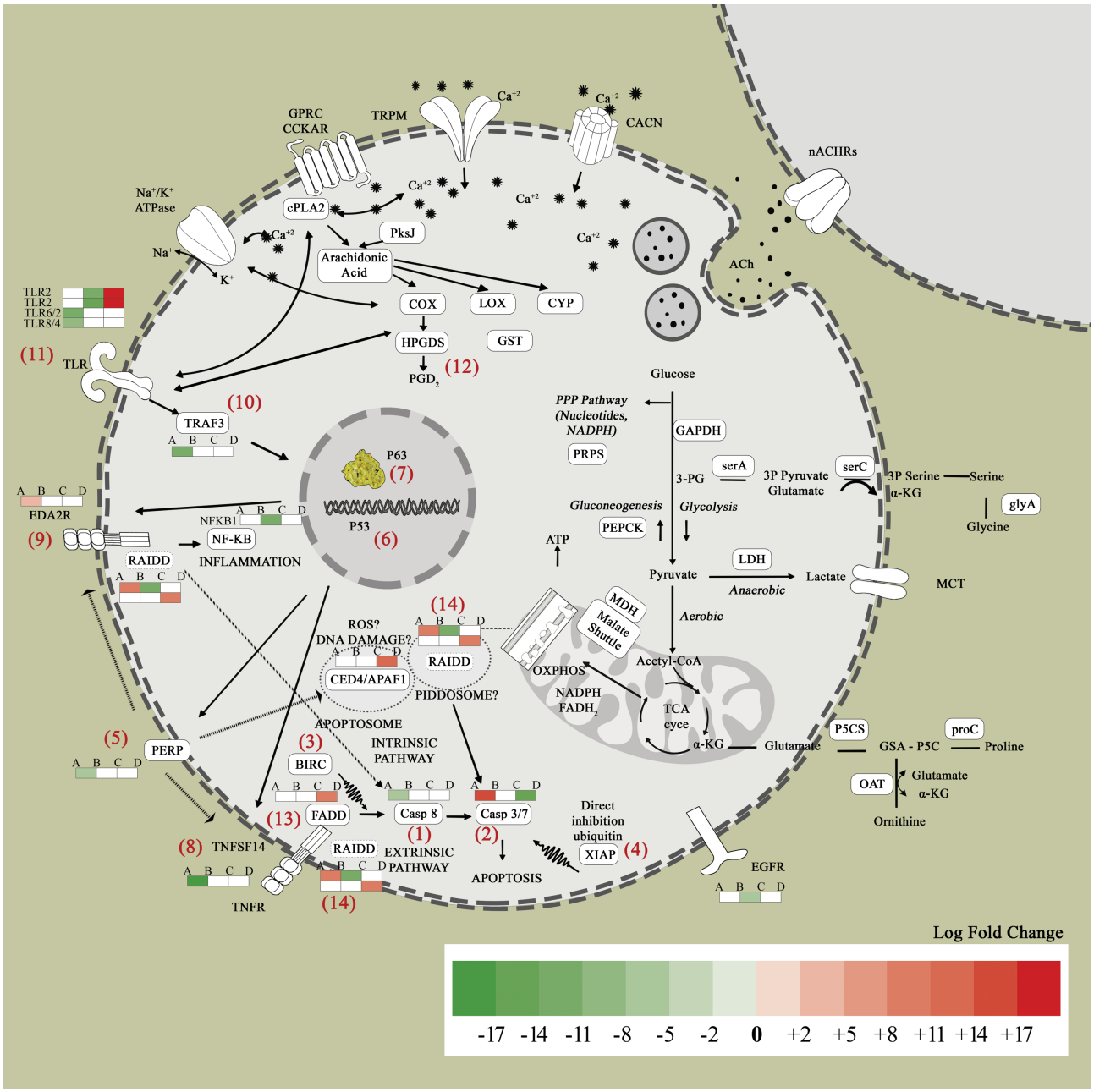


Figure 4.21. Apoptosis in the hypothesized model. In the legend, green and red colors represent downregulation and upregulation with higher color intensity denoting greater log-fold change.

In the study, it was seen that apoptosis was regulated in both directions, in salinity increase and decrease (Table 4.17). A contig mapped to initiator caspase, CASP8 (Figure 4.21(1)) was downregulated in BA(↑), but an executioner caspase, CASP7 (Figure 4.21(2)) was upregulated in BA(↑). CASP7 was also downregulated in DC(↓) (Table 4.17). Likewise, contigs mapping to apoptotic regulators (IAPs), BIRCs (Figure 4.21(3)) and XIAPs (Figure 4.21(4)) were also regulated in both directions (Table 4.17). IAPs inhibit apoptosis by binding to TNF or directly inhibit executioner caspases (Scott et al., 2005; Meng et al., 2013). Regulation of these IAPs in the study likely ensured survival and improved stress tolerance by inhibiting apoptosis (Meng et al., 2013).

Apoptosis probably played an important role in adaptation to stress both in high and low salinity as related contigs were regulated. Regulation of proapoptotic (caspases) and antiapoptotic (IAPs) genes was probably related to stress duration and intensity and were tuning survival, stress tolerance and apoptosis.

Salinity increase can be a stress factor to trigger apoptosis as normally mussels were at the home condition at 18‰ and salinity was gradually increased and decreased. However, due to the effect of low salinity on metabolism, low salinity conditions were also stressful in terms of energy budget when compared to high salinity. Especially, downregulation of apoptosis effector PERP (Figure 4.21(5)) with salinity increase in BA(↑) (Table 4.17) was notable in this perspective, as it is a novel effector of p53-dependent apoptosis (Attardi et al., 2000). PERP (Figure 4.21(5)) is the transcriptional target of p53 and p63 genes (Kazan et al, 2017) and is specifically expressed on p53 mediated apoptosis (McDonnell et al., 2019). Under stress conditions which culminate in DNA damage, cell cycle is suspended to prevent faulty replication, and is continued after the repair is completed. If the DNA damage is beyond repair, the cell goes to apoptosis (Attardi et al., 2000). P53 prevents proliferation of cells with damaged DNA by inducing cell cycle arrest or apoptosis. In this manner, acting as a 'guardian of the genome', p53 regulates hundreds to thousands of genes involved in related cellular processes such as energy metabolism, translation and also other feedback mechanisms (Fischer, 2017). Contigs that are involved in triggering and execution of intrinsic and extrinsic pathway of apoptosis in low salinity conditions in the study was likely related to PERP regulation.

For expression of PERP, besides p53, p63 is also necessary (Haupt et al., 2003; Ihrie et al., 2005). P63 has at least six isoforms, including i) transactivating p63 (TAp63) isoforms which bind to p53 response elements and induce cell cycle arrest and apoptosis, and ii) N-terminally truncated p63 (ΔNp63) isoforms which also bind to p53 response elements and negatively regulate p53, p63 and p73 activities (Sun et al., 2011). As isoforms have opposite and competitive effects, enhancing apoptosis or survival, p63 is referred to as 'Janus faced' (Caron de Fromentel et al., 2012). In this study, regulation of PERP indicates mainly involvement of TAp63 isoforms as it (PERP) is the effector of apoptosis. However, the induction mechanism of PERP is not precisely understood and is associated with both extrinsic and intrinsic pathways of apoptosis. Expression of PERP above the threshold level is correlated with cleavage of CASP8 and BID (McDonnell et al., 2019). Factors controlling PERP expression were found to be cellular state, p53/p63 mediated transcription and autophagy-lysosomal protein degradation (McDonnell et al., 2019). Besides its induction not being fully understood, BID has not been described in mollusks (Estévez-Calvar et al., 2013).

4.2.3.1. Extrinsic Pathway

Extrinsic Pathway Receptors

Contigs belonging to the extrinsic pathway of apoptosis were also regulated in the study. Death receptors of the extrinsic pathway (Figure 4.20(9)) belong to the tumor necrosis factor/nerve growth factor (TNF/NGF) receptor superfamily (Guicciardi and Gores, 2003). TNF family controls processes such as differentiation, proliferation, inflammation, and apoptosis. Between timepoints A and B, a contig mapping to TNFSF14 (Figure 4.21(8)) was downregulated and a contig mapping to TNFRSF27 (Figure 4.21(9)) was upregulated (Table 4.17). TNFSF14 promotes apoptosis (Coleman, 2019) and it is an inducer of NF-κB, which mainly regulates the response of inflammation, infection, and stress (D'Ignazio et al., 2018). It is also a ligand of lymphotoxin beta receptor (LTBR) and TNFRSF14 (Uniprot, n.d. (e); Liu et al., 2014a), and LTBR promotes apoptosis via TRAF3 (Uniprot, n.d. (h)), which was also downregulated in BA(↑) (Figure 4.21(10)). Another contig that belongs to the TNF family, TNFRSF27, is a receptor for EDA-A2 isoform of ectodysplasin. TNFRSF27 activates NF-κB, JNK pathways (Uniprot, n.d. (f)) and i) is a direct target of p53 (Lu et al., 2020), ii) is involved in 'ectodermal cell differentiation' (GO:0010668), and iii) is an 'intrinsic apoptotic signaling pathway by p53 class mediator' (GO:0072332) in humans. Regulation of these contigs can be related to innate receptors that were D.E. in the study (Table 4.18), as TNF synthesis is initiated by innate sensors in many types of cells (Ware, 2013).

Innate Receptors

Innate sensors are pathogen recognition receptors (PRRs) that recognize pathogens from common properties of molecules such as recognition of double-stranded RNA of viruses or pathogen-associated molecular patterns (PAMPs, e.g. LPS or peptidoglycan (PGN)) (Pålsson-McDermott and O'Neill, 2007). After recognition, signal transduction pathways activate immune processes such as inflammation and apoptosis. The main innate receptors that were D.E. in the study included CLRs, TLRs, RLRs, and NLRs. CLRs are involved in many immune and biological processes such as pathogen recognition (Gerdol and Venier, 2015), complement activation (Gerdol and Venier, 2015), inflammation (Cummings and McEver, 2009), phagocytosis (Song et al., 2010), and particle capture in feeding (Gerdol and Venier, 2015). RLRs recognize viral RNA and DNA (Gerdol and Venier, 2015). NLRs recognize peptidoglycan and flagellin of bacteria (Song et al., 2010). And lastly, TLRs recognize conserved PAMPs of bacteria, viruses, protozoa and fungi (Pålsson-McDermott and O'Neill, 2007).

In the study, CLRs were regulated in both directions in salinity increase and decrease (Table 4.18). RLRs also were regulated in both directions in salinity increase (Table 4.18). NLRs and TLRs (Figure 4.21(11)) were parallelly regulated (Table 4.18) with EDA2R (TNFRSF27) and TNFSF14, respectively (Table 4.17). Contigs mapping to NLRs (Table 4.18) were upregulated with increase (in BA(↑)) and downregulated with decrease (in DC(↓)), in line with the regulation of EDA2R (Table 4.17), as stated above. NLRs have not been identified in bivalves (Gerdol and Venier, 2015), however, Gerdol and Venier (2015) identified one NLR-like sequence in *M. galloprovincialis*. Consistently in our study, contigs mapping to NLRs in KO terms (EggNOG, KofamKOALA and KAAS) were not matching to any known proteins of bivalves in blastx hits.

Other than these main receptors, lectins, peptidoglycan recognition protein (PGRP), scavenger receptor class F member 1 (SCARF1) (Table 4.19), and many contigs with C1Q domains were also D.E. in both directions in salinity increase and decrease (Table 4.18). TNF regulation in the study can be related to these receptors, however, the most conspicuous and possible candidate is TLR regulation that was regulated inversely with salinity. TLRs (Figure 4.21(11)) were downregulated with salinity increase in BA(↑) and upregulated with salinity decrease in DC(↓) (Table 4.18) in line with TNFSF14 (Figure 4.21(8)) (Table 4.17). TLRs are important for discriminating self and non-self as it recognizes PAMPs of pathogens, but not of hosts (Erridge, 2010). Activation of TLR signaling is triggered with ligand binding and TLR dimerization (Figure 4.21(11)) which are tightly regulated processes (O'Neill and Bowie, 2007) due to their immunostimulatory effects. As salinity was the only variable in our experiment, it might have had some kind of indirect effect on TLR regulation. Modulation of TLRs from endogenous sources such as prostaglandins (Yoon et al. 2008) rather than pathogens has also been suggested (Erridge, 2010). In BA(↑), HPGDS was downregulated that catalyzes the conversion of prostaglandin H_2 to D_2 (Table 4.11). PGD_2 is a key mediator in inflammation and immune response, and also suggested to regulate TLR activity (Yoon et al., 2008). Therefore, in our study, TLR regulation can be related to PGD_2 activity, although this point requires further research.

It was also found that a p63 (Figure 4.21(7)) isoform, TAp63α (Figure 4.22(1)), induced by TLR3 (Figure 4.22(2)) initiated apoptosis of both intrinsic and extrinsic pathways in some endothelial cells of human (Sun et al., 2011). TLR3 was triggered by endogenous dsRNA (or exogenous analogs) which activated the signaling pathway that leads to the regulation of TAp63α. TAp63α binds to DNA through p53- or p63-responsive elements (Figure 4.22(3)) to regulate proapoptotic Noxa (Figure 4.22(4)) of intrinsic pathway and TNF receptor (tumor necrosis factor-related apoptosis-inducing ligand (TRAIL) receptor (Figure 4.22(5))) of extrinsic pathway. The hypothetical model of the process is given in Figure 4.22. In this study, we also considered the involvement of p63 gene

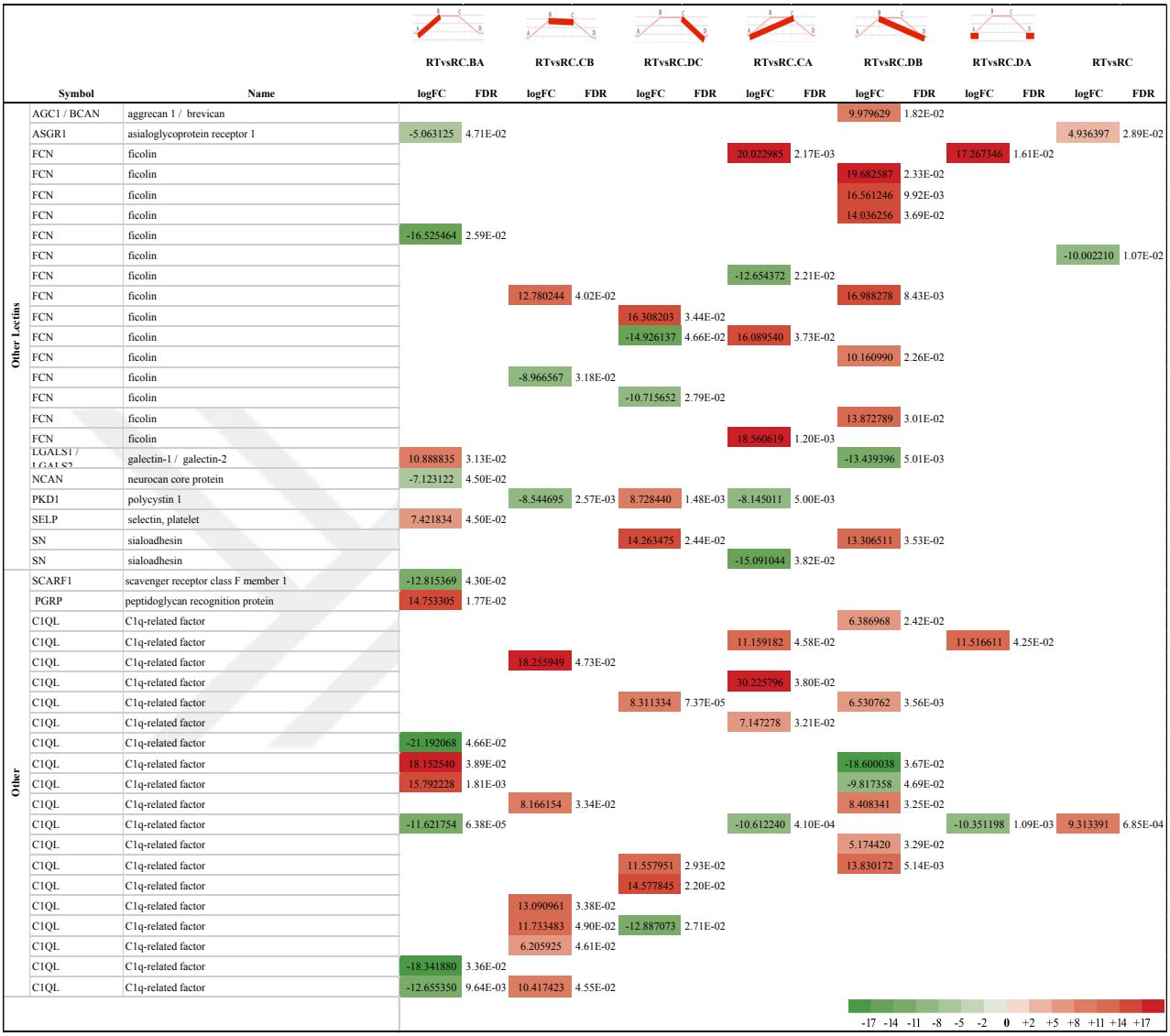
(probably TAp63 isoform) in our apoptosis model with a similar regulation, due to PERP downregulation in BA(↑) (Table 4.17).

Table 4.18. Regulation of contigs of the main innate receptors. In the legend, green and red colors represent downregulation and upregulation with higher color intensity denoting greater log-fold change.

		Symbol	Name	RTvsRC.BA logFC	RTvsRC.BA FDR	RTvsRC.CB logFC	RTvsRC.CB FDR	RTvsRC.DC logFC	RTvsRC.DC FDR	RTvsRC.CA logFC	RTvsRC.CA FDR	RTvsRC.DB logFC	RTvsRC.DB FDR	RTvsRC.DA logFC	RTvsRC.DA FDR	RTvsRC logFC	RTvsRC FDR
Innate Sensors (Pathogen Recognition Receptors)	CLR (lectins)	CD207 / CLEC17A	CD207 antigen / C-type lectin superfamily 17 member A	-10.637482	4.31E-02	11.315130	3.09E-02					19.202896	1.21E-04				
		CLEC17A / CD207	C-type lectin superfamily 17 member A / CD207 antigen	17.387745	2.65E-02					23.764054	1.94E-03			23.233946	4.22E-03		
		VCAN / AGC1 / NCAN / CLEC10A	versican core protein / aggrecan 1 / neurocan core protein / C-type lectin domain family 10 member A			-7.856964	3.21E-02	8.614681	1.32E-02	-8.833866	1.18E-02						
		CLEC10A / AGC1	C-type lectin domain family 10 member A / aggrecan 1									14.259789	1.66E-03				
		CLEC10A	C-type lectin domain family 10 member A					18.694139	3.32E-02			19.708921	2.05E-02				
		CLEC10A / FCER2	C-type lectin domain family 10 member A / low affinity immunoglobulin epsilon Fc receptor											-14.327149	6.49E-03		
		CLEC10A / NCAN	C-type lectin domain family 10 member A / neurocan core protein			-11.833061	1.68E-02					-11.734162	3.44E-02				
		ASGR2 / CLEC17A / CLEC4E / CLEC10A	asialoglycoprotein receptor 2 / C-type lectin superfamily 17 member A / C-type lectin domain family 4 member E / C-type lectin domain family 10 member A			-22.269505	3.08E-02										
		CLEC10A / AGC1 / CLEC4E	C-type lectin domain family 10 member A / aggrecan 1 / C-type lectin domain family 4 member E							-19.044135	1.53E-02						
		CLEC10A / CLEC4E	C-type lectin domain family 10 member A / C-type lectin domain family 4 member E	13.084160	2.28E-02												
		CLEC10A / CLEC4E / MRC	C-type lectin domain family 10 member A / C-type lectin domain family 4 member E / mannose receptor, C type							-7.939903	2.30E-02						
		CLEC4M / AGC1 / BCAN / CLEC4F / CLEC17A / CLEC10A	C-type lectin domain family 4 member M / aggrecan 1 / brevican / C-type lectin domain family 4 member F / C-type lectin superfamily 17 member A / C-type lectin domain family 10 member A			10.998009	1.47E-02										
		CLEC17A / CLEC4M / BCAN / NCAN / CLEC10A	C-type lectin superfamily 17 member A / C-type lectin domain family 4 member M / brevican / neurocan core protein / C-type lectin domain family 10 member A	-17.030086	3.17E-02												
		CLEC10A / COLEC12 / MRC	C-type lectin domain family 10 member A / collectin sub-family member 12 / mannose receptor, C type			6.148256	2.75E-03	-5.001676	2.23E-02								
		CLEC4E	C-type lectin domain family 4 member E	-16.931001	1.33E-02					-17.330534	1.33E-02			-18.007281	1.29E-02		
		CLEC4E	C-type lectin domain family 4 member E	12.228009	3.45E-02												
		CLEC4E	C-type lectin domain family 4 member E	-17.920541	8.69E-03	19.467337	7.28E-03										
		CLEC4E / MRC	C-type lectin domain family 4 member E / mannose receptor, C type			-9.994062	1.68E-02	13.062212	6.34E-04	-10.450531	8.90E-03						
		COLEC12 / CLEC4G	collectin sub-family member 12 / C-type lectin superfamily 4 member G					21.856780	3.02E-03								
		CLEC4M	C-type lectin domain family 4 member M	-11.856084	8.94E-03									-13.877200	2.54E-03		
		CLEC4M	C-type lectin domain family 4 member M							16.054302	2.37E-02						
		CLEC4M	C-type lectin domain family 4 member M			9.464432	1.88E-02					16.302714	2.56E-05				
		CLEC4F / CLEC17A / NCAN / CLEC4M / BCAN	C-type lectin domain family 4 member F / C-type lectin superfamily 17 member A / neurocan core protein / C-type lectin domain family 4 member M / brevican			11.159161	1.26E-02					9.899319	2.11E-02				
		CLEC4M	C-type lectin domain family 4 member M					-11.023412	4.39E-02	11.831965	3.96E-02						
		CLEC4M	C-type lectin domain family 4 member M									15.556748	2.06E-03	13.576001	1.04E-02		
		COLEC12 / CLEC4M	collectin sub-family member 12 / C-type lectin domain family 4 member M					-13.988474	4.12E-02	21.058294	5.13E-03						
		CLEC7A	C-type lectin domain family 7 member A			-13.795637	1.91E-02										
		MRC / KLRB	mannose receptor, C type / killer cell lectin-like receptor subfamily B	14.368046	6.03E-03	-11.775809	2.67E-02										
		MRC / CLEC17A / CLEC4F	mannose receptor, C type / C-type lectin superfamily 17 member A / C-type lectin domain family 4 member F			14.797720	4.47E-03										
		AGC1 / CLEC4F / CLEC17A	aggrecan 1 / C-type lectin domain family 4 member F / C-type lectin superfamily 17 member A			6.540026	1.52E-02										
		FCER2 / CLEC4F / NCAN	low affinity immunoglobulin epsilon Fc receptor / C-type lectin domain family 4 member F / neurocan core protein					21.532091	1.60E-02								
	RLR	DDX58 / IFIH1	ATP-dependent RNA helicase DDX58 / interferon-induced helicase C domain-containing protein 1	-10.108261	1.11E-02	10.271893	1.12E-02										
		DDX58 / IFIH1	ATP-dependent RNA helicase DDX58 / interferon-induced helicase C domain-containing protein 1	7.017617	4.63E-02												
	NLR	NLRC4 / NLRP3	NLR family CARD domain-containing protein 4 / NACHT, LRR and PYD domains-containing protein 3	21.319341	1.75E-03									16.261020	2.90E-02		
		NLRC4 / NLRP3	NLR family CARD domain-containing protein 4 / NACHT, LRR and PYD domains-containing protein 3	8.804246	1.45E-02							-8.293659	3.13E-02				
		NLRC4 / NLRP3	NLR family CARD domain-containing protein 4 / NACHT, LRR and PYD domains-containing protein 3											10.400476	4.26E-02		
		NLRP3	NACHT, LRR and PYD domains-containing protein 3									6.717345	2.26E-02				
		NLRP3	NACHT, LRR and PYD domains-containing protein 3					-14.724923	1.06E-02								
	TLR	TLR13 / TLR2	toll-like receptor 13 / toll-like receptor 2			-16.227972	1.52E-02	19.333157	2.87E-03								
		TLR2	toll-like receptor 2			-12.245666	2.43E-02	18.053097	7.93E-04								
		TLR2 / TLR6	toll-like receptor 2 / toll-like receptor 6	-13.909191	1.67E-02									-18.425885	3.80E-03		
		TLR4 / TLR8	toll-like receptor 4 / toll-like receptor 8	-10.606568	4.58E-02												

-17 -14 -11 -8 -5 -2 0 +2 +5 +8 +11 +14 +17

Table 4.19. Regulation of contigs of the other innate receptors. In the legend, green and red colors represent downregulation and upregulation with higher color intensity denoting greater log-fold change.



			RTvsRC.BA		RTvsRC.CB		RTvsRC.DC		RTvsRC.CA		RTvsRC.DB		RTvsRC.DA		RTvsRC	
	Symbol	Name	logFC	FDR	logFC	FDR	logFC	FDR	logFC	FDR	logFC	FDR	logFC	FDR	logFC	FDR
Other Lectins	AGC1 / BCAN	aggrecan 1 / brevican									9.979629	1.82E-02				
	ASGR1	asialoglycoprotein receptor 1	-5.063125	4.71E-02											4.936397	2.89E-02
	FCN	ficolin							20.022985	2.17E-03			17.267346	1.61E-02		
	FCN	ficolin									19.682587	2.33E-02				
	FCN	ficolin									16.561246	9.92E-03				
	FCN	ficolin									14.036256	3.69E-02				
	FCN	ficolin	-16.525464	2.59E-02												
	FCN	ficolin													-10.002210	1.07E-02
	FCN	ficolin							-12.654372	2.21E-02						
	FCN	ficolin			12.780244	4.02E-02					16.988278	8.43E-03				
	FCN	ficolin					16.308203	3.44E-02								
	FCN	ficolin					-14.926137	4.66E-02	16.089540	3.73E-02						
	FCN	ficolin									10.160990	2.26E-02				
	FCN	ficolin			-8.966567	3.18E-02										
	FCN	ficolin					-10.715652	2.79E-02								
	FCN	ficolin									13.872789	3.01E-02				
	FCN	ficolin							18.560619	1.20E-03						
	LGALS1 / LGALS2	galectin-1 / galectin-2	10.888835	3.13E-02							-13.439396	5.01E-03				
	NCAN	neurocan core protein	-7.123122	4.50E-02												
	PKD1	polycystin 1			-8.544695	2.57E-03	8.728440	1.48E-03	-8.145011	5.00E-03						
	SELP	selectin, platelet	7.421834	4.50E-02												
	SN	sialoadhesin					14.263475	2.44E-02			13.306511	3.53E-02				
	SN	sialoadhesin							-15.091044	3.82E-02						
Other	SCARF1	scavenger receptor class F member 1	-12.815369	4.30E-02												
	PGRP	peptidoglycan recognition protein	14.753305	1.77E-02												
	C1QL	C1q-related factor									6.386968	2.42E-02				
	C1QL	C1q-related factor							11.159182	4.58E-02			11.516611	4.25E-02		
	C1QL	C1q-related factor			18.255949	4.73E-02										
	C1QL	C1q-related factor							30.225796	3.80E-02						
	C1QL	C1q-related factor					8.311334	7.37E-05			6.530762	3.56E-03				
	C1QL	C1q-related factor							7.147278	3.21E-02						
	C1QL	C1q-related factor	-21.192068	4.66E-02												
	C1QL	C1q-related factor	18.152540	3.89E-02							-18.600038	3.67E-02				
	C1QL	C1q-related factor	15.792228	1.81E-03							-9.817358	4.69E-02				
	C1QL	C1q-related factor			8.166154	3.34E-02					8.408341	3.25E-02				
	C1QL	C1q-related factor	-11.621754	6.38E-05					-10.612240	4.10E-04			-10.351198	1.09E-03	9.313391	6.85E-04
	C1QL	C1q-related factor									5.174420	3.29E-02				
	C1QL	C1q-related factor					11.557951	2.93E-02			13.830172	5.14E-03				
	C1QL	C1q-related factor					14.577845	2.20E-02								
	C1QL	C1q-related factor			13.090961	3.38E-02										
	C1QL	C1q-related factor			11.733483	4.90E-02	-12.887073	2.71E-02								
	C1QL	C1q-related factor			6.205925	4.61E-02										
	C1QL	C1q-related factor	-18.341880	3.36E-02												
	C1QL	C1q-related factor	-12.655350	9.64E-03	10.417423	4.55E-02										

-17 -14 -11 -8 -5 -2 **0** +2 +5 +8 +11 +14 +17

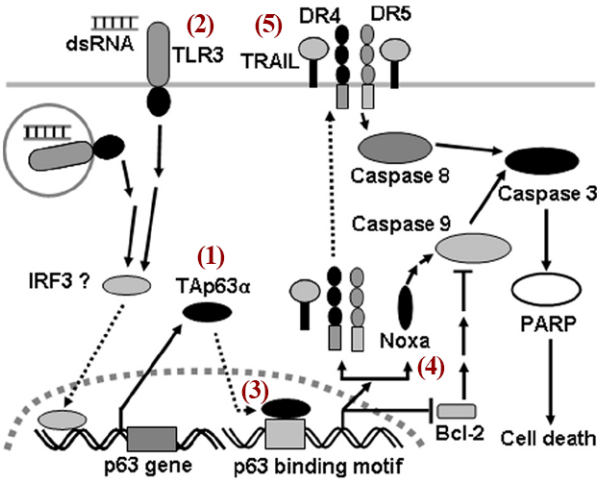


Figure 4.22. Hypothetical model of the pathway which activated TAp63α dependent apoptosis by TLRs (Sun et al., 2011).

Extrinsic Pathway Adaptors

FADD (Figure 4.20(10), Figure 4.21(13)) was another upregulated contig in DC(↓) that is involved in the extrinsic pathway of apoptosis. It is an adaptor molecule that mediates apoptotic signals from various receptors such as FAS, TRAIL and TNF (Figure 4.21(8)). It recruits initiator caspase 8 (Figure 4.20(11), Figure 4.21(1)) which initiates caspase cascade to execute apoptosis (Uniprot, n.d. (d); Estévez-Calvar et al., 2013). In *Crassotrea hongkongensis*, FADD-CASP 8 also activates inflammatory response (Vogeler et al., 2021). Upregulation of FADD with salinity decrease (in DC(↓)) was in line with downregulation of TNFSF14 with salinity increase (in BA(↑)), both having higher expression in lower salinity conditions.

4.2.3.2. Extrinsic/Intrinsic Pathway. Two RAIDD (Figure 4.20(14), Figure 4.21(14)) contigs were also D.E. (Table 4.17). One of the RAIDD contigs was upregulated in DC(↓) and the other was upregulated in BA(↑) and downregulated in CB(→). RAIDD is an adaptor protein that recruits CASP2, and can be involved in apoptosis in two ways. First (Figure 4.20(14)), in the intrinsic pathway of vertebrates, it is involved in the formation of PIDDosome complex (Figure 4.20(16)) with p53-induced death domain protein 1 (PIDD1) (Figure 4.20(15)) and the CASP2 to activate stress-induced apoptosis (Uniprot, n.d. (g)). And second (Figure 4.20(17)), in the extrinsic pathway, it can bind with TNF receptors and TRADD to activate apoptosis (Uniprot, n.d. (g); Vogeler et al., 2021). RAIDD regulation in this study could also be through the intrinsic pathway, besides the extrinsic pathway, as PIDD and RAIDD homologue genes were identified in bivalves suggesting the formation of PIDDosome in bivalves for apoptosis (Vogeler et al., 2021). The RAIDD and TNFRSF27 contigs

were upregulated in BA(↑), suggesting that apoptosis was likely triggered with salinity increase as well.

4.2.3.3. Intrinsic Pathway. A contig mapping to APAF1/ CED-4 (Figure 4.20(13), Figure 4.21(15)) was also upregulated in DC(↓). This gene is involved in apoptosome formation in the intrinsic apoptotic pathway that is triggered by stress signals, such as DNA damage or oxidative stress. In this study, energy metabolism was altered with salinity change and low salinity was associated with high energy expenditure and high metabolic rate. High metabolic rate can increase ROS production which can cause oxidative stress, however, no antioxidant enzymes were found to be D.E. in DC(↓). DNA damage response was also examined and no significant D.E. genes were found (Table 4.20). Only ATP-dependent DNA helicase PIF1 (K15255, EC:3.6.4.12) that is involved in mitochondrial and nuclear genome stability (Nextprot, n.d.) were downregulated between DC(↓) (Table 4.20).

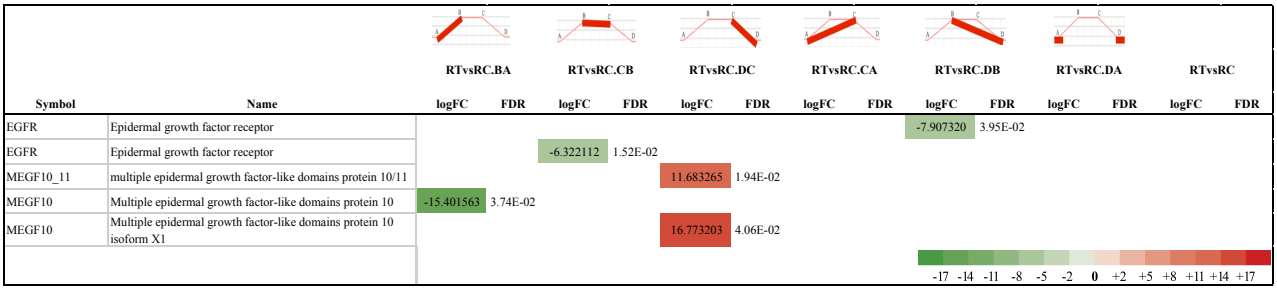
Table 4.20. Regulation of contigs of DNA damage response. In the legend, green and red colors represent downregulation and upregulation with higher color intensity denoting greater log-fold change.

		RTvsRC.BA		RTvsRC.CB		RTvsRC.DC		RTvsRC.CA		RTvsRC.DB		RTvsRC.DA		RTvsRC	
Symbol	Name	logFC	FDR	logFC	FDR	logFC	FDR	logFC	FDR	logFC	FDR	logFC	FDR	logFC	FDR
PIF1	ATP-dependent DNA helicase PIF1					-11.183092	9.81E-03			-11.534593	6.01E-03				

-17 -14 -11 -8 -5 -2 0 +2 +5 +8 +11 +14 +17

4.2.3.4. Other Antiapoptotic and Proapoptotic Genes. Lastly, EGFR and MEGF10 were examined in D.E. lists in relation to apoptosis (Table 4.21). EGFR promotes cell proliferation and survival, and negatively regulates apoptosis. MEGF 10 is a membrane receptor that is involved in the clearance of apoptotic cells (Uniprot, n.d. (j)). It is also a negative regulator of the cell cycle (Zhao et al., 2012). EGFR was not D.E. with salinity increase in BA(↑) and salinity decrease in DC(↓) in the study. MEGF 10 was inversely regulated with salinity, downregulated with salinity increase in BA(↑) and upregulated with salinity decrease in DC(↓). Regulation of MEGF10 supported regulation of PERP and apoptosis at the lower salinity condition, likely due to its involvement in the clearance of apoptotic cells.

Table 4.21. Regulation of contigs of EGFR and MEGF 10. In the legend, green and red colors represent downregulation and upregulation with higher color intensity denoting greater log-fold change.



Symbol	Name	RTvsRC.BA logFC	RTvsRC.BA FDR	RTvsRC.CB logFC	RTvsRC.CB FDR	RTvsRC.DC logFC	RTvsRC.DC FDR	RTvsRC.CA logFC	RTvsRC.CA FDR	RTvsRC.DB logFC	RTvsRC.DB FDR	RTvsRC.DA logFC	RTvsRC.DA FDR	RTvsRC logFC	RTvsRC FDR
EGFR	Epidermal growth factor receptor									-7.907320	3.95E-02				
EGFR	Epidermal growth factor receptor			-6.322112	1.52E-02										
MEGF10_11	multiple epidermal growth factor-like domains protein 10/11					11.683265	1.94E-02								
MEGF10	Multiple epidermal growth factor-like domains protein 10	-15.401563	3.74E-02												
MEGF10	Multiple epidermal growth factor-like domains protein 10 isoform X1					16.773203	4.06E-02								

4.3. Gene Set Enrichment Analysis

Summaries of enriched Gene Ontology (GO) terms having FDR < 0.25 (for salinity increase Figure B.1-B.4, for salinity acclimation Figure B.5-B.8, for salinity decrease Figure B.9-B.12 in Appendix B) and top 50 enriched GOs by NES scores (Table 4.22-4.27) were interpreted. 417, 257, and 388 gene ontology terms were enriched (with FDR < 0.25), for salinity increase, high salinity acclimation, and salinity decrease, respectively. Broadly, gene enrichments were grouped under ciliary activity (Table 4.22), energy metabolism, oxidative phosphorylation (Table 4.23), gene expression regulation (Table 4.24), protein metabolism (Table 4.25), nucleotide metabolism (Table 4.26), and DNA damage (Table 4.27). Group enrichments were interlinked with each other, presenting a starting point to hypothesize about the details of the actual processes.

4.3.1. Ciliary Activity

GOs involved with ciliary activity were notably greater in BA(↑) and CB(→). Cell projection assembly was enriched in salinity increase and high salinity acclimation in both Revigo summarizations (Figure B.2, Figure B.3, Figure B.6, Figure B.7, Figure B.11 in Appendix B) and top 50 enriched GOs list (Table 4.22 (1)). Cillium is a microtubule-based organelle of eukaryotic cells that assemble and disassemble with environmental signals (Pedersen et al., 2012), and is mainly involved in motility and sensing. Non-motile cilia consist of lipid and membrane proteins, TRP channels, GCPRs, receptor tyrosine kinases (RTKs), and extracellular matrix receptor protein complexes (Pedersen et al., 2012), which enable sensing of extracellular signals such as osmolarity, chemicals and light (Adams, 2010). Cillium is also rich in signaling effector proteins and transcription factors, which enable transmitting signals to the cell for response (Pedersen et al., 2012). It also acts as a mechanoreceptor responder, via opening calcium channels for calcium influx (Adams, 2010). In multicellular organisms, it usually helps the movement of materials and fluid; for example, it is

involved in mucociliary clearance inhibiting entrance of dust, smog and pathogens to the lungs in the respiratory epithelium (Kummer, 2008). Another example involves helping to transport food and mix it with digestive juices in the digestive track of snails (Dar et al., 2017). In bivalves, many tissues are ciliated, such as gills, mantle, and palps, helping with various organismal processes (Gosling, 2008).

Table 4.22. GOs of cilliary activity enriched in top 50 list by NES scores.

		 RTvsRC.BA	 RTvsRC.CB	 RTvsRC.DC
Cilliary Activity	Biological Process	(1) cell projection assembly (GO:0030031) (1) cell projection organization (GO:0030030) (1) plasma membrane bounded cell projection assembly (GO:0120031) (1) plasma membrane bounded cell projection organization (GO:0120036) (1) cilium assembly (GO:0060271) (1) cilium organization (GO:0044782) (2) exocytosis (GO:0006887)	(1) cilium assembly (GO:0060271) (1) cell projection assembly (GO:0030031) (1) cilium organization (GO:0044782) (1) plasma membrane bounded cell projection assembly (GO:0120031) (1) plasma membrane bounded cell projection organization (GO:0120036) (1) cell projection organization (GO:0030030) (2) exocytosis (GO:0006887) (2) regulation of postsynaptic membrane potential (GO:0060078) (2) regulation of membrane potential (GO:0042391)	
	Cellular Component	(1) plasma membrane bounded cell projection (GO:0120025) (1) cilium (GO:0005929)	(1) cilium (GO:0005929)	(1) cilium (GO:0005929)
	Molecular Function		(2) transmitter-gated ion channel activity (GO:0022824) (2) transmitter-gated channel activity (GO:0022835) (2) neurotransmitter receptor activity (GO:0030594)	

Bivalve gills have three kinds of cilia: frontal, latero-frontal, and lateral, each with a specific function (Meseck et al., 2020). Frontal cilia create water currents that allow gas exchange, food intake, and waste removal (Thomsen et al., 2016; Ward et al., 1998; Meseck et al., 2020), and the other two enhance further movement and selective capturing of the particles (Meseck et al., 2020). Under the environmental change, gill ciliary activity is involved in the adaptation by adjusting the rate of beating of the cilia, which ensures a slower rate of exposure to changing environmental conditions (Deaton, 2008).

As gill ciliary activity generates water currents for filter-feeding and gas exchange, it can also affect energy production; for example, an increase of beating frequency was suggested to improve oxygen flux to intracellular mitochondria (Doeller et., 1993). The subject is controversial and Jørgensen (1990) suggested that filtration efficiency does not change according to physiological needs, such as nutritional requirements (in Riisgård et al., 2015). However, it is known that environmental variables such as temperature reduce beating rate (Galtsoff, 1964 in Lavaud et al., 2018), and changes in salinity have been observed to reduce filtration rate via the closure of the valve gap (Riisgård et al., 2015). Additionally, utilization of oxygen can also vary according to the species. For some species the rate of oxygen usage depends directly on ambient partial pressure (PO_2) (e.g. in *Modiolus demissus*), for others, efficiency is increased with strategies, such as increasing ventilation rate. In *M. edulis*, a species that is closely related to *M. galloprovincialis*, oxygen extraction efficiency can more than treble as PO_2 falls from 160 to 20mmHg (Taylor & Brand, 1975 in Gosling, 2003).

Ciliary activity is also a highly energy-consuming process. A continuous supply of ATP is needed for dynein ATPases that drive ciliary activity (Doeller et al., 1993). In the absence of oxygen, cilia can be temporarily activated, however, aerobic respiration is needed for rapid and continuous activity (Aiello, 1960). Moreover, anaerobic metabolism was seen to be obligatory for ciliary activity; although the ciliary activity of excised gills resumed with the addition of activatory substances (Aiello, 1960), the activity of lateral cilia stopped when glycolysis was inhibited.

In most bivalves such as *M. edulis*, the beating of the lateral ciliary activity is controlled by innervation from the central nervous system (Catapane et al., 1978). Neurotransmitter release (Table 4.22 (2)) regulates ciliary activity and alters membrane potential (Table 4.22 (2)) and cilia beating rate, which were also found to be correlated (Catapane et al., 2016). The neurotransmitter serotonin has an excitatory effect, increasing cilia beating rate and causing prolonged membrane depolarization, while dopamine has an inhibitory effect, decreasing beating rate and causing hyperpolarized resting membrane (Catapane et al., 2016, Catapane et al., 1978; Carroll and Catapane, 2007).

Another neurotransmitter, acetylcholine, generated in the nerve-free tissue of the gill plates also regulates ciliary activity in *M. edulis* (Bülbring et al., 1953; Aiello, 1960). Low concentration of acetylcholine has an excitatory effect, and vice versa (Aiello and Paparo, 1974). Cholinergic ciliary stimulation is linked to cytosolic calcium increase and signaling (Zagoory et al., 2002; Jokura et al., 2020; Catapane et al., 2016). Nicotinic acetylcholine receptor and calcium signaling that are involved in the regulation of ciliary activity were also D.E. in the differentially expressed gene lists, in agreement with GSEA analysis (Nicotinic acetylcholine receptor in BA(↑), dynein light chain in BA(↑), calcium-related channels in BA(↑), CB(→), and DC(↓)).

4.3.2. Oxidative Phosphorylation

Gene ontology terms related to oxidative phosphorylation were enriched in salinity decrease both in Revigo summarizations (Figure B.10, Figure B.11, Figure B.12 in Appendix B), and top 50 enriched GO list (Table 4.23). In oxidative phosphorylation, electrons of NADH and $FADH_2$ are transferred to O_2 to generate massive amounts of ATP in the electron transport chain of mitochondria. Therefore, enrichment of terms of oxidative phosphorylation reflects energy production. In differential gene expression (DGE) analysis, contigs of oxidative phosphorylation genes were found to be downregulated with salinity increase, in line with high glycolytic rate and energy expenditure of low salinity. The related contigs were not D.E. in salinity decrease, however overall same trend related with high energy expenditure of low salinity was observed (FUCA and LCT were upregulated

in DC(↓)). The reason was probably related to the acclimation period, the duration of the exposure to 18 ppt: Timepoint A was after the acclimation period at steady state, and mussels had been at 18 ppt for three weeks at the time of sampling, whereas at the time of sampling at timepoint D, mussels did not have any period of acclimation to 18 ppt. In GSEA, the same processes were also enriched in salinity decrease verifying results of DGE analysis. This was also seen in ribosomal proteins (Table 4.9). Oxidative phosphorylation and ribosomal genes were D.E. in salinity increase in DGE analysis, but enriched in salinity decrease in GSEA. This was probably due to the utilization of whole gene lists in GSEA but a subset in DGE analysis (*i.e.* those which have FDR<0.05), with DGE analysis providing the most important hits.

Table 4.23. GOs of oxidative phosphorylation enriched in top 50 list by NES scores.

		 RTvsRC.BA	 RTvsRC.CB	 RTvsRC.DC
Oxidative Phosphorylation	Biological Process			energy coupled proton transport, down electrochemical gradient (GO:0015985) ATP biosynthetic process (GO:0006754) ATP synthesis coupled proton transport (GO:0015986)
	Cellular Component			mitochondrial protein-containing complex (GO:0098798) proton-transporting ATP synthase complex (GO:0045259) respiratory chain complex (GO:0098803) respirasome (GO:0070469) mitochondrial matrix (GO:0005759) proton-transporting ATP synthase complex, coupling factor F(o) (GO:0045263)
	Molecular Function			

4.3.3. Gene Expression Regulation

Another group enriched in GSEA was gene expression regulation. GO terms linked to gene expression regulation were enriched in all of the treatments (Figure B.2, Figure B.3, Figure B.6, Figure B.7, Figure B.10, Figure B.11, Figure B.12 in Appendix B) while negative regulation of gene expression was enriched in salinity increase (Figure B.2 in Appendix B, Table 4.24). Gene expression regulation is the major adaptive mechanism for stress response and ensures proper adaptation to stronger stress (De Nadal, 2011), this being particularly important for long-term chronic stress like the one applied in this experiment. With the environmental change, regulation of gene expression ensures the production of proteins that are needed for adapting to the new conditions. GO terms that are related to protein synthesis, ribosomal subunits (Table 4.25 (3), Figure B.11 in Appendix B), tRNA processing and modification were enriched (Table 4.25(5), Figure B.12 in Appendix B) with salinity decrease, probably helping to adapt to the salinity change. This is in agreement with DGE analysis, where ribosomal genes were downregulated with salinity increase and protein turnover was higher in the low salinity condition. Other GO terms linked to protein metabolism were also enriched in all of the treatments (Table 4.25, Fig.18, Figure B.3, Figure B.4, Figure B.6, Figure B.7, Figure

B.8, Figure B.10, Figure B.11, Figure B.12 in Appendix B). Especially protein catabolic processes were highly enriched for salinity increase in both Revigo summarizations (Figure B.2, Figure B.3, Figure B.4 in Appendix B) and top 50 enriched GO list (Table 4.25 (1)).

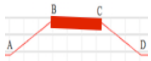
Table 4.24. GOs of gene expression regulation enriched in top 50 list by NES scores.

		 RTvsRC.BA	 RTvsRC.CB	 RTvsRC.DC
Gene Expression Regulation	Biological Process	mRNA metabolic process (GO:0016071) mRNA processing (GO:0006397) RNA splicing (GO:0008380) RNA splicing, via transesterification reactions with bulged adenosine as nucleophile (GO:0000377) mRNA splicing, via spliceosome (GO:0000398) RNA splicing, via transesterification reactions (GO:0000375) ncRNA metabolic process (GO:0034660) RNA catabolic process (GO:0006401) negative regulation of gene expression (GO:0010629)	mRNA processing (GO:0006397) RNA splicing via transesterification reactions (GO:0000375) RNA splicing (GO:0008380) RNA splicing via transesterification reactions with bulged adenosine as nucleophile (GO:0000377) mRNA splicing via spliceosome (GO:0000398) mRNA metabolic process (GO:0016071) positive regulation of transcription DNA-templated (GO:0045893) regulation of transcription by RNA polymerase II (GO:0006357) positive regulation of nucleic acid-templated transcription (GO:1903508) positive regulation of RNA metabolic process (GO:0051254) positive regulation of RNA biosynthetic process (GO:1902680)	mRNA processing (GO:0006397) ncRNA metabolic process (GO:0034660) RNA modification (GO:0009451) mRNA metabolic process (GO:0016071) ncRNA processing (GO:0034470) histone methylation (GO:0016571)
	Cellular Component			spliceosomal complex (GO:0005681) DNA-directed RNA polymerase complex (GO:0000428)
	Molecular Function			

4.3.4. Protein Metabolism

Proteins are continuously synthesized, modified, and degraded if they are functionally expired, misfolded or damaged beyond repair. For a protein to be functional, it must be folded in its native conformation. Stressors like oxidative stress, temperature, salinity and other factors can impair folding and cause dysfunction of proteins (Wang et al., 2004). Also, newly synthesized proteins can undergo partial degradation for modification (Donohue and Osna, 2004). Proteolysis is the degradation of proteins by hydrolysis at peptide bonds to polypeptides and amino acids, with protease enzymes or without enzymes. Two major pathways of proteolysis are lysosomal and ubiquitin-proteasome pathway (UPP) (Cooper, 2000). In the lysosomal pathway, proteins to be degraded are encapsulated in membrane vesicles and transported to the lysosome where they can be digested by catalytic enzymes including cathepsins, other proteases, and other hydrolytic enzymes. In UPP, proteins to be degraded are tagged with ubiquitin in the process of ubiquitination, and degraded by 26S proteasome. Proteosomal, ubiquitin-dependent protein catabolism was highly enriched in top 50 enriched gene ontology terms of salinity increase in our study (Table 4.25) matching with altered protein turnover rates at low salinities in the DGE analysis. GOs related to post-translational modifications of proteins were enriched in treatments (Table 4.25, Figure B.4, Figure B.6, Figure B.7, Figure B.8, Figure B.10, Figure B.11, Figure B.12 in Appendix B). In our study, among these GOs, some related to methylation were enriched in salinity increase (in Revigo summarizations, Figure B.2, Figure B.4 in Appendix B) and decrease (in top 50 GOs and in Revigo summarizations, Table 4.25, Figure B.10, Figure B.11, Figure B.12 in Appendix B).

Table 4.25. GOs of protein metabolism enriched in top 50 list by NES scores.

		 RTvsRC.BA	 RTvsRC.CB	 RTvsRC.DC
Protein Metabolism	Biological Process	(1) cellular protein catabolic process (GO:0044257) (1) protein catabolic process (GO:0030163) (1) proteolysis involved in cellular protein catabolic process (GO:0051603) (1) ubiquitin-dependent protein catabolic process (GO:0006511) (1) modification-dependent macromolecule catabolic process (GO:0043632) (1) proteasomal protein catabolic process (GO:0010498) (1) modification-dependent protein catabolic process (GO:0019941) (1) proteasome-mediated ubiquitin-dependent protein catabolic process (GO:0043161) (2) establishment of protein localization to organelle (GO:0072594) (2) intracellular protein transport (GO:0006886)	(2) intracellular protein transport (GO:0006886) (2) Golgi vesicle transport (GO:0048193) (2) export from cell (GO:0140352) (2) secretion by cell (GO:0032940) (2) exocytosis (GO:0006887) (2) cotranslational protein targeting to membrane (GO:0006613) protein homooligomerization (GO:0051260)	lipoprotein metabolic process (GO:0042157) (5) tRNA modification (GO:0006400) (5) tRNA processing (GO:0008033) (3) ribonucleoprotein complex biogenesis (GO:0022613) (6) macromolecule methylation (GO:0043414) (6) methylation (GO:0032259) (6) protein methylation (GO:0006479) (6-7) protein alkylation (GO:0008213)
	Cellular Component	(1) endopeptidase complex (GO:1905369) (1) proteasome complex (GO:0000502) (1) peptidase complex (GO:1905368) (1) ubiquitin ligase complex (GO:0000151) (1) proteasome core complex (GO:0005839) (4) endoplasmic reticulum (GO:0005783) (4) nuclear outer membrane-endoplasmic reticulum membrane network (GO:0042175) (4) endoplasmic reticulum membrane (GO:0005789) (4) endoplasmic reticulum subcompartment (GO:0098827) (4) peroxisome (GO:0005777) (4) Golgi apparatus (GO:0005794) (6-7) transferase complex (GO:1990234)	(1) proteasome complex (GO:0000502) (1) endopeptidase complex (GO:1905369) (4) endoplasmic reticulum (GO:0005783) (4) Golgi membrane (GO:0000139)	(1) proteasome complex (GO:0000502) (1) endopeptidase complex (GO:1905369) (1) peptidase complex (GO:1905368) (3) ribosomal subunit (GO:0044391) (3) large ribosomal subunit (GO:0015934) (4) endoplasmic reticulum protein-containing complex (GO:0140534) (6-7) transferase complex (GO:1990234)
	Molecular Function	(5) catalytic activity, acting on a tRNA (GO:0140101)	(5) catalytic activity acting on a tRNA (GO:0140101) (7) transferase activity transferring acyl groups (GO:0016746) (7) transferase activity transferring acyl groups other than amino-acyl groups (GO:0016747)	(6) S-adenosylmethionine-dependent methyltransferase activity (GO:0008757) (6) methyltransferase activity (GO:0008168) (6-7) transferase activity, transferring one-carbon groups (GO:0016741) (6-7) transferase activity, transferring alkyl or aryl (other than methyl) groups (GO:0016765)

Amino acids derived from the degradation of proteins can also be recycled to synthesize new proteins, converted to other amino acids or used in energy metabolism by converting to TCA cycle intermediates or glucose. We found an alteration in energy metabolism with salinity change, explained in greater detail in Results 4.2.1., Energy Metabolism and Salinity section. Also, amino acids can be utilized as osmolytes to buffer osmotic changes and maintain cell volume and osmolarity in marine invertebrates (Pourmozaffar et al., 2019). In this study, enrichment of protein catabolism was likely activated by cellular needs driven by osmoregulation, energy metabolism and the requirements of the new salinity conditions.

Enriched cellular components, endoplasmic reticulum (ER), golgi apparatus and peroxisomes are also related to protein metabolism (Table 4.25(4)). ER is involved in the transportation and post-translational modifications of proteins. Secretory pathway and integral membrane proteins are synthesized in ribosomes of the rough ER. After translation in the cytoplasm or the ER, post-translational modifications are applied that lead to the maturation of the proteins in the ER including protein folding, glycosylation, assembly and proteolytic processing (Wilk-Blaszczak, (n. d.)). Proteins can be transported to golgi apparatus that modifies and sorts proteins for further maturation and later sends them to proper destinations to be used in the cell or secreted by exocytosis. The smooth ER is also involved in carbohydrate metabolism, detoxification process and lipid, phospholipid and steroid synthesis. Golgi apparatus also synthesizes glycolipids and sphingomyelin (Cooper, 2000). Peroxisomes are membrane-closed organelles that can oxidize fatty acids and amino acids (Cooper,

2020). They are also involved in the metabolism of ROS species, lipid catabolism and biosynthesis adjusted according to metabolic needs (Islinger et al., 2012).

4.3.5. Nucleotide Metabolism

Another enriched category was nucleotide metabolism. Nucleotides are very important building blocks of nucleic acids, enzyme cofactors, pathway intermediates and energy currency (Lehninger et al., 2005, pp. 273). GOs related with ribonucleoside triphosphates (NTPs) were enriched in all treatments in Revigo summarizations (Figure B.2, Figure B.4, Figure B.6, Figure B.10, Figure B.11 in Appendix B) and in salinity increase (BA(↑)) and decrease (DC(↓)) in top 50 enriched GO terms in our study (Table 4.26). The result is matching with DGE analysis, where PRPS that is involved in nucleotide synthesis and cdd that is involved in recycling of pyrimidines (Frances & Cordelier, 2020), were D.E. in salinity increase (BA(↑)) and decrease (DC(↓)), respectively. In top 50 enriched GO terms, rather than pyrimidines, processes involving purine ribonucleoside triphosphate and formation (GO:0009205, GO:0009145) were enriched in salinity decrease (Table 4.26 (2)). Nucleoside-triphosphatase regulator activity (GO:0060589) which can modulate ATPase or GTPase (EMBL, n.d) and GTPase regulator activity (GO:0030695) were enriched in salinity increase in top 50 enriched GO terms. Small GTPase mediated signal transduction (GO:0007264, Figure B.2 in Appendix B), GTPase binding (GO:0051020, Fig.20), GTPase regulator activity (GO:0030695, Figure B.4 in Appendix B) and ATPase-coupled transmembrane transporter activity (GO:0042626, Figure B.4 in Appendix B) were also enriched in Revigo summarizations in salinity increase.

Table 4.26. GOs of nucleotide metabolism enriched in top 50 list by NES scores.

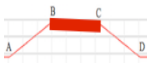
		 RTvsRC.BA	 RTvsRC.CB	 RTvsRC.DC
Nucleotide Metabolism	Biological Process			(1) ribonucleoside triphosphate metabolic process (GO:0009199) (1) ribonucleoside triphosphate biosynthetic process (GO:0009201) (2) purine ribonucleoside triphosphate metabolic process (GO:0009205) (1) nucleoside triphosphate biosynthetic process (GO:0009142) (2) purine nucleoside triphosphate biosynthetic process (GO:0009145)
	Cellular Component			
	Molecular Function	(3) nucleoside-triphosphatase regulator activity (GO:0060589) (3) GTPase regulator activity (GO:0030695)		

4.3.6. DNA Repair

DNA repair (GO:0006281) was enriched in all treatments in Revigo summarizations (Figure B.2, Figure B.6, Figure B.10 in Appendix B). In top 50 enriched list, cellular response to DNA damage stimulus (GO:0006974) and DNA repair (GO:0006281) was enriched in salinity decrease.

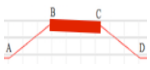
This enrichment could have originated due to altered metabolism and salinity stress. In this study, salinity change seems to have altered metabolic processes, energy expenditure and metabolic rate, all of which also agree with literature, as high salinity is associated with low energy expenditure and vice versa in *Mytilus* species (Freitas et al., 2017; Riisgard et al., 2013; Tedengren and Kautsky, 1986; Tedengren and Kautsky, 1987; Sanders et al., 2018). Metabolic processes can also increase ROS and cause DNA damage. In DGE analysis, UCP4 that decreases ROS formation and protects from oxidative stress was found to be regulated with altered energy metabolism. Antioxidant enzyme GST which protects cells from oxidative stress was also regulated parallelly. Additionally, genes involved in DNA damage response were examined, but only PIF1, which is involved in genome stability was found to D.E. in DC(↓). Although we could not find a noteworthy DNA damage response in DGE analysis, apoptosis can also be related to a mild case of DNA damage, as it was enriched in GSEA. Initiation of apoptosis and IAPs can manage and enhance adaptation to stress, caused by altered metabolism in the study.

Table 4.27. GOs of DNA damage and repair enriched in top 50 list by NES scores.

		 RTvsRC.BA	 RTvsRC.CB	 RTvsRC.DC
DNA Damage and Repair	Biological Process			DNA repair (GO:0006281) cellular response to DNA damage stimulus (GO:0006974)
	Cellular Component			
	Molecular Function			

Other than these groups, generic gene ontology terms of top 50 list that are involved in cellular processes are given in Table 4.28. We applied long-term gradual salinity stress and both GSEA and DGE analysis results were compatible in this regard.

Table 4.28. Generic GOs enriched in top 50 list by NES scores.

		 RTvsRC.BA	 RTvsRC.CB	 RTvsRC.DC
Others	Biological Process	cellular response to organonitrogen compound (GO:0071417) exocytosis (GO:0006887) organelle assembly (GO:0070925) metal ion transport (GO:0030001)	response to organic substance (GO:0010033) isoprenoid biosynthetic process (GO:0008299) exocytosis (GO:0006887) potassium ion transport (GO:0006813)	cellular protein-containing complex assembly (GO:0034622)
	Cellular Component	organelle subcompartment (GO:0031984) microbody (GO:0042579) intracellular protein-containing complex (GO:0140535)	spindle pole (GO:0000922) synapse (GO:0045202) organelle subcompartment (GO:0031984) intracellular protein-containing complex (GO:0140535)	oxidoreductase complex (GO:1990204) organelle inner membrane (GO:0019866) intracellular protein-containing complex (GO:0140535)
	Molecular Function	cation channel activity (GO:0005261)	signaling receptor binding (GO:0005102) G protein-coupled peptide receptor activity (GO:0008528) peptide receptor activity (GO:0001653) magnesium ion binding (GO:0000287) protein serine/threonine kinase activity (GO:0004674) cation channel activity (GO:0005261)	4 iron, 4 sulfur cluster binding (GO:0051539) ligase activity (GO:0016874)

4.4. Pathway Enrichment Analysis

Pathway enrichment analysis was conducted using significant lists of DGE analysis using ComPath with pathway databases WikiPathways, Reactome and KEGG, to highlight the most prominent pathways for different salinity treatments. Top fifty enriched pathways having FDR < 0.05 were interpreted (Table 4.29-4.34). Pathways related to immune system, metabolism, calcium signaling, cellular homeostasis and processes such as growth, proliferation, etc. and their respective signaling pathways were enriched.

4.4.1. Immune System

Pathways of immune system and innate immune system were enriched in all of the contrasts (Table 4.29). Other enrichments that were related to immune response were pathways of pathogen recognition receptors; C-type lectins (CLRs), Toll-like receptors (TLRs), RIG- like receptors (RLRs) and NOD-like receptors (NLRs), complement system, apoptosis and their respective signaling pathways (Table 4.29). Pathways of pathogen recognition receptors, NLRs, TLRs and CLRs were enriched in all of the three treatments, whereas RLRs were enriched in BA(↑) and CB(→). This was in agreement with DGE analysis except no NLR contig was D.E in CB(→). Additionally, TLRs in BA(↑) and CB(→), and RLRs in BA(↑) were enriched in all of the three databases. TLRs were enriched in both BA(↑) and CB(→) but higher number of pathways were enriched in BA(↑).

Pathways related to complement system were also enriched in all contrasts being higher in BA(↑) and CB(→) (Table 4.29). Complement system is part of innate (and adaptive in other organisms) immunity that helps to fight against pathogens by inflammation, opsonization and killing of pathogens (Janeway et al., 2001). Most of the complement cascade enzymes are inactive when not triggered. When triggered, each enzyme activates the next enzyme in line through proteolytic cleavage (Alberts et al., 2008). Complement activation can be caused by Ca^{+2} dependent mannan-binding lectin which is a CLR (Gerdol and Venier, 2015). Mannose receptor, C type (MRC) was D.E in BA(↑) and CB(→) in DGE analysis (Table 4.18), which is parallel to pathway enrichments of the complement system. Other than via the lectin pathway, complement system can be triggered by the classical pathway, which is activated by binding of C1q protein to the pathogen's surface for phagocytosis, and by the alternative pathway which is activated by the surface of bacteria itself (Alberts et al., 2008). Blood coagulation can also trigger the complement cascade (Janeway et al., 2001).

Another pathway group that is related to immune response was apoptosis. Pathways of apoptosis were enriched in all of the contrasts, with enrichment higher in BA(↑) and DC(↓) than in CB(→) (Table 4.29). Conversely, in CB(→), pathways related to survival, such as PI3K-AKT signaling pathway (Janku et al., 2018) (Table 4.34) that is activated by cellular stimuli and regulates transcription, translation, proliferation, growth, and survival (GenomeNet, n.d) and pathways of growth factors (EGFR, FGFR) (Table 4.30) were enriched. This was in line with DGE analysis as PERP in BA(↑) and FADD, APAF1, and RAIDD in DC(↓) were D.E.

Other enriched pathways of the immune response were the signaling pathways that are mostly involved in immune response, including MAPK (Mitogen-activated protein kinase) and NF-κB (Nuclear Factor kappa B) (Table 4.34). NF-κB is a transcription factor that is involved in proinflammatory gene expression like cytokines, chemokines and adhesion molecules (Lawrence, 2009; Song et al., 2010) produced in response to stimuli like stress and free radicals. NF-κB is also important for cell survival, as it activates genes that inhibit proapoptotic signaling (Piva et al., 2006). Similarly, MAPK pathway can be stimulated by stress, cytokines, hormones, bacteria and participate in immune function and cell death (Song et al., 2010). Other than immune response, MAPK pathway also participates in many processes including cell differentiation and proliferation (Song et al., 2010). Pathways related to NF-κB signaling were enriched in BA(↑) and DC(↓), and MAPK signaling was enriched in CB(→) in the study.

Table 4.29. Enriched pathways related to immune system.

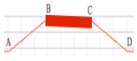
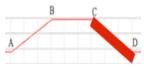
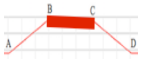
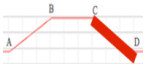
				 RTvsRC.BA	 RTvsRC.CB	 RTvsRC.DC
Immune System	Immune System		KEGG			
			Reactome	Immune System Innate Immune System	Immune System Innate Immune System Inflammasomes	Immune System Innate Immune System Interferon Signaling Cytokine Signaling in Immune system
			Wikipathways			
	Pathogen Recognition Receptors	CLRs	KEGG	C-type lectin receptor signaling pathway - Homo sapiens (human)	C-type lectin receptor signaling pathway - Homo sapiens (human)	
			Reactome	C-type lectin receptors (CLRs) Dectin-2 family	C-type lectin receptors (CLRs) Dectin-2 family	Dectin-2 family
			Wikipathways			
		NLRs	KEGG	NOD-like receptor signaling pathway - Homo sapiens (human)	NOD-like receptor signaling pathway - Homo sapiens (human)	NOD-like receptor signaling pathway - Homo sapiens (human)
			Reactome		The NLRP3 inflammasome Nucleotide-binding domain, leucine rich repeat containing receptor (NLR) signaling pathways	
			Wikipathways	Nucleotide-binding Oligomerization Domain (NOD) pathway		Nucleotide-binding Oligomerization Domain (NOD) pathway
		RLRs	KEGG	RIG-I-like receptor signaling pathway - Homo sapiens (human) Cytosolic DNA-sensing pathway - Homo sapiens (human)	RIG-I-like receptor signaling pathway - Homo sapiens (human)	
			Reactome	DDX58/IFIH1-mediated induction of interferon-alpha/beta Negative regulators of DDX58/IFIH1 signaling Regulation of innate immune responses to cytosolic DNA		
			Wikipathways	RIG-I-like Receptor Signaling	RIG-I-like Receptor Signaling	
		TLRs	KEGG	Toll-like receptor signaling pathway - Homo sapiens (human)	Toll-like receptor signaling pathway - Homo sapiens (human)	
			Reactome	Toll-Like Receptors Cascades Toll Like Receptor 4 (TLR4) Cascade Trafficking and processing of endosomal TLR Regulation of TLR by endogenous ligand Toll Like Receptor 3 (TLR3) Cascade	Toll-Like Receptors Cascades	Regulation of TLR by endogenous ligand Transfer of LPS from LBP carrier to CD14
			Wikipathways	Toll-like Receptor Signaling Toll-like Receptor Signaling Pathway Regulation of toll-like receptor signaling pathway Simplified Depiction of MYD88 Distinct Input-Output Pathway TLR4 Signaling and Tolerance	Toll-like Receptor Signaling Toll-like Receptor Signaling Pathway Regulation of toll-like receptor signaling pathway	
	Complement System		KEGG	Complement and coagulation cascades - Homo sapiens (human)	Complement and coagulation cascades - Homo sapiens (human)	
			Reactome	Formation of Fibrin Clot (Clotting Cascade) Common Pathway of Fibrin Clot Formation	Formation of Fibrin Clot (Clotting Cascade)	
			Wikipathways	Complement and Coagulation Cascades Human Complement System Fibrin Complement Receptor 3 Signaling Pathway	Complement and Coagulation Cascades Human Complement System	Human Complement System
	Cell Death		KEGG	Apoptosis - Homo sapiens (human) Phagosome - Homo sapiens (human) Apoptosis - multiple species - Homo sapiens (human) TNF signaling pathway - Homo sapiens (human) Necroptosis - Homo sapiens (human)	Apoptosis - Homo sapiens (human) Phagosome - Homo sapiens (human)	Apoptosis - multiple species - Homo sapiens (human) Phagosome - Homo sapiens (human)
			Reactome	Apoptosis Programmed Cell Death Intrinsic Pathway for Apoptosis Caspase-mediated cleavage of cytoskeletal proteins Death Receptor Signalling via Death Receptors in the presence of ligand SMAC-mediated apoptotic response SMAC-mediated dissociation of IAP:caspase complexes SMAC binds to IAPs Apoptotic cleavage of cellular proteins Apoptotic factor-mediated response TRIF-mediated programmed cell death Apoptotic execution phase Cell death signalling via NRAGE, NRIF and NADE Regulation of necroptotic cell death RIPK1-mediated regulated necrosis Regulated Necrosis		SMAC-mediated apoptotic response SMAC-mediated dissociation of IAP:caspase complexes SMAC binds to IAPs Apoptotic factor-mediated response Intrinsic Pathway for Apoptosis Cytochrome c-mediated apoptotic response Activation of caspases through apoptosome-mediated cleavage
			Wikipathways	Apoptosis Apoptosis Modulation and Signaling TNF related weak inducer of apoptosis (TWEAK) Signaling Pathway Apoptosis Modulation by HSP70 Nanomaterial induced apoptosis Fas Ligand (FasL) pathway and Stress induction of Heat Shock Proteins (HSP) regulation	Apoptosis Apoptosis Modulation and Signaling	Apoptosis
	Proapoptotic Signal Transducer		KEGG			
			Reactome	TRAF3-dependent IRF activation pathway TRAF6 mediated NF-kB activation TRAF6 mediated IRF7 activation	TRAF6 mediated NF-kB activation	
			Wikipathways			

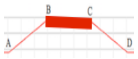
Table 4.30. Enriched pathways related to cellular processes.

		 RTvsRC.BA	 RTvsRC.CB	 RTvsRC.DC
Processes such as proliferation, motility differentiation etc.	KEGG	TNF signaling pathway - Homo sapiens (human)	EGFR tyrosine kinase inhibitor resistance - Homo sapiens (human) ErbB signaling pathway - Homo sapiens (human) Neurotrophin signaling pathway - Homo sapiens (human)	
	Reactome		Constitutive Signaling by EGFRvIII Signaling by EGFRvIII in Cancer GAB1 signalosome Signaling by EGFRvIII in Cancer PI3K events in ERBB2 signaling Constitutive Signaling by Ligand-Responsive EGFR Cancer Variants Signaling by EGFR in Cancer Signaling by Ligand-Responsive EGFR Variants in Cancer RAF/MAP kinase cascade Downstream signaling of activated FGFR2 Signaling by FGFR2 amplification mutants Signaling by FGFR2 fusions Signaling by EGFR Signaling by ERBB2 Signaling by PTK6 Inhibition of Signaling by Overexpressed EGFR Signaling by Overexpressed Wild-Type EGFR in Cancer	Signaling by FGFR2 amplification mutants Signaling by FGFR2 fusions RAF/MAP kinase cascade
	Wikipathways	Ectoderm Differentiation	ESC Pluripotency Pathways ErbB Signaling Pathway	Ectoderm Differentiation

4.4.2. Metabolism

Pathways related to protein, lipid and carbohydrate metabolism were enriched. Pathways related to protein metabolism, and post-translational modification and transportation of proteins were highly enriched in BA(↑). In DGE analysis and GSEA analysis, protein metabolism and turnover were also found to be altered in BA(↑). For lipids, pathways related to the metabolism of fatty acids were enriched with all contrasts being prominently higher in DC(↓). Pathways of membrane lipids that are also involved in cell-cell communication, glycosphingolipid (D'Angelo et al., 2013) and sphingolipids (Merrill, 2008) were enriched in BA(↑) and CB(→). In DGE analysis contigs related to lipid metabolism were D.E. in all of the contrasts (Table 4.11).

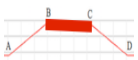
Table 4.31. Enriched pathways related to metabolism of proteins, carbohydrates and lipids.

		 RTvsRC.BA	 RTvsRC.CB	 RTvsRC.DC
Protein/Lipid/Carbohydrate Metabolism	KEGG	Proteoglycans in cancer - Homo sapiens (human) Lysosome - Homo sapiens (human) Glycosphingolipid biosynthesis - lacto and neolacto series - Homo sapiens (human) Central carbon metabolism in cancer - Homo sapiens (human)	Proteoglycans in cancer - Homo sapiens (human) Lysosome - Homo sapiens (human) Central carbon metabolism in cancer - Homo sapiens (human)	Cholesterol metabolism - Homo sapiens (human)
	Reactome	Metabolism of proteins Transport of gamma-carboxylated protein precursors from the endoplasmic reticulum to the Golgi apparatus Post-translational protein modification Gamma carboxylation, hypusine formation and arylsulfatase activation Gamma-carboxylation of protein precursors Gamma-carboxylation, transport, and amino-terminal cleavage of proteins Removal of aminoterminal propeptides from gamma-carboxylated proteins Deubiquitination Plasma lipoprotein assembly, remodeling, and clearance ECM proteoglycans	Plasma lipoprotein assembly, remodeling, and clearance Plasma lipoprotein clearance Biosynthesis of DPAn-3-derived 13-series resolvins Biosynthesis of DPAn-3-derived protectins and resolvins Biosynthesis of electrophilic ω-3 PUFA oxo-derivatives	Plasma lipoprotein assembly, remodeling, and clearance Plasma lipoprotein clearance Transport of small molecules LDL clearance Biosynthesis of DPAn-3-derived 13-series resolvins Biosynthesis of DPAn-3-derived protectins and resolvins Biosynthesis of electrophilic ω-3 PUFA oxo-derivatives Biosynthesis of DPAn-3-derived maresins Biosynthesis of aspirin-triggered D-series resolvins LDL remodeling Biosynthesis of DPAn-3 SPMs Biosynthesis of D-series resolvins Biosynthesis of E-series 18(R)-resolvins Biosynthesis of DPA-derived SPMs Biosynthesis of E-series 18(S)-resolvins Biosynthesis of EPA-derived SPMs Synthesis of Lipoxins (LX) HDL clearance Post-translational protein modification
	Wikipathways	Degradation pathway of sphingolipids, including diseases	Degradation pathway of sphingolipids, including diseases	

4.4.3. Calcium Signaling

Pathways related to calcium signaling, presynaptic depolarization and calcium channel opening were enriched in BA(↑) and response to elevated platelet cytosolic Ca^{2+} was enriched in DC(↓). Opening of the voltage-gated calcium channels causes calcium influx which causes neurotransmitter release (Reactome, 2004). In line with this, both in DGE and GSEA analysis, contigs and GO terms related to cell-cell signaling and ciliary activity were regulated. Response to elevated platelet cytosolic Ca^{2+} pathway is related to calcium increase and protein kinase C (PKC) activation.

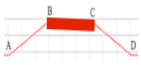
Table 4.32. Enriched pathways related to cell-cell and calcium signaling.

		 RTvsRC.BA	 RTvsRC.CB	 RTvsRC.DC
Cell-Cell Signaling / Calcium Signalling	KEGG			
	Reactome	Presynaptic depolarization and calcium channel opening		Response to elevated platelet cytosolic Ca2+ TRP channels
	Wikipathways			

4.4.4. Structural Integrity of Tissues and Cells

Pathways related to supporting the structural integrity of tissues and cells were also enriched. These were pathways of extracellular matrix (ECM), cytoskeleton and cell-matrix adhesions. The extracellular matrix is composed of secreted molecules that provide structural support to the cells. The cytoskeleton is a system of filaments that determines cell shape and motility (Ray and Fry, 2015). Focal adhesions are plasma membrane-associated macromolecules that connect and transmit regulatory signals between the actin cytoskeleton and extracellular matrix via integrin receptors (Kuo, 2014), which enables regulation of cell behavior and gene expression. Focal adhesions are cell-matrix adhesions that are important for many processes such as cell motility, cell proliferation, cell differentiation, regulation of gene expression processes, and cell survival (WikiPathways, n.d. (c)). These pathways may be altered due to volume changes that may occur from salinity stress in the study. It is known that volume changes act as a signal that modulates metabolism, growth and development (in Low and Taylor, 1998). Mechanical stimuli are converted to chemical signals for metabolic reactions via transmembrane integrins which connect ECM and cytoskeleton at focal adhesions (Low and Taylor, 1998).

Table 4.33. Enriched pathways related to ECM, cytoskeleton and cell-matrix adhesions.

		 RTvsRC.BA	 RTvsRC.CB	 RTvsRC.DC
Cell-Matrix Adhesions ECM Cytoskeleton	**KEGG**	Regulation of actin cytoskeleton - Homo sapiens (human)	Focal adhesion - Homo sapiens (human) Rap1 signaling pathway - Homo sapiens (human)	Focal adhesion - Homo sapiens (human) ECM-receptor interaction - Homo sapiens (human) Rap1 signaling pathway - Homo sapiens (human)
	Reactome	Extracellular matrix organization ECM proteoglycans		Extracellular matrix organization Integrin cell surface interactions Reelin signalling pathway
	Wikipathways	Focal Adhesion	Focal Adhesion-PI3K-Akt-mTOR-signaling pathway Focal Adhesion Regulation of Actin Cytoskeleton	Focal Adhesion-PI3K-Akt-mTOR-signaling pathway Focal Adhesion

4.4.5. Signaling Pathways

Additionally, signaling pathways that regulate many cellular functions, such as Ras signaling pathway that controls survival, cell proliferation, growth, migration and differentiation (WikiPathways, n.d. (a)), and RAC1/PAK1/p38/MMP2 pathway that is involved in growth and cell proliferation (WikiPathways, n.d. (b)), were enriched (Table 4.34). Other pathway enrichments are given in Table 4.35. Overall, GSEA and DGE analyses were in line with pathway enrichments.

Table 4.34. Enriched pathways related to signaling.

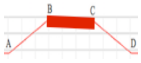
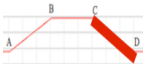
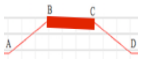
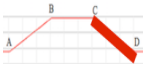
		 RTvsRC.BA	 RTvsRC.CB	 RTvsRC.DC
PI3K-Akt Signaling Pathway	**KEGG**	PI3K-Akt signaling pathway - Homo sapiens (human)	PI3K-Akt signaling pathway - Homo sapiens (human)	PI3K-Akt signaling pathway - Homo sapiens (human)
	Reactome		Constitutive Signaling by Aberrant PI3K in Cancer PI3K events in ERBB2 signaling PI3K/AKT Signaling in Cancer PI5P, PP2A and IER3 Regulate PI3K/AKT Signaling Negative regulation of the PI3K/AKT network PIP3 activates AKT signaling PI-3K cascade:FGFR2 PI3K Cascade Insulin receptor signalling cascade	
	Wikipathways	PI3K-Akt Signaling Pathway	PI3K-Akt Signaling Pathway	PI3K-Akt Signaling Pathway
Ras Signaling Pathway	**KEGG**		Ras signaling pathway - Homo sapiens (human)	
	Reactome			
	Wikipathways		Ras Signaling	
RAC1/PAK1 /p38/MMP2 Pathway	**KEGG**			
	Reactome			
	Wikipathways		RAC1/PAK1/p38/MMP2 Pathway	RAC1/PAK1/p38/MMP2 Pathway
MAPK Signaling Pathway	**KEGG**		MAPK signaling pathway - Homo sapiens (human)	
	Reactome		MAPK1/MAPK3 signaling MAPK family signaling cascades	MAPK1/MAPK3 signaling
	Wikipathways		MAPK Signaling Pathway	
NF-kB Signaling Pathway	**KEGG**	NF-kappa B signaling pathway - Homo sapiens (human)	NF-kappa B signaling pathway - Homo sapiens (human)	NF-kappa B signaling pathway - Homo sapiens (human)
	Reactome	NF-kB activation through FADD/RIP-1 pathway mediated by caspase-8 and -10 TNF receptor superfamily (TNFSF) members mediating non-canonical NF-kB pathway		
	Wikipathways			

Table 4.35. Generic pathways enriched.

		 RTvsRC.BA	 RTvsRC.CB	 RTvsRC.DC
Other	**KEGG**	Viral carcinogenesis - Homo sapiens (human) Pathways in cancer - Homo sapiens (human)	Endocytosis - Homo sapiens (human) Pathways in cancer - Homo sapiens (human) MicroRNAs in cancer - Homo sapiens (human) Relaxin signaling pathway - Homo sapiens (human) Phospholipase D signaling pathway - Homo sapiens (human)	Vitamin digestion and absorption - Homo sapiens (human) Biotin metabolism - Homo sapiens (human)
	Reactome	Activation of IRF3/IRF7 mediated by TBK1/IKK epsilon Hemostasis	Hemostasis IRS-mediated signalling PKMTs methylate histone lysines Signaling by Non-Receptor Tyrosine Kinases Intracellular signaling by second messengers	Transport of small molecules Defects in vitamin and cofactor metabolism Metabolism of proteins Metabolism of water-soluble vitamins and cofactors Metabolism of vitamins and cofactors Hemostasis Platelet degranulation Platelet activation, signaling and aggregation
	Wikipathways	Vitamin B12 Metabolism Vitamin D Receptor Pathway	Vitamin B12 Metabolism AGE/RAGE pathway Folate Metabolism Phase I biotransformations, non P450 NAD metabolism, sirtuins and aging	GPCRs, Class B Secretin-like Copper homeostasis

5. CONCLUSIONS AND RECOMMENDATIONS

5.1. Conclusions

M. galloprovincialis is an economically and ecologically important species. It is sessile and faces highly changing environmental conditions. It is also exposed to a high amount of microbial challenge due to being a filter feeder. The ability to survive in these environmental conditions makes *M. galloprovincialis* an ideal species to study animal adaptation and stress response. In this study, we examined the long-term stress response of *M. galloprovincialis* to gradual salinity increase, acclimation, and decrease, to account for the lower and upper limits of salinity encountered by this species in the Bosphorous and adjacent seas. We found that the mussels adapted to changing salinities by altering energy, carbohydrate, lipid, nitrogen, and nucleotide metabolisms. Results of DGE, GSEA and pathway enrichments were compatible. In addition to these groups, GO terms related to DNA repair and gene expression regulation and pathways related to immune system were enriched in GSEA and pathway enrichment analysis, respectively.

Firstly, gill cilia are involved probably in osmosensing and commanding the cellular response (Pedersen et al., 2012). Bivalves are filter feeders, whose gills are specialized in capturing food particles, besides respiration. Gill filaments are ciliated and are recruited in feeding, respiration and sensing environmental signals. Cilia assembles and disassembles with changing salinities, and act as a pivotal osmosensor and commander, sensing and transmitting extracellular signals via receptors, effector proteins and transcription factors to cells for the response (Pedersen et al., 2012). Contigs of cholinergic ciliary stimulation (acetylcholine receptors, voltage-gated calcium channels and dyneins) that are linked to membrane depolarization, cytosolic calcium increase (Zagoory et al., 2002; Jokura et al., 2020; Catapane et al., 2016) and cell-to-cell signaling (Clapham, 2007) were differentially expressed in this study. Those contigs that were involved in calcium regulation and signaling were TRPMs, voltage-gated calcium channels and stanniocalcin.

Secondly, since *M. galloprovincialis* is an osmoconformer, changing salinities causes alteration of cell volume as extracellular fluid becomes isosmotic and cells swell or shrink due to osmosis (Deaton, 2008; Toyohara, 2005a). Cell volume regulation is an essential response as uncontrolled levels of volume change can cause dysfunctioning of the cell and leads to apoptosis (Gutierre et al., 2014 cited in Rivera-Ingraham and Lignot, 2017; Gómez-Angelats and Cidlowski, 2002 cited in Rivera-Ingraham and Lignot, 2017). Cell volume regulation in the study was mainly

enhanced by changing the permeability of water and ions across the cell membrane (Deaton, 2008) and by alteration of nitrogen metabolism (Peteiro et al., 2018). Permeability and fluidity of the membrane are altered by the change in lipid composition of the membrane which triggers signaling cascades that lead to osmolyte regulation (Bhoite and Roy, 2013; Ortiz et al., 2017; Nelson et al., 2011). In the study, change in lipid composition of the membrane by arachidonic acid metabolism and polyketide synthase probably lead to osmolyte and volume regulation. For example, regulation of Na^+/K^+ pump in the study was in line with alteration of membrane lipid composition with arachidonic acid metabolism, as eicosanoids are modulators of this pump (Therien and Blostein, 2000). Our findings match with the literature that arachidonic acid metabolism is involved in a signaling cascade that leads to osmolyte release triggered by cell swelling (Lambert, 2004; Meng et al. 2013) and Na^+/K^+ pump is involved in volume regulation due to the Donnan effect and swelling tendency caused by osmotic pressure (Mongin and Orlov, 2001). In cell volume regulation, nitrogen metabolism was also altered. For euryhaline marine invertebrates, free amino acids, their derivatives, and methylamines are also used to buffer osmotic changes (Pourmozaffar et al., 2019). With increases in salinity, free amino acids and their derivatives are increased, whereas, with a decrease in salinity, free amino acids and amino-nitrogens are decreased due to ammonia excretion (Gosling, 2004; Meng et al., 2013).

Under hyperosmotic stress, intracellular organic osmolytes such as alanine, betaine (glycine betaine), proline, and glycine are accumulated to maintain cell volume (Deaton, 2001). In bivalves, serine, proline, and glycine are among the most common amino acids involved in osmoregulation (Deaton, 2001; Hanson and Dietz, 1976). In this study, genes involved in the synthesis of these amino acids were upregulated with salinity increase. Additionally, contigs that are intermediates of proline synthesis, P5CS and OAT, were upregulated with salinity decrease, showing the possibility of involvement of proline in responding to chronic salinity decrease as well. A more probable scenario is that ornithine and α-ketoglutarate can form with OAT, rather than synthesis of proline with proC that can also feed the TCA cycle for energy production (α-ketoglutarate) at low salinities. Another organic osmolyte, betaine (glycine betaine) was also regulated in the study. Choline dehydrogenase (betA) catalyzes the oxidation of choline to betaine aldehyde and is involved in the synthesis of betaine (glycine betaine). betA was upregulated with salinity decrease and not differentially expressed with salinity increase. In bivalves and also in other species betaine is accumulated with hyperosmotic stress as an osmoprotectant (de Vooys and Geenevasen, 2002; Deaton, 2001). Due to regulation in the study, other functions likely determined its regulation more so than the osmoprotective function such as the role of betaine in one-carbon metabolism, nucleotide, DNA, creatine, and phospholipid synthesis. It was not differentially expressed in salinity increase (and upregulated with decrease)

supporting its function with high energy metabolism (as low salinity is high energy expenditure in *Mytilus*), as further metabolization of choline may supply electron carriers (NADH) and ubiquinol for oxidative phosphorylation (Mailloux et al., 2016).

Protein turnover was also higher at lower salinity, represented by regulation of FUCA (is involved in the first step of glycoprotein degradation), cathepsin B,L (cysteine proteases that participate in protein turnover), and ribosomal proteins (involved in protein synthesis and ribosomal biogenesis); all downregulated with salinity increase. Protein synthesis is one of the most energy-consuming processes in the cell (Guimaraes & Zavolan, 2016), and in the study, high protein turnover was probably increasing energy demand of low salinity. GOs related to protein catabolic processes were also highly enriched for salinity increase in GSEA analysis. Amino acids derived from the degradation of proteins can also be recycled to synthesize new proteins, converted to other amino acids or used in energy metabolism by converting to TCA cycle intermediates or glucose. In this study, nitrogen metabolism was likely activated by cellular needs driven by osmoregulation, energy metabolism and the requirements of the new salinity conditions. Regulation of cell volume by nitrogen metabolism in bivalves increases demands of oxidative metabolism, mobilization of reserves, and oxygen consumption rates (Peteiro et al., 2018). Additionally, ionic regulation such as Na^+/K^+ pump that requires a large portion of the cell's energy (Deaton, L. 2008; Mongin and Orlov, 2009; Sardini et al., 2003) cause increase in energy demand (at low salinity/steady-state) with implications on energy production and metabolism.

M. galloprovincialis belongs to the family Mytilidae that includes euryoxic and facultative anaerobes (De Zwaan and Mathieu,1992). As they inhabit intertidal and shallow waters, they are exposed to air with tides. Besides tides, dissolved oxygen levels can change due to other factors like eutrophication, and changes in salinity and/or temperature. Because of fluctuations in environmental O_2 concentrations, bivalves evolved adaptations to tolerate anoxic conditions. Alteration of energy metabolism in the study was observed both in the genes of anaerobic and aerobic metabolism. In aerobic organisms, energy is harnessed through the process of oxidative phosphorylation (Berg et al., 2002b). Oxidative phosphorylation contigs were downregulated with salinity increase (in BA(↑)), matching with high energy expenditure of low salinity in *Mytilus* species in the literature (Freitas et al., 2017; Riisgard et al., 2013; Tedengren and Kautsky, 1987; Sanders et al., 2018). Additionally, a contig of the anaerobic metabolism, specifically L-lactate dehydrogenase, was also downregulated with salinity increase, in parallel with the regulation of oxidative phosphorylation contigs. Normally, the production of lactate from pyruvate happens when there is not sufficient oxygen (Melkonian and Schury, 2020). In this study, no indication of oxygen deprivation was found, such as differential

expression of hypoxia-inducible factors (HIFs). Parallel regulation of aerobic and anaerobic metabolism contigs in the study could help in providing additional energy to the cells; and involvement of functional anaerobism when energy production of aerobiosis is not sufficient was suggested previously in bivalves (De Zwaan and Mathieu, 1992). This regulation was accompanied by a high glycolytic rate (GADPH was downregulated with salinity increase also). Carbohydrate catabolism in the study was also in agreement with the regulation of energy metabolism, as carbohydrates are the priority respiratory substrates in bivalves (Hawkins et al., 1985).

A notable regulation of carbohydrate metabolism was parallel regulation of reciprocally regulated processes; glycolysis and gluconeogenesis. Normally these are reciprocal processes regulated by allosteric enzymes according to the energy charge of the cell. In our study, contigs of these processes, GADPH and PEPCK were both downregulated in salinity increase (in BA(↑)). Parallel regulation of these processes is also seen in some cancer types that rely on oxidative phosphorylation in limited glucose supply, where PEPCK is regulated to replenish glycolysis intermediates by utilizing TCA metabolites and carbon metabolites, as alternative carbon sources (Leithner, 2015, Leithner et al., 2014). Likewise, in lung cancer cells, lactate is converted to phosphoenolpyruvate with PEPCK in glucose deprivation (Leithner et al., 2014). Regulation of PEPCK was found to be mediated by P53 via SIRT6 in cancer metabolism (Zhang et al., 2014 in Leithner et al., 2014). In our study, SIRT6 was also upregulated with salinity increase in BA(↑), which in return probably downregulates PEPCK (as there was no more need to utilize TCA metabolites as an alternative carbon source) and decreases glucose uptake as high salinity is a relatively low energy expenditure state, when compared to low salinity.

In addition, reactive oxygen species (ROS) are produced as byproducts due to electron leakage in the electron transfer chain of oxidative phosphorylation and are increased under stress conditions. Mitochondrial uncoupling protein, UCP4 was parallelly regulated with oxidative phosphorylation contigs (downregulated with salinity increase) which decrease ROS generation with little impact on membrane potential and ATP generation (Ramsden et al., 2012). To assess oxidative status, antioxidant enzymes were also examined. Antioxidant expression was in opposite direction with salinity; Glutathione s-transferases (GSTs) contigs were downregulated with salinity increase. GST can increase with exposure to H_2O_2, protecting cells from oxidative stress and lipid peroxidation (Halliwell and Gutteridge, 2015). GSTs are also involved in the conversion of unstable leukotriene A4 to leukotriene C4 (NCBI, n. d.). In the study, phospholipase activity in arachidonic acid metabolism causes hydrolysis of phospholipids that can further result in the generation of eicosanoids, and lipid peroxidation by the enzymes LOX and COX (Speed and Blair, 2011). GST downregulation

with salinity increase, parallel to both phospholipase activity and aerobic metabolism, could therefore be a response to both protect from ROS due to energy metabolism, and lipid peroxidation due to COX and LOX. DNA damage response was also examined and no significant differentially expressed genes were found except ATP-dependent DNA helicase PIF1 (downregulated with salinity decrease) that is involved in mitochondrial and nuclear genome stability (Nextprot, n.d.). Although we could not find a noteworthy DNA damage response in DGE analysis, GO terms related to it were enriched in GSEA analysis. This enrichment could have originated due to altered metabolism and salinity stress.

Finally related with nucleotide metabolism, PRPS was downregulated with salinity increase, having the same direction of regulation with contigs of energy metabolism, protein turnover and arachidonic acid metabolism. PRPS catalyzes the generation of PRPP, which is a key molecule in nucleotide synthesis, and is very important in many respects since the generation of many key molecules such as the energy currency ATP, nucleic acids DNA and RNA, cofactors (e.g. NAD), second messengers (e.g. c-AMP), and pathway intermediates (e.g. UDP-glucose) depends on it (Hove-Jensen et al., 2016).

High salinity is associated with low energy expenditure and vice versa in *Mytilus* species (Freitas et al., 2017; Riisgard et al., 2013; Tedengren and Kautsky, 1987; Sanders et al., 2018). In this study, altered nitrogen metabolism and ion channel activity for osmolyte and volume regulation probably caused an increase in energy demand which reflects on energy production and metabolism. Besides metabolism, salinity change also alters inflammatory and immune responses, affecting lysozyme activity, humoral responses, immune-related genes, and apoptosis (Pourmozaffar et al., 2019). For example, alteration of membrane phospholipids and further metabolization of arachidonic acid lead to eicosanoids that can bind to their receptors and mediate immune and inflammatory responses. We observed apoptosis initiation with the participation of TP53 apoptosis effector (PERP), TLRs and TNFSF14 in our experiment (also downregulated with salinity increase), which may also be caused by stress (can be related to a mild case of DNA repair, as it was enriched in GSEA) that was probably related to energy need and altered metabolism due to low salinities. Regulation of PERP also indicated p53 and p63 originated apoptosis. Inhibitor of apoptosis (IAPs) regulation probably increased stress tolerance in the study. MEGF 10 was inversely regulated with salinity, downregulated with salinity increase and upregulated with salinity decrease. Regulation of MEGF10 supported regulation of PERP and apoptosis at the low salinity condition, as it is involved in the clearance of apoptotic cells. Pathway enrichment analysis also supported this result: pathways of apoptosis were enriched in all of the contrasts, with enrichment higher in salinity increase and decrease, rather than during the (high salinity) acclimation period. Conversely, during acclimation, pathways related to

survival such as PI3K-AKT signaling pathway (Janku et al., 2018) that is activated by cellular stimuli and regulates transcription, translation, proliferation, growth, and survival (GenomeNet, n.d), and pathways of growth factors (EGFR, FGFR) were enriched. In this context, we generated a hypothesized pathway matching with these regulations, given in Figure 4.23.

Along with the regulation direction given in the DGE analysis, we have seen sub-processes in GSEA. Additionally, we saw the plasticity of the response more clearly when we examined contrasts in GSEA. For example, in DGE analysis, oxidative phosphorylation contigs were differentially expressed in salinity increase, but not in decrease. The reason was probably related to the acclimation period as salinity increase was after acclimation to steady-state condition, and mussels were more acclimated to low salinity whereas mussels were acclimated to high salinity before salinity decrease. On the other hand, in GSEA the result was vice versa; the same processes were also enriched in salinity decrease verifying plasticity of the regulation and results of DGE. The same patterns were also seen in ribosomal proteins. This was probably due to the utilization of whole gene lists in GSEA but a subset in DGE analysis (*i.e.* those which have FDR<0.05), with DGE analysis providing the most important hits.

To sum up, we found regulation of cholinergic ciliary activity, nitrogen metabolism, and arachidonic acid metabolism in osmostress adaptation. Energy metabolism was regulated in line with the literature. In addition to the existing literature, we encountered two important metabolic regulations; first, functional anerobism that was suggested in bivalves before and second, regulation of PEPCK with OXPHOS and glycolysis genes.

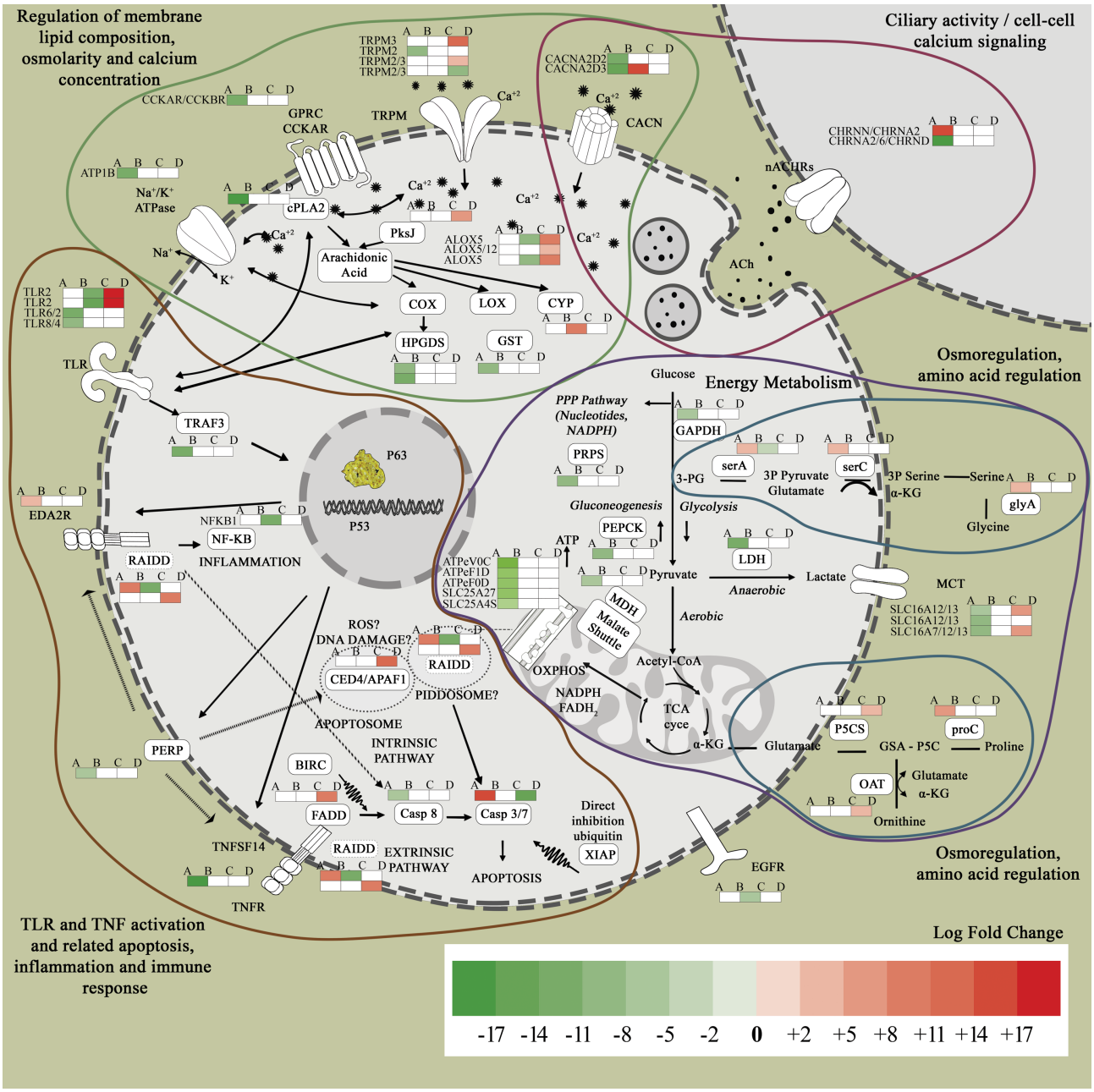


Figure 4.23. Hypothesized model of the study with regulations. In the legend, green and red colors represent downregulation and upregulation with higher color intensity denoting greater log-fold change.

5.1.1. Effect of Salinity on Distribution

Salinity and temperature are among the most important factors that affect the distribution of bivalves (Gosling, 2004, pp. 55). Their distribution is mainly affected by temperature on large geographic scales and by salinity in coastal and estuarine regions (Gosling, 2004, pp. 55). In addition, other environmental factors such as water turbidity, substrate type, food availability, and occurrence

of competitors and predators, among others, also act synergistically in determining their distribution (Gosling, 2004, pp. 55).

The results of our study suggest that high salinity (39 ‰) can affect the distribution and prevalence of this species positively in terms of energy budget. When we look at the distribution of this species, we see that this species is frequently found in the high salinities in our experiment. As its name implies, the Mediterranean mussel M. galloprovincialis is native to the Mediterranean Sea, which has high salinities throughout the basin (36.2-39 ‰). It is found along the coasts of Algeria, Bosnia and Herzegovina, Croatia, Egypt, Slovenia, France, Greece, Italy, Libya, Morocco, Spain, Tunisia, and Turkey (ISSG, 2015). But due to synergetic effects of other environmental factors such as warmer waters and substrate type, it is absent from Fethiye to Samandağ (Deniz Haber Ajansı, 2009). In addition, nutrient availability may have affected the situation as oligotrophy of the Mediterranean Sea increases along west-east and north-south directions, and primary production decreases along west-east directions (Siokou-Frangou et al., 2010). However, this species is also native to the Black Sea where salinity is 18 ‰ and highly nutrient rich nutrient rich due to river inflows (Türkoğlu and Koray, 2002); it is found along the coasts of Bulgaria, Romania, Russian Federation, Turkey, and Ukraine (ISSG, 2015).

Our results with energy metabolism can also suggest that high salinity can increase the invasive capacity of the Mediterranean mussel. As an example, the effect of salinity and temperature on relative frequencies of native M. trossulus and invasive M. galloprovincialis in central California was examined by Braby and Somero (2005). Accordingly, it was found that their distribution followed the estuarine-to-oceanic gradient pattern and also suggested a differential response of these species to salinity and temperature. M. galloprovincialis was most prevalent in oceanic habitats within the central California hybrid zone, where salinity is high and temperature is low. It is known that M. galloprovincialis tolerates higher temperatures in its biogeographic range, so Braby and Somero (2005) suggested that the main factor affecting its distribution could be low salinity.

5.2. Limitations of the Study

Due to working with a non-model organism and in order to find enriched pathways between contrasts, pathway enrichment analysis was conducted using a set of gene symbols (significant contigs in DGE analysis) against public databases (WikiPathways, Reactome and KEGG), which must be considered with its limitations. Bulk selection of gene symbols can result in false negatives when queried against databases in pathway enrichment analysis as different symbols can be used

between databases and contigs. Also, the results are closely linked to the data scope each database has. However, the analysis was still useful for underlining the prominent pathways, albeit with these limitations. Similarly, de novo assembly construction, mapping, and annotation for non-model organisms are also linked to data entries of the databases, which should be considered in the interpretation of the results and the context of the species.

Another point to consider is the reproducibility of the RNA-Seq studies (Yu, 2020). The Sequencing Quality Control (SEQC) project assessed the performance of RNA-Seq studies by analyzing RNA samples with multiple replicates across laboratories and platforms (SEQC/MAQC-III Consortium, 2014; Yu, 2020). They found relative expression levels were reproducible and accurate across platforms with the use of specific filters whereas RNA-Seq does not provide absolute measurements and even in qPCR gene-specific biases were observed (SEQC/MAQC-III Consortium, 2014). In our study, due to budget constraints, the tanks that were designed as technical replicates (Tank A and B) were later used as biological replicates of experimental conditions. So each replicate of an experiment condition is prepared by pooling the samples of the related tank for that condition. Since it is not possible to realize artifacts that can occur in a single tank without replicate tanks, the design was adapted in this way and the tank effect was incorporated into the model.

5.3. Recommendations

During 1850s, Louis Pasteur found the inhibiting effect of oxygen on fermentation (Lehninger et al., 2005, pp. 533, 560). ATP production through fermentation was far more inefficient compared to ATP production through respiration which makes aerobic metabolism advantageous when oxygen is available. Under aerobic conditions, generated ATP and citrate acts as allosteric inhibitors of 6-phosphofructokinase (EC:2.7.1.11) of the glycolysis (Berg et al., 2002a). Therefore, glycolytic pathway is faster in anaerobic conditions, although energy produced is significantly less when compared to aerobic conditions. This reverse relation between O_2 consumption and glycolytic rate is called the Pasteur effect (Lehninger et al., 2005, pp. 533, 560).

Later, during1920s, Otto Warburg found metabolic phenotype in tumour tissues that presented a a reverse case of the Pasteur effect (Koppenol et al., 2011), where lactate is produced (with high rate of glucose uptake and glycolysis) in the presence of oxygen (aerobic glycolysis). This process was referred to as the Warburg effect (DeBerardinis and Chandel, 2020). To some extent, other cells such as microbes also use aerobic glycolysis for the anabolic reactions during rapid proliferation (Lunt and Vander Heiden, 2011), but in cancer tissues that exhibit the Warburg effect, production of lactate

from glucose was 10-fold higher, when compared to normal tissues, showing distorted proportion of the regulation (Koppenol et al., 2011).

Tumour cells can experience hypoxia due to lack of capillary network for sufficient O_2 delivery (Lehninger et al., 2005, pp. 533, 560) but also, in many cancer cells, respiration is retained with Warburg effect indicating glycolytic reprogramming, rather than dysfunctioning of the respiration (Koppenol et al., 2011). As ATP production is inefficient in fermentation compared to respiration, several explanations are made with regards to this phenomenon (Zu and Guppy, 2004). One of the explanations involves feeding of the branching pathways from glycolysis to ensure macromolecular synthesis that is needed for the proliferation of tumour cells (DeBerardinis and Chandel, 2020); in Warburg effect, metabolic pathways are enhanced, which supports macromolecular synthesis, such as pentose phosphate pathway, nucleotide biosynthesis, amino acid biosynthesis and lipid homeostasis (DeBerardinis and Chandel, 2020; Su et al., 2014).

In this study, two important regulation was especially notable. The first one was a Warburg effect-like regulation of vertebrates with a profile of respiratory gene expression that is seen in cancer tissues (Koppenol et al., 2011). In the significant list of the DGE analysis, LDHA (anaerobic metabolism) and oxidative phosphorylation (aerobic metabolism) genes were parallelly downregulated with salinity increase in BA(↑), and no indication of oxygen deprivation was found. This regulation could be to provide additional energy; involvement of functional anaerobism when energy production of aerobiosis is not sufficient was suggested before in bivalves (De Zwaan and Mathieu, 1992). In the study, this regulation was accompanied by high glycolytic rate (GADPH), protein turnover and altered nucleotide metabolism in parallel.

The second notable regulation was the parallel regulation of reciprocally regulated processes; glycolysis and gluconeogenesis. Normally these two processes are regulated by allosteric enzymes, according to the energy charge of the cell. In our study, contigs of these processes, GADPH and PEPCK, were both downregulated in salinity increase in BA(↑). Parallel regulation of these processes is also seen in some cancer types that rely on oxidative phosphorylation in limited glucose supply, where PEPCK is regulated to replenish glycolysis intermediates by utilizing TCA metabolites and carbon metabolites, as alternative carbon sources (Leithner, 2015, Leithner et al., 2014). Likewise, in lung cancer cells, lactate is converted to phosphoenolpyruvate with PEPCK in glucose deprivation (Leithner et al., 2014). Regulation of PEPCK was found to be mediated by P53 via SIRT6 in cancer metabolism (Zhang et al., 2014 in Leithner et al., 2014). In our study, SIRT6 was also upregulated with salinity increase in BA(↑), which probably downregulates PEPCK (as there was no more need

to utilize TCA metabolites as an alternative carbon source) and decreased glucose uptake as high salinity is a low energy expenditure state.

Cancer cells have deregulated proliferation and survival mechanisms such as depressing cell death (Evan and Vousden, 2001), and these regulations (Warburg effect and PEPCK) in cancer provide metabolites and ensure macromolecular synthesis that is needed for the uncontrolled proliferation of tumour cells. Likewise, Warburg effect-like regulation with respiration (contigs of oxidative phosphorylation and LDHA) and parallel regulation of PEPCK (contig of gluconeogenesis) with GADPH in our study probably resulted from the need for energy and metabolites required to respond to low salinity stress (steady-state).

As another important point, parallelly, we observed apoptosis initiation with the participation of TP53 apoptosis effector (PERP), TLRs and TNFSF14 in our experiment, which may also be caused by stress that was probably related to energy need and altered metabolism due to low salinity. Regulation of PERP also indicated p53 and p63 originated apoptosis. Induction of apoptosis and IAPs probably managed and enhanced adaptation and durability to stress, by balancing between survival and death, caused by the altered metabolism in the study.

Enrichment of cancer-related genes and metabolic routes were mentioned in the study of Moreira et al. (2015) in *M. galloprovincialis*. The result in our study indicated *M. galloprovincialis* as a candidate species for studying metabolic regulation and pathways that may contribute to our understanding of cancer. Especially our results related to apoptosis initiation may be particularly promising in this perspective.

REFERENCES

Adams, M., 2010. The primary cilium: an orphan organelle finds a home. Nature Education, 3(9), 54.

Adamus, T. & Kortylewski, M., 2018. The revival of CpG oligonucleotide-based cancer immunotherapies. Contemporary Oncology, 22(1A), 56-60.

Agarwal, R., Raza, H., Allyn, D. L., Bickers, D. R. & Mukhtar, H., 1992. Glutathione s-transferase-dependent conjugation of eukotriene A4-methyl ester to leukotriene C4-methyl ester in mammalian skin. Biochem Pharmacol., 44(10), 2047-2053.

Ahern, G. P., 2013. Transient receptor potential channels and energy homeostasis. Trends Endocrinol Metab., 24(11), 554-560.

Aiello, E., 1960. Factors affecting ciliary activity on the gill of the mussel *Mytilus edulis*. Physiological Zoology, 33(2), 120-135.

Aiello, E., & Paparo, A., 1974. A role for acetylcholine in the regulation of ciliary activity. Comparative and General Pharmacology, 5(3), 285–297.

Alberts, B., Johnson, A., Lewis, J., Raff, M., Roberts, K., & Walter, P., 2008. Molecular Biology of the Cell, Fifith Edition., Garland Science, New York, NY.

Alberty, R. A., 2005. Thermodynamic properties of oxidoreductase, transferase, hydrolase, and ligase reactions. Archives of Biochemistry and Biophysics, 435(2), 363-368.

Allam, B. & Raftos, D., 2015. Immune responses to infectious diseases in bivalves. Journal of Invertebrate Pathology, 131, 121-36.

Almeida, E. A., Dias Bainy, A. C., Dafre, A. L., Gomes, O. F., Medeiros, M. H. G., & Di Mascio, P., 2005. Oxidative stress in digestive gland and gill of the brown mussel (*Perna perna*) exposed to air and re-submersed. Journal of Experimental Marine Biology and Ecology, 318(1), 21-30.

Altiok, H., Sur, H. I., Muftuoglu, A. E., & Yuce, H., 2010. Temperature, salinity and flow variations in the Strait of Istanbul (Bosphorus). Rapport Commission Internationale de La Mer Mediterranee, 39, 85.

Anders, S., Pyl, P. T., & Huber, W., 2015. HTSeq-A Python framework to work with high-throughput sequencing data. Bioinformatics, 31(2), 166-169.

Andrews, S., 2010. FastQC: A quality control tool for high throughput sequence data., http://www.bioinformatics.babraham.ac.uk/projects/fastqc/ (accessed January 2021).

Anestis, A., Lazou, A., Pörtner, H. O., Michaelidis, B., 2007. Behavioral, metabolic, and molecular stress responses of marine bivalve *Mytilus galloprovincialis* during long-term acclimation at increasing ambient temperature. American Journal of Physiology - Regulatory Integrative and Comparative Physiology, 293(2), 911-921.

Anestis, A., Pörtner, H. O., Karagiannis, D., Angelidis P., Staikou, A., Michaelidis B., 2010. Response of *Mytilus galloprovincialis* (L.) to increasing seawater temperature and to marteliosis: Metabolic and physiological parameters. Comparative Biochemistry and Physiology, 156, 57-66.

Anju, A., Jeswin, J., Thomas, P. C., & Vijayan, K. K., 2013. Molecular cloning, characterization and expression analysis of F-type lectin from pearl oyster *Pinctada fucata*. Fish & Shellfish Immunology, 35(1), 170-174.

Aramaki, T., Blanc-Mathieu, R., Endo, H., Ohkubo, K., Kanehisa, M., Goto, S., & Ogata, H., 2020. KofamKOALA: KEGG ortholog assignment based on profile HMM and adaptive score threshold. Bioinformatics, 36(7), 2251-2252.

Artigaud, S., Lacroix, C., Richard, J., Flye-Sainte-Marie, J., Bargelloni, L., & Pichereau, V., 2015. Proteomic responses to hypoxia at different temperatures in the great scallop (*Pecten maximus*). PeerJ, 2015(3).

Ashburner, M., Ball, C. A., Blake, J. A., Botstein, D., Butler, H., Cherry, J. M., Davis, A. P., Dolinski, K., Dwight, S. S., Eppig, J. T., Harris, M. A., Hill, D. P., Issel-Tarver, L., Kasarskis, A., Lewis, S., Matese, J. C., Richardson, J. E., Ringwald, M., Rubin, G. M., & Sherlock, G., 2000. Gene ontology: tool for the unification of biology. The Gene Ontology Consortium. Nature genetics, 25(1), 25-29.

Aslan, I., & Aslan, M., 2017. Plasma Polyunsaturated Fatty Acids After Weight Loss Surgery. 10.1016/B978-0-12-804011-9.00058-3.

Attardi, L. D., Reczek, E. E., Cosmas, C., Demicco, E. G., McCurrach, M. E., Lowe, S. W., & Jacks, T., 2000. PERP, an apoptosis-associated target of p53, is a novel member of the PMP-22/gas3 family. Genes & Development, 14(6), 704-718.

Ayala, A., Muñoz, M. F., & Argüelles, S., 2014. Lipid peroxidation: production, metabolism, and signaling mechanisms of malondialdehyde and 4-hydroxy-2-nonenal. Oxidative Medicine and Cellular Longevity, 2014, 360438.

Azzu, V., & Brand, M. D., 2010. The on-off switches of the mitochondrial uncoupling proteins. Trends in Biochemical Sciences, 35(5), 298-307.

Babraham Bioinformatics, n.d. https://www.bioinformatics.babraham.ac.uk/projects/fastqc/Help/3%20Analysis%20Modules/ (accessed November 2020).

Badariotti, F., Kypriotou, M., Lelong, C., Dubos, M. P., Renard, E., Galera, P., & Favrel, P., 2006. The phylogenetically conserved molluscan chitinase-like protein 1 (Cg-Clp1), homologue of human HC-gp39, stimulates proliferation and regulates synthesis of extracellular matrix components of mammalian chondrocytes. The Journal of Biological Chemistry, 281(40), 29583-29596.

Bafaro, E., Liu, Y., Xu, Y., & Dempski, R. E., 2017. The emerging role of zinc transporters in cellular homeostasis and cancer. Signal Transduction and Targeted Therapy, 2(1), 1-12.

Bakan, G. & Büyükgüngör, H., 2000. The Black Sea. Marine Pollution Bulletin, 41, 24-43.

Bakker, J., 1997. Physiology of Tissue Oxygen Delivery. In Pinsky M.R. (Eds.), Applied Cardiovascular Physiology. Update in Intensive Care and Emergency Medicine, 28, 64-75, Springer, Berlin, Heidelberg.

Baltaci, A. K., & Yuce, K., 2018. Zinc transporter proteins. Neurochemical Research, 43(3), 517-530.

Bamji-Mirza, M. & Yao, Z. n.d. AOCS Lipid Library. https://lipidlibrary.aocs.org/chemistry/physics/animal-lipids/phospholipases (accessed June 2021).

Bär, R., Rouholahnejad, E., Rahman, K., Abbaspour, K. C. & Lehmann, A., 2015. Climate change and agricultural water resources: A vulnerability assessment of the Black Sea catchment. Environmental Science & Policy, 46, 57-69.

Bayne, B. L., 1976. Marine Mussels, Their Ecology and Physiology. Cambridge University Press, Cambridge.

Bayne, B.L., Widdows, J. & Thompson, R.J., 1976. Physiology: II. In B.L. Bayne (Eds.), Marine Mussels: Their Ecology and Physiology, 207-60, Cambridge University Press, Cambridge.

Behari, J., 2011. Fatty Liver. In Monga, S.P.S., Molecular Pathology of Liver Diseases, Springer US.

Benjamini, Y. & Hochberg, Y., 1995. Controlling the false discovery rate: a practical and powerful approach to multiple testing. Journal of the Royal Statistical Society. Series B (Methodological), 57, 289-300.

Berg, J. M., Tymoczko, J. L., & Stryer, L., 2002a. The glycolytic pathway is tightly controlled. Biochemistry, 5.

Berg, J., Tymoczko, J. L., & Stryer, L., 2002b. Chapter 18: Oxidative Phosphorylation. Biochemistry, 6.

Besser, J., Carleton, H. A., Gerner-Smidt, P., Lindsey, R. L., & Trees, E., 2018. Next-generation sequencing technologies and their application to the study and control of bacterial infections. Clinical Microbiology and Infection, 24(4), 335-341.

Beşiktepe, Ş. T., Sur, H. İ., Özsoy, E., Latif, M. A., Oğuz, T. & Ünlüata, Ü., 1994. The circulation and hydrography of the Marmara Sea. Prog. Oceanog., 34, 285-334.

Bethoux, J. P., Gentili, B., Raunet, J. & Talliez, D., 1990. Warming trends in the western Mediterranean deep water. Nature, 347, 660-662.

Bethoux, J. P., Gentili, B., Tailliez, D., 1998. Warming and freshwater budget change in the Mediterranean since the 1940s, their possible relation to the greenhouse effect. Geophysical Research Letters, 25, 1023-1026.

Bhoite, S., & Roy, R., 2013. Role of membrane lipid in osmoregulatory processes during salinity adaptation: a study with chloride cell of mud crab, *Scylla serrata*. Marine and Freshwater Behaviour and Physiology, 46(5), 287-300.

Birkbeck, T. H., & McHenery, J. G., 1984. Chitinase in the mussel, *Mytilus edulis* (L.). Comparative Biochemistry and Physiology Part B: Biochemistry, 77(4), 861-865.

Blaustein, M. P., 1985. Intracellular Calcium as a Second Messenger. In R. P. Rubin, G. B. Weiss, & J. W. Putney (Eds.), Calcium in Biological Systems, 23-33, Boston, MA: Springer US.

Bolger, A. M., Lohse, M., & Usadel, B., 2014. Trimmomatic: a flexible trimmer for Illumina sequence data. Bioinformatics, 30(15), 2114-2120.

Boonmee, A., Heude Berthelin, C., Kingtong, S., Pauletto, M., Bernay, B., Adeline, B., … Kellner, K., 2016. Differential protein expression during sperm maturation and capacitation in an hermaphroditic bivalve, *Pecten maximus* (Linnaeus, 1758). Journal of Molluscan Studies, 82(4), 575-584.

Borza, C., Muntean, D., Dehelean, C., Savoiu, G., Serban, C., Simu, G., Andoni, M., Butur, M., & Drag, S., 2013. Oxidative Stress and Lipid Peroxidation - A Lipid Metabolism Dysfunction. Lipid Metabolism.

Boudjema, K., Kourdali, S., Bounakous, N., Meknachi, A., & Badis, A., 2014. Catalase activity in brown mussels (*Perna perna)* under acute cadmium, lead, and copper exposure and depuration tests. Journal of Marine Biology, 2014.

Bourdon J. C., 2007. p53 Family isoforms. Current Pharmaceutical Biotechnology, 8(6), 332-336.

Box, A., Sureda, A., & Deudero, S., 2009. Antioxidant response of the bivalve *Pinna nobilis* colonised by invasive red macroalgae *Lophocladia lallemandii*. Comparative Biochemistry and Physiology Part C: Toxicology & Pharmacology, 149(4), 456-460.

Braby, C. E., & Somero, G. N., 2006. Ecological gradients and relative abundance of native (*Mytilus trossulus*) and invasive (*Mytilus galloprovincialis*) blue mussels in the California hybrid zone. Marine Biology, 148(6), 1249-1262.

Bradley, T. J., 2009. Animal Osmoregulation. Oxford University Press.

Brandão, V. C. M., Meola, J., Garcia, S. B., Candido-Dos-Reis, F. J., Poli-Neto, O. B., Nogueira, A. A., & Rosa-E-Silva, J. C., 2018. Increased expression levels of metalloprotease, tissue inhibitor of metalloprotease, metallothionein, and p63 in ectopic endometrium: an animal experimental study. Revista Brasileira de Ginecologia e Obstetricia, 40(11), 705-712.

Breheny, P., Stromberg, A., & Lambert, J., 2018. P-Value histograms: Inference and diagnostics. High-Throughput, 7(3), 1-13.

Brightbill, H. D., & Modlin, R. L., 2000. Toll-like receptors: molecular mechanisms of the mammalian immune response. Immunology, 101(1), 1-10.

Brown, J., Wang, H., Hajishengallis, G. N., & Martin, M., 2011. TLR-signaling networks: an integration of adaptor molecules, kinases, and cross-talk. Journal of Dental Research, 90(4), 417- 427.

Buckley, B. A., Owen, M. E. & Hofmann, G. E., 2001. Adjusting the thermostat: the threshold induction temperature for the heat shock response in intertidal mussels (genus Mytilus) changes as a function of thermal history. The Journal of Experimental Biology, 204(20), 3571-3579.

Burg, M. B. & Ferraris, J. D., 2008. Intracellular Organic Osmolytes: Function and Regulation. Journal of Biological Chemistry, 283(12), 7309-7313.

Bülbring, E., Burn, J. H., & Shelley, H. J., 1953. Acetylcholine and ciliary movement in the gill plates of *Mytilus edulis*. Proceedings of the Royal Society of London. Series B, Containing Papers of a Biological Character. Royal Society (Great Britain), 141(905), 445-466.

Cao, R., Liu, Y., Wang, Q., Yang, D., Liu, H., Ran, W., ... Zhao, J., 2018. Seawater acidification reduced the resistance of *Crassostrea gigas* to *Vibrio splendidus* challenge: An energy metabolism perspective. Frontiers in Physiology, 9, 1-14.

Carmeliet, P., 2005. VEGF as a key mediator of angiogenesis in cancer. Oncology; 69, 4-10.

Caron de Fromentel, C., Aberdam, E., & Aberdam, D., 2012. The two faces of p63, Janus of the p53 gene family. Medecine Sciences: M/S, 28(4), 381-387.

Catapane, B. Y. E. J., Sciences, N., College, M. E., & Stefano, G. B., 1978. Pharmacological study of the reciprocal dual innervation of the lateral ciliated gill epithelium by the CNS of *Mytilus Edulis* (Bivalvia). Journal of Experimental Biology, 74(1), 101-113.

Carroll, M. A., & Catapane, E. J., 2007. The nervous system control of lateral ciliary activity of the gill of the bivalve mollusc, *Crassostrea virginica*. Comparative Biochemistry and Physiology. Part A, Molecular & Integrative Physiology, 148(2), 445-450.

Catapane, E., Nelson, M., Adams, T., & Carroll, M., 2016. Innervation of gill lateral cells in the bivalve mollusc *Crassostrea virginica* affects cellular membrane potential and cilia activity. Journal of Pharmacological Reports, 1(2).

Cavaletto, M., Ghezzi, A., Burlando, B., Evangelisti, V., Ceratto, N., & Viarengo, A., 2002. Effect of hydrogen peroxide on antioxidant enzymes and metallothionein level in the digestive gland of *Mytilus galloprovincialis*. Comparative Biochemistry and Physiology Part C: Toxicology & Pharmacology, 131(4), 447-455.

Celikyilmaz-Aydemir, G., 2011. Vulnerability of the Black Sea to the Impacts of Climate Change. In Lagutov, V. (Eds.), Environmental Security in Watersheds: The Sea of Azov, 173-180, Springer, Netherlands.

Chakarov, S., Petkova, R., Russev, G., & Zhelev, N., 2014. DNA damage and mutation. Types of DNA damage. BioDiscovery, 11, e8957.

Changeux J. P., 2020. Discovery of the first neurotransmitter receptor: the acetylcholine nicotinic receptor. Biomolecules, 10(4), 547.

Chen, Y., McCarthy, D., Ritchie, M., Robinson, M., & Smyth, G., 2008. edgeR: differential analysis of sequence read count data User's Guide. (accessed June 2020).

Chen, J., Xiao, S., & Yu, Z., 2011. F-type lectin involved in defense against bacterial infection in the pearl oyster (*Pinctada martensii*). Fish & Shellfish Immunology, 30(2), 750-754.

Chen, Y., Lun, A. T., & Smyth, G. K., 2016. From reads to genes to pathways: differential expression analysis of RNA-Seq experiments using Rsubread and the edgeR quasi-likelihood pipeline. F1000Research, 5.

Chen, Y., Xu, K., Li, J., Wang, X., Ye, Y., & Qi, P., 2018. Molecular characterization of complement component 3 (C3) in *Mytilus coruscus* improves our understanding of bivalve complement system. Fish & Shellfish Immunology, 76, 41-47.

Chen, Y., McCarthy, D., Ritchie, M., Robinson, M., Smyth, G., & Hall, E., 2020. edgeR: differential analysis of sequence read count data User's Guide. R Package, 1-121.

Choi, M. K., Son, S., Hong, M., Choi, M. S., Kwon, J. Y., & Lee, J., 2016. Maintenance of Membrane Integrity and Permeability Depends on a Patched-Related Protein in *Caenorhabditis elegans*. Genetics, 202(4), 1411-1420.

Clapham, D. E., 2007. Calcium Signaling. Cell, 131(6), 1047-1058.

Clausen, L., Abildgaard, A. B., Gersing, S. K., Stein, A., Lindorff-Larsen, K., & Hartmann-Petersen, R., 2019. Protein stability and degradation in health and disease. Advances in Protein Chemistry and Structural Biology, 114, 61-83.

Coleman, W. B., 2019. Chapter 9 - Modulation of the Epigenome (Methylome) to Improve Chemotherapeutic Efficacy. In D. E. B. T.-T. C. S. P. to E. R. to C. Johnson (Eds.), Cancer Sensitizing Agents for Chemotherapy, 3, 187-202, Academic Press.

Conesa, A., Madrigal, P., Tarazona, S., Gomez-Cabrero, D., Cervera, A., McPherson, A., Szcześniak, M. W., Gaffney, D. J., Elo, L. L., Zhang, X., & Mortazavi, A., 2016. A survey of best practices for RNA-seq data analysis. Genome Biology, 17(1), 13.

Cooper, E. L., 2018. Advances in Comparative Immunology. Springer International Publishing.

Cooper, G. M., 2000. The Cell: A Molecular Approach. 2nd edition. Sunderland (MA): Sinauer Associates.

Cooper, J. A., 2020. Peroxisome. Encyclopedia Britannica, https://www.britannica.com/science/peroxisome (accessed July 2021).

Cornet, M., 2006. Effects of seawater salinity fluctuations on primary tissue culture from the mussel *Mytilus galloprovincialis* Potential application to the detection of seawater genotoxicity. Toxicology in Vitro, 20, 1500-1505.

Coscia, M. R., Giacomelli, S., Oreste, U., 2011. Toll- like receptors: An overview from invertebrates to vertebrates. Invertebrate Survival Journal, 1(8),210-226.

Costea, I., Mack, D. R., Israel, D., Morgan, K., Krupoves, A., Seidman, E., Deslandres, C., Lambrette, P., Grimard, G., Levy, E., & Amre, D. K., 2010. Genes involved in the metabolism of poly-unsaturated fatty-acids (PUFA) and risk for Crohn's disease in children & young adults. Plos One, 5(12), e15672.

Creative Enzymes, n.d. Enzyme Definition and Classification. https://www.creative enzymes.com/resource/enzyme-definition-and-classification_18.html (accessed November 2020).

Croft, D., Mundo, A. F., Haw, R., Milacic, M., Weiser, J., Wu, G., ... & D'Eustachio, P., 2014. The Reactome pathway knowledgebase. Nucleic Acids Research, 42(D1), D472-D477.

Croom, E., 2012. Metabolism of xenobiotics of human environments. Progress in Molecular Biology and Translational Science, 112, 31-88.

Cuesta, S. M., Rahman, S. A., & Thornton, J. M., 2016. Exploring the chemistry and evolution of the isomerases. Proceedings of the National Academy of Sciences, 113(7), 1796-1801.

Cummings, R. D. & McEver, R. P., 2009. Chapter 31 C-type Lectins. In Varki A., Cummings R. D., Esko J. D., et al. (Eds.), Essentials of Glycobiology. 2nd edition. Cold Spring Harbor (NY): Cold Spring Harbor Laboratory Press.

D'Angelo, G., Capasso, S., Sticco, L., & Russo, D., 2013. Glycosphingolipids: Synthesis and functions. FEBS Journal, 280(24), 6338-6353.

D'Ignazio, L., Batie, M., & Rocha, S., 2018. TNFSF14/LIGHT, a non-canonical NF-κB stimulus, induces the HIF Pathway. Cells, 7(8), 102.

Dar, M. A., Pawar, K. D., & Pandit, R. S., 2017. Gut microbiome analysis of snails: a biotechnological approach. Organismal and Molecular Malacology. Intech. p, 189-217.

De Nadal, E., Ammerer, G. & Posas, F., 2011. Controlling gene expression in response to stress. Nature Reviews Genetics, 12(12), 833-845.

De Vooys, C. G. N., Geenevasen, J. A. J., 2002. Biosynthesis and role in osmoregulation of glycine-betaine in the Mediterranean mussel *Mytilus galloprovincialis* LMK. Comparative Biochemistry and Physiology, 132, 409-414.

De Zwaan, A., 1977. Anaerobic energy metabolism in bivalve molluscs. Oceanogr. Mar. Biol. 15, 103-187.

De Zwaan, A., 1983. Carbohydrate Catabolism in Bivalves. In P. W. B. T.-M. B. and M. B. Hochachka (Eds.), Metabolic Biochemistry and Molecular Biomechanics, 137-175, Academic Press.

De Zwaan, A., & Mathieu, M., 1992. Cellular Energy Metabolism in the Mytilidae: An Overview. In E. Gosling (Eds.), The Mussel Mytilus: Ecology, Physiology, Genetics and Culture, 223-307, Elsevier B.V.

Deaton, L., 2001. Hyperosmotic volume regulation in the gills of the ribbed mussel, *Geukensia demissa*: rapid accumulation of betaine and alanine. Journal of Experimental Marine Biology and Ecology, 260, 185-197.

Deaton, L., 2008. Osmotic and Ionic Regulation: Cells and Animals. In Evans, D. H. Osmotic and Ionic Regulation: Cells and Animals, 107-135, CRC Press.

DeBerardinis, R. J., & Chandel, N. S., 2020. We need to talk about the Warburg effect. Nature Metabolism, 2(2), 127-129.

Deitmer, J. W., Theparambil, S. M., Ruminot, I., Noor, S. I., & Becker, H. M., 2019. Energy dynamics in the brain: contributions of astrocytes to metabolism and pH homeostasis. Frontiers in Neuroscience, 13, 1301.

Demonbreun, A. R., Fallon, K. S., Oosterbaan, C. C., Bogdanovic, E., Warner, J. L., Sell, J. J., … McNally, E. M., 2019. Recombinant annexin A6 promotes membrane repair and protects against muscle injury. Journal of Clinical Investigation, 129(11), 4657-4670.

Deniz Haber Ajansı, 2009. https://www.denizhaber.net/akdeniz-sahillerinde-midye-neden-yok-haber-17186.htm (accessed October 2021).

Dickson, R. R., Meincke, J., Malmberg, S. A., & Lee, A. J., 1988. The "great salinity anomaly" in the northern North Atlantic 1968-1982. Progress in Oceanography, 20(2), 103-151.

Di Meo, S., Reed, T. T., Venditti, P., & Victor, V. M., 2016. Role of ROS and RNS sources in physiological and pathological conditions. Oxidative Medicine and Cellular Longevity, 2016, 1245049.

Dineley, K. E., Votyakova, T. V., & Reynolds, I. J., 2003. Zinc inhibition of cellular energy production: Implications for mitochondria and neurodegeneration. Journal of Neurochemistry, 85(3), 563-570.

Doeller, J. E., Kraus, D. W., Shick, J. M., & Gnaiger, E., 1993. Heat flux, oxygen flux, and mitochondrial redox state as a function of oxygen availability and ciliary activity in excised gills of *Mytilus edulis*. The Journal of Experimental Zoology, 265(1), 1-8.

Doğru-Abbasoğlu, S., Koçak-Toker, N., & Uysal, M., 2018. Chapter 24 - Carnosine as a Putative Antioxidant in Usage Against Liver Disease. In V. B. Patel, R. Rajendram, & V. R. B. T.-T. L. Preedy (Eds.), 295-304, Academic Press, Boston.

Domingo-Fernández, D., Hoyt, C. T., Bobis-Álvarez, C., Marín-Llaó, J., & Hofmann-Apitius, M., 2019. ComPath: an ecosystem for exploring, analyzing, and curating mappings across pathway databases. NPJ Systems Biology and Applications, 5, 3.

Donohue, T. M. & Osna, N. A., 2004. Intracellular Proteolytic Systems in Alcohol-Induced Tissue Injury, https://pubs.niaaa.nih.gov/publications/arh27-4/317-324.htm (accessed March 2021).

Durack, P. J. & Wijffels, S. E., 2010. Fifty-year trends in global ocean salinities and their relationship to broad-scale warming. Journal of Climate, 23, 4342-4362.

Dutka, T. L., & Lamb, G. D., 2007. Na^+-K^+ pumps in the transverse tubular system of skeletal muscle fibers preferentially use ATP from glycolysis. American Journal of Physiology - Cell Physiology, 293(3), C967-C977.

Dutton, J. M. & Hofmann, G. E., 2009. Biogeographic variation in *Mytilus galloprovincialis* heat shock gene expression across the eastern Pacific range. Journal of Experimental Marine Biology and Ecology, 376, 37-42.

Eierman, L. E. & Hare, M. P., 2014. Transcriptomic analysis of candidate osmoregulatory genes in the eastern oyster *Crassostrea virginica*. BMC Genomics, 15, 503.

Eierman, L. E. & Hare, M. P., 2016. Reef-specific patterns of gene expression plasticity in eastern oysters (*Crassostrea virginica*). Journal of Heredity, 107(1), 90-100.

Ellington, W. R., 1983. The recovery from anaerobic metabolism in invertebrates. Journal of Experimental Zoology, 228(3), 431-444.

Elmore S., 2007. Apoptosis: a review of programmed cell death. Toxicologic Pathology, 35(4), 495-516.

EMBL, n.d. https://www.ebi.ac.uk/QuickGO/term/GO:0060589 (accessed May 2021).

Erickson, G. R., & Guilak, F., 1999. Osmotic stress initiates intracellular calcium waves in chondrocytes through extracellular influx and the inositol phosphate pathway. American Society of Mechanical Engineers, Bioengineering Division (Publication) BED, 44, 43-44.

Erridge, C., 2010. Endogenous ligands of TLR2 and TLR4: agonists or assistants?. Journal of Leukocyte Biology, 87(6), 989-999.

Estévez-Calvar, N., Romero, A., Figueras, A., & Novoa, B., 2013. Genes of the mitochondrial apoptotic pathway in *Mytilus galloprovincialis*. Plos One, 8(4).

Evan, G. I., & Vousden, K. H., 2001. Proliferation, cell cycle and apoptosis in cancer. Nature, 411(6835), 342-348.

Evans, R. C., & Blackwell, K. T., 2015. Calcium: amplitude, duration, or location?. The Biological Bulletin, 228(1), 75-83.

Evans, J. H., Gerber, S. H., Murray, D., & Leslie, C. C., 2004. The calcium binding loops of the cytosolic phospholipase A_2 C2 domain specify targeting to Golgi and ER in live cells. Molecular Biology of the Cell, 15(1), 371-383.

Fabregat, A., Jupe, S., Matthews, L., Sidiropoulos, K., Gillespie, M., Garapati, P., ... & D'Eustachio, P., 2018. The reactome pathway knowledgebase. Nucleic Acids Research, 46(D1), D649-D655.

Farooqui, A. A., & Farooqui, T., 2016. Chapter 15 - Biochemical Aspects of n-6 and n-3 Fatty Acid-Derived Lipid Mediators in the Brain. In R. R. Watson & F. B. T.-H. of L. in H. F. De Meester (Eds.), 457-474, AOCS Press.

Featherstone, C., & Jackson, S. P., 1999. DNA double-strand break repair. Current Biology: CB, 9(20), R759-R761.

Fernández, B., Campillo, J. A., Martínez-Gómez, C., & Benedicto, J., 2010. Antioxidant responses in gills of mussel (*Mytilus galloprovincialis*) as biomarkers of environmental stress along the Spanish Mediterranean coast. Aquatic Toxicology, 99(2), 186-197.

Fernández, J. A., Skryma, R., Bidaux, G., Magleby, K. L., Scholfield, C. N., McGeown, J. G., Prevarskaya, N., & Zholos, A. V., 2011. Voltage- and cold-dependent gating of single TRPM8 ion channels. The Journal of General Physiology, 137(2), 173-195.

Fernández-Reiriz, M., Range, P., Álvarez-Salgado, X., Labarta, U., 2011. Physiological energetics of juvenile clams Ruditapes decussatus in a high CO_2 coastal ocean. Marine Ecology Progress Series, 433, 97-105.

Fields, P. A., Zuzow, M. J. & Tomanek, L., 2011. Proteomic responses of blue mussel (*Mytilus*) congeners to temperature acclimation. The Journal of Experimental Biology, 215, 1106-1116.

Figueras, A., Moreira, R., Sendra, M., & Novoa, B., 2019. Genomics and immunity of the Mediterranean mussel *Mytilus galloprovincialis* in a changing environment. Fish & Shellfish Immunology, 90, 440-445.

Figueroa-Soto, C. G., & Valenzuela-Soto, E. M., 2018. Glycine betaine rather than acting only as an osmolyte also plays a role as regulator in cellular metabolism. Biochimie, 147, 89-97.

Fischer, M., 2017. Census and evaluation of p53 target genes. Oncogene, 36(28), 3943-3956.

Frances, A., & Cordelier, P., 2020. The emerging role of cytidine deaminase in human diseases: a new opportunity for therapy? Molecular Therapy, 28(2), 357-366.

Freitas, R., De Marchi, L., Bastos, M., Moreira, A., Velez, C., Chiesa, S., ... Soares, A. M. V. M., 2017. Effects of seawater acidification and salinity alterations on metabolic, osmoregulation and oxidative stress markers in *Mytilus galloprovincialis*. Ecological Indicators, 79, 54-62.

Fribley, A., Zhang, K., Kaufman, R. J., 2009. Regulation of apoptosis by the unfolded protein response. Methods in molecular biology, 559,191-204.

Fuhrmann, M., Delisle, L., Petton, B., Corporeau, C., & Pernet, F., 2018. Metabolism of the Pacific oyster, *Crassostrea gigas*, is influenced by salinity and modulates survival to the Ostreid herpesvirus OsHV-1. Biology Open, 7(2), 1-10.

Galluzzi, L., Kepp, O., & Kroemer, G., 2014. 5 - Pathophysiology of Cancer Cell Death. In J. E. Niederhuber, J. O. Armitage, J. H. Doroshow, M. B. Kastan, & J. E. B. T.-A. C. O. Fifth E. Tepper (Eds.), 69-77.e3, Elsevier.

Galtsoff, P.S., 1964. The American oyster *Crassostrea virginica* Gmelin. US Fish and Wildlife Services. Fishery Bulletin, 64, 480.

GBIF, 2021. *Mytilus galloprovincialis* (Lamarck, 1819) in the Global Biodiversity Information Facility, GBIF Backbone Taxonomy, https://www.gbif.org/species/2285683, Checklist dataset https://doi.org/10.15468/39omei (accessed June 2021).

Gene Ontology Consortium, 2021. The Gene Ontology resource: enriching a GOld mine. Nucleic Acids Research, 49(D1), D325-D334.

GenomeNet, n. d. (a) https://www.genome.jp/dbget-bin/www_bget?ko:K12657 (accessed December 2020).
GenomeNet, n. d. (b). https://www.genome.jp/dbget-bin/www_bget?ko:K01229 (accessed January 2021).

Gerber, S., Cadet, P., Sheehan, M., Stefano, G. B., & Mantione, J. J., 2007. Vertebrate interleukins originated in invertebrates?. Invertebrate Survival Journal, 4(2), 95-100.

Gerdol, M., Manfrin, C., De Moro, G., Figueras, A., Novoa, B., Venier, P., & Pallavicini, A., 2011. The C1q domain containing proteins of the Mediterranean mussel *Mytilus galloprovincialis*: A widespread and diverse family of immune-related molecules. Developmental and Comparative Immunology, 35(6), 635-643.

Gerdol, M., & Venier, P., 2015. An updated molecular basis for mussel immunity. Fish & Shellfish Immunology, 46(1), 17-38.

Gerdol, M., Venier, P., & Pallavicini, A., 2015. The genome of the Pacific oyster *Crassostrea gigas* brings new insights on the massive expansion of the C1q gene family in Bivalvia. Developmental and Comparative Immunology, 49(1), 59-71.

Gestal, C., Pallavicini, A., Venier, P., Novoa, B., & Figueras, A., 2010. MgC1q, a novel C1q-domain-containing protein involved in the immune response of *Mytilus galloprovincialis*. Developmental and Comparative Immunology, 34(9), 926-934.

Giannetto, A., Maisano, M., Cappello, T., Oliva, S., Parrino, V., Natalotto, A., De Marco, G., Barberi, C., Romeo, O., Mauceri, A., & Fasulo, S., 2015. Hypoxia-Inducible Factor α and Hif-prolyl Hydroxylase Characterization and Gene Expression in Short-Time Air-Exposed *Mytilus galloprovincialis*. Marine Biotechnology, 17(6), 768-781.

Giglia-Mari, G., Zotter, A., & Vermeulen, W., 2011. DNA damage response. Cold Spring Harbor Perspectives in Biology, 3(1), 1-19.

Gilek, M., Littorin, B., & Saetre, P., 2001. Spatial patterns of abundance and growth of *Mytilus edulis* on boulders in the Northern Baltic Sea proper. Hydrobiologia, 452(1), 59-68.

Gilles, R., 1988. Comparative aspects of cell osmoregulation and volume control. Kidney and Blood Pressure Research, 11(3-5), 277-288.

Goda, N. & Kanai, M., 2012. Hypoxia-inducible factors and their roles in energy metabolism. International Journal of Hematology, 95, 457-463.

Gómez-Angelats, M., & Cidlowski, J. A., 2002. Invited review: cell volume control and signal transduction in apoptosis. Toxicologic Pathology, 30(5), 541-551.

González, A., Schmid, A., Sternfeld, L., Krause, E., Salido, G. M., & Schulz, I., 1999. Cholecystokinin-evoked Ca^{2+} waves in isolated mouse pancreatic acinar cells are modulated by activation of cytosolic phospholipase A_2, phospholipase D, and protein kinase C. Biochemical and Biophysical Research Communications, 261(3), 726-733.

Gonzalez, I., 2014. Tutorial Statistical analysis of RNA-Seq data. Plateforme Bioinformatique. IMT Universite Toulouse III. http://www.nathalievialaneix.eu/doc/pdf/tutorial-rnaseq.pdf (accessed November 2020).

Gosling, E., 2003. Circulation, Respiration, Excretion and Osmoregulation. In Gosling E., Bivalve Molluscs, Biology, Ecology and Culture, 201-225, Blackwell Publishing.

Gosling, E., 2004. Bivalve molluscs: Biology, Ecology and Culture. Blackwell Science.

Gosling, E., 2008. Bivalve molluscs: Biology, Ecology and Culture. John Wiley & Sons.

Götz, S., Garcia-Gomez, J. M., Terol, J., Williams, T. D., Nagaraj, S. H., Nueda, M. J., Robles, M., Talon, M., Dopazo, J. and Conesa, A., 2008. High-throughput functional annotation and data mining with the Blast2GO suite. Nucleic Acids Research, 36(10), 3420-35.

Grabherr, M. G., Haas, B. J., Yassour, M., Levin, J. Z., Thompson, D. A., Amit, I., et al., 2013. Trinity: reconstructing a full-length transcriptome without a genome from RNA-Seq data. Nature Biotechnology, 29(7), 644-652.

Gracey, A. Y., Chaney, M. L., Boomhower, J. P., Tyburczy, W. R., Connor, K. & Somero, G. N., 2008. Rhythms of gene expression in a fluctuating intertidal environment. Current Biology, 18, 1501-1507.

Grada, A. & Weinbrecht, K., 2013. Next-generation sequencing: methodology and application. Journal of Investigative Dermatology, 133(8), e11.

Gravato, C., Oliveira, M., & Santos, M. A., 2005. Oxidative stress and genotoxic responses to resin acids in Mediterranean mussels. Ecotoxicology and Environmental Safety, 61(2), 221-229.

Green, T. J., Helbig, K., Speck, P., & Raftos, D. A., 2016. Primed for success: Oyster parents treated with poly(I:C) produce offspring with enhanced protection against Ostreid herpesvirus type I infection. Molecular Immunology, 78, 113-120.

Grimm, C., Kraft, R., Sauerbruch, S., Schultz, G., & Harteneck, C., 2003. Molecular and functional characterization of the melastatin-related cation channel TRPM3. The Journal of Biological Chemistry, 278(24), 21493-21501.

Grover, A., 2002. Molecular biology of stress responses. Cell stress & Chaperones, 7(1), 1-5.

Guerini, D., 1998. The Ca^{2+} pumps and the Na^{+} / Ca^{2+} exchangers. BioMetals, 11, 319-330.

Guicciardi M.E., & Gores, G.J., 2003. The Death Receptor Family and the Extrinsic Pathway. In Yin XM., Dong Z. (Eds.), Essentials of Apoptosis, Humana Press, Totowa, NJ.

Guimaraes, J. C., & Zavolan, M., 2016. Patterns of ribosomal protein expression specify normal and malignant human cells. Genome Biology, 17(1), 1-13.

Gutierre, S. M. M., Vitule, J. R. S., Freire, C. A. & Prodocimo, V., 2014. Physiological tools to predict invasiveness and spread via estuarine bridges: tolerance of Brazilian native and worldwide introduced freshwater fishes to increased salinity. Marine and Freshwater Research, 65, 425-436.

Haas, E., & Stanley, D. W., 2007. Phospholipase A1. In S. J. Enna & D. B. B. T. T. C. P. R. Bylund (Eds.), 1-4, Elsevier.

Haase V. H., 2013. Regulation of erythropoiesis by hypoxia-inducible factors. Blood Reviews, 27(1), 41-53.

Hakem, R., 2008. DNA-damage repair; the good, the bad, and the ugly. EMBO Journal, 27(4), 589-605.

Halliwell, B., & Gutteridge, J. M., 2015. Free Radicals in Biology and Medicine. Oxford University Press, USA.

Hambidge, M., Cousins, R. J., & Costello, R. B., 2000. Zinc and health: Current status and future directions-Introduction. Journal of Nutrition, 130(5), 1341S.

Hamer, B., Hamer, D. P., Muller, W.E.G. & Batel, R., 2004. Stress-70 proteins in marine mussel *Mytilus galloprovincialis* as biomarkers of environmental pollution: a field study. Environment International, 30, 873-882.

Hamer, B. et al., *20*08. Effect of hypoosmotic stress by low salinity acclimation of Mediterranean mussels *Mytilus galloprovincialis* on biological parameters used for pollution assessment. Aquatic Toxicology, 89, 137-151.

Hamid, R., Khan, M. A., Ahmad, M., Ahmad, M. M., Abdin, M. Z., Musarrat, J., & Javed, S., 2013. Chitinases: An update. Journal of Pharmacy & Bioallied Sciences, 5(1), 21-29.

Han, J. S., Lee, J. H., Kong, J., Ji, Y., Kim, J., Choe, S. S., & Kim, J. B., 2019. Hypoxia restrains lipid utilization via protein kinase A and adipose triglyceride lipase downregulation through hypoxia-inducible factor. Molecular and Cellular Biology, 39(2), e00390-18.

Hanna, V. S., & Hafez, E. A. A., 2018. Synopsis of arachidonic acid metabolism: A review. Journal of Advanced Research, 11, 23-32.

Hanson, J. A., & Dietz, T. H., 1976. The role of free amino acids in cellular osmoregulation in the freshwater bivalve *Ligumia subrostrata* (Say). Canadian Journal of Zoology, 54(11), 1927-1931.

Hasegawa, P. M., Bressan, R. A., Zhu, J.-K., & Bohnert, H. J., 2000. Plant cellular and molecular responses to high salinity. Annual Review of Plant Physiology and Plant Molecular Biology, 51(1), 463-499.

Haupt, S., Berger, M., Goldberg, Z., & Haupt, Y., 2003. Apoptosis - The p53 network. Journal of Cell Science, 116(20), 4077-4085.

Hawkins, A. J. S., 1985. Relationships between the synthesis and breakdown of protein, dietary absorption and turnovers of nitrogen and carbon in the blue mussel, *Mytilus edulis* L. Oecologia, 66(1), 42-49.

Hecox-Lea, B.J., Mark Welch, D.B., 2018. Evolutionary diversity and novelty of DNA repair genes in asexual *Bdelloid rotifers*. BMC Evolutionary Biology, 18, 177.

Henry, R. P., 2001. Environmentally mediated carbonic anhydrase induction in the gills of euryhaline crustaceans. The Journal of Experimental Biology, 204, 991-1002.

Henry, R. P., Gehnrich,S., Weihrauch, D. & Towle, D. W., 2003. Salinity-mediated carbonic anhydrase induction in the gills of the euryhaline green crab, *Carcinus maenas*. Comparative Biochemistry and Physiology, 136, 243-258.

Hibino, T., Loza-Coll, M., Messier, C., Majeske, A. J., Cohen, A. H., Terwilliger, D. P., Buckley, K. M., Brockton, V., Nair, S. V., Berney, K., Fugmann, S. D., Anderson, M. K., Pancer, Z., Cameron, R. A., Smith, L. C., & Rast, J. P., 2006. The immune gene repertoire encoded in the purple sea urchin genome. Developmental Biology, 300(1), 349-365.

Hiom, K., 2001. Recombination: Homologous recombination branches out. Current Biology, 11(7), 278-280.

Hirao, K., Nagano, A. J & Awazu, A., 2015. Noise-plasticity correlations of gene expression in the multicellular organism *Arabidopsis thaliana*, Journal of Theoretical Biology, 387, 13-22.

Hochachka, P.W., 1986. Metabolic arrest. Intensive care medicine, 12, 127-133.

Hochachka, P., & Mustafa, T., 1972. Invertebrate facultative anaerobiosis. Science, 178(4065), 1056-1060.

Hofmann, G. E., 2005. Patterns of Hsp gene expression in ectothermic marine organisms on small to large biogeographic scales. Integrative and Comparative Biology, 45,247-255.

Hosoi, M., Takeuchi, K., Sawada, H. and Toyohara H., 2005. Expression and functional analysis of mussel taurine transporter, as a key molecule in cellular osmoconforming. The Journal of Experimental Biology, 208, 4203-4211.

Hosoi, M., Shinzato, C., Takagi, M., Hosoi-Tanabe, S. Sawada, H., Terasawa, E. & Toyohara, H., 2007. Taurine transporter from the giant Pacific oyster *Crassostrea gigas*: function and expression in response to hyper- and hypo-osmotic stress. Fisheries Science, 73(2),385-394.

Hou, Q., Ufer, G., & Bartels, D., 2016. Lipid signalling in plant responses to abiotic stress. Plant Cell and Environment, 39(5), 1029-1048.

Houston, A. I., McNamara, J. M., Barta, Z., & Klasing, K. C., 2007. The effect of energy reserves and food availability on optimal immune defence. Proceedings of the Royal Society B: Biological Sciences, 274(1627), 2835-2842.

Houten, S. M., & Wanders, R. J., 2010. A general introduction to the biochemistry of mitochondrial fatty acid β-oxidation. Journal of Inherited Metabolic Disease, 33(5), 469-477.

Houtkooper, R. H., Pirinen, E., & Auwerx, J., 2012. Sirtuins as regulators of metabolism and healthspan. Nature Reviews Molecular Cell Biology, 13(4), 225-238.

Hove-Jensen, B., Andersen, K. R., Kilstrup, M., Martinussen, J., Switzer, R. L., & Willemoës, M., 2016. Phosphoribosyl diphosphate (PRPP): biosynthesis, enzymology, utilization, and metabolic significance. Microbiology and Molecular Biology Reviews: MMBR, 81(1), e00040-16.

Hu, M., Li, L., Sui, Y., Li, J., Wang, Y., Lu, W., Dupont, S., 2015. Effect of pH and temperature on antioxidant responses of the thick shell mussel *Mytilus coruscus*. Fish & shellfish Immunology, 46, 573-583.

Hu, D., Ansari, D., Bauden, M., Zhou, Q., & Andersson, R., 2019. The emerging role of calcium-activated chloride channel regulator 1 in cancer. Anticancer Research, 39(4), 1661-1666.

Huerta-Cepas J et al., 2019. eggNOG 5.0: a hierarchical, functionally and phylogenetically annotated orthology resource based on 5090 organisms and 2502 viruses. Nucleic Acids Research, 47(D1), D309-D314.

Ihrie, R. A., Marques, M. R., Nguyen, B. T., Horner, J. S., Papazoglu, C., Bronson, R. T., … Attardi, L. D., 2005. Perp is a p63-regulated gene essential for epithelial integrity. Cell, 120(6), 843-856.

Isani, G. Monari, M. Andreani, G. Fabbri, M. et al., 2002. Effect of copper exposure on superoxide dismutase (SOD) - glutathione peroxidase (Se-GPx) and catalase (CAT) activities in bivalve mollusc *Scapharca inaequivalvis*. Agris, 56, 53-54.

Islinger, M., Grille, S., Fahimi, H. D., & Schrader, M., 2012. The peroxisome: An update on mysteries. Histochemistry and Cell Biology, 137(5), 547-574.

ISSG, 2015. Invasive Species Specialist Group, The Global Invasive Species Database. Version 2015.1, http://www.iucngisd.org/gisd/speciesname/Mytilus+galloprovincialis (accessed January 2021).

Ivanina, A. V., Borah, B., Rimkevicius, T., Macrander, J., Piontkivska, H., Sokolova, I. M., & Beniash, E., 2018. The role of the Vascular Endothelial Growth Factor (VEGF) signaling in biomineralization of the Oyster *Crassostrea gigas*. Frontiers in Marine Science, 5, 1-14.

Jäättelä, M., & Kallunki, T., 2016. Lysosome and Cancer. In Lysosomes: Biology, Diseases, and Therapeutics, 181-207.

Janero, D. R., Hreniuk, D., Sharif, H. M., & Prout, K. C., 1993. Hydroperoxide-induced oxidative stress alters pyridine nucleotide metabolism in neonatal heart muscle cells. The American Journal of Physiology, 264(6 Pt 1), C1401-C1410.

Janeway Jr, C. A., Travers, P., Walport, M., & Shlomchik, M. J., 2001. The complement system and innate immunity. In Immunobiology: The Immune System in Health and Disease. 5th edition. Garland Science.

Janku, F., Yap, T. A., & Meric-Bernstam, F., 2018. Targeting the PI3K pathway in cancer: are we making headway? Nature Reviews Clinical Oncology, 15(5), 273-291.

Jastroch, M., Divakaruni, A. S., Mookerjee, S., Treberg, J. R., & Brand, M. D., 2010. Mitochondrial proton and electron leaks. Essays in Biochemistry, 47, 53-67.

Jiao, Y., Cao, Y., Zheng, Z., Liu, M., & Guo, X., 2019. Massive expansion and diversity of nicotinic acetylcholine receptors in lophotrochozoans. BMC Genomics, 20(1), 1-15.

Jillette, N., Cammack, L., Lowenstein, M. & Henry, R. P., 2011. Down-regulation of activity and expression of three transport-related proteins in the gills of the euryhaline green crab, *Carcinus maenas*, in response to high salinity acclimation. Comparative Biochemistry and Physiology, 158, 189-193.

Johannesson, K., Kautsky, N., Tedengren, M., 1990. Genotypic and phenotypic differences between Baltic and North Sea populations of *Mytilus edulis* evaluated through reciprocal transplantations. II. Genetic variation. Marine Ecology Progress Series, 59, 211-219.

Jokura, K., Nishino, J. M., Ogasawara, M., & Nishino, A., 2020. An α7-related nicotinic acetylcholine receptor mediates the ciliary arrest response in pharyngeal gill slits of Ciona. Journal of Experimental Biology, 223(10).

Jørgensen, C. B., 1990. Bivalve Filter Feeding: Hydrodynamics, Bio-energetics, Physiology and Ecology, Olsen & Olsen, Fredensborg, Denmark.

Julien, O. & Wells, J., 2017. Caspases and their substrates. Cell Death & Differentiation, 24(8), 1380-1389.

Kalkan, E., 2013. Investigating the Role of the Turkish Straits System as a Phylogeographical Break in the Mediterranean-Black Sea Transition, Ph. D. Boğaziçi University, Turkey.

Kanehisa, M. & Goto, S., 2000. KEGG: Kyoto encyclopedia of genes and genomes. Nucleic Acids Research, 28, 27-30.

Kanehisa, M., Sato, Y., Kawashima, M., Furumichi, M., & Tanabe, M., 2016. KEGG as a reference resource for gene and protein annotation. Nucleic Acids Research, 44, D457-D462.

Kanehisa, M., Furumichi, M., Tanabe, M., Sato, Y., & Morishima, K., 2017. KEGG: new perspectives on genomes, pathways, diseases and drugs. Nucleic Acids Research, 45, D353-D361.

Kannan, K. & Jain, S. K., 2000. Oxidative stress and apoptosis. Pathophysiology. 7(3),153-163.

Kano, M., Shoda, J., Satoh, S., Kobayashi, M., Matsuzaki, Y., Abei, M., & Tanaka, N., 2002. Increased expression of gallbladder cholecystokinin: A receptor in prairie dogs fed a high-cholesterol diet and its dissociation with decreased contractility in response to cholecystokinin. Journal of Laboratory and Clinical Medicine, 139(5), 285-294.

Kautsky, N., Johannesson, K., Tedengren, M., 1990. Genotypic and phenotypic differences between Baltic and North Sea populations of *Mytilus edulis* evaluated through reciprocal transplantations. I. Growth and morphology. Marine Ecology Progress Series, 59, 203-210.

Kazan, H. H., Özen, C., & Muyan, M., 2017. PERP (PERP, TP53 apoptosis effector). Atlas of Genetics and Cytogenetics in Oncology and Haematology.

Kelder, T., Van Iersel, M. P., Hanspers, K., Kutmon, M., Conklin, B. R., Evelo, C. T., & Pico, A. R., 2012. WikiPathways: building research communities on biological pathways. Nucleic Acids Research, 40(D1), D1301-D1307.

Kelley, M. R., & Fishel, M. L., 2013. Dna repair and cancer therapeutics. In Tan, D and Lynch, H. T. Principles of Molecular Diagnostic and Personalised Cancer Medicine, 566-579, Lippincott Williams & Wilkins.

Kellner, K., Heude-Berthelin, C., & Mathieu, M., 2002. Immunocytochemical demonstration of glucagon-like peptides in *Mytilus edulis* cerebral ganglia and an in vitro effect of vertebrate glucagon on glycogen metabolism. Tissue & Cell, 34(2), 109-116.

Kendziorski, C., Irizarry, R. A., Chen, K. S., Haag, J. D., & Gould, M. N., 2005. On the utility of pooling biological samples in microarray experiments. Proceedings of the National Academy of Sciences of the United States of America, 102(12), 4252-4257.

Kim, C., Kim, J. Y., & Kim, J. H., 2008a. Cytosolic phospholipase A_2, lipoxygenase metabolites, and reactive oxygen species. Journal of Biochemistry and Molecular Biology, 41(8), 555-559.

Kim, J. Y., Kim, Y. M., Cho, S. K., Choi, K. S., & Cho, M., 2008b. Noble tandem-repeat galectin of Manila clam *Ruditapes philippinarum* is induced upon infection with the protozoan parasite *Perkinsus olseni*. Developmental and Comparative Immunology, 32(10), 1131-1141.

Kim, D., Langmead, B. & Salzberg, S. L., 2015. HISAT: a fast spliced aligner with low memory requirements. Nature Methods, 12, 357-360.

King, S. M., 2018. Composition and Assembly of Axonemal Dyneins. In S. M. King (Eds.), Dyneins: Structure, Biology and Disease, 162-201, Academic Press.

Kisic, B., Miric, D., Zoric, L., & Ilic, A. 2012. Role of lipid peroxidation in the pathogenesis of age-related cataract. In Lipid Peroxidation. IntechOpen, 10.5772/45942.

Koppenol, W., Bounds, P. & Dang, C., 2011. Otto Warburg's contributions to current concepts of cancer metabolism. Nature Reviews Cancer, 11(5), 325-337.

Kopylova E., Noé L. & Touzet H., 2012. SortMeRNA: Fast and accurate filtering of ribosomal RNAs in metatranscriptomic data, Bioinformatic, doi: 10.1093/bioinformatics/bts611.

Korotkova, M., & Lundberg, I. E., 2014. The skeletal muscle arachidonic acid cascade in health and inflammatory disease. Nature Reviews Rheumatology, 10(5), 295-303.

Korycan, S. A., & Storey, K. B., 1983. Organ-specific metabolism during anoxia and recovery from anoxia in the cherrystone clam, *Mercenaria mercenaria*. Canadian Journal of Zoology, 61(12), 2674-2681.

Kugel, S., & Mostoslavsky, R., 2014. Chromatin and beyond: The multitasking roles for SIRT6. Trends in Biochemical Sciences, 39(2), 72-81.

Kumar, V., Abbas, A. K., Aster, J. C., 2015. Chapter 2 Cellular responses to stress and toxic insults: adaptation, injury, and death. In Robbins and Cotran Pathologic Basis of Disease. 9th ed.

Kummer, W., Lips, K. S., & Pfeil, U. 2008. The epithelial cholinergic system of the airways. Histochemistry and Cell Biology, 130(2), 219-234.

Kuo, J. C., 2014. Focal adhesions function as a mechanosensor. Progress in Molecular Biology and Translational Science, 126, 55-73.

Kutmon, M., Riutta, A., Nunes, N., Hanspers, K., Willighagen, E. L., Bohler, A., ... & Pico, A. R., 2016. WikiPathways: capturing the full diversity of pathway knowledge. Nucleic Acids Research, 44(D1), D488-D494.

Kvansakul, M., 2017. Viral Infection and Apoptosis. Viruses, 9(12), 356.

Lambert, I. H., 2004. Regulation of the cellular content of the organic osmolyte taurine in mammalian cells. Neurochemical Research, 29(1), 27-63.

Lane, A. N., & Fan, T. W., 2015. Regulation of mammalian nucleotide metabolism and biosynthesis. Nucleic Acids Research, 43(4), 2466-2485.

Lankisch, T. O., Nozu, F., Owyang, C., & Tsunoda, Y., 1999. High-affinity cholecystokinin type A receptor/cytosolic phospholipase A_2 pathways mediate Ca^{2+} oscillations via a positive feedback regulation by calmodulin kinase in pancreatic acini. European Journal of Cell Biology, 78(9), 632-641.

Latz, E., Xiao, T. & Stutz, A., 2013. Activation and regulation of the inflammasomes. Nature Reviews Immunology, 13(6), 397-411.

Lavaud, R., La Peyre, M. K., Casas, S. M., Bacher, C., & La Peyre, J. F., 2017. Integrating the effects of salinity on the physiology of the eastern oyster, *Crassostrea virginica*, in the northern Gulf of Mexico through a Dynamic Energy Budget model. Ecological Modelling, 363, 221-233.

Law, C. W., Y. Chen, W. Shi, & G. K. Smyth., 2014. Voom: Precision weights unlock linear model analysis tools for RNA-seq read counts. Genome Biology, 15(2), 1-17.

Law, C. W., Alhamdoosh, M., Su, S., Dong, X., Tian, L., Smyth, G. K., & Ritchie, M. E., 2016. RNA-seq analysis is easy as 1-2-3 with limma, Glimma and edgeR. F1000Research, 5.

Lawrence T., 2009. The nuclear factor NF-kappaB pathway in inflammation. Cold Spring Harbor Perspectives in Biology, 1(6), a001651.

Leblanc, N., Ledoux, J., Saleh, S., Sanguinetti, A., Angermann, J., O'Driscoll, K., Britton, F., Perrino, B. A., & Greenwood, I. A., 2005. Regulation of calcium-activated chloride channels in smooth muscle cells: a complex picture is emerging. Canadian Journal of Physiology and Pharmacology, 83(7), 541-556.

Lehninger, A. L., Nelson, D. L., & Cox, M. M., 2005. Lehninger principles of biochemistry. New York: W.H. Freeman.

Lei, C., Hao, R., Zheng, Z., Deng, Y., Wang, Q., & Li, J., 2017. Molecular cloning and characterisation of scavenger receptor class B in pearl oyster *Pinctada fuctada martensii*. Electronic Journal of Biotechnology, 30, 12-17.

Leithner, K., Hrzenjak, A., & Olschewski, H., 2014. Gluconeogenesis in cancer: door wide open. Proceedings of the National Academy of Sciences of the United States of America, 111(42), E4394.

Leithner, K., 2015. PEPCK in cancer cell starvation. Oncoscience, 2(10), 805-806.

Leulier, F., & Lemaitre, B., 2008. Toll-like receptors--taking an evolutionary approach. Nature Reviews Genetics, 9(3), 165-178.

Li, W., & Godzik, A., 2006. Cd-hit: A fast program for clustering and comparing large sets of protein or nucleotide sequences. Bioinformatics, 22(13), 1658-1659.

Li, H., Handsaker, B., Wysoker, A., Fennell, T., Ruan, J., Homer, N., Marth, G., Abecasis, G., Durbin, R., 2009. The Sequence Alignment/Map format and SAMtools. Bioinformatics, 25(16), 2078-2079.

Liao, H., Yang, Z., Dou, Z., Sun, F., Kou, S., Zhang, Z., ... Bao, Z., 2019. Impact of ocean acidification on the energy metabolism and antioxidant responses of the Yesso scallop (*Patinopecten yessoensis*). Frontiers in Physiology, 10, 1-10.

Lieber, M. R., Gu, J., Lu, H., Shimazaki, N., & Tsai, A. G., 2010. Nonhomologous DNA end joining (NHEJ) and chromosomal translocations in humans. Sub-cellular Biochemistry, 50, 279-296.

Litwack, G., 2017. Erythropoietin, Academic Press.

Liu, L., Yang, J., Qiu, L., Wang, L., Zhang, H., Wang, M., Vinu, S. S., & Song, L., 2011. A novel scavenger receptor-cysteine-rich (SRCR) domain containing scavenger receptor identified from mollusk mediated PAMP recognition and binding. Developmental and Comparative Immunology, 35(2), 227-239.

Liu, W., Zhan, C., Cheng, H., Kumar, P. R., Bonanno, J. B., Nathenson, S. G., & Almo, S. C., 2014a. Article mechanistic basis for functional promiscuity in the TNF and TNF receptor superfamilies: structure of the LIGHT: DcR3 assembly. Structure/Folding and Design, 22(9), 1252-1262.

Liu, H. H., Xiang, L. X., & Shao, J. Z., 2014b. A novel C1q-domain-containing (C1qDC) protein from *Mytilus coruscus* with the transcriptional analysis against marine pathogens and heavy metals. Developmental and Comparative Immunology, 44(1), 70-75.

Liu, C. L., & Shi, G. P., 2019. Calcium-activated chloride channel regulator 1 (CLCA1): More than a regulator of chloride transport and mucus production. The World Allergy Organization Journal, 12(11), 100077.

Lockwood, B. L., Sanders, J. G. & Somero, G. N., 2010. Transcriptomic responses to heat stress in invasive and native blue mussels (genus *Mytilus*): molecular correlates of invasive success, The Journal of Experimental Biology, 213, 3548-3558.

Lockwood, B. & Somero, G., 2011. Transcriptomic responses to salinity stress in invasive and native blue mussels (genus *Mytilus*), Molecular Ecology, 20, 517-529.

Lodish H, Berk A, Zipursky SL, et al., 2000. Molecular Cell Biology. 4th edition. W. H. Freeman and Company. New York.

Lopez-Maury, L., Marguerat, S., & Bahler, J., 2008. Tuning gene expression to changing environments: from rapid responses to evolutionary adaptation. Nature Reviews Genetics, 9, 583-593.

Low, S. Y., & Taylor, P. M., 1998. Integrin and cytoskeletal involvement in signalling cell volume changes to glutamine transport in rat skeletal muscle. The Journal of Physiology, 512 (Pt 2), 481-485.

Lu, S., Wang, J., Chitsaz, F., Derbyshire, M. K., Geer, R. C., Gonzales, N. R., Gwadz, M., Hurwitz, D. I., Marchler, G. H., Song, J. S., Thanki, N., Yamashita, R. A., Yang, M., Zhang, D., Zheng, C., Lanczycki, C. J., & Marchler-Bauer, A., 2020. CDD/SPARCLE: the conserved domain database in 2020. Nucleic Acids Research, 48(D1), D265-D268.

Lunt, S. Y., & Vander Heiden, M. G., 2011. Aerobic glycolysis: meeting the metabolic requirements of cell proliferation. Annual Review of Cell and Developmental Biology, 27, 441-464.

Ma, S. et al., 2012. Activation of the cold-sensing TRPM8 channel triggers UCP1-dependent thermogenesis and prevents obesity. Journal of Molecular cell Biology, 4, 88-96.

MacEwan, D. J., 2002. TNF ligands and receptors - A matter of life and death. British Journal of Pharmacology, 135(4), 855-875.

Madhavan, G., 2006. Functional Metabolism: Regulation and Adaptation. (Eds. Storey K. B.), Annals of Biomedical Engineering, 34(6), 1070.

Mahdi, J. G., & Kelly, D. R., 2008. Lyases. Biotechnology: Second, Completely Revised Edition, 8-12, 41-171.

Mailloux, R. J., Young, A., Chalker, J., Gardiner, D., O'Brien, M., Slade, L., & Brosnan, J. T., 2016. Choline and dimethylglycine produce superoxide/hydrogen peroxide from the electron transport chain in liver mitochondria. FEBS Letters, 590(23), 4318-4328.

Manubolu, M., Goodla, L., Pathakoti, K., & Malmlöf, K., 2018. Enzymes as Direct Decontaminating Agents-mycotoxins. In C. S. Nunes & V. B. T.-E. in H. and A. N. Kumar (Eds.), 313-330, Academic Press.

Mardis, E. R. 2013. Next-generation sequencing platforms. Annual Review of Analytical Chemistry, 6, 287-303.

Maret, W., 2000. The function of zinc metallothionein: a link between cellular zinc and redox state. The Journal of Nutrition, 130(5), 1455S-1458S.

Marreiro, D. D., Cruz, K. J., Morais, J. B., Beserra, J. B., Severo, J. S., & de Oliveira, A. R., 2017. Zinc and oxidative stress: current mechanisms. Antioxidants, 6(2), 24.

Martin, M., 2011. Cutadapt removes adapter sequences from high-throughput sequencing reads. EMBnet.journal, 17(1), 10-12.

Marvyn, P. M., Bradley, R. M., Button, E. B., Mardian, E. B., & Duncan, R. E., 2015. Fasting upregulates adipose triglyceride lipase and hormone-sensitive lipase levels and phosphorylation in mouse kidney. Biochemistry and Cell Biology, 93(3), 262-267.

Matsuura, K., Canfield, K., Feng, W., & Kurokawa, M., 2016. Metabolic regulation of apoptosis in cancer. International Review of Cell and Molecular Biology, 327, 43-87.

McCarthy, D., J., Chen, Y., Smyth, G. K., 2012. Differential expression analysis of multifactor RNA-Seq experiments with respect to biological variation. Nucleic Acids Research, 40(10), 4288-4297.

McDonald, J. H., Seed, R. & Koehn, R. K., 1991. Allozymes and morphometric characters of three species of *Mytilus* in the Northern and Southern Hemispheres, Marine Biology, 111, 323-333.

McDonnell, S. J., Spiller, D. G., White, M. R. H., Prior, I. A., & Paraoan, L., 2019. ER stress-linked autophagy stabilizes apoptosis effector PERP and triggers its co-localization with SERCA2b at ER–plasma membrane junctions. Cell Death Discovery, 5(1), 1-12.

Mehnert, C. S., Rampelt, H., Gebert, M., Oeljeklaus, S., Schrempp, S. G., Kochbeck, L., Guiard, B., Warscheid, B., & van der Laan, M., 2014. The mitochondrial ADP/ATP carrier associates with the inner membrane presequence translocase in a stoichiometric manner. The Journal of Biological Chemistry, 289(39), 27352-27362.

Melkonian, E. A., Schury, M. P., 2020. Biochemistry, Anaerobic Glycolysis. In StatPearls. Treasure Island (FL): StatPearls Publishing.

Meng, J., Zhu, Q., Zhang, L., Li, C., Li, L., She, Z., Huang, B. & Zhang, G., 2013. Genome and Transcriptome Analyses Provide Insight into the Euryhaline Adaptation Mechanism of *Crassostrea gigas*. Plos One, 8(3), e58563.

Meng, J., Wang, T., Li, L., & Zhang, G., 2018. Inducible variation in anaerobic energy metabolism reflects hypoxia tolerance across the intertidal and subtidal distribution of the Pacific oyster (*Crassostrea gigas*). Marine Environmental Research, 138, 135-143.

Mercer, T., Gerhardt, D., Dinger, M. et al., 2012. Targeted RNA sequencing reveals the deep complexity of the human transcriptome. Nature biotechnology, 30, 99-104.

Merrill, A. H., 2008. Sphingolipids. In Vance D. E., Vance C. E. (Eds.), Biochemistry of Lipids, Lipoproteins and Membranes, 363-397, Elsevier.

Meseck, S. L., Sennefelder, G., Krisak, M., & Wikfors, G. H., 2020. Physiological feeding rates and cilia suppression in blue mussels (*Mytilus edulis*) with increased levels of dissolved carbon dioxide. Ecological Indicators, 117, 106675.

Metz, J. G., Roessler, P., Facciotti, D., Levering, C., Dittrich, F., Lassner, M., … Browse, J., 2001. Production of polyunsaturated fatty acids by potyketide synthases in both prokaryotes and eukaryotes. Science, 293(5528), 290-293.

Metzker, M. L., 2010. Sequencing technologies - the next generation. Nature Reviews, 11, 31.

Michigan State University, n. d. College of Natural Science Research Technology Support Facility. FastQC tutorial & FAQ. https://rtsf.natsci.msu.edu/genomics/tech-notes/fastqc-tutorial-and-faq/ (accessed November 2020).

Milan, M., Coppe, A., Reinhardt, R. et al., 2011. Transcriptome sequencing and microarray development for the Manila clam, *Ruditapes philippinarum*: genomic tools for environmental monitoring. BMC Genomics, 12, 234.

Milisav, I., Poljšak, B. & Ribarič, S., 2017. Reduced risk of apoptosis: mechanisms of stress responses. Apoptosis, 22, 265-283.

Minárik, P., Tomaásková, N., Kollárová, M., & Antalík, M., 2002. Malate dehydrogenases structure and function. General Physiology and Biophysics, 21(3), 257-265.

Miyamoto, T., & Amrein, H., 2017. Gluconeogenesis: An ancient biochemical pathway with a new twist. Fly, 11(3), 218-223.

Modica, T. M. E., Dituri, F., Mancarella, S., Pisano, C., Fabregat, I., and Giannelli, G., 2019. Calcium regulates HCC proliferation as well as EGFR recycling/degradation and could be a new therapeutic target in HCC. Cancers, 11(10).

Mohamed, M. M., & Sloane, B. F., 2006. Multifunctional enzymes in cancer. Nature Reviews Cancer, 6(10), 764-775.

Mongin, A. A., & Orlov, S. N., 2001. Mechanisms of cell volume regulation and possible nature of the cell volume sensor. Pathophysiology, 8(2), 77-88.

Mongin, A. A., & Orlov, S. N., 2009. Mechanisms of cell volume regulation. Physiology and Maintenance-Volume I: General Physiology, 1, 130.

Monroig, Ó., Tocher, D. R., & Navarro, J. C., 2013. Biosynthesis of polyunsaturated fatty acids in marine invertebrates: Recent advances in molecular mechanisms. Marine Drugs, 11(10), 3998-4018.

Morandell, S. & Yaffe, M. B., 2012. Exploiting synthetic lethal interactions between DNA damage signaling, checkpoint control, and p53 for targeted cancer therapy. Progress in Molecular Biology and Translational Science, 110, 289-314.

Moreira, R., Pereiro, P., Canchaya, C., Posada, D., Figueras, A. & Novoa, B., 2015. Rna-Seq in *Mytilus galloprovincialis*: comparative transcriptomics and expression profiles among different tissues. BMC Genomics, 16, 728.

Moriya, Y., Itoh, M., Okuda, S., Yoshizawa, A., & Kanehisa, M., 2007. KAAS: an automatic genome annotation and pathway reconstruction server. Nucleic Acids Research, 35, W182-W185.

Mors, O., Li, Q., Christensen, J. H., Børglum, A. D., Lazarus, R., Qvist, P., … Lescai, F., 2015. Experimental validation of methods for differential gene expression analysis and sample pooling in RNA-seq. BMC Genomics, 16(1), 1-8.

Muttray, A., F., Schulte, P., M. & Baldwin, S. A., 2008. Invertebrate p53-like mRNA isoforms are differentially expressed in mussel haemic neoplasia, Marine Environmental Research, 66(4), 412-421.

Mutz, K. O., Heilkenbrinker, A., Lönne, M., Walter, J. G. & Stahl, F., 2013. Transcriptome analysis using next-generation sequencing. Current Opinion in Biotechnology, 24, 22-30.

Nagalakshmi, U., Wang, Z., Waern, K., Shou, C., Raha, D., Gerstein, M., & Snyder, M., 2008. The transcriptional landscape of the yeast genome defined by RNA sequencing. Science, 320(5881), 1344-1349.

Napoli, M., & Flores, E. R., 2017. The p53 family orchestrates the regulation of metabolism: physiological regulation and implications for cancer therapy. British Journal of Cancer, 116(2), 149-155.

NCBI, n. d. National Center for Biotechnology Information. PubChem Compound Summary for CID 5280383, Leukotriene A4. https://pubchem.ncbi.nlm.nih.gov/compound/Leukotriene-A4. (accessed March 2021).

Nelson, D., L. & Cox, M., 2008. Lehninger Principles of Biochemistry (7th Edition), WH Freeman.

Nelson, J., Gibbons, E., Pickett, K. R., Streeter, M., Warcup, A. O., Yeung, C. H.-Y., Judd, A. M. & Bell, J. D, 2011. Relationship between membrane permeability and specificity of human secretory phospholipase A_2 isoforms during cell death. Biochimica et Biophysica Acta (BBA)-Biomembranes, 1808(7), 1913-1920.

Nextprot, n.d. https://www.nextprot.org/entry/NX_Q9H611/ (accessed April 2021).

NHGRI, 2020. National Human Genome Research Institute. https://www.genome.gov/about-genomics/fact-sheets/Sequencing-Human-Genome-cost (accessed June 2021).

Nobel Prize, 2021. Nobel Prize Outreach AB Press release. https://www.nobelprize.org/prizes/medicine/2011/press-release/ (accessed July 2021).

Nørregaard, R., Kwon, T. H., & Frøkiær, J., 2015. Physiology and pathophysiology of cyclooxygenase-2 and prostaglandin E2 in the kidney. Kidney Research and Clinical Practice, 34(4), 194-200.

Oancea, E., Vriens, J., Brauchi, S., Jun, J., Splawski, I., & Clapham, D. E., 2009. TRPM1 forms ion channels associated with melanin content in melanocytes. Science Signaling, 2(70), ra21-ra21.

O'Connor, C. M. & Adams, J. U., 2010. Essentials of Cell Biology. Cambridge, MA: NPG Education.

Oda, T., Abe, T., Yanagisawa, H., & Kikkawa, M., 2016. Structure and function of outer dynein arm intermediate and light chain complex. Molecular Biology of the Cell, 27(7), 1051-1059.

Ogata, H., Goto, S., Sato, K., Fujibuchi, W., Bono, H., & Kanehisa, M., 1999. KEGG: Kyoto encyclopedia of genes and genomes. Nucleic Acids Research, 27(1), 29-34.

Oktay, M., Albayrak Sönmez, A., Gümüşkaya Öcal, B., Genel, N., Hücümenoğlu, S., Alper, M., 2013. Prostat adenokarsinomlarında annexin A2, A7 Ve A11 immünhistokimyasal ekspresyonu ve prognostik faktörlerle ilişkisi. Düzce Tıp Dergisi. 15(1), 14-18.

O'Neill L. A., Bowie A. G., 2007 The family of five: TIR-domain-containing adaptors in Toll-like receptor signalling. Nature Reviews Immunology, 7, 353-364.

Orhan, H. & Şahin, G., 1995. Clinical and toxicological importance of glutathione s-transferases. Turkiye Klinikleri J Med Sci.15(5), 303-15.

Ortiz, G. G., Pacheco Moisés, F. P., Mireles-Ramírez, M., Flores-Alvarado, L. J., González-Usigli, H., Sánchez-González, V. J., ... Rivero-Moragrega, P., 2017. Oxidative stress: love and hate history in central nervous system. Advances in Protein Chemistry and Structural Biology, 108, 1-31.

Pålsson-McDermott, E. M., & O'Neill, L. A., 2007. Building an immune system from nine domains. Biochemical Society Transactions, 35(6), 1437-1444.

Panigrahy, D., Kaipainen, A., Greene, E. R., & Huang, S., 2010. Cytochrome P450-derived eicosanoids: the neglected pathway in cancer. Cancer Metastasis Reviews, 29(4), 723-735.

Papa, S., & Skulachev, V. P., 1997. Reactive oxygen species, mitochondria, apoptosis and aging. Molecular and Cellular Biochemistry, 174(1-2), 305-319.

Pedersen, L., Schrøder, J., Satir, P., & Christensen, S., 2012. The ciliary cytoskeleton. Comprehensive Physiology, 2, 779-803.

Pelzel, Heather & Nickells, Robert. 2010. Retinal ganglion cell death in glaucoma. Ocular Disease: Mechanisms and Management, 207-213.

Pertea, M., Pertea, G. M., Antonescu, C. M., Chang, T. C., Mendell, J. T. & Salzberg, S. L., 2015. StringTie enables improved reconstruction of a transcriptome from RNA-seq reads. Nature Biotechnology, 33, 290-295.

Peteiro, L. G., Woodin, S. A., Wethey, D. S., Costas-Costas, D., Martínez-Casal, A., Olabarria, C., & Vázquez, E., 2018. Responses to salinity stress in bivalves: Evidence of ontogenetic changes in energetic physiology on *Cerastoderma edule*. Scientific Reports, 8(1), 1-9.

Philipp, E. E. R., Kraemer, L., Melzner, F., Poustka, A. J., Thieme, S., Findeisen, U., Schreiber, S. & Rosenstiel, P., 2012. Massively parallel RNA sequencing identifies a complex immune gene repertoire in the lophotrochozoan *Mytilus edulis.* Plos One*,* 7(3), e33091.

Phillips, J. W., & Hird, F. J., 1977. Gluconeogenesis in vertebrate livers. Comparative Biochemistry and Physiology. B, Comparative Biochemistry, 57(2), 127-131.

Pikuleva, I. A., & Waterman, M. R., 2013. Cytochromes P450: roles in diseases. Journal of Biological Chemistry, 288(24), 17091-17098.

Pirahanchi, Y., Jessu, R., Aeddula, N. R., 2021. Physiology, Sodium Potassium Pump. In StatPearls [Internet]. Treasure Island (FL): StatPearls, https://www.ncbi.nlm.nih.gov/books/NBK537088/ (accessed March 2021).

Piva, R., Belardo, G., & Santoro, M. G., 2006. NF-kappaB: a stress-regulated switch for cell survival. Antioxidants & Redox Signaling, 8(3-4), 478-486.

Pollutri, D., & Penzo, M., 2020. Ribosomal protein L10: from function to dysfunction. Cells, 9(11), 2503.

Pourmozaffar, S., Tamadoni Jahromi, S., Rameshi, H., Sadeghi, A., Bagheri, T., Behzadi, S., Gozari, M., Zahedi, M. R., & Abrari Lazarjani, S., 2019. The role of salinity in physiological responses of bivalves. Reviews in Aquaculture, 1-19.

Prado-Alvarez, M., Rotllant, J., Gestal, C., Novoa, B., & Figueras, A., 2009. Characterization of a C3 and a factor B-like in the carpet-shell clam, *Ruditapes decussatus*. Fish & Shellfish Immunology, 26(2), 305-315.

Prego-Faraldo, M. V., Martínez, L., & Méndez, J., 2018. RNA-Seq analysis for assessing the early response to DSP toxins in *Mytilus galloprovincialis* digestive gland and gill. Toxins, 10(10), 417.

Prentis, P. J & Pavasovic, A., 2014. The *Anadara trapezia* transcriptome: A resource for molluscan physiological genomics. Marine Genomics, 18, 113-115.

Purves, J., Cockayne, A., Moody, P. C., & Morrissey, J. A., 2010. Comparison of the regulation, metabolic functions, and roles in virulence of the glyceraldehyde-3-phosphate dehydrogenase homologues gapA and gapB in *Staphylococcus aureus*. Infection and Immunity, 78(12), 5223-5232.

Pytharopoulou, S., Grintzalis, K., Sazakli, E., Leotsinidis, M., Georgiou, C., & Kalpaxis, D., 2011. Translational responses and oxidative stress of mussels experimentally exposed to Hg, Cu and Cd: One pattern does not fit at all. Aquatic Toxicology, 105, 157-165.

R Core Team 2019. R: A language and environment for statistical computing. R Foundation for Statistical Computing, Vienna, Austria. URL: https://www.R-project.org/.

Rahman, M. A., Henderson, S., Miller-Ezzy, P., Li, X. X., & Qin, J. G. 2019. Immune response to temperature stress in three bivalve species: Pacific oyster *Crassostrea gigas*, Mediterranean mussel *Mytilus galloprovincialis* and mud cockle *Katelysia rhytiphora*. Fish & Shellfish Immunology, 86, 868-874.

Ramsden, D. B., Ho, P. W., Ho, J. W., Liu, H. F., So, D. H., Tse, H. M., Chan, K. H., & Ho, S. L., 2012. Human neuronal uncoupling proteins 4 and 5 (UCP4 and UCP5): structural properties, regulation, and physiological role in protection against oxidative stress and mitochondrial dysfunction. Brain and Behavior, 2(4), 468-478.

Ray, P. D., & Fry, R. C., 2015. Chapter 2 - The Cell: The Fundamental Unit in Systems Biology. In R. C. B. T.-S. B. in T. and E. H. Fry (Eds.), 11-42, Academic Press, Boston.

Reactome, 2004. https://reactome.org/content/detail/R-HSA-112308 (accessed June 2021).

Reactome, 2009. https://reactome.org/content/detail/R-HSA-444120 (accessed December 2020).

Reactome, 2014. https://reactome.org/content/detail/R-HSA-5333671 (accessed February 2021).

Reglero, A., & Cabezas, J. A., 1976. Glycosidases of molluscs: purification and properties of alpha-L-fucosidase from *Chamelea gallina* L. European Journal of Biochemistry, 66(2), 379-387.

Reidelberger R. D., 1994. Cholecystokinin and control of food intake. The Journal of Nutrition, 124(8 Suppl), 1327S-1333S.

Reimand, J., Isserlin, R., Voisin, V., Kucera, M., Tannus-lopes, C., Rostamianfar, A., Wadi, L., Meyer, M., Wong, J., Xu, C., Merico, D., & Bader, G. D., 2019. Pathway enrichment analysis and visualization of omics data using g: Profiler , GSEA , Cytoscape and EnrichmentMap. Nature Protocols, 14, 482-517.

Rey-Campos, M., Moreira, R., Valenzuela-Muñoz, V., Gallardo-Escárate, C., Novoa, B., & Figueras, A., 2019. High individual variability in the transcriptomic response of Mediterranean mussels to Vibrio reveals the involvement of myticins in tissue injury. Scientific Reports, 9(1), 1-15.

Ricciotti, E., & FitzGerald, G. A., 2011. Prostaglandins and inflammation. Arteriosclerosis, Thrombosis, and Vascular biology, 31(5), 986-1000.

Richmond, G. S., & Smith, T. K., 2011. Phospholipases A_1. International journal of molecular sciences, 12(1), 588-612.

Riisgård, H. U., Bøttiger, L., Pleissner, D., 2012. Effect of salinity on growth of mussels, Mytilus edulis, with special reference to Great Belt (Denmark). Open Journal of Marine Science, 2, 167-176.

Riisgård, H.U., Lüskow, F., Pleissner, D., Lundgreen, K., López, M., 2013. Effect of salinity on filtration rates of mussels *Mytilus edulis* with special emphasis on dwarfed mussels from the low-saline Central Baltic Sea. Helgoland Marine Research, 67, 591-598.

Riisgård, H. U., Funch, P., & Larsen, P. S., 2015. The mussel filter-pump-present understanding, with a re-examination of gill preparations. Acta Zoologica, 96(3), 273-282.

Rismani-Yazdi, H., Haznedaroglu, B. Z., Bibby, K., & Peccia, J., 2011. Transcriptome sequencing and annotation of the microalgae *Dunaliella tertiolecta*: pathway description and gene discovery for production of next-generation biofuels. BMC Genomics, 12, 148.

Ritchie, M.E., Phipson, B., Wu, D., Hu, Y., Law, C.W., Shi, W., & Smyth, G.K., 2015. limma powers differential expression analyses for RNA-sequencing and microarray studies. Nucleic Acids Research, 43(7), e47.

Rivera-Ingraham, G. A., & Lignot, J. H., 2017. Osmoregulation, bioenergetics and oxidative stress in coastal marine invertebrates: raising the questions for future research. Journal of Experimental Biology, 220(10), 1749-1760.

Robinson, M. D., McCarthy, D. J. & Smyth, G. K., 2010. edgeR: a Bioconductor package for differential expression analysis of digital gene expression data. Bioinformatics, 26(1), 139-140.

Roch, G. J., & Sherwood, N. M., 2011. Stanniocalcin has deep evolutionary roots in eukaryotes. Genome Biology and Evolution, 3, 284-294.

Rocher, B., Bultelle, F., Chan, P., Foll, F. Le, Letendre, J., Monsinjon, T., Olivier, S., Péden, R., Poret, A., Vaudry, D., & Knigge, T., 2015. 2-DE Mapping of the blue mussel gill proteome: the usual suspects revisited. Proteomes, 3(1), 3-41.

Romero, A., Dios, S., Poisa-Beiro, L., Costa, M. M., Posada, D., Figueras, A., & Novoa, B., 2011. Individual sequence variability and functional activities of fibrinogen-related proteins (FREPs) in the

Mediterranean mussel (*Mytilus galloprovincialis*) suggest ancient and complex immune recognition models in invertebrates. Developmental and Comparative Immunology, 35(3), 334-344.

Romero, A., Novoa, B., & Figueras, A., 2015. The complexity of apoptotic cell death in molluscs: an update. Fish and Shellfish Immunology, 46(1), 79-87.

Roos, W. P. and Kaina, B., 2006. DNA damage-induced cell death by apoptosis. Trends in Molecular Medicine, 12(9), 440-450.

Rudnick, G., Krämer, R., Blakely, R. D., Murphy, D. L., & Verrey, F., 2014. The SLC6 transporters: perspectives on structure, functions, regulation, and models for transporter dysfunction. Pflügers Archiv-European Journal of Physiology, 466(1), 25-42.

Ruprecht, J. J., & Kunji, E. R. S., 2020. The SLC25 mitochondrial carrier family: structure and mechanism. Trends in Biochemical Sciences, 45(3), 244-258.

Salvi, F., & Gadda, G., 2013. Human choline dehydrogenase: medical promises and biochemical challenges. Archives of Biochemistry and Biophysics, 537(2), 243-252.

Samanta, A., Hughes, T., & Moiseenkova-Bell, V. Y., 2018. Transient receptor potential (TRP) channels. Sub-cellular Biochemistry, 87, 141-165.

Sanders, T., Schmittmann, L., Nascimento-Schulze, J. C., & Melzner, F., 2018. High calcification costs limit mussel growth at low salinity. Frontiers in Marine Science, 5(OCT), 1-9.

Sanders, T., Thomsen, J., Müller, J. D., Rehder, G., & Melzner, F., 2020. Decoupling salinity and carbonate chemistry: low calcium ion concentration rather than salinity limits calcification in Baltic Sea mussels. Biogeosciences Discussions, 18(8), 2573-2590.

Sanderson, S. M., Xiao, Z., Wisdom, A. J., Bose, S., Liberti, M. V., Reid, M. A., … Locasale, J. W., 2020. The Na^+/K^+ ATPase regulates glycolysis and modifies immune metabolism in tumors. bioRxiv, 2020.03.31.018739.

Sardini, A., Amey, J. S., Weylandt, K. H., Nobles, M., Valverde, M. A., & Higgins, C. F., 2003. Cell volume regulation and swelling-activated chloride channels. Biochimica et Biophysica Acta - Biomembranes, 1618(2), 153-162.

Schurch, N. J., Schofield, P., Gierliński, M., Cole, C., Sherstnev, A., Singh, V., ... & Barton, G. J., 2016. How many biological replicates are needed in an RNA-seq experiment and which differential expression tool should you use?. Rna, 22(6), 839-851.

Scott, F. L., Denault, J. B., Riedl, S. J., Shin, H., Renatus, M., & Salvesen, G. S., 2005. XIAP inhibits caspase-3 and -7 using two binding sites: evolutionary conserved mechanism of IAPs. EMBO Journal, 24(3), 645-655.

Seagroves, T. N., Ryan, H. E., Lu, H., Wouters, B. G., Knapp, M., Thibault, P., Laderoute, K., & Johnson, R. S., 2001. Transcription factor HIF-1 is a necessary mediator of the pasteur effect in mammalian cells. Molecular and Cellular Biology, 21(10), 3436-3444.

Sepp, M., Sokolova, N., Jugai, S., Mandel, M., Peterson, P., & Vendelin, M., 2014. Tight coupling of Na^+/K^+ ATPase with glycolysis demonstrated in permeabilized rat cardiomyocytes. Plos One, 9(6), e99413.

Seppey, M., Manni, M., & Zdobnov, E. M., 2019. BUSCO: assessing genome assembly and annotation completeness. Methods in Molecular Biology, 1962, 227–245.

Han, J. S., Lee, J. H., Kong, J., Ji, Y., Kim, J., Choe, S. S., & Kim, J. B., 2019. Hypoxia restrains lipid utilization via protein kinase A and adipose triglyceride lipase downregulation through hypoxia-inducible factor. Molecular and Cellular Biology, 39(2), e00390-18.

Pagnon, J., Matzaris, M., Stark, R., Meex, R. C. R., Macaulay, S. L., Brown, W., … Watt, M. J., 2012. Identification and functional characterization of protein kinase A phosphorylation sites in the major lipolytic protein, adipose triglyceride lipase. Endocrinology, 153(9), 4278–4289.

Pierce, S. K., & Warren, J. W., 2001. The taurine efflux portal used to regulate cell volume in response to hypoosmotic stress seems to be similar in many cell types: lessons to be learned from molluscan red blood cells. American Zoologist, 41(4), 710-720.

SEQC/MAQC-III Consortium., 2014. A comprehensive assessment of RNA-seq accuracy, reproducibility and information content by the sequencing quality control consortium. Nature Biotechnology 32, 903-914.

Sillanpää, J. K., Cardoso, J. C. dos R., Félix, R. C., Anjos, L., Power, D. M., & Sundell, K., 2020. Dilution of seawater affects the Ca^{2+} transport in the outer mantle epithelium of *Crassostrea gigas*. Frontiers in Physiology, 11, 1-15.

Sims, D., Sudbery, I., Ilott, N. E., Heger, A., & Ponting, C. P., 2014. Sequencing depth and coverage: key considerations in genomic analyses. Nature Reviews Genetics, 15(2), 121-132.

Singh, R., Mailloux, R. J., Puiseux-Dao, S., & Appanna, V. D., 2007. Oxidative stress evokes a metabolic adaptation that favors increased NADPH synthesis and decreased NADH production in *Pseudomonas fluorescens*. Journal of Bacteriology, 189(18), 6665-6675.

Sinicrope, F. A., Rego, R. L., Okumura, K., Foster, N. R., O'Connell, M. J., Sargent, D. J., & Windschitl, H. E., 2008. Prognostic impact of bim, puma, and noxa expression in human colon carcinomas. Clinical Cancer Research, 14(18), 5810-5818.

Siokou-Frangou, I., Christaki, U., Mazzocchi, M. G., Montresor, M., Ribera D'Alcala, M., Vaque, D., & Zingone, A., 2010. Plankton in the open Mediterranean Sea: a review. Biogeosciences, 7(5), 1543-1586.

Slenter, D. N., Kutmon, M., Hanspers, K., Riutta, A., Windsor, J., Nunes, N., ... & Willighagen, E. L., 2018. WikiPathways: a multifaceted pathway database bridging metabolomics to other omics research. Nucleic Acids Research, 46(D1), D661-D667.

Smucker, R. A., & Wright, D. A., 1984. Chitinase activity in the crystalline style of the american oyster *Crassostrea virginica*. Comparative Biochemistry and Physiology Part A: Physiology, 77(2), 239-241.

Song, L., Wang, L., Qiu, L., & Zhang, H. 2010. Bivalve immunity. Advances in experimental medicine and biology, 708, 44–65.

Speed, N., & Blair, I. A., 2011. Cyclooxygenase- and lipoxygenase-mediated DNA damage. Cancer Metastasis Reviews, 30(3-4), 437-447.

Spooner, P. M., Chernick, S. S., Garrison, M. M., & Scow, R. O., 1979. Insulin regulation of lipoprotein lipase activity and release in 3T3-L1 adipocytes. Separation and dependence of hormonal effects on hexose metabolism and synthesis of RNA and protein. Journal of Biological Chemistry, 254(20), 10021-10029.

Stabili, L., Acquaviva, M. I., & Cavallo, R. A., 2005. *Mytilus galloprovincialis* filter feeding on the bacterial community in a Mediterranean coastal area (Northern Ionian Sea, Italy). Water Research, 39(2), 469-477.

Steinbauer, B., Mehnert, T., & Beyer, K. (2003). Hydration and lateral organization in phospholipid bilayers containing sphingomyelin: A 2H-NMR study. Biophysical Journal, 85(2), 1013-1024.

Storey, K., & Storey, J., 1990. Metabolic rate depression and biochemical adaptation in anaerobiosis, hibernation and estivation. The Quarterly Review of Biology, 65(2), 145-174.

Storey, K. B., & Storey, J. M. 2004. Oxygen limitation and metabolic rate depression. Journal of Comparative Physiology, 131, 311-319.

Su, M. A., Huang, Y. T., Chen, I. T., Lee, D. Y., Hsieh, Y. C., Li, C. Y., ... & Wang, H. C. (2014). An invertebrate Warburg effect: a shrimp virus achieves successful replication by altering the host metabolome via the PI3K-Akt-mTOR pathway. Plos Pathogens, 10(6), e1004196.

Subramanian, A., Tamayo, P., Mootha, V. K., Mukherjee, S., Ebert, B. L., Gillette, M. A., Paulovich, A., Pomeroy, S. L., Golub, T. R., Lander, E. S., & Mesirov, J. P., 2005. Gene set enrichment analysis: a knowledge-based approach for interpreting genome-wide expression profiles. Proceedings of the National Academy of Sciences, 102(43), 15545-15550.

Suhaili, S. H., Karimian, H., Stellato, M., Lee, T. H., & Aguilar, M. I., 2017. Mitochondrial outer membrane permeabilization: a focus on the role of mitochondrial membrane structural organization. Biophysical Reviews, 9(4), 443-457.

Sun, R., Zhang, Y., Lv, Q., Liu, B., Jin, M., Zhang, W., ... Duan, Z., 2011. Toll-like receptor 3 (TLR3) induces apoptosis via death receptors and mitochondria by up-regulating the transactivating p63 isoform α (TAP63α). Journal of Biological Chemistry, 286(18), 15918-15928.

Sun, S., & Zhou, J., 2018. Molecular mechanisms underlying stress response and adaptation. Thoracic Cancer, 9(2), 218-227.

Supek, F., Bošnjak, M., Škunca, N., & Šmuc, T., 2011. Revigo summarizes and visualizes long lists of gene ontology terms. Plos One, 6(7).

Szabadfi, K., Pinter, E., Reglodi, D., & Gabriel, R. 2014. Neuropeptides, trophic factors, and other substances providing morphofunctional and metabolic protection in experimental models of diabetic retinopathy. International Review of Cell and Molecular Biology, 311, 1-121.

Tagliarolo, M., Clavier, J., Chauvaud, L., Koken, M. & Grall, J., 2012. Metabolism in blue mussel: intertidal and subtidal beds compared. Aquatic Biology, 17, 167-180.

Tang, X., Metzger, D., Leeman, S., & Amar, S., 2006. LPS-induced TNF-alpha factor (LITAF)-deficient mice express reduced LPS-induced cytokine: evidence for LITAF-dependent LPS signaling pathways. Proceedings of the National Academy of Sciences of the United States of America, 103(37), 13777-13782.

Tao, M., Isas, J. M., & Langen, R. (2020). Annexin B12 trimer formation is governed by a network of protein-protein and protein-lipid interactions. Scientific Reports, 10(1), 1-11.

Taylor, A.C. & Brand, A.R., 1975. A comparative study of the respiratory responses of the bivalves *Arctica islandica* L. and *Mytilus edulis* L. to declining oxygen tension. Proceedings of the Royal Society of London. Series B. Biological Sciences, 190(1101), 443-456.

Tedengren, M., & Kautsky, N., 1986. Comparative study of the physiology and its probable effect on size in Blue Mussels (*Mytilus Edulis* L.) from the North Sea and the Northern Baltic Proper. Ophelia, 25(3), 147-155.

Tedengren, M., & Kautsky, N., 1987. Comparative stress response to diesel oil and salinity changes of the blue mussel, *Mytilus edulis* from the Baltic and North seas. Ophelia, 28(1), 1-9.

Tehrani, H. S., & Moosavi-Movahedi, A. A., 2018. Catalase and its mysteries. Progress in Biophysics and Molecular Biology, 140, 5-12.

Therien, A. G., & Blostein, R., 2000. Mechanisms of sodium pump regulation. American Journal of Physiology-Cell Physiology, 279(3), C541-C566.

Thomsen, J., Himmerkus, N., Holland, N., Sartoris, F. J., Bleich, M., & Tresguerres, M., 2016. Ammonia excretion in mytilid mussels is facilitated by ciliary beating. Journal of Experimental Biology, 219(15), 2300-2310.

Ting, H. & Khasawneh, F., 2010. Platelet function and Isoprostane biology. Should Isoprostanes be the newest member of the Orphan-ligand family?. Journal of Biomedical Science, 17(1), 1-13.

Toei, M., Saum, R., & Forgac, M., 2010. Regulation and isoform function of the V-ATPases. Biochemistry, 49(23), 4715-4723.

Torres, M. A., Jones, J. D. G., & Dangl, J. L., 2006. Reactive oxygen species signaling in response to pathogens. Plant Physiology, 141(2), 373-378.

Toubiana, M., Rosani, U., Giambelluca, S., Cammarata, M., Gerdol, M., Pallavicini, A., Venier, P., & Roch, P., 2014. Toll signal transduction pathway in bivalves: complete cds of intermediate elements and related gene transcription levels in hemocytes of immune stimulated *Mytilus galloprovincialis*. Developmental and Comparative Immunology, 45(2), 300-312.

Toyohara, H., Ikeda, M., Goto, C., Sawada, Hi., Hosoi, M., Takeuchi, K., Hayashi, I., Imamura, S. & Yamashita, M., 2005a. Osmoresponsive expression of oyster amino acid transporter gene and analysis of the regulatory region involved. Fisheries Science, 71, 465-470.

Toyohara, H., Yoshida, M., Hosoi, M. & Hayashi, I., 2005b. Expression of taurine transporter in response to hypo-osmotic stress in the mantle of Mediterranean blue mussel. Fisheries Science, 71, 356-360.

Traba, J., Satrústegui, J., del Arco, A., 2009. Transport of adenine nucleotides in the mitochondria of *Saccharomyces cerevisiae*: interactions between the ADP/ATP carriers and the ATP-Mg/Pi carrier. Mitochondrion, 9 (2), 79-85.

Türkoğlu, M. & Koray, T., 2002. Phytoplankton species' succession and nutrients in the Southern Black Sea (Bay of Sinop). Turkish Journal of Botany, 26(4), 235-252.

Mehnert, C. S., Rampelt, H., Gebert, M., Oeljeklaus, S., Schrempp, S. G., Kochbeck, L., Guiard, B., Warscheid, B., & van der Laan, M., 2014. The mitochondrial ADP/ATP carrier associates with the inner membrane presequence translocase in a stoichiometric manner. The Journal of Biological Chemistry, 289(39), 27352-27362.

Treaster, S. B., Chaudhuri, A. R., & Austad, S. N., 2015. Longevity and GAPDH stability in bivalves and mammals: a convenient marker for comparative gerontology and proteostasis. Plos One, 10(11), e0143680.

TRUBA, n. d. Turkish National e-Science e-Infrastructure, https://www.truba.gov.tr (accessed August 2019).

Tseng, Y. C., Lee, J. R., Chang, J. C. H., Kuo, C. H., Lee, S. J., & Hwang, P. P., 2008. Regulation of lactate dehydrogenase in tilapia (*Oreochromis mossambicus*) gills during acclimation to salinity challenge. Zoological Studies, 47(4), 473-480.

Tsikas, D., 2017. Assessment of lipid peroxidation by measuring malondialdehyde (MDA) and relatives in biological samples: analytical and biological challenges. Analytical Biochemistry, 524, 13-30.

Tsunoda, Y., & Owyang, C., 1993. Differential involvement of phospholipase A_2/arachidonic acid and phospholipase C/phosphoinositol pathways during cholecystokinin receptor activated Ca^{2+} oscillations in pancreatic acini. Biochemical and Biophysical Research Communications, 194(3), 1194-1202.

Tsunoda, Y., & Owyang, C., 1995. High-affinity CCK receptors are coupled to phospholipase A_2 pathways to mediate pancreatic amylase secretion. The American Journal of Physiology, 269(3), G435-G444.

Turan, H., Kocatepe, D., Altan, C. O., & Erkoyuncu, İ. 2012. Soğukta saklanan tüketime hazır midyelerin (Mytilus galloprovincialis L. 1819) besin kompozisyonu ve kalite kriterlerinin incelenmesi. 11. Hatay Gıda Kongresi, 364.

Uchida, K., Dezaki, K., Damdindorj, B., Inada, H., Shiuchi, T., Mori, Y., Yada, T., Minokoshi, Y. & Tominaga, M., 2011. Lack of TRPM2 impaired insulin secretion and glucose metabolism in mice. Diabetes, 60, 119-126.

Ueland, P. M., Holm, P. I., & Hustad, S., 2005. Betaine: a key modulator of one-carbon metabolism and homocysteine status. Clinical Chemistry and Laboratory Medicine, 43(10), 1069-1075.

Uniprot, n.d. https://www.uniprot.org/keywords/KW-1278 (accessed November 2020).

Uniprot, n.d. (b) https://www.uniprot.org/uniprot/P47712 (accessed January 2021).

Uniprot, n.d. (c) https://www.uniprot.org/uniprot/O94759 (accessed February 2021).

Uniprot, n.d. (d) https://www.uniprot.org/uniprot/Q61160 (accessed February 2021).

Uniprot, n.d. (e) https://www.uniprot.org/uniprot/O43557 (accessed March 2021).

Uniprot, n.d. (f) https://www.uniprot.org/uniprot/Q8BX35 (accessed March 2021).

Uniprot, n.d. (g) https://www.uniprot.org/uniprot/P78560 (accessed March 2021).

Uniprot, n.d. (h) https://www.uniprot.org/uniprot/P36941 (accessed March 2021).

Uniprot, n.d. (i) https://www.uniprot.org/uniprot/Q91ZI0 (accessed April 2021).

Uniprot, n.d. (j) https://www.uniprot.org/uniprot/E9QJQ6 (accessed April 2021).

van Kranen, H. J., & Siezen, C. L. E., 2016. Arachidonic Acid Pathway BT. In M. Schwab (Eds.), Encyclopedia of Cancer, 1-6, Springer Berlin Heidelberg, Berlin, Heidelberg.

Vanden Abeele, F., Zholos, A., Bidaux, G., Shuba, Y., Thebault, S., Beck, B., Flourakis, M., Panchin, Y., Skryma, R., & Prevarskaya, N., 2006. Ca^{2+}-independent phospholipase A2-dependent gating of TRPM8 by lysophospholipids. The Journal of Biological Chemistry, 281(52), 40174-40182.

Venier, P., De Pittà, C., Bernante, F., Varotto, L., De Nardi, B., Bovo, G., Roch, P., Novoa, B., Figueras, A., Pallavicini, A. & Lanfranchi, G., 2009. MytiBase: a knowledgebase of mussel (*M. galloprovincialis*) transcribed sequences. BMC Genomics, 10: 72.

Venier, P., Varotto, L., Rosani, U., Millino, C., Celegato, B., Bernante, F., Lanfranchi, G., Novoa, B., Roch, P., Figueras, A., & Pallavicini, A., 2011. Insights into the innate immunity of the Mediterranean mussel *Mytilus galloprovincialis*. BMC Genomics, 12, 69.

Venugopal, S. K. & Jialal, I., 2020. Physiology, Glucagon. In StatPearls [Internet]. Treasure Island (FL): StatPearls Publishing.

Vidal-Liñán, L., Bellas, J., Etxebarria, N., Nieto, O., & Beiras, R., 2014. Glutathione s-transferase, glutathione peroxidase and acetylcholinesterase activities in mussels transplanted to harbour areas. Science of The Total Environment, 470, 107-116.

Vlahogianni, T., Dassenakis, M., Scoullos, M. J., & Valavanidis, A., 2007. Integrated use of biomarkers (superoxide dismutase, catalase and lipid peroxidation) in mussels *Mytilus galloprovincialis* for assessing heavy metals' pollution in coastal areas from the Saronikos Gulf of Greece. Marine Pollution Bulletin, 54(9), 1361-1371.

Vlahogianni, T. H., & Valavanidis, A., 2007. Heavy-metal effects on lipid peroxidation and antioxidant defence enzymes in mussels *Mytilus galloprovincialis*. Chemistry and Ecology, 23(5), 361-371.

Vogeler, S., Carboni, S., Li, X., & Joyce, A., 2021. Phylogenetic analysis of the caspase family in bivalves: implications for programmed cell death, immune response and development. BMC Genomics, 22(1), 1-17.

Wagner, G. F., Hampong, M., Park, C. M., & Copp, D. H., 1986. Purification, characterization, and bioassay of teleocalcin, a glycoprotein from salmon corpuscles of Stannius. General and Comparative Endocrinology, 63(3), 481-491.

Wagner, G. F. & Dimattia, G. E., 2006. The stanniocalcin family of proteins. Journal of Experimental Zoology Part A: Comparative Experimental Biology, 305(9), 769-780.

Walker, C. W., Van Beneden, R. J., Muttray, A. F., Böttger, S. A., Kelley, M. L., Tucker, A. E., & Thomas, W. K., 2011. p53 superfamily proteins in marine bivalve cancer and stress biology. Advances in Marine Biology, 59, 1-36.

Wang, W., Vinocur, B., Shoseyov, O., & Altman, A., 2004. Role of plant heat-shock proteins and molecular chaperones in the abiotic stress response. Trends in Plant Science, 9(5), 244-252.

Wang, L., Song, L., Zhao, J., Qiu, L., Zhang, H., Xu, W., Li, H., Li, C., Wu, L., & Guo, X., 2009. Expressed sequence tags from the zhikong scallop (*Chlamys farreri*): discovery and annotation of host-defense genes. Fish & Shellfish Immunology, 26(5), 744-750.

Wang, X., & Chapman, K. D., 2013. Lipid signaling in plants. Frontiers in Plant Science, 4, 216.

Wang, Q., Yuan, Z., Wu, H., Liu, F., & Zhao, J., 2013. Molecular characterization of a manganese superoxide dismutase and copper/zinc superoxide dismutase from the mussel *Mytilus galloprovincialis*. Fish & Shellfish Immunology, 34(5), 1345-1351.

Wang, B., Li, R., & Perrizo, W. (Eds.)., 2015. Big Data Analytics in Bioinformatics and Healthcare. IGI Global.

Wang, J., Ren, R., & Yao, C.-L., 2018a. Oxidative stress responses of *Mytilus galloprovincialis* to acute cold and heat during air exposure. Journal of Molluscan Studies, 84(3), 285-292.

Wang, W., Song, X., Wang, L., & Song, L., 2018b. Pathogen-derived carbohydrate recognition in molluscs immune defense. International Journal of Molecular Sciences, 19(3), 721.

Wang, M., Wang, L., Jia, Z., Yi, Q., & Song, L., 2018c. The various components implied the diversified Toll-like receptor (TLR) signaling pathway in mollusk *Chlamys farreri*. Fish & Shellfish Immunology, 74, 205-212.

Wang, M. H., Hsiao, G., & Al-Shabrawey, M. 2020. Eicosanoids and oxidative stress in diabetic retinopathy. Antioxidants, 9(6), 520.

Ward, J. E., Sanford, L. P., Newell, R. I. E., & MacDonald, B. A., 1998. A new explanation of particle capture in suspension-feeding bivalve molluscs. Limnology and Oceanography, 43(5), 741-752.

Ware, C. F., 2013. Protein therapeutics targeted at the TNF superfamily. Advances in Pharmacology, 66, 51-80.

Waterhouse, R. M., Zdobnov, E. M., & Kriventseva, E. V., 2011. Correlating traits of gene retention, sequence divergence, duplicability and essentiality in vertebrates, arthropods, and fungi. Genome Biology and Evolution, 3, 75-86.

Waterhouse, R. M., Seppey, M., Simão, F. A., Manni, M., Ioannidis, P., Klioutchnikov, G., … Zdobnov, E. M., 2018. BUSCO Applications from Quality Assessments to Gene Prediction and Phylogenomics. Molecular Biology and Evolution, 35(3), 543-548.

Wessner, D., Dupont, C., Charles, T. & Neufeld, J., 2018. Cultivating Microorganisms, In Microbiology, Wiley.

Whitman, D. W. & Agrawal, A. A., 2009. What is Phenotypic Plasticity and Why is it Important? In Whitman, D. W. and Ananthakrishnan, T. N. (Eds.), Phenotypic Plasticity of Insects: Mechanisms and Consequences, Scientific Publishers, 1-63.

Wight, M., & Werner, A., 2013. The functions of natural antisense transcripts. Essays in Biochemistry, 54, 91-101.

WikiPathways, n.d. (a) https://www.wikipathways.org/index.php/Pathway:WP4223 (accessed May 2021).

WikiPathways, n.d. (b) https://www.wikipathways.org/index.php/Pathway:WP3303 (accessed May 2021).

WikiPathways, n.d. (c) https://www.wikipathways.org/index.php/Pathway:WP3932 (accessed May 2021).

Wilk-Blaszczak, M., n. d. Posttranslational modifications of proteins, https://uta.pressbooks.pub/cellphysiology/chapter/posttranslational-modifications-of-proteins/ (accessed March 2021).

Willers, H., Zou, L., Pfäffle, H. N., 2012. Targeting homologous recombination repair in cancer. In Kelley M. R. (Eds.), DNA Repair in Cancer Therapy: Molecular Targets and Clinical Applications, 119-151, Elsevier, London.

Willmer, P., Stone, G. & Johnston, I., 2005. Chapter 10 Hormones and Chemical Control Systems, In Environmental Physiology of Animals. Wiley, 342-387.

Williams, M. G., 2012. PGH2 is isomerised to PGD2 by HPGDS, Reactome, https://reactome.org/content/detail/R-HSA-2161701 (accessed January 2021).

Wu, J., Bao, M., Ge, D., Huo, L., Lv, Z., Chi, C., Liao, Z., & Liu, H., 2017. The expression of superoxide dismutase in *Mytilus coruscus* under various stressors. Fish & Shellfish Immunology, 70, 361-371.

Wu, F., Falfushynska, H., Dellwig, O., Piontkivska, H., & Sokolova, I. M., 2020. Interactive effects of salinity variation and exposure to ZnO nanoparticles on the innate immune system of a sentinel marine bivalve, *Mytilus edulis*. Science of The Total Environment, 712, 136473.

Xiang, Z., Qu, F., Wang, F., Li, J., Zhang, Y., & Yu, Z., 2014. Characteristic and functional analysis of a ficolin-like protein from the oyster *Crassostrea hongkongensis*. Fish & Shellfish Immunology, 40(2), 514-523.

Xing, J., Lin, T., & Zhan, W., 2008. Variations of enzyme activities in the haemocytes of scallop *Chlamys farreri* after infection with the acute virus necrobiotic virus (AVNV). Fish & Shellfish Immunology, 25(6), 847-852.

Yamaura, K., Takahashi, K. G., & Suzuki, T., 2008. Identification and tissue expression analysis of C-type lectin and galectin in the Pacific oyster, *Crassostrea gigas*. Comparative Biochemistry and Physiology. Part B, Biochemistry & Molecular Biology, 149(1), 168-175.

Yampolsky, L.Y., Glazko, G. V. & Fry, J. D., 2012. Evolution of gene expression and expression plasticity in long-term experimental populations of *Drosophila melanogaster* maintained under constant and variable ethanol stress, Molecular Ecology, 21, 4287-4299.

Yampolsky, L.Y., Zeng, E., Lopez, J., Williams, P. J., Dick, K. B., Colbourne, J. K. & Pfrender, M. E., 2014. Functional genomics of acclimation and adaptation in response to thermal stress in Daphnia. BMC Genomics, 15, 859.

Yancey, P. H., 2005. Organic osmolytes as compatible, metabolic and counteracting cytoprotectants in high osmolarity and other stresses. Journal of Experimental Biology, 208, 2819-2830.

Yang, B., Zhang, M., Li, L., Pu, F., You, W., & Ke, C., 2015. Molecular Analysis of atypical family 18 chitinase from Fujian oyster *Crassostrea angulata* and its physiological role in the digestive system. Plos One, 10(6), e0129261.

Yang, S., Cui, J., Yang, Y., Liu, Z., Yan, H., Tang, C., ... & Gao, H., 2016. Over-expressed RPL34 promotes malignant proliferation of non-small cell lung cancer cells. Gene, 576(1), 421-428.

Yang, X., Wang, H., Huang, C., He, X., Xu, W., Luo, Y., & Huang, K., 2017. Zinc enhances the cellular energy supply to improve cell motility and restore impaired energetic metabolism in a toxic environment induced by OTA. Scientific Reports, 7(1), 1-11.

Yazdani, M., & Mahdieh, M., 2012. Salinity induced apoptosis in root meristematic cells of rice. International Journal of Bioscience, Biochemistry and Bioinformatics, 2(1), 40-43.

Yeung, B. H., Law, A. Y., & Wong, C. K., 2012. Evolution and roles of stanniocalcin. Molecular and Cellular Endocrinology, 349(2), 272-280.

Yi, C., & He, C., 2013. DNA repair by reversal of DNA damage. Cold Spring Harbor Perspectives in Biology, 5(1), a012575.

Yoon, H. J., Jeon, S.-B., Kim, I.-H., & Park, E. J., 2008. Regulation of TLR2 Expression by Prostaglandins in Brain Glia. The Journal of Immunology, 180(12), 8400-8409.

Yu L., 2020. RNA-Seq Reproducibility Assessment of the Sequencing Quality Control Project. Cancer Informatics, 19, 1176935120922498.

Yui, K., Imataka, G., Nakamura, H., Ohara, N., & Naito, Y., 2015. Eicosanoids derived from arachidonic acid and their family prostaglandins and cyclooxygenase in psychiatric disorders. Current Neuropharmacology, 13(6), 776-785.

Zagoory, O., Braiman, A., & Priel, Z., 2002. The mechanism of ciliary stimulation by acetylcholine: Roles of calcium, PKA, and PKG. Journal of General Physiology, 119(4), 329-339.

Zaitsev, Y. P., Alexandrov, B. G., Berlinsky, N. A., & Zenetos, A., 2002. Europe's biodiversity-biogeographical regions and seas: The Black Sea an oxygen-poor sea. EEA (European Environment Agency), Copenhagen.

Zenetos, A., Siokou-Frangou, I., Gotsis-Skretas, O., & Groom, S., 2002. The Mediterranean Sea-blue oxygen-rich, nutrient-poor waters. Europe's biodiversity, biogeographical regions and seas. Seas around Europe. EEA (European Environment Agency), National Centre for Marine Research (NCMR), Copenhagen.

Zhang, H., Song, L., Li, C., Zhao, J., Wang, H., Gao, Q., & Xu, W., 2007. Molecular cloning and characterization of a thioester-containing protein from Zhikong scallop *Chlamys farreri*. Molecular Immunology, 44(14), 3492-3500.

Zhang, H., Wang, L., Song, L., Song, X., Wang, B., Mu, C., & Zhang, Y., 2009. A fibrinogen-related protein from bay scallop *Argopecten irradians* involved in innate immunity as pattern recognition receptor. Fish & Shellfish Immunology, 26(1), 56-64.

Zhang, D., Ma, J., Jiang, J., Qiu, L., Zhu, C., Su, T., ... & Jiang, S., 2010. Molecular characterization and expression analysis of lipopolysaccharide and β-1, 3-glucan-binding protein (LGBP) from pearl oyster *Pinctada fucata*. Molecular Biology Reports, 37(7), 3335-3343.

Zhang, Z., Zhang, W., Jung, D. Y., Ko, H. J., Lee, Y., Friedline, R. H., Lee, E., Jun, J., Ma, Z., Kim, F., Tsitsilianos, N., Chapman, K., Morrison, A., Cooper, M. P., Miller, B. A., & Kim, J. K., 2012a. TRPM2 Ca^{2+} channel regulates energy balance and glucose metabolism. American Journal of Physiology. Endocrinology and Metabolism, 302(7), E807-E816.

Zhang, G., Fang, X., Guo, X., Li, L. I., Luo, R., Xu, F., ... & Wang, J., 2012b. The oyster genome reveals stress adaptation and complexity of shell formation. Nature, 490(7418), 49-54.

Zhang, L., Li, L. & Zhang, G., 2012c. Sequence variability of fibrinogen-related proteins (FREPs) in *Crassostrea gigas*. Chinese Science Bulletin. 57, 3312–3319.

Zhang, Y., He, X., Yu, F., Xiang, Z., Li, J., et al., 2013 Characteristic and Functional Analysis of Toll-like Receptors (TLRs) in the lophotrocozoan, *Crassostrea gigas*, Reveals Ancient Origin of TLR-Mediated Innate Immunity. PLOS ONE 8(10), e76464.

Zhang, P., Tu, B., Wang, H., Cao, Z., Tang, M., Zhang, C., Gu, B., Li, Z., Wang, L., Yang, Y., Zhao, Y., Wang, H., Luo, J., Deng, C. X., Gao, B., Roeder, R. G., & Zhu, W. G., 2014a. Tumor suppressor p53 cooperates with SIRT6 to regulate gluconeogenesis by promoting FoxO1 nuclear exclusion. Proceedings of the National Academy of Sciences of the United States of America, 111(29), 10684-10689.

Zhang, Y., Yu, F., Li, J., Tong, Y., Zhang, Y., & Yu, Z., 2014b. The first invertebrate RIG-I-like receptor (RLR) homolog gene in the pacific oyster *Crassostrea gigas*. Fish & Shellfish Immunology, 40(2), 466-471.

Zhang, J. Y., Zhang, F., Hong, C. Q., Giuliano, A. E., Cui, X. J., Zhou, G. J., Zhang, G. J., & Cui, Y. K., 2015. Critical protein GAPDH and its regulatory mechanisms in cancer cells. Cancer biology & medicine, 12(1), 10-22.

Zhao, X., Yu, H., Kong, L., & Li, Q., 2012. Transcriptomic responses to salinity stress in the Pacific oyster *Crassostrea gigas*. Plos One, 7(9), e46244.

Zheng, P., Wang, M., Li, C., Sun, X., Wang, X., Sun, Y., & Sun, S., 2017. Insights into deep-sea adaptations and host-symbiont interactions: a comparative transcriptome study on *Bathymodiolus* mussels and their coastal relatives. Molecular ecology, 26(19), 5133-5148.

Zhukova, N. V., 2019. Fatty acids of marine molluscs: impact of diet, bacterial symbiosis and biosynthetic potential. Biomolecules, 9(12), 1-25.

Zou, Y., Huang, W., Gu, Z., & Gu, X., 2011. Predominant gain of promoter TATA box after gene duplication associated with stress responses. Molecular Biology and Evolution, 28(10), 2893-2904.

Zu, X. L., & Guppy, M., 2004. Cancer metabolism: facts, fantasy, and fiction. Biochemical and Biophysical Research Communications, 313(3), 459-465.

Zyla, J., Marczyk, M., Weiner, J. et al., 2017. Ranking metrics in gene set enrichment analysis: do they matter?. BMC Bioinformatics, 18, 256.

APPENDIX A: DESCRIPTIVE STATISTICS AND DATA VALIDATION

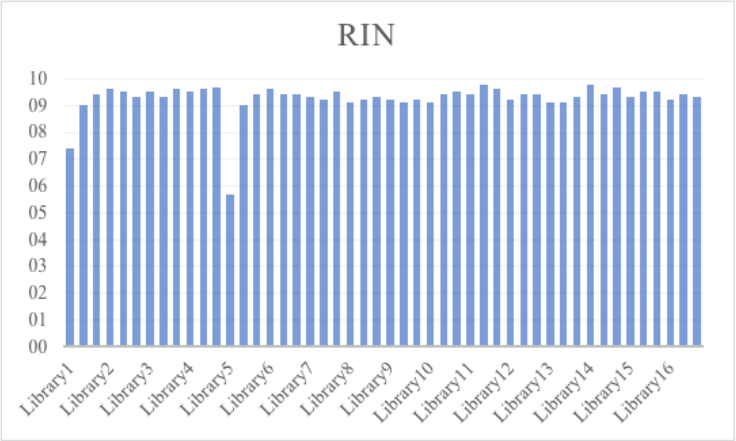


Figure A.1. Histogram of RIN values of the samples used to construct RNA-Seq libraries.

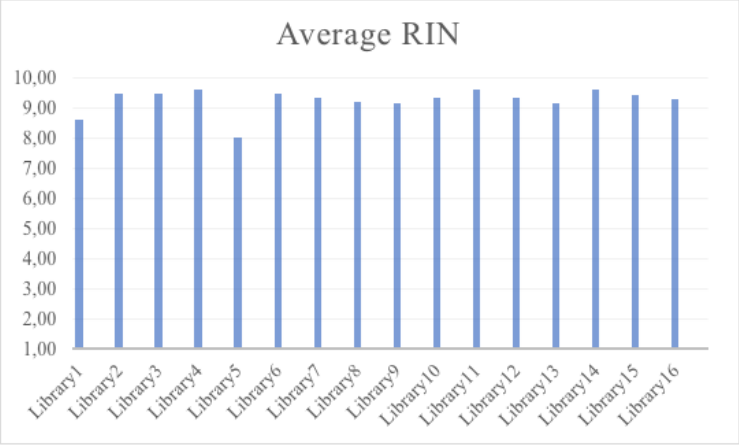


Figure A.2. Histogram of RIN values of the pooled RNA-Seq libraries.

Table A.1. RIN values of libraries used in RNA-Seq.

	Tank	Treatment	Timepoint	RIN	Average RIN
Library1	A	RT	A	7.4	8.60
				9.0	
				9.4	
Library2	A	RC	A	9.6	9.47
				9.5	
				9.3	
Library3	B	RT	A	9.5	9.47
				9.3	
				9.6	
Library4	B	RC	A	9.5	9.60
				9.6	
				9.7	
Library5	A	RT	B	5.7	8.03
				9.0	
				9.4	
Library6	A	RC	B	9.6	9.47
				9.4	
				9.4	
Library7	B	RT	B	9.3	9.33
				9.2	
				9.5	
Library8	B	RC	B	9.1	9.20
				9.2	
				9.3	
Library9	A	RT	C	9.2	9.17
				9.1	
				9.2	
Library10	A	RC	C	9.1	9.33
				9.4	
				9.5	
Library11	B	RT	C	9.4	9.60
				9.8	
				9.6	
Library12	B	RC	C	9.2	9.33
				9.4	
				9.4	
Library13	A	RT	D	9.1	9.17
				9.1	
				9.3	
Library14	A	RC	D	9.8	9.63
				9.4	

				9.7	
Library15	B	RT	D	9.3	9.43
				9.5	
				9.5	
Library16	B	RC	D	9.2	9.30
				9.4	
				9.3	
			Average	9.3	9.26
			SD	0.6	0.41

Table A.2. Sequencing statistics for libraries provided by Macrogen Inc.

	Total read bases (bp)	Total reads	GC(%)	AT(%)	Q20(%)	Q30(%)
Library1	3,361,376,960	33,280,960	38.78	61.22	98.78	95.95
Library2	3,859,031,432	38,208,232	38.64	61.36	98.86	96.11
Library3	4,314,873,722	42,721,522	38.71	61.29	98.92	96.24
Library4	4,561,187,472	45,160,272	38.76	61.24	98.87	96.15
Library5	4,578,651,988	45,333,188	38.63	61.37	98.9	96.21
Library6	3,813,115,822	37,753,622	39.25	60.75	98.94	96.32
Library7	3,880,280,014	38,418,614	38.33	61.67	98.84	96.07
Library8	4,259,695,402	42,175,202	38.98	61.02	98.84	96.12
Library9	5,476,862,562	54,226,362	39.09	60.91	98.85	96.09
Library10	5,016,965,526	49,672,926	38.75	61.25	98.84	96.07
Library11	4,180,695,626	41,393,026	38.03	61.97	98.84	96.07
Library12	4,183,320,414	41,419,014	39.07	60.93	98.92	96.27
Library13	3,750,845,686	37,137,086	39.55	60.45	98.94	96.35
Library14	4,421,791,716	43,780,116	38.77	61.23	98.89	96.15
Library15	5,199,690,080	51,482,080	38.57	61.43	98.83	96.02
Library16	4,534,732,340	44,898,340	39.03	60.97	98.84	96.05
Average	4,337,069,798	42,941,285.13	38.81	61.19	98.87	96.14
SD	561,085,273.58	5,555,299.74	0.36	0.36	0.05	0.11
Total	69,393,116,762	687,060,562				

Table A.3. Amount of reads mapping to ribosomal RNA queried against SILVA SSURef_NR99 and LSURef_NR99 databases.

	Total reads passing E-value threshold (%)
Library1	2.52
Library2	2.13
Library3	1.83
Library4	2.23
Library5	2.84
Library6	3.05
Library7	1.94
Library8	2.75
Library9	4.16
Library10	2.94
Library11	1.97
Library12	2.73
Library13	4.41
Library14	2.51
Library15	2.2
Library16	3.1
Average	2.706875
SD	0.737099891

Table A.4. Statistics of reads mapping to ribosomal RNA queried against SILVA SSURef_NR99 and LSURef_NR99 databases.

Total reads passing E-value threshold	
Library1 Results: Total reads = 16526539 Total reads passing E-value threshold = 417006 (2.52%) Total reads failing E-value threshold = 16109533 (97.48%) Minimum read length = 25 Maximum read length = 101 Mean read length = 100 By database: SILVA_138.1_SSURef_NR99_tax_silva.fasta 0.85% SILVA_138.1_LSURef_NR99_tax_silva.fasta 1.67%	Library9 Results: Total reads = 26960137 Total reads passing E-value threshold = 1122660 (4.16%) Total reads failing E-value threshold = 25837477 (95.84%) Minimum read length = 25 Maximum read length = 101 Mean read length = 100 By database: SILVA_138.1_SSURef_NR99_tax_silva.fasta 0.65% SILVA_138.1_LSURef_NR99_tax_silva.fasta 3.51%
Library2 Results: Total reads = 18991892 Total reads passing E-value threshold = 404269 (2.13%) Total reads failing E-value threshold = 18587623 (97.87%) Minimum read length = 25 Maximum read length = 101 Mean read length = 100 By database: SILVA_138.1_SSURef_NR99_tax_silva.fasta 0.62% SILVA_138.1_LSURef_NR99_tax_silva.fasta 1.51%	Library10 Results: Total reads = 24685483 Total reads passing E-value threshold = 725188 (2.94%) Total reads failing E-value threshold = 23960295 (97.06%) Minimum read length = 25 Maximum read length = 101 Mean read length = 100 By database: SILVA_138.1_SSURef_NR99_tax_silva.fasta 0.70% SILVA_138.1_LSURef_NR99_tax_silva.fasta 2.23%
Library3 Results: Total reads = 21249421 Total reads passing E-value threshold = 388000 (1.83%) Total reads failing E-value threshold = 20861421 (98.17%) Minimum read length = 25 Maximum read length = 101 Mean read length = 100 By database: SILVA_138.1_SSURef_NR99_tax_silva.fasta 0.43% SILVA_138.1_LSURef_NR99_tax_silva.fasta 1.40%	Library11 Results: Total reads = 20570574 Total reads passing E-value threshold = 404655 (1.97%) Total reads failing E-value threshold = 20165919 (98.03%) Minimum read length = 25 Maximum read length = 101 Mean read length = 100 By database: SILVA_138.1_SSURef_NR99_tax_silva.fasta 0.49% SILVA_138.1_LSURef_NR99_tax_silva.fasta 1.48%
Library4 Results: Total reads = 22454982 Total reads passing E-value threshold = 500410 (2.23%) Total reads failing E-value threshold = 21954572 (97.77%) Minimum read length = 25 Maximum read length = 101 Mean read length = 100 By database: SILVA_138.1_SSURef_NR99_tax_silva.fasta 0.48% SILVA_138.1_LSURef_NR99_tax_silva.fasta 1.75%	Library12 Results: Total reads = 20586636 Total reads passing E-value threshold = 561976 (2.73%) Total reads failing E-value threshold = 20024660 (97.27%) Minimum read length = 25 Maximum read length = 101 Mean read length = 100 By database: SILVA_138.1_SSURef_NR99_tax_silva.fasta 0.54% SILVA_138.1_LSURef_NR99_tax_silva.fasta 2.19%
Library5 Results:	Library13 Results:

Total reads = 22544561 Total reads passing E-value threshold = 640739 (2.84%) Total reads failing E-value threshold = 21903822 (97.16%) Minimum read length = 25 Maximum read length = 101 Mean read length = 100 By database: SILVA_138.1_SSURef_NR99_tax_silva.fasta 0.42% SILVA_138.1_LSURef_NR99_tax_silva.fasta 2.43%	Total reads = 18448180 Total reads passing E-value threshold = 812764 (4.41%) Total reads failing E-value threshold = 17635416 (95.59%) Minimum read length = 25 Maximum read length = 101 Mean read length = 100 By database: SILVA_138.1_SSURef_NR99_tax_silva.fasta 1.67% SILVA_138.1_LSURef_NR99_tax_silva.fasta 2.73%
Library6 Results: Total reads = 18761334 Total reads passing E-value threshold = 572006 (3.05%) Total reads failing E-value threshold = 18189328 (96.95%) Minimum read length = 25 Maximum read length = 101 Mean read length = 100 By database: SILVA_138.1_SSURef_NR99_tax_silva.fasta 0.55% SILVA_138.1_LSURef_NR99_tax_silva.fasta 2.50%	Library14 Results: Total reads = 21760437 Total reads passing E-value threshold = 546589 (2.51%) Total reads failing E-value threshold = 21213848 (97.49%) Minimum read length = 25 Maximum read length = 101 Mean read length = 100 By database: SILVA_138.1_SSURef_NR99_tax_silva.fasta 0.51% SILVA_138.1_LSURef_NR99_tax_silva.fasta 2.00%
Library7 Results: Total reads = 19101010 Total reads passing E-value threshold = 371339 (1.94%) Total reads failing E-value threshold = 18729671 (98.06%) Minimum read length = 25 Maximum read length = 101 Mean read length = 100 By database: SILVA_138.1_SSURef_NR99_tax_silva.fasta 0.40% SILVA_138.1_LSURef_NR99_tax_silva.fasta 1.55%	Library15 Results: Total reads = 25595890 Total reads passing E-value threshold = 561882 (2.20%) Total reads failing E-value threshold = 25034008 (97.80%) Minimum read length = 25 Maximum read length = 101 Mean read length = 100 By database: SILVA_138.1_SSURef_NR99_tax_silva.fasta 0.42% SILVA_138.1_LSURef_NR99_tax_silva.fasta 1.78%
Library8 Results: Total reads = 20953619 Total reads passing E-value threshold = 576657 (2.75%) Total reads failing E-value threshold = 20376962 (97.25%) Minimum read length = 25 Maximum read length = 101 Mean read length = 100 By database: SILVA_138.1_SSURef_NR99_tax_silva.fasta 0.56% SILVA_138.1_LSURef_NR99_tax_silva.fasta 2.19%	Library16 Results: Total reads = 22314635 Total reads passing E-value threshold = 691950 (3.10%) Total reads failing E-value threshold = 21622685 (96.90%) Minimum read length = 25 Maximum read length = 101 Mean read length = 100 By database: SILVA_138.1_SSURef_NR99_tax_silva.fasta 0.49% SILVA_138.1_LSURef_NR99_tax_silva.fasta 2.61%

Table A.5. Overall alignment rate of libraries using HISAT2.

	Overall alignment rate (%)
Library1	86.11
Library2	86.89
Library3	85.93
Library4	87.07
Library5	87.12
Library6	87.55
Library7	86.04
Library8	88.04
Library9	88.26
Library10	87.03
Library11	85.11
Library12	87.67
Library13	88.12
Library14	87.34
Library15	87.59
Library16	88.1
Average	87.123125
SD	0.91539222

Table A.6. Alignment statistics of libraries using HISAT2.

Library1 16526539 reads; of these: 16526539 (100.00%) were paired; of these: 3761987 (22.76%) aligned concordantly 0 times 9915359 (60.00%) aligned concordantly exactly 1 time 2849193 (17.24%) aligned concordantly >1 times ---- 3761987 pairs aligned concordantly 0 times; of these: 195877 (5.21%) aligned discordantly 1 time ---- 3566110 pairs aligned 0 times concordantly or discordantly; of these: 7132220 mates make up the pairs; of these: 4592132 (64.39%) aligned 0 times 1901877 (26.67%) aligned exactly 1 time 638211 (8.95%) aligned >1 times 86.11% overall alignment rate	Library9 26960137 reads; of these: 26960137 (100.00%) were paired; of these: 5358310 (19.87%) aligned concordantly 0 times 17974327 (66.67%) aligned concordantly exactly 1 time 3627500 (13.46%) aligned concordantly >1 times ---- 5358310 pairs aligned concordantly 0 times; of these: 311301 (5.81%) aligned discordantly 1 time ---- 5047009 pairs aligned 0 times concordantly or discordantly; of these: 10094018 mates make up the pairs; of these: 6327764 (62.69%) aligned 0 times 2911862 (28.85%) aligned exactly 1 time 854392 (8.46%) aligned >1 times 88.26% overall alignment rate
Library2 18991892 reads; of these: 18991892 (100.00%) were paired; of these: 4161992 (21.91%) aligned concordantly 0 times 11558059 (60.86%) aligned concordantly exactly 1 time 3271841 (17.23%) aligned concordantly >1 times ---- 4161992 pairs aligned concordantly 0 times; of these: 225451 (5.42%) aligned discordantly 1 time ---- 3936541 pairs aligned 0 times concordantly or discordantly; of these: 7873082 mates make up the pairs; of these: 4980399 (63.26%) aligned 0 times 2193568 (27.86%) aligned exactly 1 time 699115 (8.88%) aligned >1 times 86.89% overall alignment rate	Library10 24685483 reads; of these: 24685483 (100.00%) were paired; of these: 5313427 (21.52%) aligned concordantly 0 times 15549842 (62.99%) aligned concordantly exactly 1 time 3822214 (15.48%) aligned concordantly >1 times ---- 5313427 pairs aligned concordantly 0 times; of these: 284557 (5.36%) aligned discordantly 1 time ---- 5028870 pairs aligned 0 times concordantly or discordantly; of these: 10057740 mates make up the pairs; of these: 6401522 (63.65%) aligned 0 times 2767757 (27.52%) aligned exactly 1 time 888461 (8.83%) aligned >1 times 87.03% overall alignment rate
Library3 21249421 reads; of these: 21249421 (100.00%) were paired; of these: 4899597 (23.06%) aligned concordantly 0 times 12676279 (59.65%) aligned concordantly exactly 1 time 3673545 (17.29%) aligned concordantly >1 times ---- 4899597 pairs aligned concordantly 0 times; of these: 261602 (5.34%) aligned discordantly 1 time ---- 4637995 pairs aligned 0 times concordantly or discordantly; of these: 9275990 mates make up the pairs; of these: 5977950 (64.45%) aligned 0 times 2494552 (26.89%) aligned exactly 1 time 803488 (8.66%) aligned >1 times 85.93% overall alignment rate	Library11 20570574 reads; of these: 20570574 (100.00%) were paired; of these: 5048872 (24.54%) aligned concordantly 0 times 12240965 (59.51%) aligned concordantly exactly 1 time 3280737 (15.95%) aligned concordantly >1 times ---- 5048872 pairs aligned concordantly 0 times; of these: 268464 (5.32%) aligned discordantly 1 time ---- 4780408 pairs aligned 0 times concordantly or discordantly; of these: 9560816 mates make up the pairs; of these: 6127236 (64.09%) aligned 0 times 2598447 (27.18%) aligned exactly 1 time 835133 (8.73%) aligned >1 times 85.11% overall alignment rate
Library4 22454982 reads; of these: 22454982 (100.00%) were paired; of these: 4875612 (21.71%) aligned concordantly 0 times 13759687 (61.28%) aligned concordantly exactly 1 time 3819683 (17.01%) aligned concordantly >1 times ----	Library12 20586636 reads; of these: 20586636 (100.00%) were paired; of these: 4226992 (20.53%) aligned concordantly 0 times 13015160 (63.22%) aligned concordantly exactly 1 time 3344484 (16.25%) aligned concordantly >1 times

4875612 pairs aligned concordantly 0 times; of these: 278224 (5.71%) aligned discordantly 1 time ---- 4597388 pairs aligned 0 times concordantly or discordantly; of these: 9194776 mates make up the pairs; of these: 5806285 (63.15%) aligned 0 times 2575229 (28.01%) aligned exactly 1 time 813262 (8.84%) aligned >1 times 87.07% overall alignment rate	---- 4226992 pairs aligned concordantly 0 times; of these: 237310 (5.61%) aligned discordantly 1 time ---- 3989682 pairs aligned 0 times concordantly or discordantly; of these: 7979364 mates make up the pairs; of these: 5076801 (63.62%) aligned 0 times 2211149 (27.71%) aligned exactly 1 time 691414 (8.67%) aligned >1 times 87.67% overall alignment rate
Library5 22544561 reads; of these: 22544561 (100.00%) were paired; of these: 4737372 (21.01%) aligned concordantly 0 times 14134687 (62.70%) aligned concordantly exactly 1 time 3672502 (16.29%) aligned concordantly >1 times ---- 4737372 pairs aligned concordantly 0 times; of these: 258722 (5.46%) aligned discordantly 1 time ---- 4478650 pairs aligned 0 times concordantly or discordantly; of these: 8957300 mates make up the pairs; of these: 5805416 (64.81%) aligned 0 times 2391208 (26.70%) aligned exactly 1 time 760676 (8.49%) aligned >1 times 87.12% overall alignment rate	Library13 18448180 reads; of these: 18448180 (100.00%) were paired; of these: 3632711 (19.69%) aligned concordantly 0 times 11986696 (64.97%) aligned concordantly exactly 1 time 2828773 (15.33%) aligned concordantly >1 times ---- 3632711 pairs aligned concordantly 0 times; of these: 203457 (5.60%) aligned discordantly 1 time ---- 3429254 pairs aligned 0 times concordantly or discordantly; of these: 6858508 mates make up the pairs; of these: 4383142 (63.91%) aligned 0 times 1899963 (27.70%) aligned exactly 1 time 575403 (8.39%) aligned >1 times 88.12% overall alignment rate
Library6 18761334 reads; of these: 18761334 (100.00%) were paired; of these: 3920614 (20.90%) aligned concordantly 0 times 12053556 (64.25%) aligned concordantly exactly 1 time 2787164 (14.86%) aligned concordantly >1 times ---- 3920614 pairs aligned concordantly 0 times; of these: 208647 (5.32%) aligned discordantly 1 time ---- 3711967 pairs aligned 0 times concordantly or discordantly; of these: 7423934 mates make up the pairs; of these: 4671605 (62.93%) aligned 0 times 2094966 (28.22%) aligned exactly 1 time 657363 (8.85%) aligned >1 times 87.55% overall alignment rate	Library14 21760437 reads; of these: 21760437 (100.00%) were paired; of these: 4622508 (21.24%) aligned concordantly 0 times 13594901 (62.48%) aligned concordantly exactly 1 time 3543028 (16.28%) aligned concordantly >1 times ---- 4622508 pairs aligned concordantly 0 times; of these: 260954 (5.65%) aligned discordantly 1 time ---- 4361554 pairs aligned 0 times concordantly or discordantly; of these: 8723108 mates make up the pairs; of these: 5509404 (63.16%) aligned 0 times 2422352 (27.77%) aligned exactly 1 time 791352 (9.07%) aligned >1 times 87.34% overall alignment rate
Library7 19101010 reads; of these: 19101010 (100.00%) were paired; of these: 4337928 (22.71%) aligned concordantly 0 times 11544062 (60.44%) aligned concordantly exactly 1 time 3219020 (16.85%) aligned concordantly >1 times ---- 4337928 pairs aligned concordantly 0 times; of these: 233665 (5.39%) aligned discordantly 1 time ---- 4104263 pairs aligned 0 times concordantly or discordantly; of these: 8208526 mates make up the pairs; of these: 5332147 (64.96%) aligned 0 times 2176017 (26.51%) aligned exactly 1 time 700362 (8.53%) aligned >1 times	Library15 25595890 reads; of these: 25595890 (100.00%) were paired; of these: 5276795 (20.62%) aligned concordantly 0 times 15880085 (62.04%) aligned concordantly exactly 1 time 4439010 (17.34%) aligned concordantly >1 times ---- 5276795 pairs aligned concordantly 0 times; of these: 282113 (5.35%) aligned discordantly 1 time ---- 4994682 pairs aligned 0 times concordantly or discordantly; of these: 9989364 mates make up the pairs; of these: 6354008 (63.61%) aligned 0 times 2752705 (27.56%) aligned exactly 1 time

86.04% overall alignment rate	882651 (8.84%) aligned >1 times 87.59% overall alignment rate
Library8 20953619 reads; of these: 20953619 (100.00%) were paired; of these: 4188748 (19.99%) aligned concordantly 0 times 13426272 (64.08%) aligned concordantly exactly 1 time 3338599 (15.93%) aligned concordantly >1 times ---- 4188748 pairs aligned concordantly 0 times; of these: 232363 (5.55%) aligned discordantly 1 time ---- 3956385 pairs aligned 0 times concordantly or discordantly; of these: 7912770 mates make up the pairs; of these: 5011582 (63.34%) aligned 0 times 2211083 (27.94%) aligned exactly 1 time 690105 (8.72%) aligned >1 times 88.04% overall alignment rate	Library16 22314635 reads; of these: 22314635 (100.00%) were paired; of these: 4440433 (19.90%) aligned concordantly 0 times 14496336 (64.96%) aligned concordantly exactly 1 time 3377866 (15.14%) aligned concordantly >1 times ---- 4440433 pairs aligned concordantly 0 times; of these: 238544 (5.37%) aligned discordantly 1 time ---- 4201889 pairs aligned 0 times concordantly or discordantly; of these: 8403778 mates make up the pairs; of these: 5310999 (63.20%) aligned 0 times 2335314 (27.79%) aligned exactly 1 time 757465 (9.01%) aligned >1 times 88.10% overall alignment rate

Table A.7. Statistics of alignment files.

Library1 41536805 + 0 in total (QC-passed reads + QC-failed reads) 0 + 0 duplicates 36925230 + 0 mapped (88.90%:nan%) 41536805 + 0 paired in sequencing 20774452 + 0 read1 20762353 + 0 read2 33138950 + 0 properly paired (79.78%:nan%) 34289463 + 0 with itself and mate mapped 2635767 + 0 singletons (6.35%:nan%) 1053535 + 0 with mate mapped to a different chr 678668 + 0 with mate mapped to a different chr (mapQ>=5)	Library9 64554842 + 0 in total (QC-passed reads + QC-failed reads) 0 + 0 duplicates 58213745 + 0 mapped (90.18%:nan%) 64554842 + 0 paired in sequencing 32289934 + 0 read1 32264908 + 0 read2 52694628 + 0 properly paired (81.63%:nan%) 54411238 + 0 with itself and mate mapped 3802507 + 0 singletons (5.89%:nan%) 1568040 + 0 with mate mapped to a different chr 1072660 + 0 with mate mapped to a different chr (mapQ>=5)
Library2 47689480 + 0 in total (QC-passed reads + QC-failed reads) 0 + 0 duplicates 42694759 + 0 mapped (89.53%:nan%) 47689480 + 0 paired in sequencing 23850925 + 0 read1 23838555 + 0 read2 38407608 + 0 properly paired (80.54%:nan%) 39739710 + 0 with itself and mate mapped 2955049 + 0 singletons (6.20%:nan%) 1231849 + 0 with mate mapped to a different chr 800012 + 0 with mate mapped to a different chr (mapQ>=5)	Library10 60645876 + 0 in total (QC-passed reads + QC-failed reads) 0 + 0 duplicates 54227967 + 0 mapped (89.42%:nan%) 60645876 + 0 paired in sequencing 30331138 + 0 read1 30314738 + 0 read2 48820266 + 0 properly paired (80.50%:nan%) 50463473 + 0 with itself and mate mapped 3764494 + 0 singletons (6.21%:nan%) 1503146 + 0 with mate mapped to a different chr 974991 + 0 with mate mapped to a different chr (mapQ>=5)
Library3 53589967 + 0 in total (QC-passed reads + QC-failed reads) 0 + 0 duplicates 47592360 + 0 mapped (88.81%:nan%) 53589967 + 0 paired in sequencing 26802754 + 0 read1 26787213 + 0 read2 42667878 + 0 properly paired (79.62%:nan%) 44204817 + 0 with itself and mate mapped 3387543 + 0 singletons (6.32%:nan%) 1405686 + 0 with mate mapped to a different chr 901489 + 0 with mate mapped to a different chr (mapQ>=5)	Library11 51284424 + 0 in total (QC-passed reads + QC-failed reads) 0 + 0 duplicates 45140648 + 0 mapped (88.02%:nan%) 51284424 + 0 paired in sequencing 25653176 + 0 read1 25631248 + 0 read2 40054210 + 0 properly paired (78.10%:nan%) 41569108 + 0 with itself and mate mapped 3571540 + 0 singletons (6.96%:nan%) 1403702 + 0 with mate mapped to a different chr 926978 + 0 with mate mapped to a different chr (mapQ>=5)
Library4 56325655 + 0 in total (QC-passed reads + QC-failed reads) 0 + 0 duplicates 50501145 + 0 mapped (89.66%:nan%) 56325655 + 0 paired in sequencing 28170478 + 0 read1 28155177 + 0 read2 45450656 + 0 properly paired (80.69%:nan%) 47070428 + 0 with itself and mate mapped 3430717 + 0 singletons (6.09%:nan%) 1490823 + 0 with mate mapped to a different chr 963771 + 0 with mate mapped to a different chr (mapQ>=5)	Library12 51071737 + 0 in total (QC-passed reads + QC-failed reads) 0 + 0 duplicates 45981067 + 0 mapped (90.03%:nan%) 51071737 + 0 paired in sequencing 25543332 + 0 read1 25528405 + 0 read2 41676416 + 0 properly paired (81.60%:nan%) 43028515 + 0 with itself and mate mapped 2952552 + 0 singletons (5.78%:nan%) 1235049 + 0 with mate mapped to a different chr 815338 + 0 with mate mapped to a different chr (mapQ>=5)
Library5 56016637 + 0 in total (QC-passed reads + QC-failed reads) 0 + 0 duplicates 50194428 + 0 mapped (89.61%:nan%)	Library13 45245049 + 0 in total (QC-passed reads + QC-failed reads) 0 + 0 duplicates 40849145 + 0 mapped (90.28%:nan%)

56016637 + 0 paired in sequencing 28018149 + 0 read1 27998488 + 0 read2 45491734 + 0 properly paired (81.21%:nan%) 46976609 + 0 with itself and mate mapped 3217819 + 0 singletons (5.74%:nan%) 1338154 + 0 with mate mapped to a different chr 865849 + 0 with mate mapped to a different chr (mapQ>=5)	45245049 + 0 paired in sequencing 22630405 + 0 read1 22614644 + 0 read2 37201034 + 0 properly paired (82.22%:nan%) 38349129 + 0 with itself and mate mapped 2500016 + 0 singletons (5.53%:nan%) 1041259 + 0 with mate mapped to a different chr 686426 + 0 with mate mapped to a different chr (mapQ>=5)
Library6 45706956 + 0 in total (QC-passed reads + QC-failed reads) 0 + 0 duplicates 41025099 + 0 mapped (89.76%:nan%) 45706956 + 0 paired in sequencing 22859359 + 0 read1 22847597 + 0 read2 36992664 + 0 properly paired (80.93%:nan%) 38180409 + 0 with itself and mate mapped 2844690 + 0 singletons (6.22%:nan%) 1102877 + 0 with mate mapped to a different chr 727013 + 0 with mate mapped to a different chr (mapQ>=5)	Library14 54103376 + 0 in total (QC-passed reads + QC-failed reads) 0 + 0 duplicates 48577254 + 0 mapped (89.79%:nan%) 54103376 + 0 paired in sequencing 27059577 + 0 read1 27043799 + 0 read2 43781198 + 0 properly paired (80.92%:nan%) 45300442 + 0 with itself and mate mapped 3276812 + 0 singletons (6.06%:nan%) 1390055 + 0 with mate mapped to a different chr 911861 + 0 with mate mapped to a different chr (mapQ>=5)
Library7 47943913 + 0 in total (QC-passed reads + QC-failed reads) 0 + 0 duplicates 42597384 + 0 mapped (88.85%:nan%) 47943913 + 0 paired in sequencing 23980619 + 0 read1 23963294 + 0 read2 38298214 + 0 properly paired (79.88%:nan%) 39623992 + 0 with itself and mate mapped 2973392 + 0 singletons (6.20%:nan%) 1190802 + 0 with mate mapped to a different chr 770112 + 0 with mate mapped to a different chr (mapQ>=5)	Library15 64252873 + 0 in total (QC-passed reads + QC-failed reads) 0 + 0 duplicates 57881842 + 0 mapped (90.08%:nan%) 64252873 + 0 paired in sequencing 32136308 + 0 read1 32116565 + 0 read2 52494186 + 0 properly paired (81.70%:nan%) 54138365 + 0 with itself and mate mapped 3743477 + 0 singletons (5.83%:nan%) 1491558 + 0 with mate mapped to a different chr 966340 + 0 with mate mapped to a different chr (mapQ>=5)
Library8 51620337 + 0 in total (QC-passed reads + QC-failed reads) 0 + 0 duplicates 46595484 + 0 mapped (90.27%:nan%) 51620337 + 0 paired in sequencing 25817970 + 0 read1 25802367 + 0 read2 42305478 + 0 properly paired (81.96%:nan%) 43616426 + 0 with itself and mate mapped 2979058 + 0 singletons (5.77%:nan%) 1197764 + 0 with mate mapped to a different chr 794709 + 0 with mate mapped to a different chr (mapQ>=5)	Library16 54416910 + 0 in total (QC-passed reads + QC-failed reads) 0 + 0 duplicates 49093978 + 0 mapped (90.22%:nan%) 54416910 + 0 paired in sequencing 27217475 + 0 read1 27199435 + 0 read2 44530848 + 0 properly paired (81.83%:nan%) 45885154 + 0 with itself and mate mapped 3208824 + 0 singletons (5.90%:nan%) 1242942 + 0 with mate mapped to a different chr 821309 + 0 with mate mapped to a different chr (mapQ>=5)

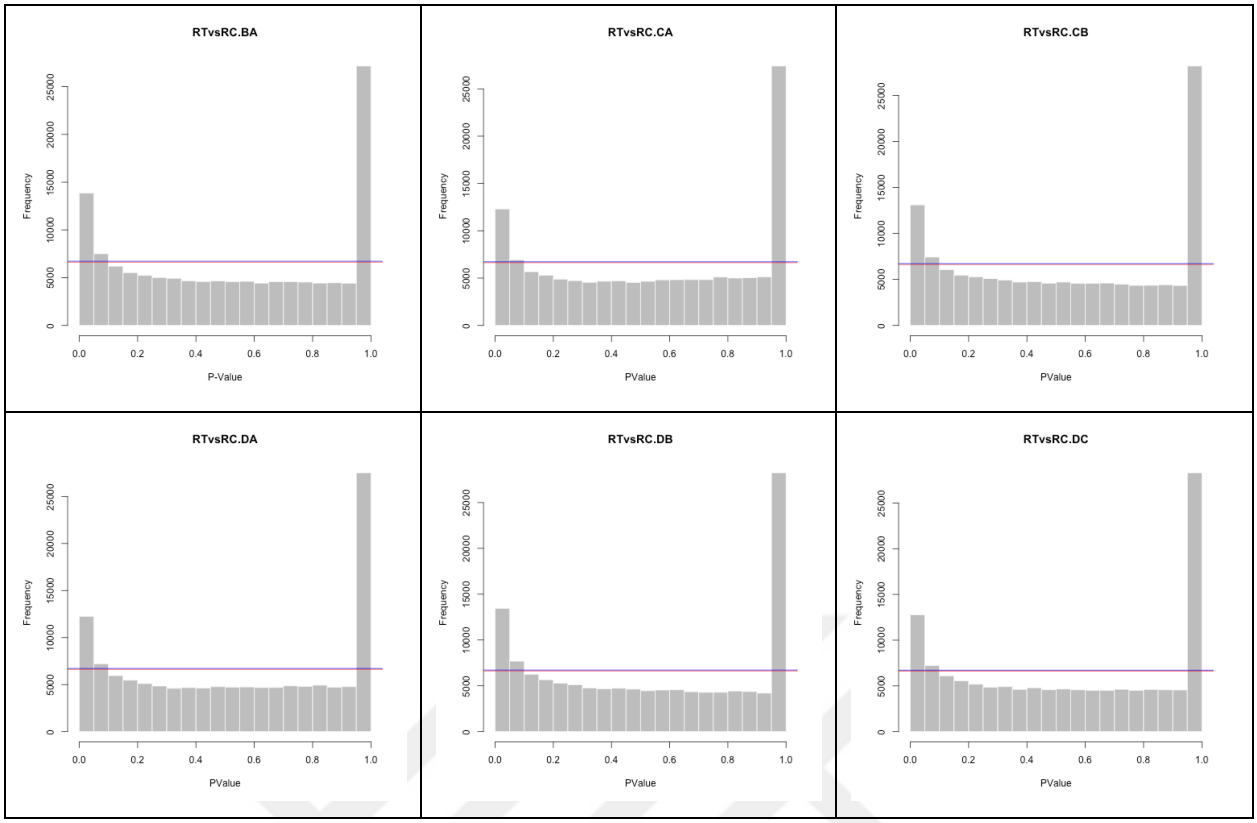


Figure A.3. P-value histogram of the contrasts with filtering F2. F2 keep contigs having worthwhile expression in at least 2 libraries. Higher criticism threshold, calculated as qbinom(0.95, length(pValues), 0.05) (R Core Team, 2019) , coloured red. Quality control threshold, calculated as qbinom(1 – 0.05*0.05, length(pValues), 0.05), coloured blue (Breheny et al., 2018).

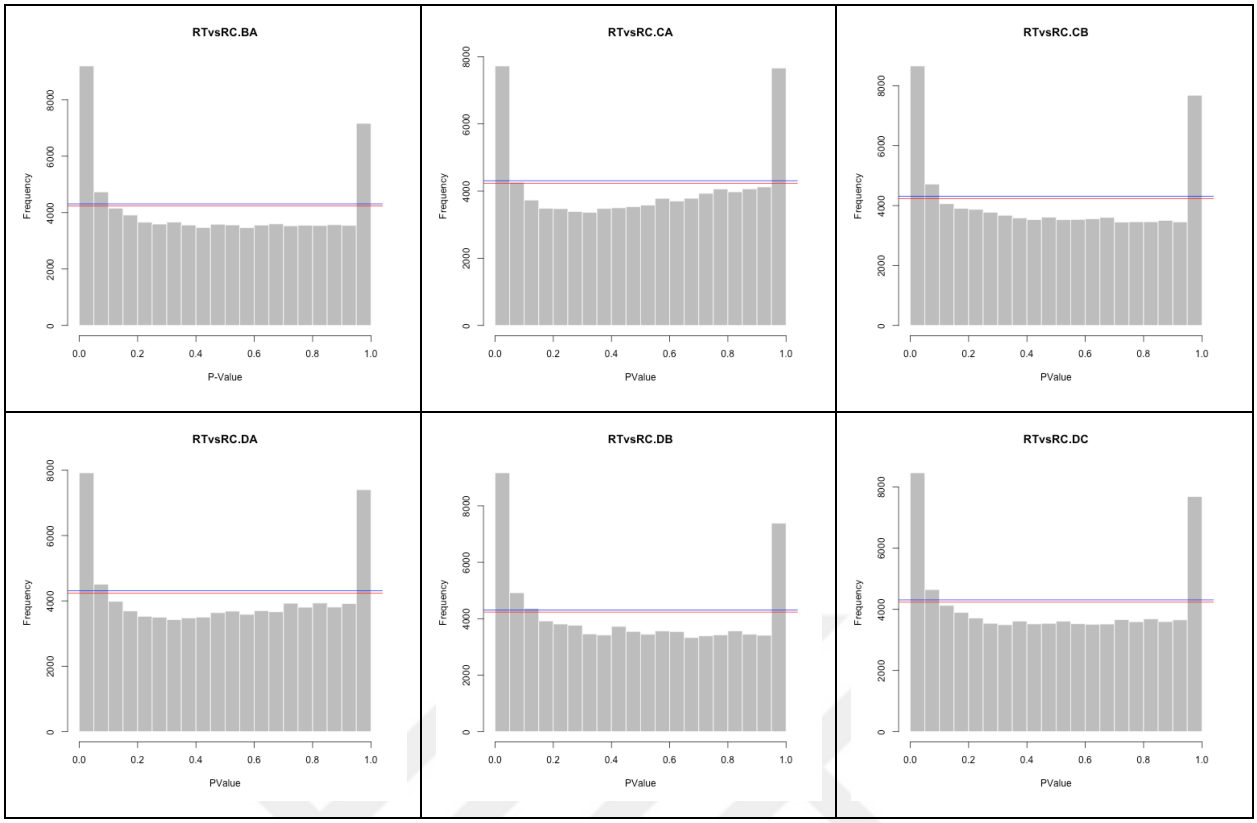


Figure A.4. P-value histogram of the contrasts with filtering F4. F4 keep contigs having worthwhile expression in at least 4 libraries. Higher criticism threshold, calculated as qbinom(0.95, length(pValues), 0.05) (R Core Team, 2019) , coloured red. Quality control threshold, calculated as qbinom(1 – 0.05*0.05, length(pValues), 0.05), coloured blue (Breheny et al., 2018).

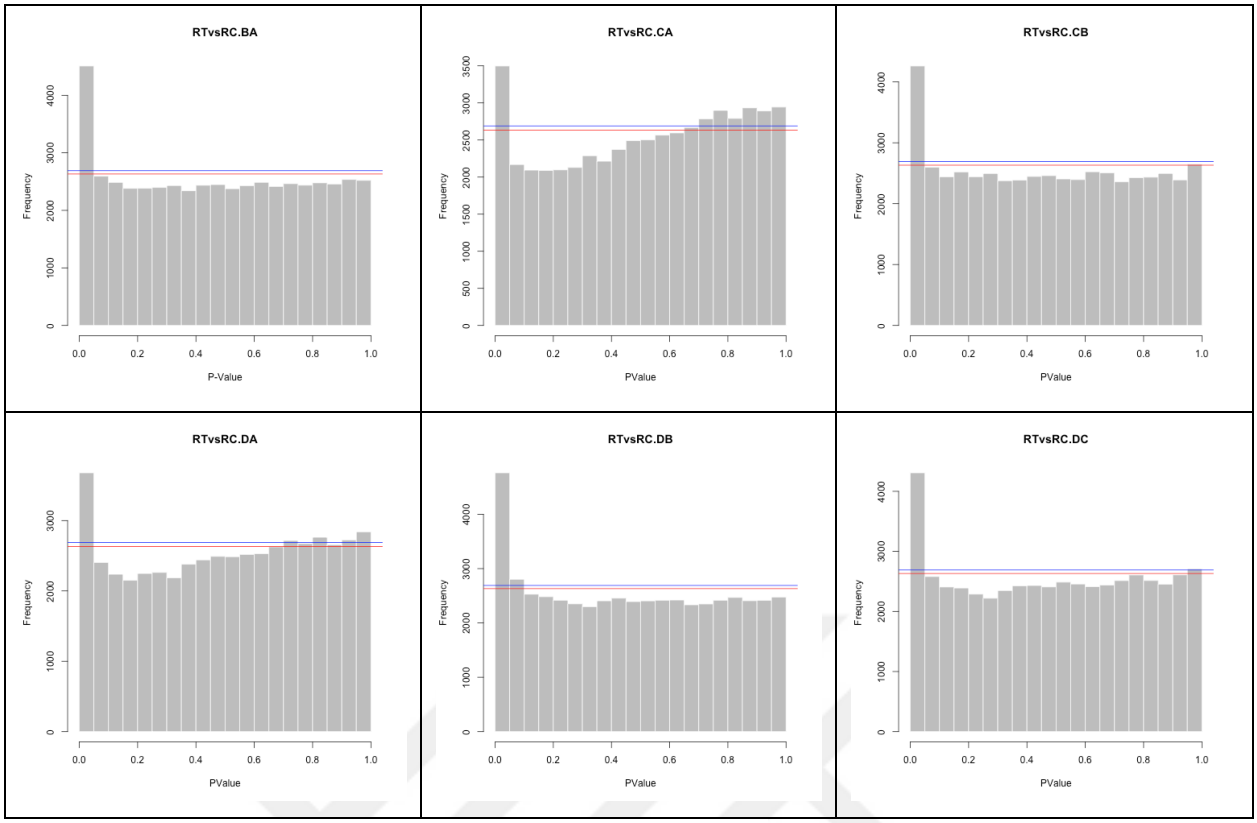


Figure A.5. P-value histogram of the contrasts with filtering F8. F8 keep contigs having worthwhile expression in at least 8 libraries. Higher criticism threshold, calculated as qbinom(0.95, length(pValues), 0.05) (R Core Team, 2019), coloured red. Quality control threshold, calculated as qbinom(1 – 0.05*0.05, length(pValues), 0.05), coloured blue (Breheny et al., 2018).

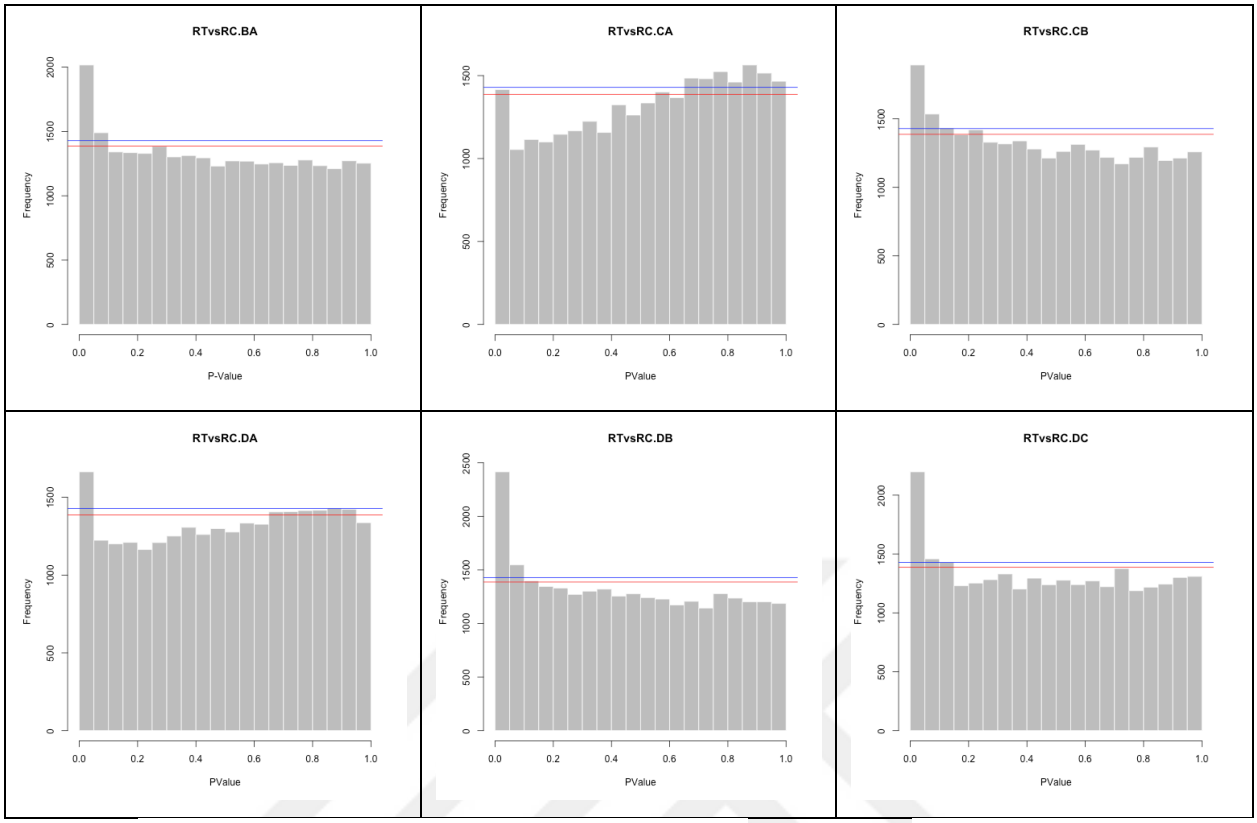


Figure A.6. P-value histogram of the contrasts with filtering F15. F15 keep contigs having worthwhile expression in at least 15 libraries. Higher criticism threshold, calculated as qbinom(0.95, length(pValues), 0.05) (R Core Team, 2019), coloured red. Quality control threshold, calculated as qbinom(1 – 0.05*0.05, length(pValues), 0.05), coloured blue (Breheny et al., 2018).

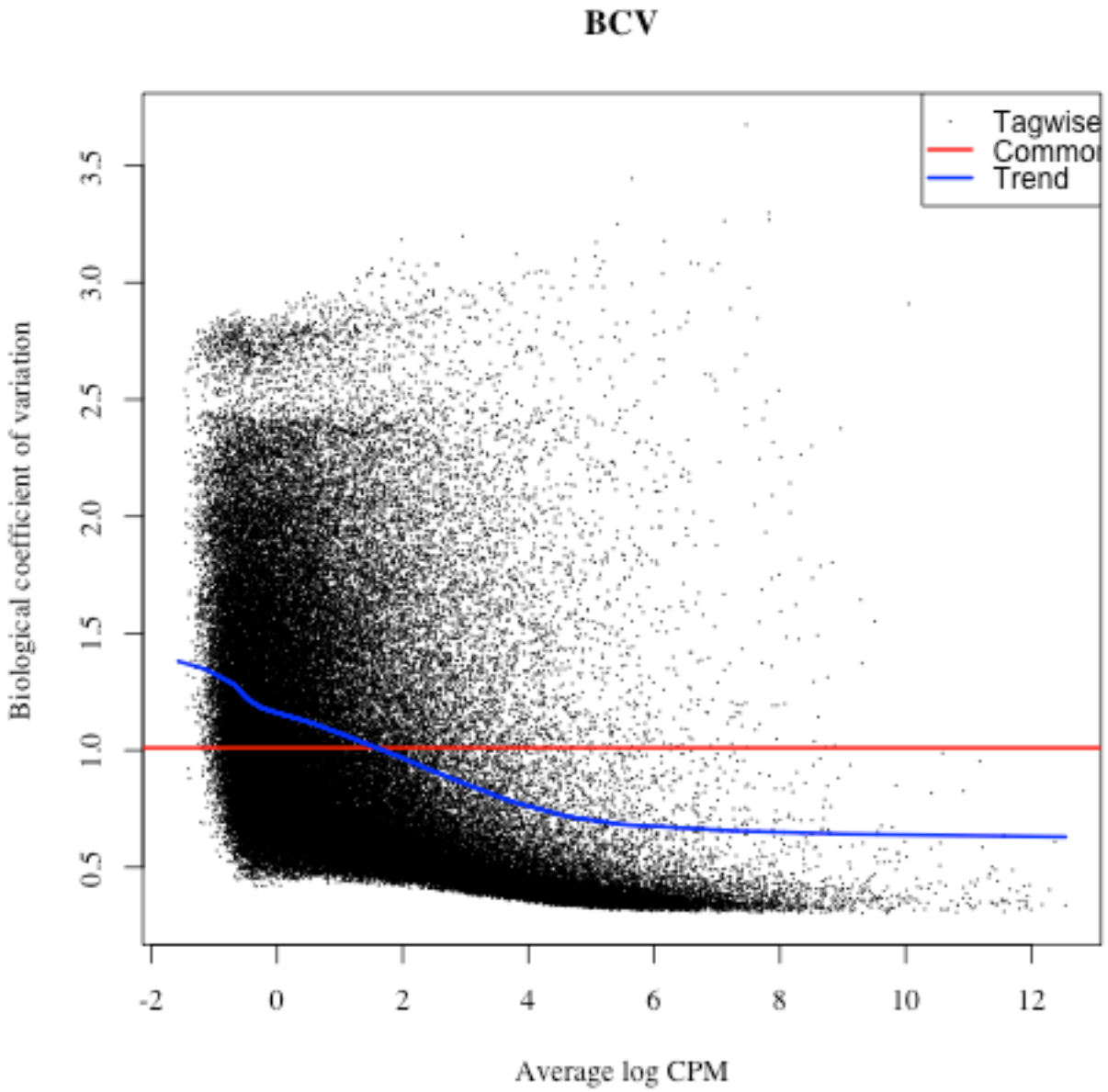


Figure A.7. Biological coefficient of variation (BCV) plot showing square-root estimates of common, tagwise and trended dispersions. BCV is plotted against average abundance of each gene.

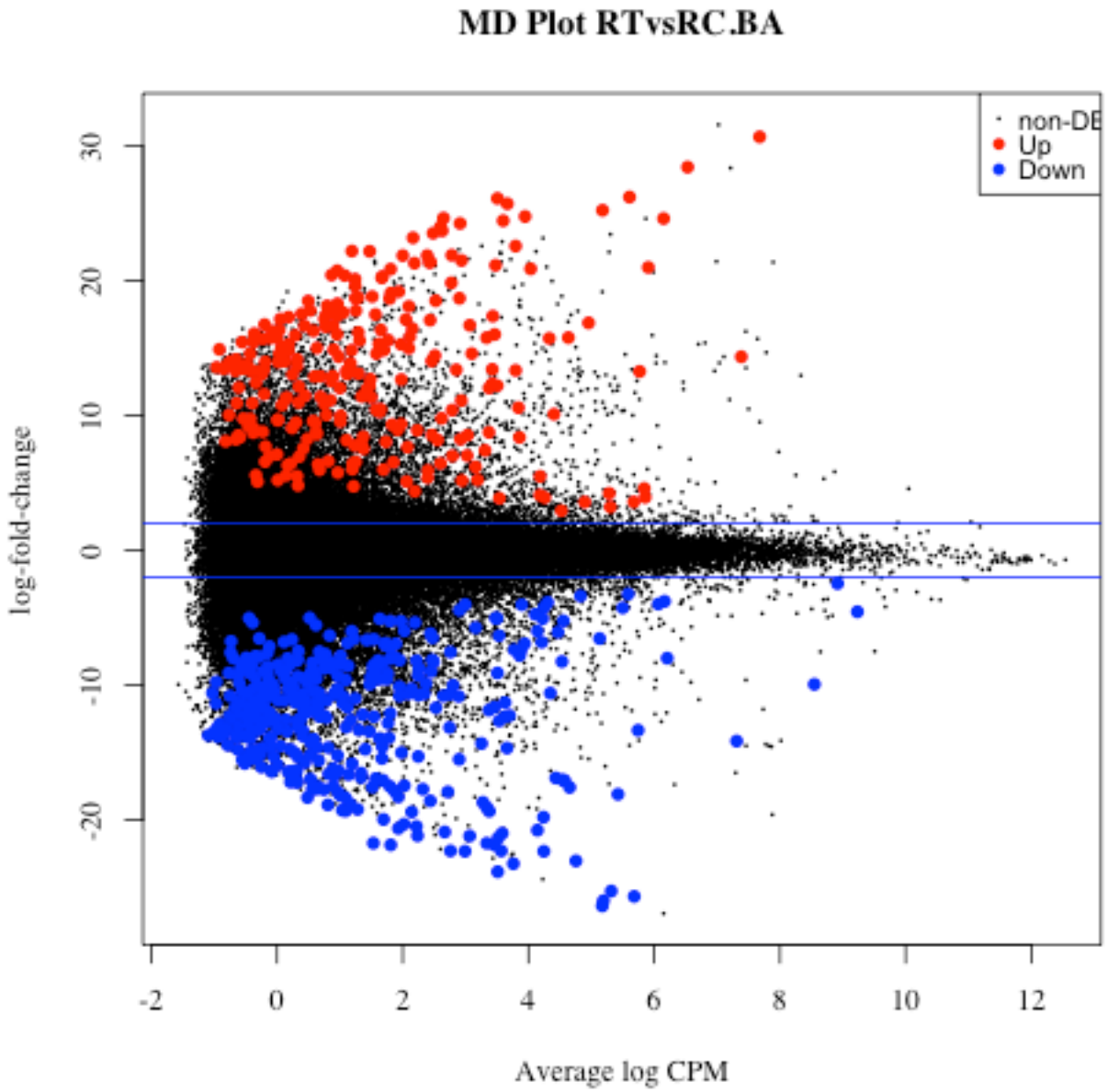


Figure A.8. MD plot of the contrast BA. The blue lines indicate 2-fold changes.

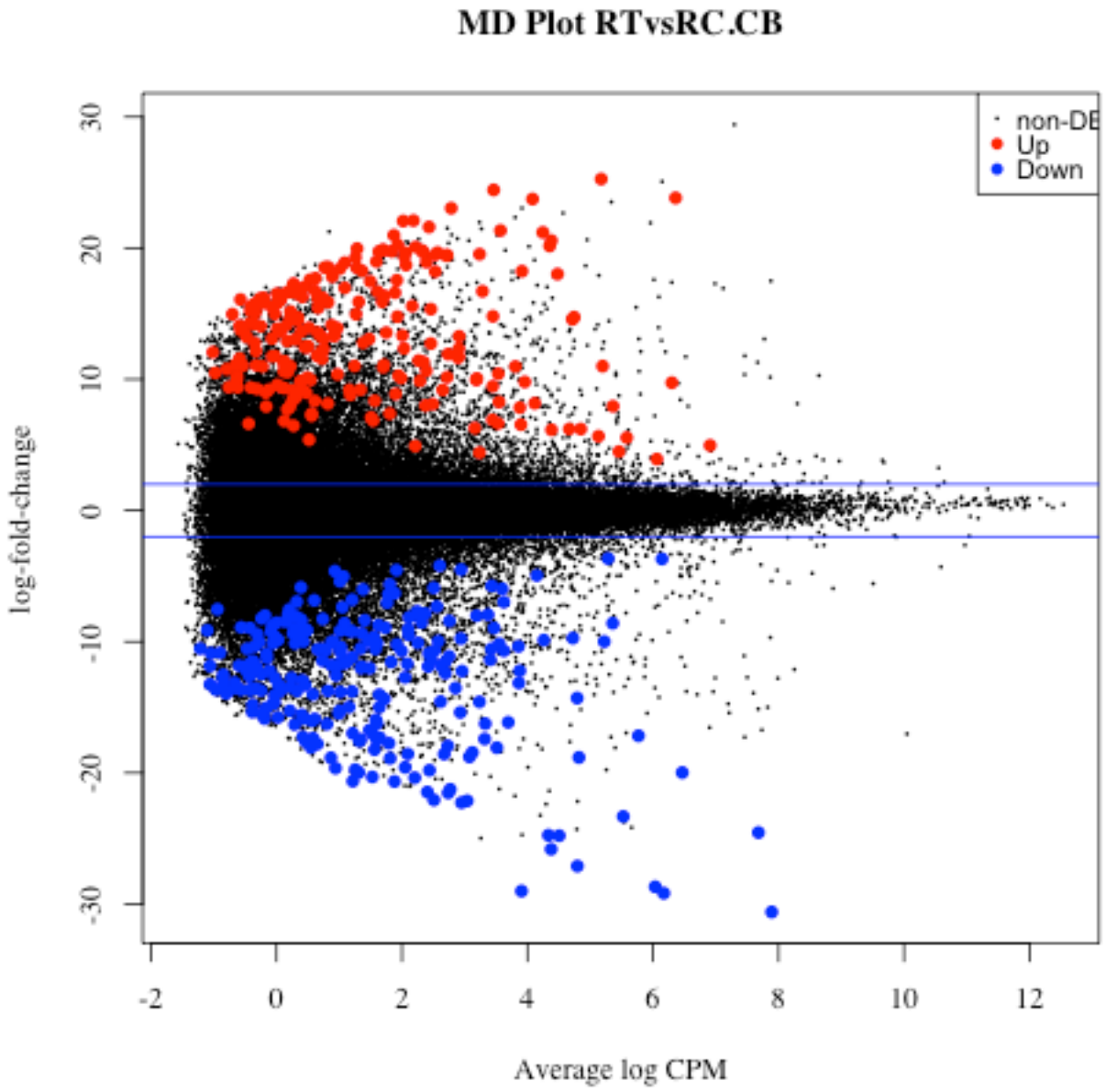


Figure A.9. MD plot of the contrast CB. The blue lines indicate 2-fold changes.

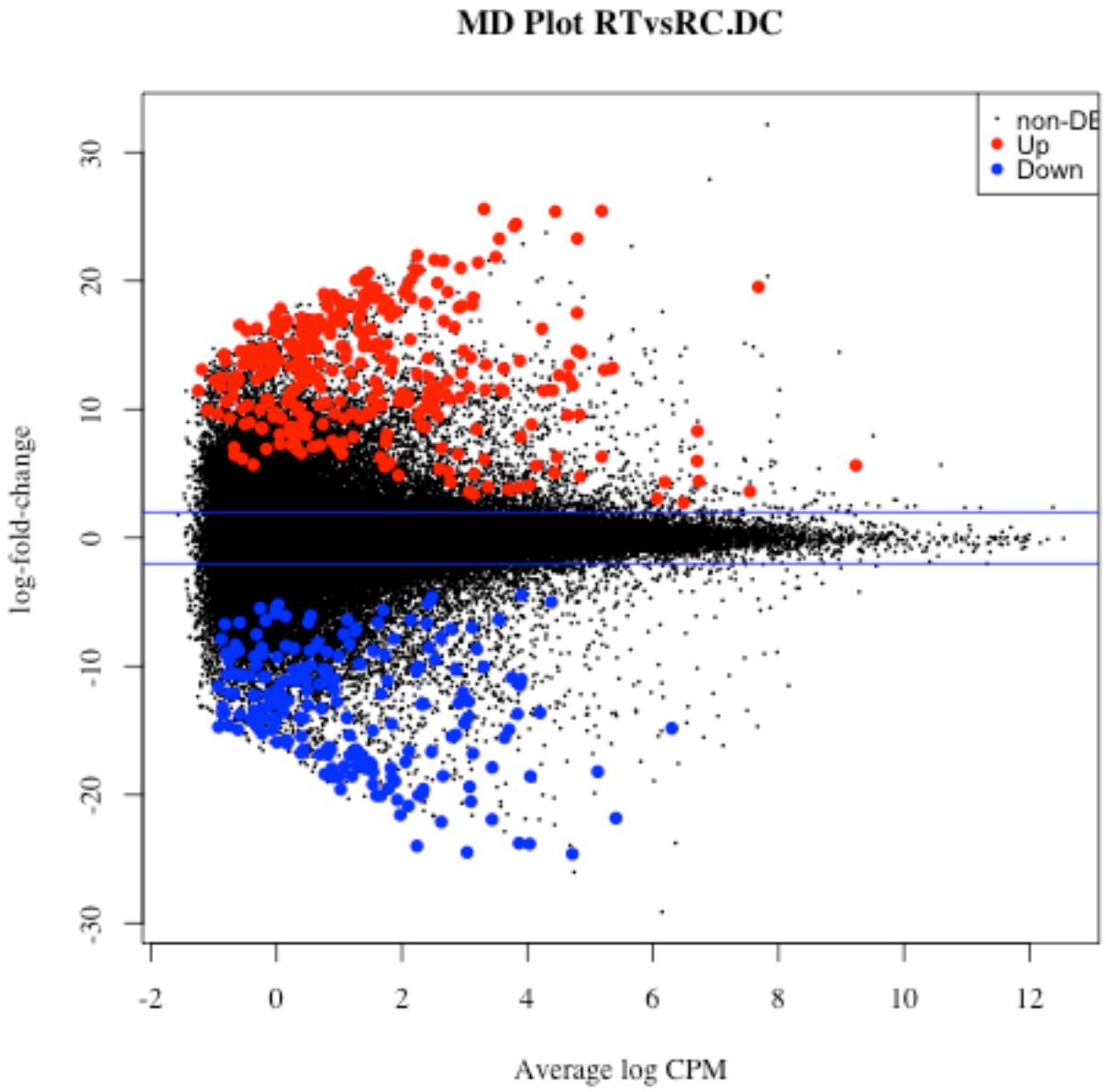


Figure A.10. MD plot of the contrast DC. The blue lines indicate 2-fold changes.

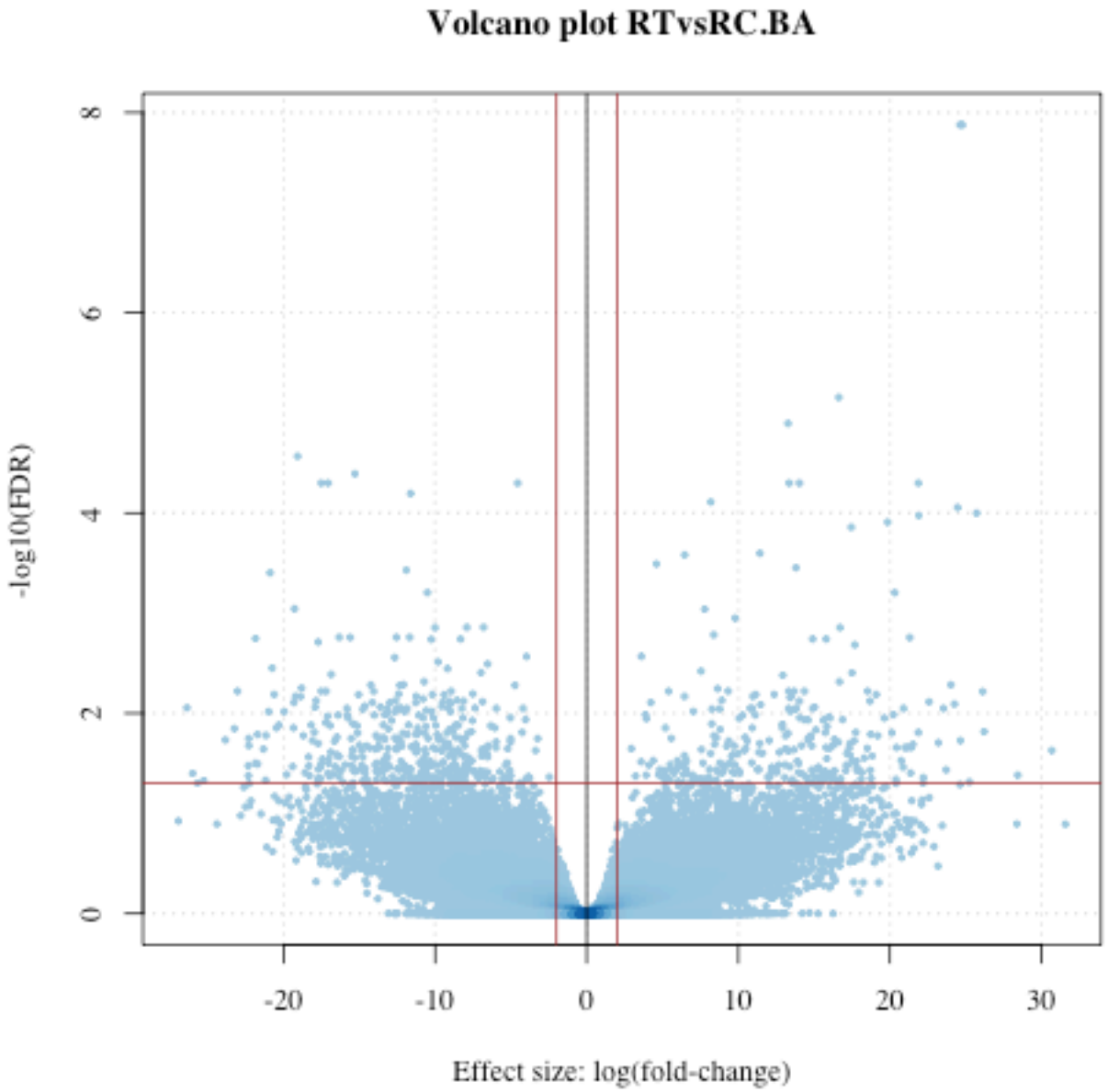


Figure A.11. Volcano plot of the contrast BA. The vertical red lines indicate 2-fold changes. The horizontal red line indicates the value of -log10(0.05).

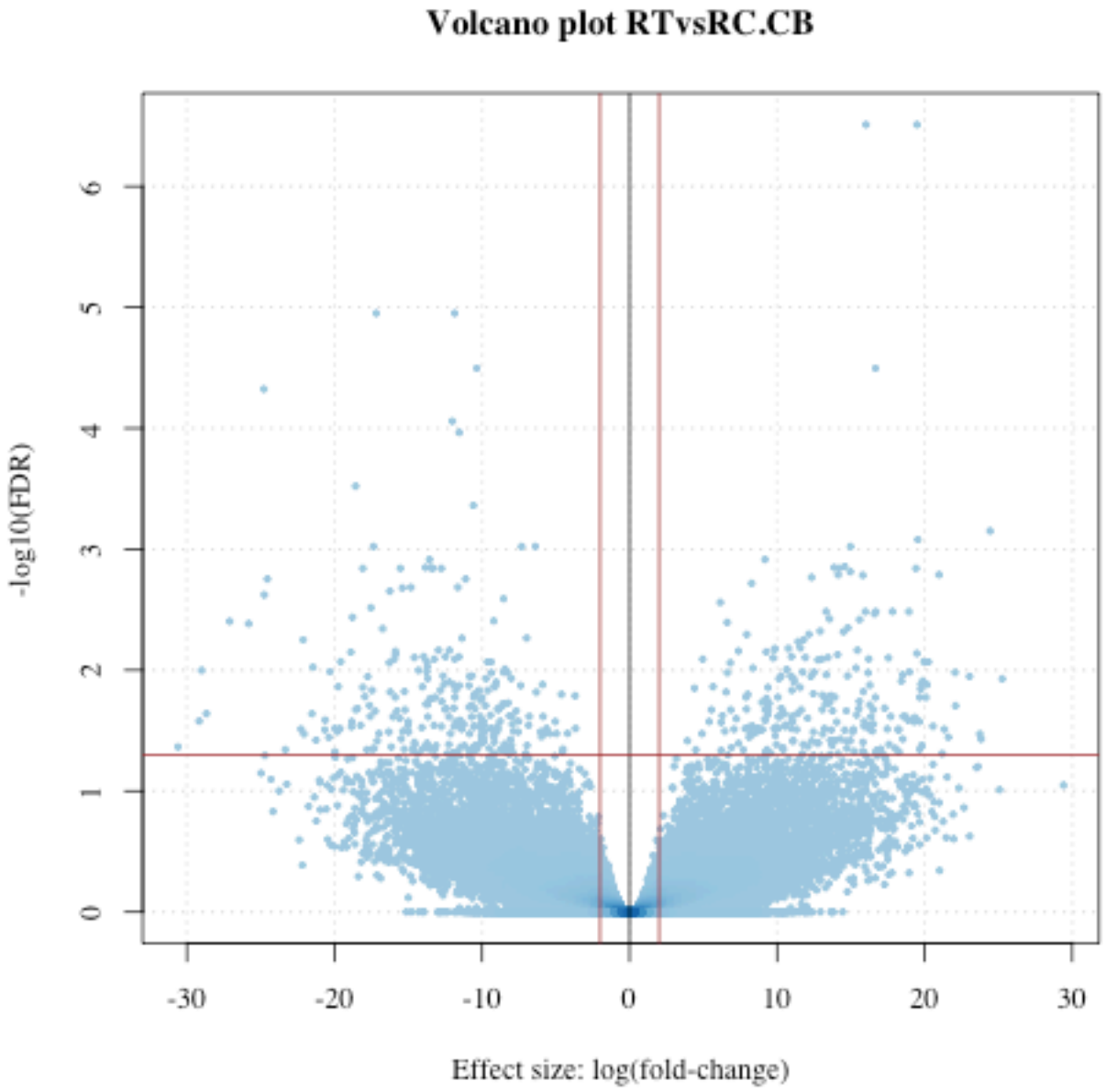


Figure A.12. Volcano plot of the contrast CB. The vertical red lines indicate 2-fold changes. The horizontal red line indicates the value of -log10(0.05).

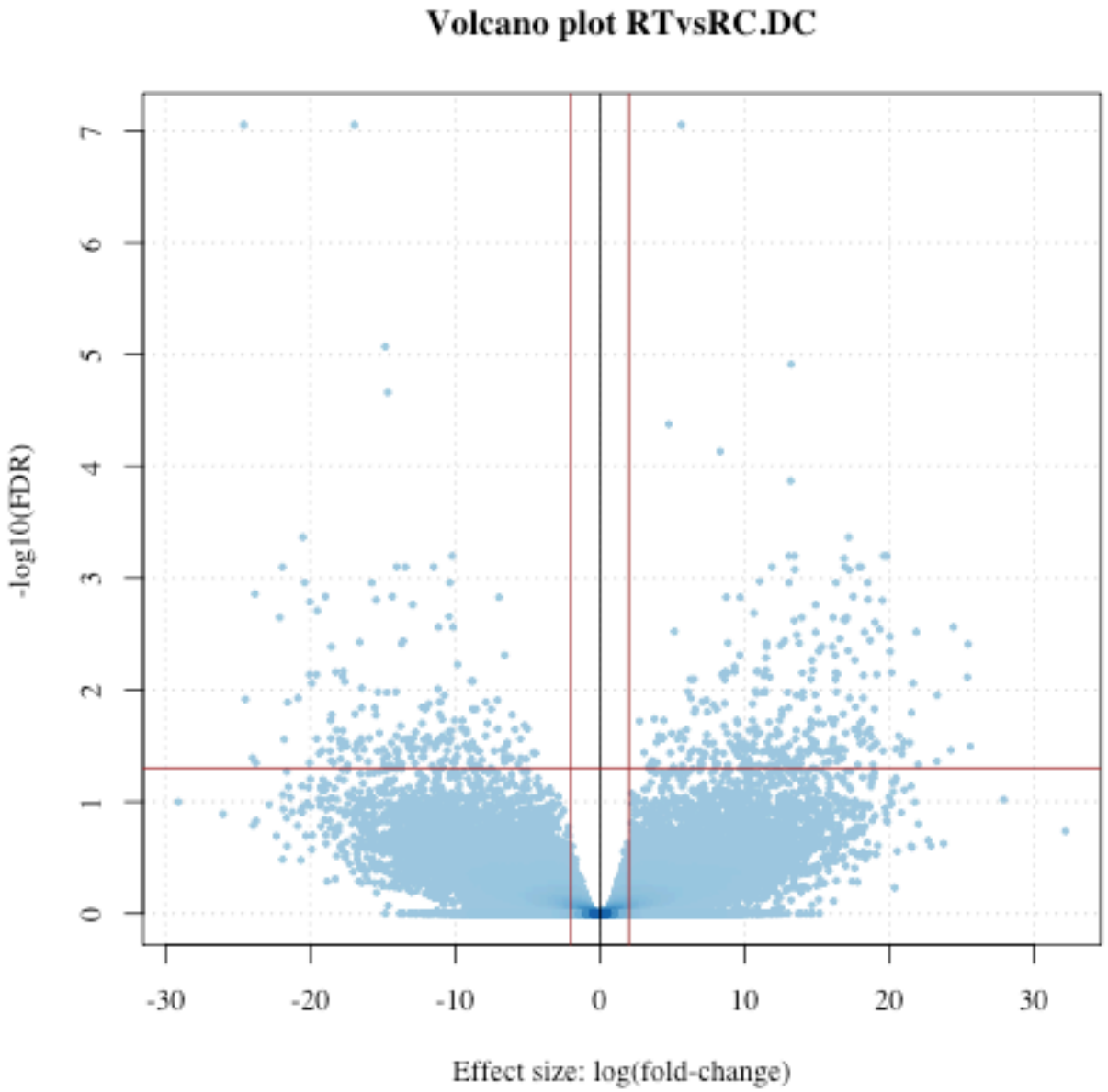


Figure A.13. Volcano plot of the contrast DC. The vertical red lines indicate 2-fold changes. The horizontal red line indicates the value of -log10(0.05).

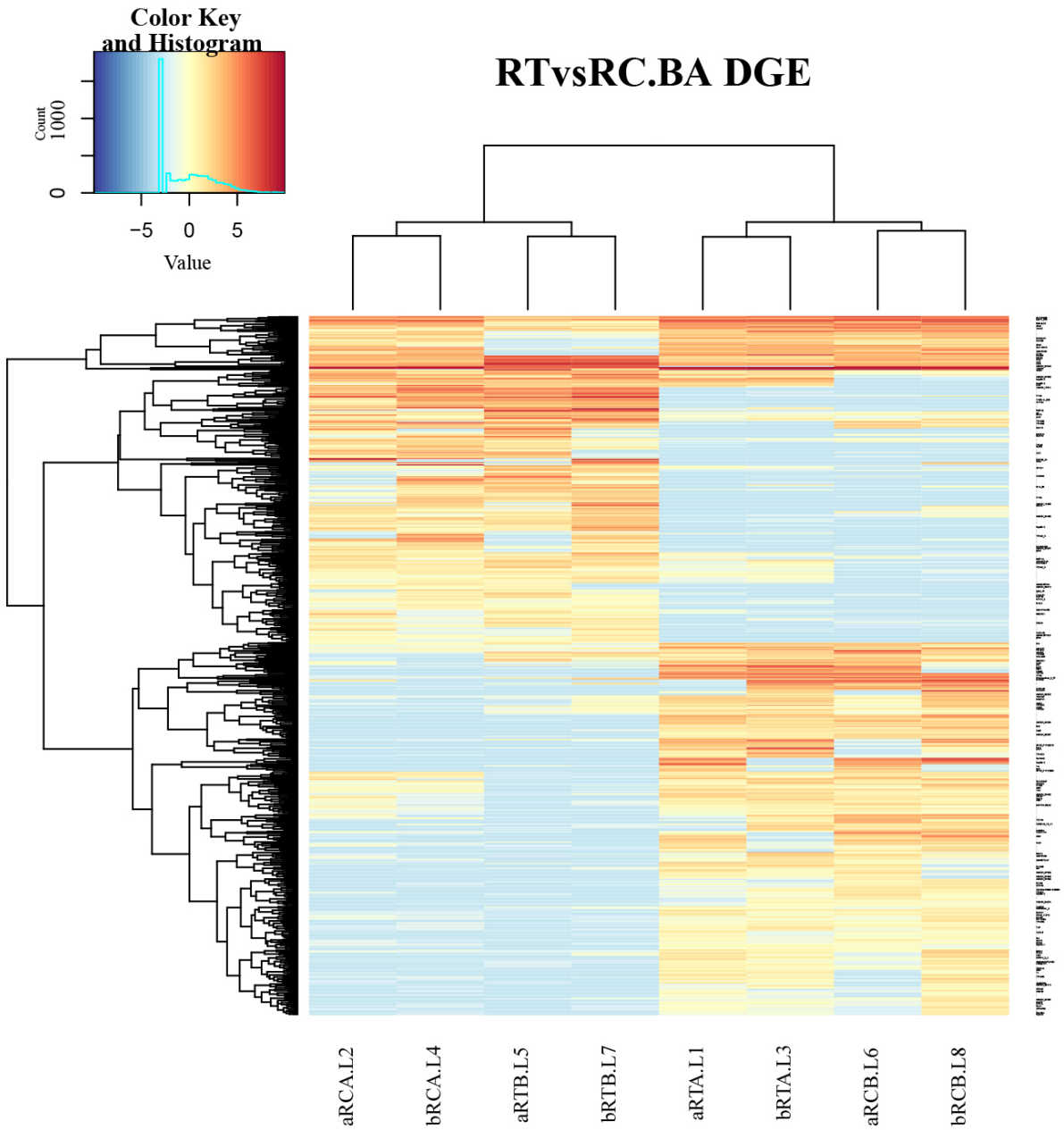


Figure A.14. Heatmap of the differentially expressed genes for the contrast BA.

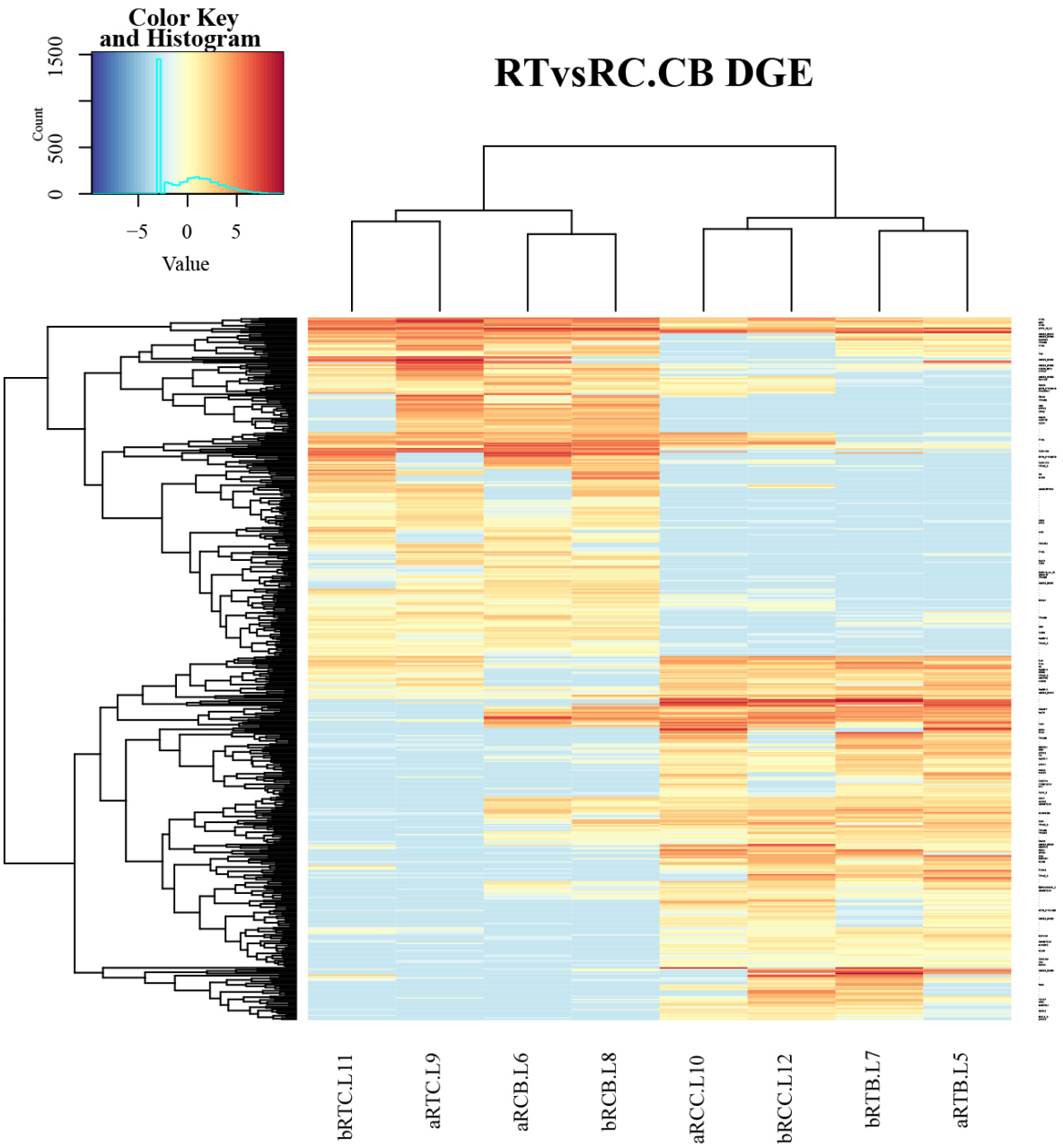


Figure A.15. Heatmap of the differentially expressed genes for the contrast CB.

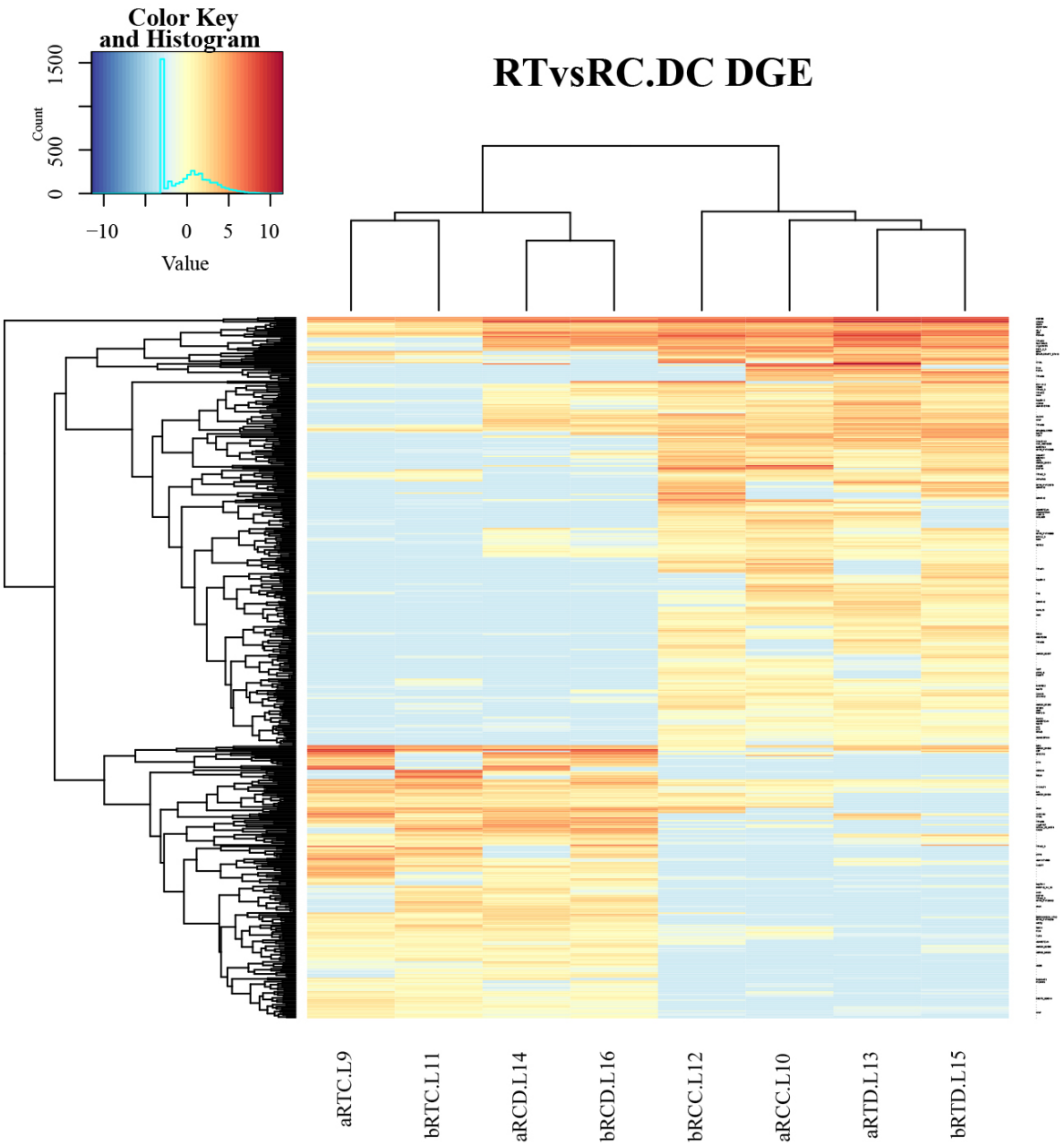


Figure A.16. Heatmap of the differentially expressed genes for the contrast DC.

APPENDIX B: GSEA ANALYSIS

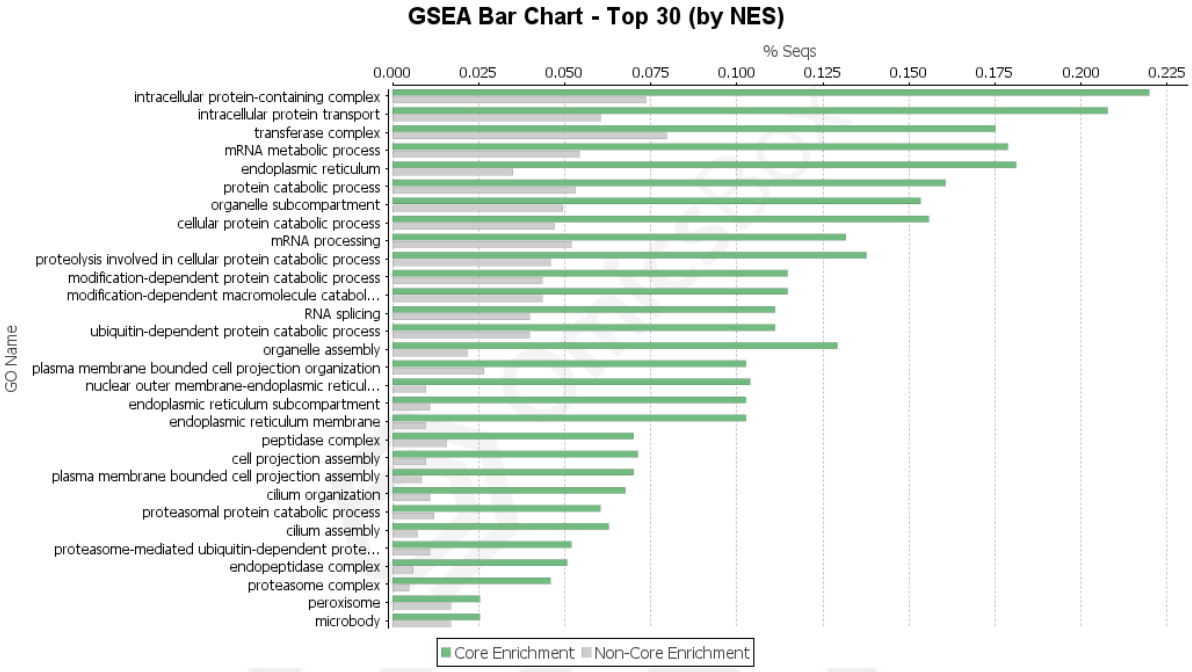


Figure B.1. Gene ontology terms enrcihed in salinity increase.

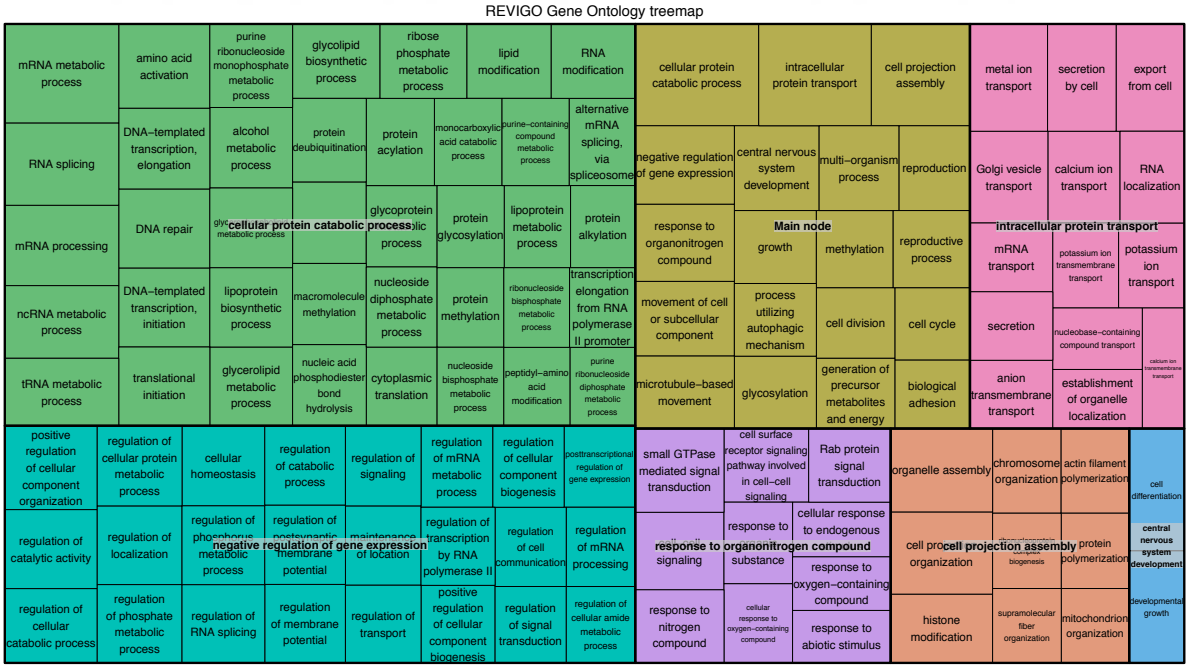


Figure B.2. Summarization of the enriched GOs for salinity increase, biological processes having FDR < 0.25 were summarized to 19 main nodes by Revigo. Each rectangle is a representative of a cluster. Superclusters are generated by loosely related terms and visualized with the same colour. (Supek et al., 2011).

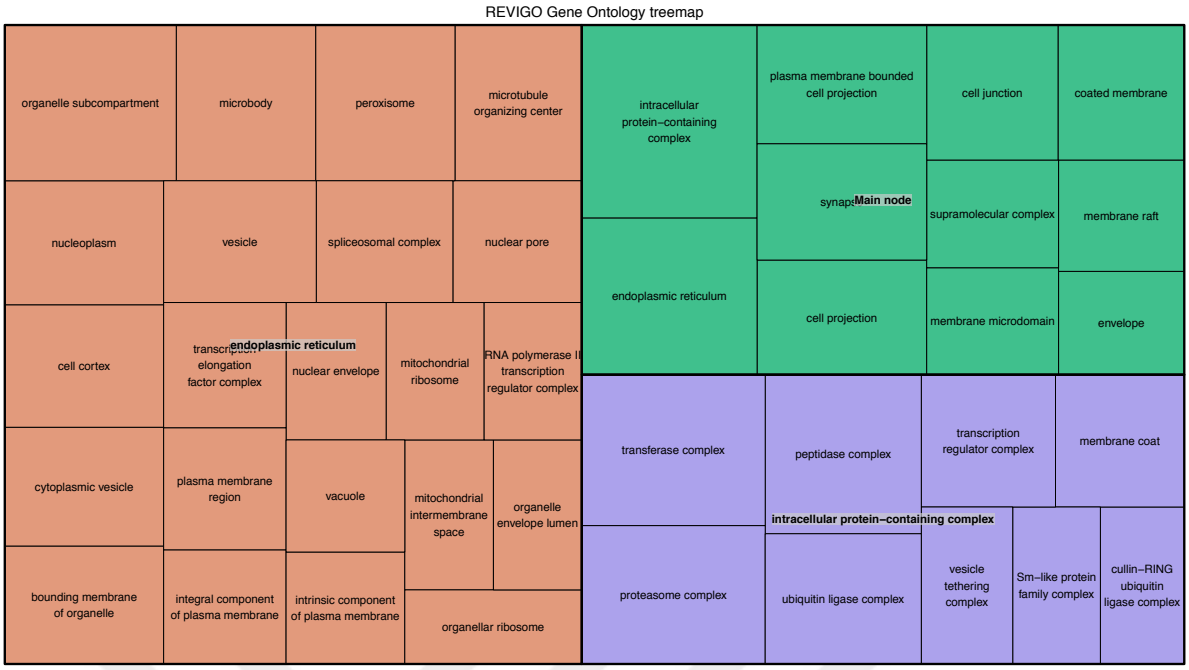


Figure B.3. Summarization of the enriched GOs for salinity increase, cellular components having FDR < 0.25 were summarized to 11 main nodes by Revigo. Each rectangle is a representative of a cluster. Superclusters are generated by loosely related terms and visualized with the same colour. (Supek et al., 2011).

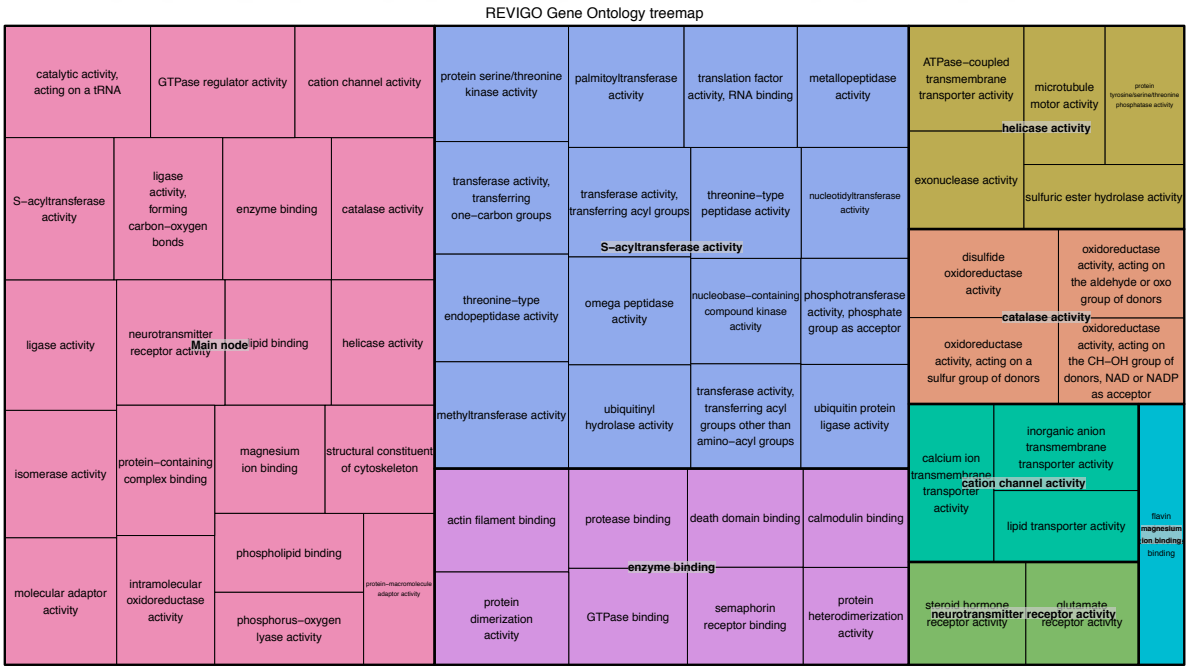


Figure B.4. Summarization of the enriched GOs for salinity increase, molecular functions having FDR < 0.25 were summarized to 20 main nodes by Revigo. Each rectangle is a representative of a cluster. Superclusters are generated by loosely related terms and visualized with the same colour. (Supek et al., 2011).

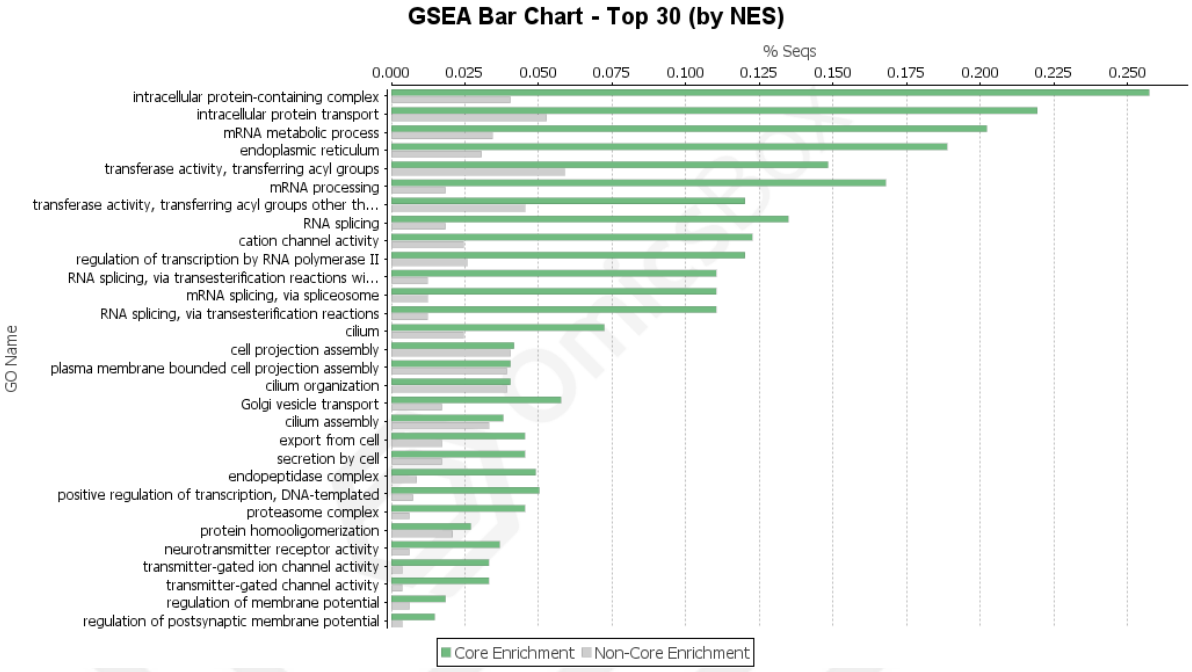


Figure B.5. Gene ontology terms enrcihed in high salinity acclimation.

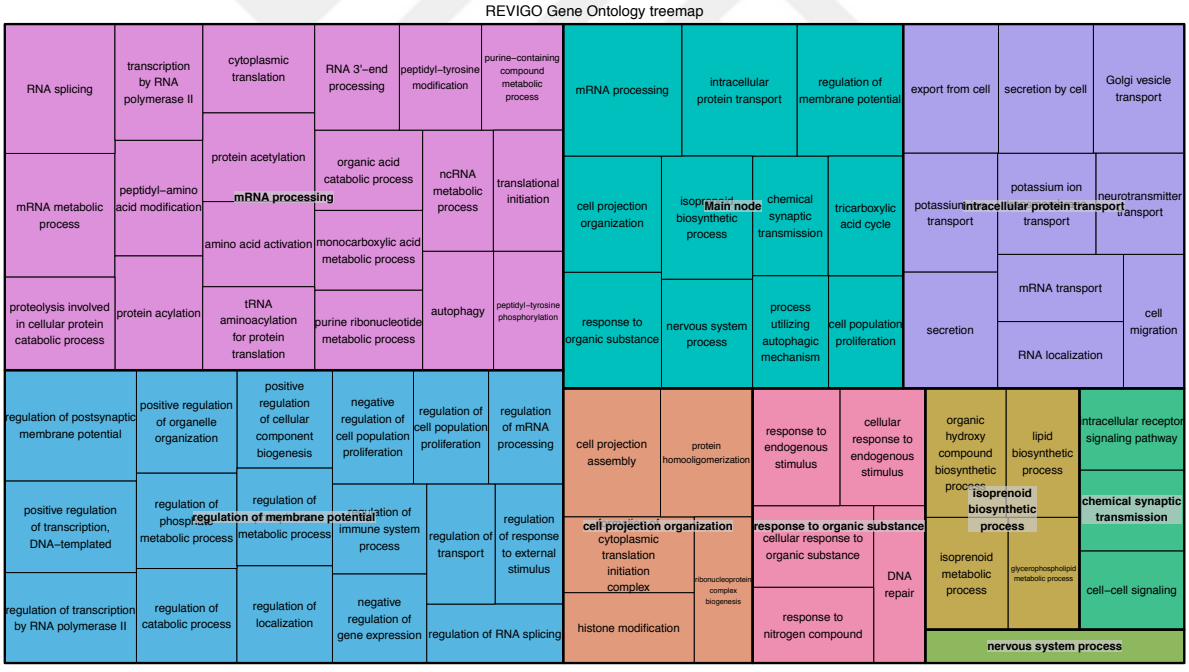


Figure B.6. Summarization of the enriched GOs for high salinity acclimation, biological processes having FDR < 0.25 were summarized to 11 main nodes by Revigo. Each rectangle is a representative of a cluster. Superclusters are generated by loosely related terms and visualized with the same colour. (Supek et al., 2011).

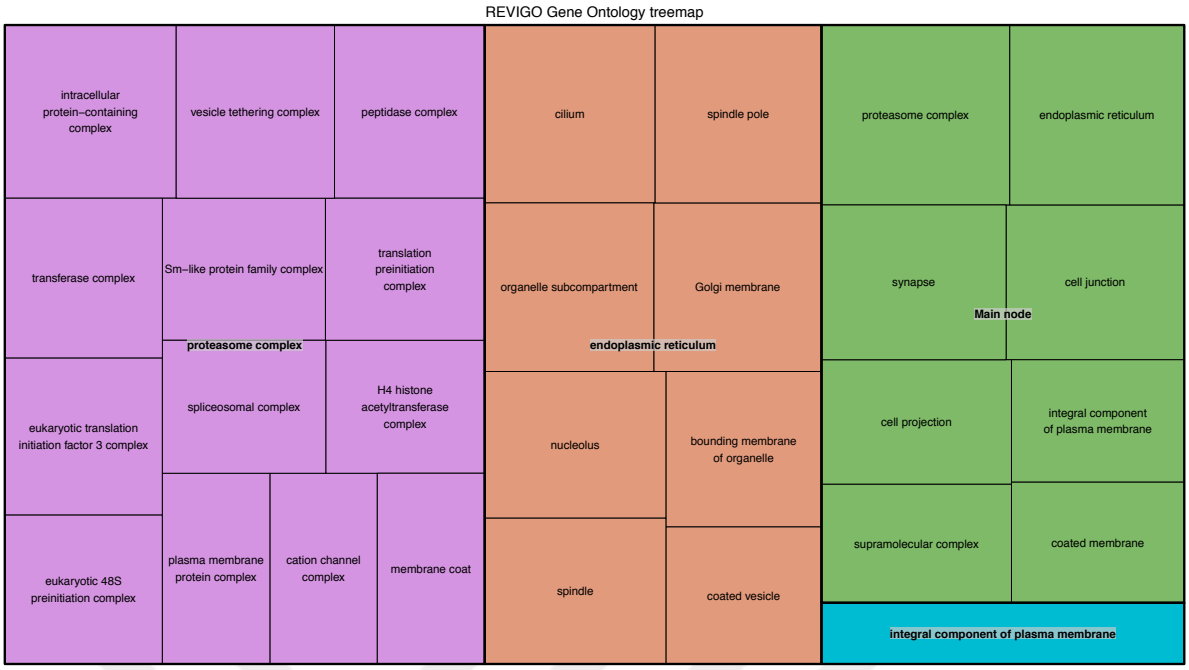


Figure B.7. Summarization of the enriched GOs for high salinity acclimation, cellular components having FDR < 0.25 were summarized to 8 main nodes by Revigo. Each rectangle is a representative of a cluster. Superclusters are generated by loosely related terms and visualized with the same colour. (Supek et al., 2011).

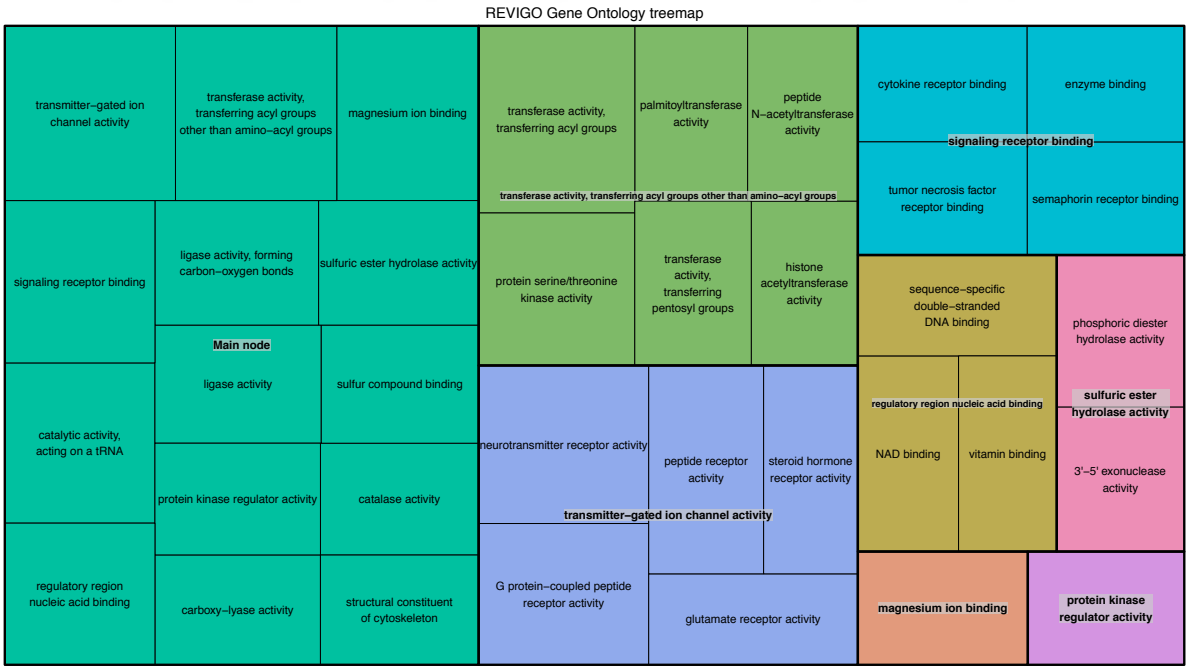


Figure B.8. Summarization of the enriched GOs for high salinity acclimation, molecular functions having FDR < 0.25 were summarized to 14 main nodes by Revigo. Each rectangle is a representative of a cluster. Superclusters are generated by loosely related terms and visualized with the same colour. (Supek et al., 2011).

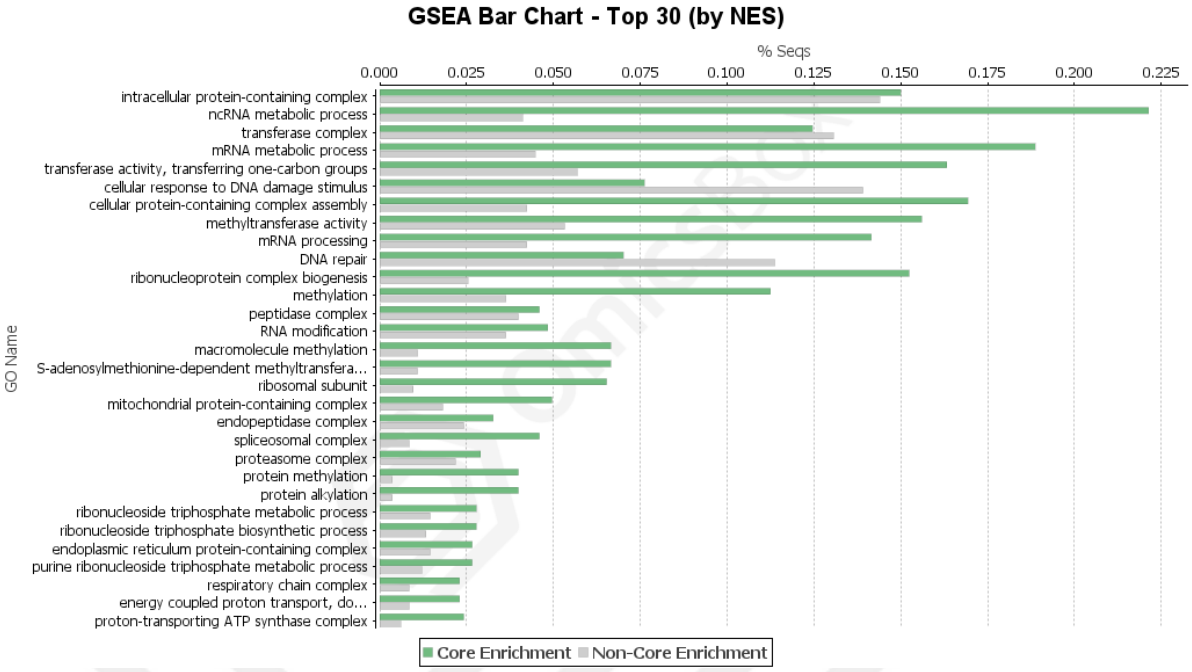


Figure B.9. Gene ontology terms enrcihed in salinity decrease.

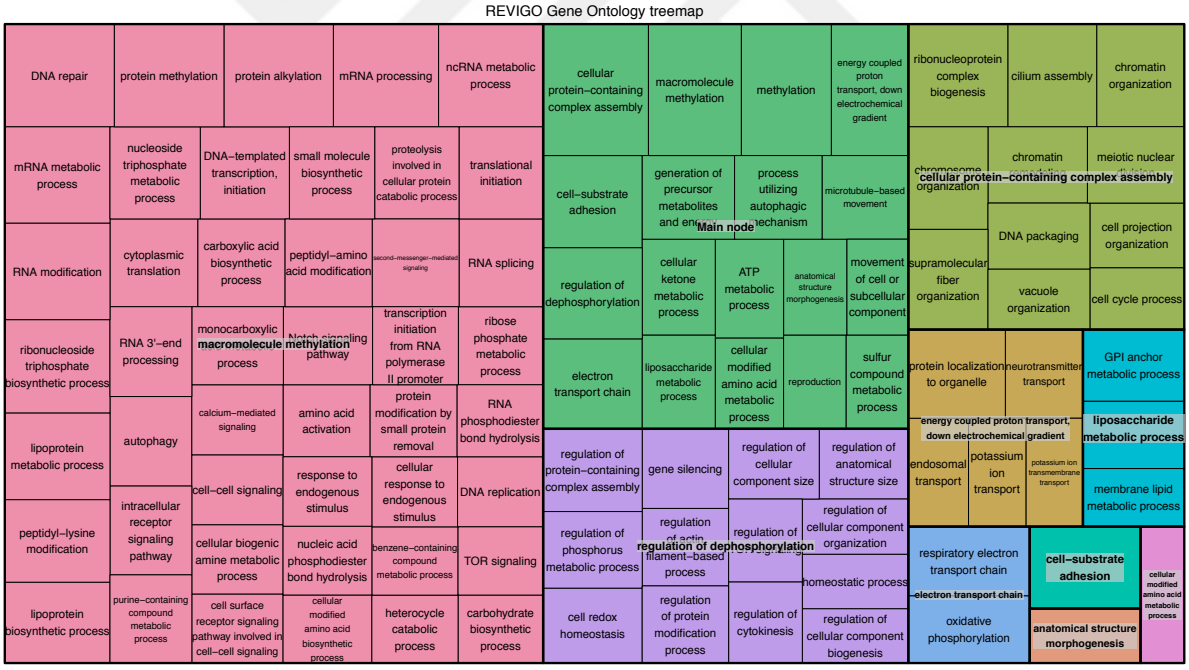


Figure B.10. Summarization of the enriched GOs for salinity decrease, biological processes having FDR < 0.25 were summarized to 18 main nodes by Revigo. Each rectangle is a representative of a cluster. Superclusters are generated by loosely related terms and visualized with the same colour. (Supek et al., 2011).

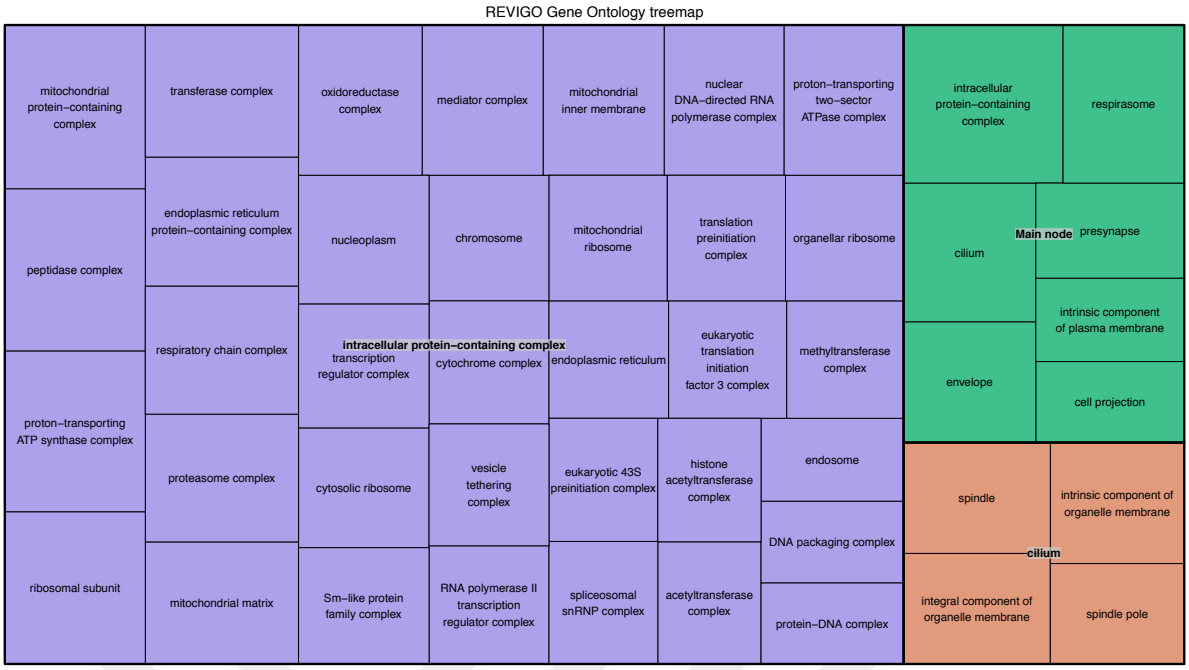


Figure B.11. Summarization of the enriched GOs for salinity decrease, cellular components having FDR < 0.25 were summarized to 7 main nodes by Revigo. Each rectangle is a representative of a cluster. Superclusters are generated by loosely related terms and visualized with the same colour. (Supek et al., 2011).

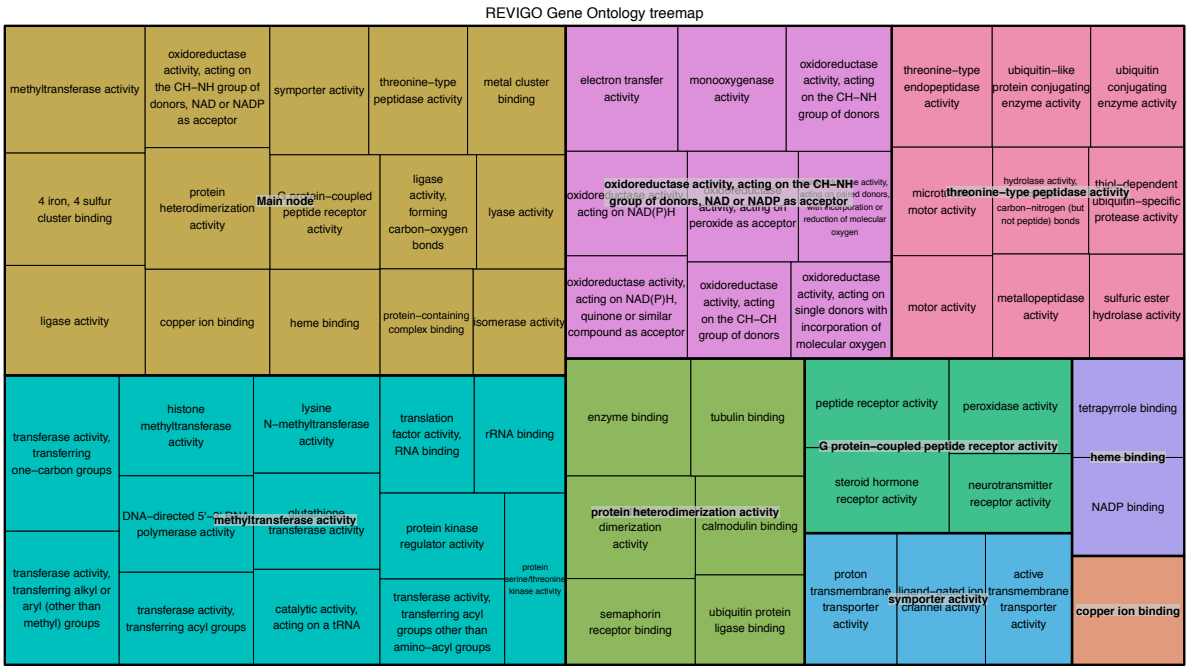


Figure B.12. Summarization of the enriched GOs for salinity decrease, molecular functions having FDR < 0.25 were summarized to 15 main nodes by Revigo. Each rectangle is a representative of a cluster. Superclusters are generated by loosely related terms and visualized with the same colour. (Supek et al., 2011).